Thermo Chemical Conversion of Biomass and Wastes

Nordic graduate school BiofuelGS-2
Chalmers, Göteborg 19-23 November 2007

Henrik Thunman and Bo Leckner

Welcome to the course Thermo Chemical conversion of biomass and wastes

The course will start 11.00 on the 19th of November in the seminar room at the division of Energy Technology at Chalmers. The seminar room is located on Hörsalsvägen 7b 3rd floor.

The course is given within the Nordic graduate school BiofuelGS-2 (Biofuel Science and Technology – 2) and in co-operation with the national research program CECOST, (The Centre for Combustion Science and Technology). The major part of the coarse material is included in here and to be able to get out as much as possible from the course we want the students to get familiar with the material and prepare themselves for the first assignment taking place already after the first lecture. Written examination 7th of December 9.00-13.00 at home University.

This material together with some complementing material will be handed out to the students at the first lecture.

Once more welcome to the course

Henrik Thunman and Bo Leckner

Content

Preliminary schedule

	Monday		Tuesday	Wednesday	Thursday	Friday
		8.00-9.45	Heat and mass transfer, HT	Conversion of thermally large particles HT	Conversion technologies: Great combustion HT Fluidised bed combustion BLe	The integration of thermo chemical conversion of solid biomass and wastes into the energy system, HT
		10.00-10.20	Heat balance exercise	Repetition	Repetition	Assignment 4
11.00-12.30	Introduction, HT Fuel characteristics BL	10.20-11.30	Heat balance exercise Assignment 1	Tutorials, Assignment 3	Assignment 4	Assignment 4
12.30-13.30	Lunch	11.30-12.30	Lunch	Lunch	Lunch	Lunch
13.30-15.15	Fuel resources and emission norms. BL	12.30-14.15	Conversion of thermally small particles HT	Char combustion (1h) BLe Comprehensive modelling of thermally large particles, HT	Boilers, Furnaces and Gasifiers BLe	Assignments 1-4
15.30-18.00	Heat balance exercise at Chalmers Power Station Per Löveryd Assignment 1	14.15-16.30	Tutorials, Assignment 2	Tutorials, Assignment 2 and 3	Assignment 4	
		19.00-	Course dinner			

NOMENCLATURE

ROMAN LETTER

A	[m^2]	area
a_1, a_2		constants
A_{int}	[m^2/m^3]	intrinsic area
a	[m^2/s]	thermal diffusivity, $k_c/\rho c_p$
Bi_t	[-]	thermal Biot number $h_c r_{car}/k_c$
Bi_m	[-]	mass Biot number $h_m r_{car}/D_{AB,eff}$
C	[$mole/m^3$]	molecular concentration
c_1		area factor
c_p	[J/kg·K]	specific heat at constant pressure
D_{AB}	[m^2/s]	molecular diffusivity of species A in B
$D_{AB,eff}$	[m^2/s]	effective molecular diffusivity of species A in B inside a porous structure
Dr	[-]	drying number
d	[m]	diameter, or characteristic length
E	[J/mole]	activation energy
f		function
HHV	[J/kg]	higher heating value
H	[J/kg]	heat of reaction
H_m	[J/kg]	heat of vaporisation
H_v	[J/kg]	heat of pyrolysis or devolatilisation
H_C	[J/kg]	heat of char conversion
H_{vol}	[J/kg]	heat of volatiles
h_{rad}	[W/(K m^2)]	radiative heat transfer coefficient
h_c	[W/(K m^2)]	heat transfer coefficient
h_c^*	[W/(K m^2)]	heat transfer coefficient corrected for gas flowing out from particle
$h_{c,eff}$	[W/(K m^2)]	effective heat transfer coefficient
h_m	[m/s]	mass transfer coefficient

k_c	[W/(K·m)]	heat conductivity
k_{rad}	[W/(K m)]	effective radiative conductivity
$k_{rv,0}$	[1/s]	pre-exponential factor for devolatilisation
$k_{rm,0}$	[1/s]	pre-exponential factor for drying
$k_{rC,0}$	[[]/([]s)]	pre-exponential factor for char conversion
L	[m]	Length
LHV	[J/kg]	lower heating value
Nu	[-]	Nusselt number, $h_c d / k_c$
M_i	[kg/mole]	molecular weight of species *i*
m	[kg]	mass
n	[- , mole/s]	reaction order or shape factor in (Chapter 4), or molar flow (Chapter 8)
P	[Pa]	pressure
Pe_t	[-]	thermal Peclet number
Pe_m	[-]	mass Peclet number
Pr	[-]	Prandtl number, $c_p\mu / k_c$
q	[J/s]	heat flow
Re	[-]	Reynolds number, ud/ν
r	[m]	radius
r_{car}	[.m]	characteristic radius or legth
R_v	[1/s]	rate of volatile release
R_m	[1/s]	rate of moisture release
R_C	[1/s]	rate of char conversion
$R_{C,eff}$	[1/s]	effective rate of char conversion
$\mathcal{R}$	[J/mole K]	gas constant 8.314
S	[J/(s m^3)]	heat source
S_m	[J/(s m^3)]	heat for vaporisation
S_v	[J/(s m^3)]	heat for devolatilisation
Sc	[-]	Schmidt number, ν/D_{AB}
Sh	[-]	Sherwood number, $h_m d/D_{AB}$
s	[m^2]	permeability
T	[K]	temperature
T_m	[K]	temperature at which moisture is released
T_v	[K]	temperature at which volatiles are released
T_b	[K]	background temperature for radiation
T_∞	[K]	temperature if surroundings
Th	[-]	$R(k_r/D_{eff})^{1/2}$
t	[s]	time
t_{dry}	[s]	time of drying
t_{ign}	[s]	time of ignition
t_{vol}	[s]	time of devolatilisation

t_{char}	[s]	time of char conversion
u	[m/s]	gas velocity
V	[m^3]	volume
W		generic variable
X	[-]	molar fraction
X_m	[-]	mass of moisture related to initial mass of moisture (Chapter 5)
x	[m]	length coordinate
Y	[kg/kg]	mass fraction

GREEK LETTER

Λ	[m^2/m^3]	effective intrinsic area
α	[-]	dimensionless constant
β	[-]	dimensionless temperature gradient at the drying front, or empirical exponent
Ω	[-]	stoichiometric coefficient
Γ	[ ]	shape factor
ν	[-]	gas voidage
μ	[Pa·s]	dynamic viscosity
θ	[-]	dimensionsless temperature (Chapter 3), or volumetric shrinkage factor (Chapter 5)
ρ	[kg/m^3]	density (in Chapter 5 related to initial time)
σ	[W/m^2K^4]	Stafan Boltzmann constant, 5.67×10^{-8}
τ	[-]	time constant *or* tortuosity
ξ	[-, m]	dimensionless length coordinate Chapter 3, length co-ordinate Chapter 5
ψ	[-]	dimensionless concentration (Chapter 3), or mass fraction of released gas not leaving through cracks (Chapter 5)
(δx)	[m]	length of one computational cell
ε	[-]	emissivity
Φ	[-, m^2/m^3]	split factor
φ	[m]	ratio between shrinkage in radial and axial direction
ω	[-]	ratio of solid and initial volume
ψ	[-]	mass fraction of released gas not leaving through cracks
ζ	[-]	ratio of initial volume of solid and gas to that occupied of gas only (V_0/V_g)
χ		generic variable
ϑ	[m/(Pa s)]	pressure-velocity coefficient

SUPERSCRIPT

0	reference
-	average value
·	per unit time
″	per unit area
‴	per unit volume
I	convective term
II	diffusive
III	source term
i, ii, iii	reaction 1, 2 and 3

SUBSCRIPT

0	initial state (for reaction rate it is the pre-exponential factor)
car	characteristic
v	volatiles
m	moisture
C	char
s	solid phase
g	gas phase
df	dry substanse
a	ash
B	cell on the bottom side of the active cell P
b	boundary at the bottom
c	convective
E	cell on the bottom side of the active cell P
e	boundary to the east
g	gas phase
i	counter
j	counter
k	counter
m	moisture (or mass)
N	cell on the north side of the active cell P
n	boundary to the north
P	active cell
per	perpendicular
par	parallel
S	cell on the south side of the active cell P
s	solid phase or boundary to the south

surf	surface
T	cell on the bottom side of the active cell P
t	boundary at the top
V	volume
v	volatiles
W	cell on the west side of the active cell P
w	boundary to the west
ξ	length coordinate
∞	ambient condition

CHAPTER 2

SOLID FUELS

LINDA JOHANSSON, HENRIK THUNMAN

Fossil fuels consist primarily of natural gas, petroleum-derived fuels, and coal. Biomass fuels are primarily wood, agricultural residues, and refuse. Solid fuels contain carbon, hydrogen, oxygen, nitrogen, sulphur, water, and ash. To characterise the solid fuel, the fuel is divided into moisture, volatile matter and fixed carbon. The composition of various fuels with a special focus on biofuels is given in Table 2.1. The composition of solid fuels is reported on an as-received basis, on a dry basis, or on a dry, ash-free basis. The basis of the calculation must always be specified.

Moisture can exist in two forms in solid fuels: as free water and as bound water. Free water is unbound. It is found between the cell walls in wood or in the larger pores of low-grade coal and is drawn into the pores by capillary attraction. Bound water is held by physical adsorption and exhibits a small heat of sorption. Green wood typically consists of 50 % water. A wood air-dried for a considerable time, up to one year depending on conditions, the moisture falls to 15-20 %. Lignite coals contain 20 to 40 % moisture, most of which is free water, whereas bituminous coals contain about 5 to 10 % moisture that is bound water, but also some surface (free) water. As we shall see, fuel moisture influences the rate of combustion and the overall efficiency of the combustion system.

Volatiles are the part of the fuel that is released as gases due to heating of the fuel. The volatile gas is mainly composed by carbon monoxide, carbon dioxide, hydrogen, water vapour, and various hydrocarbons. Wood typically consists of 80-90 % volatiles, lignite coals 40 %, bituminous coal 30% and anthracite 5-10 %. The remaining part of the combustible part of the fuel is fixed carbon. Ash is the inorganic residue remaining after the fuel is completely

Table 2.1 Composition of various fuels

	Fixed carbon (dry)%	Volatile matter (dry)%	Ash (dry) %	carbon	hydrogen	oxygen	nitrogen	sulphur	clorine	SiO_2	$AlzO_3$	TiO_2	Fe_2O_2	CaO	MgO	Na_2O	K_2O	SO_3	P_2O_5
				% on dry and ash free						% on ash									
Bituminous coal	55	35	10	83	5	10	1	1	0.1	70	40	1	15	7	2	2	2	5	1
Red oak sawdust	13	86	0.3	50	6	44	0.03	0.01	0.01	21	3	0.3	3	11	4	1	22	3	1
Alder/fir sawdust	19	77	4	51	6	39	0.46	0.05	0.02	35	12	1	8	25	4	2	6	0.6	2
Forest residuals	14	82	4	50	5	40	1.08	0.11	0.04	18	4	1	2	45	7	2	9	3	7
Pine sawdust	15	82	3	54	6	40	0.1	0.04	0.02	18	3	0.3	2	56	6	2	8	2	2
Bagasse	12	86	2	49	6	43	0.16	0.04	0.03	47	18	3	14	4	3	1	4	2	3
Switch grass, average	15	79	5	47	6	41	0.7	0.1	0.02	62	2	0.3	1	10	4	0.5	9	1	4
Miscantus	16	80	3	48	6	43	0.4	0.05	0.08	56	1	0.0	1	14	1	0.2	19	2	6
Straw (DK)	15	81	4	48	6	42	0.6	0.09	0.17	55	1	0.2	1	12	2	2	13	2	4
Rice hulls	16	63	20	47	6	44	0.6	0.05	0.12	91	1	0.0	0.1	3	0.0	0.2	4	1	0.4
Almond shells	21	76	3	49	6	41	0.8	0.04	<0.01	9	3	0.1	2	11	3	2	49	1	4
Olive pits	16	82	2	53	7	38	0.4	0.05	0.04	31	9	0.3	7	15	4	28	4	0.6	2
Dry sewage sludge	10	52	38	46	6	41	5	1.2	0.25	37	15	1	5	21	3	0.5	1	3	13
RDF	15	77	8	48	7	44	0.6	0	1.3	40	24	2	2	23	3	2	2	2	1

Table 2.2 Typical ash and moisture content of various fuels, and energy per unit volume related to that of coal.

Fuel	Ash %	Moisture %	Volume $(m^3/m^3\ coal)_{MJ}$
Coal	10	10	1
Wood pellets	0.2-0.5	5	2
Wood powder	0.2-0.5	5	4
Wood chips	0.2-0.5	50	7
Saw dust	0.2-0.5	50	9
Bark	1	50	8
Straw briquettes	5	<18	3
Straw bale	5	<18	13
Straw natural	5	<18	20

burned. Wood usually has only a few tenths of a percent of ash, while coal typically has 10 % or more of ash. Typically the ash begins to soften at 1200 °C and becomes fluid at 1300 °C, although this varies significantly between fuels depending on the composition of ash. Ash characteristics play an important role in system design in order to minimize slagging, fouling, erosion, and corrosion. For transportation, the energy per unit volume is the most important factor shown in Table 2.2 for various biofuels related to coal.

BIOFUELS

The plant matter include cellulose, hemicellulose, lignin and other compounds for example lipids, proteins, simple sugars, starches, water, hydrocarbons and ash [1]. Cellulose is the chief cell wall component in wood. Hemicellulose associated with cellulose in the cell walls. Lignin is the third major wall component in the cell walls of wood serving as a cement between wood fibres, as a stiffening agent within the fibres, and as a barrier to the degradation of the cell wall. The concentration of each component in plant matter depends on species, type of plant tissue, stage of growth, and growing conditions. Irrespective of studied plant matter, biomass is highly oxygenated, with respect to fossil fuels as coals, due to the carbonate structure of biomass.

Biomass includes all kind of materials that were directly or indirectly formed through the current photosynthesis. In the photosynthesis reaction atmospheric carbon dioxide is transferred to organic bound carbon in biomass by reacting with water in the presence of sunlight. Primary the sugar glucose is formed:

$$6CO_2 + 6H_2O \rightarrow C_6H_{12}O_6 + 6O_2$$

Four main classes of biofuels can be found [1]:

a-b	Wood and woody materials
c-d	Herbaceous and other annual growth materials
e-f	Agricultural wastes and residues
g-h	Refuse-derived fuels (RDF) and organic waste materials

In Table 2.3 compositions and heating values of some biofuels from the different classes of biofuels are presented. For comparison, coal is included as well. The principal component of biomass is carbon, typically varying between 40 and slightly more than 50 % of the dry fuel. The highest carbon content is recorded for wood pellets and the lowest for RDF. Oxygen is the second most abundant component ranging between slightly less than 30 and slightly more than 40 % (dry fuel). The third major component is hydrogen, showing concentrations between 5 and 7 %.

Table 2.3 Composition in mass-% of dry fuel and heating values (LHV) in MJ per kg dry fuel. The first class of biofuels is represented by the fuels labelled a and b, the second class of fuel c – d, the third class of fuel e – f and the fourth class of fuel g – h. Fuel analyses are from reference 4, citied by reference 3, except for a [5] and h [6].

Label	Fuel	C	H	O	N	S	Cl	Ash	LHV
a	Wood pellets	50.6	6.0	43.1	0.08	<0.01	<0.01	0.3	19.1
b	Willow wood	49.9	5.9	41.8	0.61	0.07	<0.01	1.71	18.4
c	Wheat straw	44.9	5.5	41.8	0.44	0.16	0.23	7.02	16.8
d	Switchgrass	46.7	5.8	37.4	0.77	0.19	0.19	8.97	16.9
e	Almond shells	49.3	6.0	40.6	0.76	0.04	<0.01	3.29	18.3
f	Olive pitts	52.8	6.7	38.3	0.45	0.05	0.04	1.72	20.2
g	Mixed paper	48.0	6.6	36.8	0.14	0.07	-	8.33	19.5
h	MSW*	42.4	6.1	35.1	2.2	0.24	0.73	-	16.0
i	Coal, lvb**	87.5	4.3	1.6	1.25	0.75	0.16	4.51	34.1
j	Lignite	61.0	4.1	18.5	1.02	1.81	0.04	13.69	22.5

* municipal solid waste (MSW)

** low volatile bituminous (lvb)

WOOD AND WOODY MATERIALS

The yield of woody fuels per land area may differ, e.g. tree plantations growing new hybrid hardwoods, such as hybrid poplar, yield 5 to 10 times the annual biomass of a natural forest [7]. However, the building up of the plant starts with a stem of a tree, which is composed of wood and an outermost layer of bark. The innermost wood is considerably darker than the portion adjacent to the bark. The light wood is termed sapwood and the dark wood heartwood. The sapwood is most recently formed, and contains the only living cells found in mature wood. Growth rings indicate the age of the tree. Each growing season a new layer of wood is inserted between existing wood and the bark. This is termed a growth ring. The lighter-colour portion of the growth ring is produced first and therefore called earlywood or springwood. The darker part is produced later and is called latewood or summerwood. Most wood cells have their long axis oriented parallel to the long axis of the tree stem. However, some cells have their long axis oriented perpendicular to the stem. Aggregations of these transversely oriented cells are called rays.

Besides cellulose, hemi-cellulose and lignin dry wood consists of resins (extractives), and ash-forming minerals. Wood extractives include oils, resins, gums, fats, waxes, etc, that ordinarily do not exceed a few percent. However, extractives from bark range from 20 to

40 %. The constituents which making up the ash remaining after combustion of the wood are in the range from 0.2 to 1 % by weight and consists mainly of calcium, potassium, magnesium, manganese, and sodium oxides and small amounts of other oxides, such as iron and aluminium [7]. The mineral matter is dispersed throughout the cells in molecular form.

Wood can be divided into hardwood and softwood, the hardwoods are generally denser than the softwoods. Hardwoods refer to broad-leafed trees that shed their leaves at the end of each growing season. The wood of hardwood contains vessels that are responsible for water conduction and fibers that perform the supporting role, Figure 2.1. Softwoods are evergreen trees with needles, sometimes called conifers because their seeds are formed in cones. In softwood there is cells called longitudinal tracheids, which have the roles of conduction and support, Figure 2.2.

Bark differs from hardwood and softwood in both structure and composition. Structurally, bark appears more sponge-like than an organized fibre [7]. Bark pores twist and intermix in an irregular pattern. Bark contains more resin and more ash than wood, typically 1 to 3 %.

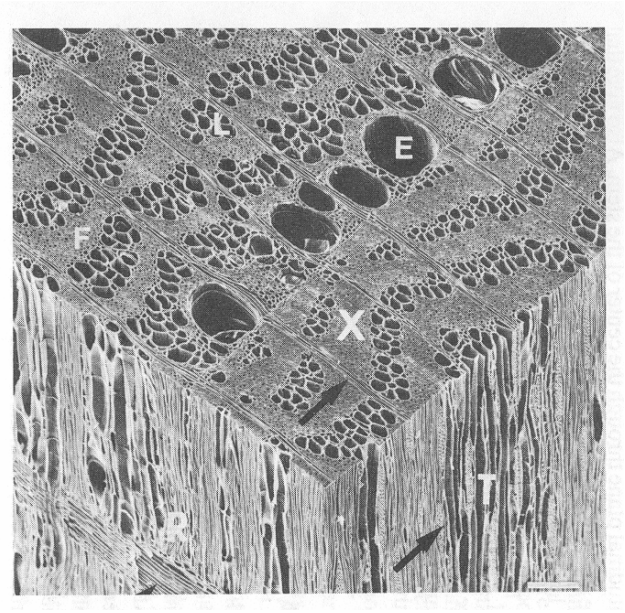

Figure 2.1

Diffuse-porous hardwood with fairly uniform vessel diameters across entire growth ring. Formation of vessels from individual vessel elements (E) shown in both radial (R) and tangential (T) views. Note presence of one-cell wide and multicell-wide rays in tangential view (arrows) [2].

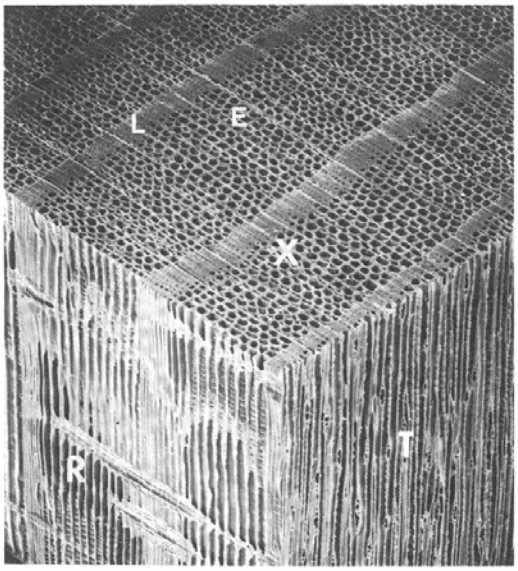

Figure 2.2

Softwood growth increments. Note the wide latewood zone in cross-sectional view (X). Individual latewood cells with tick walls and small radial diameters are visible. Arrows indicate wood rays in all three planes of study. (R, radial; T, tangential) [2].

Sometimes wood is pelletised or briquettised to improve storage and shipping, or made into charcoal. Charcoal is made by heating wood in the absence of air to produce char. Charcoal is a relatively clean-burning fuel. Charcoal can be pulverized easily and made into briquettes by the addition of a binder such as starch.

HERBACEOUS AND OTHER ANNUAL GROWTH MATERIALS

Herbaceous and other annual growth materials, i.e. straw and grasses, typically contain significantly higher amounts of chlorine than woody fuels. The straw and grass presented in Table 2.3 contain 20 times or more chlorine than the woody fuels. The high chlorine content makes great demands on the boilers where these fuels are burnt because chlorine may cause corrosion problems as well as emissions of chlorinated hydrocarbons together with hydrochlorine. The ash content in straw and grasses is, besides the chlorine content, much higher compared to woody fuels. Another important ash constitute is potassium that contribute to depositions on tubes and agglomeration of fluidized beds.

AGRICULTURAL WASTES AND RESIDUES

Agricultural wastes comprise crop residues as well as manure. Crop residues are the plant parts left in the field after harvest and the remainders left after processing the crop, e.g. nut husks and olive pits. Agricultural wastes also include animal manures. For example in India considerable amount of dried cattle dung is used as a fuel for cooking. Different agricultural wastes and residues may differ much in structure and chemical content. For example almond shells in Table 2.3contain four times or less chlorine and twice as much ash as olive pits. Consequently, it is important to distinguish different agricultural wastes and residues.

REFUSE-DERIVED FUELS (RDF) AND COMBUSTIBLE WASTE

Often refuse with considerable energy content and other waste are disposed in landfills or incinerated without energy recovery. Relatively recently, efforts have been made to burn waste materials with the purpose of also producing heat and power. Since large quantities of these waste materials are generated, they represent a significant energy resource. However, not the all waste is biofuel. In Sweden, 85 % of the combustible waste may be considered as biofuel, and the remaining part as fossil fuel [8].

From January 2002 it became illegal to deposit separated combustible waste in landfills in Sweden. Year 2002, about 40 %, $1.7*10^6$ tons, of the Swedish household waste was incinerated with energy recovery. In addition, $1.1*10^6$ tons of industrial waste was incinerated [9]. A total of 8.6 TWh of heat and electricity was generated from waste, where 95 % consisting of heat in district heating plants. Heat generated from waste contributed to 10 % of the district heating in Sweden [9].

Refuse can be burned directly in specially designed boilers, or it can be processed before combustion to separate combustibles from the non-combustibles. Processing includes shredding, magnetic separation, screening, and air classification. Processing facilitates recovery of metals and glass as well as controlling the fuel size. The processed refuse is called *refuse-derived fuel* (RDF), ref [7].

RDF can be processed into several forms depending on how it is utilized. For example, coarse RDF is obtained when 95 % of the mass passes through a 15 cm screen [7] and fluff RDF when 95 % of the mass passes through a 5 cm screen. The RDF can be compressed into pellets or briquettes for better storage and shipping or thermally converted to liquid and gaseous fuels. Typical materials found in Swedish municipal solid waste are listed in Table 2.4.

Table 2.4 Typical sorting analysis of municipal solid waste in Sweden, recycled material is excluded, [10] citied by [11].

Material category	**Subcategory**	**Wet mass-%**
Paper	Newspapers Cardboards Wrapping Cardboards Writing papers Paper sacks Soft papers	18.4
Diapers		7.9
Plastic	Soft plastics Hard plastics Wrapping plastics	8.1
Laminate	Milk packages Butter packages Metal laminates	4.1
Glass		2.2
Kitchen sweeping and garden trash	Kitchen sweepings Garden sweepings	49.2
Remaining combustible		3.5
Metal		2.6
Remaining incombustible		1.5
Hazardous waste		0.4

PEAT

Peat is formed from decaying woody plants, reeds, sedges, and mosses in wet environments from which air is largely excluded, such as watery bogs, usually occurring in northern climates. In the presence of bacterial action, chemical decomposition proceeds by a process called humification [7]:

$$\underset{\text{Cellulose}}{2C_6H_{10}O_5} \xrightarrow[\text{Heating}]{\text{Bacterial action}} \underset{\text{Peat}}{C_8H_{10}O_5} + CH_4 + 2CO_2$$

The rate of formation of a peat bed is about 3 cm per 100 years, and formally peat can be regarded a renewable resource, but practically it is not. Peat is usually dark-brown in colour and fibrous in character. Since freshly harvested peat typically contains 80 to 90 % water, it must be dried before use it as a fuel. Peat contains 1 to 10 % ash.

COAL

Coal is a heterogeneous mineral, whose combustible part consists principally of carbon, hydrogen, and oxygen, with minor amounts of sulphur and nitrogen. Other constituents are the ash-forming inorganic compounds, distributed throughout the coal. When heated, coal gives off gases, leaving a residue called char (When the heating is carried out with the purpose of producing a solid carbonaceous residue, it is called coke, in Swedish koks). This residue is porous and consists of carbon and remaining mineral ash.

Coal was formed by accumulation of wood and other biomass that was later covered, compacted, and transformed into rock over a period of hundreds of thousands of years. Most bituminous coal seams were deposited in wetlands that were regularly flooded with nutrient-containing water that supported abundant peat-forming vegetation. The lower levels of the wetlands were anaerobic and acidic, which promoted structural changes and biochemical decomposition of the plant remnants. This microbial and chemical alteration of the cellulose, lignin, and other plant substances, and later the increasing depth of burial, resulted in a decrease in the percentage of moisture and a gradual increase in the percentage of carbon. This change from peat through the stages of lignite, bituminous coal, and ultimately to anthracite (the process called coalification) is characterized physically by decreasing porosity and increasing gelification and vitrification. Chemically, the process is accompanied by a

decrease in the volatile matter content, as well as an increase in the percentage of carbon, a gradual decrease in the percentage of oxygen, and, as the anthracite stage is approached, a decrease in the percentage of hydrogen.

The chemical composition of coal cannot be described in as straightforward manner such as was done for wood. A vast array of organic compounds has been identified in coal. Benzenoid ring units play an important role in the coal structure. Hydrogen, oxygen, nitrogen, and sulphur are attached to the carbon skeleton. Inorganic minerals form the ash, which remains when coal is burned.

Nitrogen in coal is organic and varies up to a few percent by mass. Sulphur in coal has organic and inorganic forms. The organic sulphur, which is bound into the coal, varies widely from a fraction of a percent to 8 %. Inorganic sulphur is predominantly found as iron pyrite (FeS_2) and varies from zero up to a few percent. Pyritic sulphur may be removed by coal cleaning methods, while organic sulphur is distributed throughout and requires chemical degradation to release the sulphur.

The mineral matter in coal consists of minerals such as kaolinite, detrital clay, pyrite, and calcite, and hence includes oxides of silicon, aluminium, iron, and alkali metals. Minor but significant amounts of magnesium, sodium, potassium, manganese, and phosphorus are found. Mineral matter in coal varies widely and is present in molecular form, as bands between layers of coal, and is in some instances added from the overburden during mining.

Coal may be classified according to rank and grade. *Coal rank* expresses the progressive metamorphism of coal from lignite (low rank) to anthracite (high rank). Rank is based on heating value, which is calculated on a dry ash-free basis for low-rank coals, and on percentage of fixed carbon, calculated on a dry ash-free basis, for higher-rank coal.

The lowest ranked coal is lignite. Lignite is also referred to as brown coal. Chemically, lignite is close to peat, and it contains a large percentage of water and volatiles. Mechanically, lignite is easily fractured, but not spongy like peat. Sub-bituminous coal is dull-black, shows little woody material, and often appears banded in the ground as well as in the particles themselves. The coal usually fractures along the banded planes. Also, the moisture content of sub-bituminous coal is reduced. Bituminous coal is a dark black colour and is often banded. The moisture content is low and the volatile content ranges from high to medium. Bituminous coal is more resistant to disintegration in air than lignite and sub-bituminous coals. Anthracite coal is hard and brittle and has a bright lustre. It has almost no volatiles or moisture. Anthracite is not banded.

The *grade of coal*, which is independent of rank, depends on the ash content, ash fusion temperature, sulphur content, and the presence of other deleterious constituents. Grade of coal is used more qualitatively than rank. The grade of coal can be improved by coal cleaning methods to remove some ash and pyrite sulphur.

Mechanical cleaning processes include crushing, washing, dewatering, and drying. Coarse and medium sizes coal particles are cleaned by gravity separation, while the finer sizes are cleaned by froth floatation. Typically coal has a density of 1100 to 1300 kg/m^3. When tiny particles are added to water, bringing the density to about 1500 kg/m^3, then coal particles float while free mineral impurities tend to sink. In froth flotation the small coal particles are buoyed up to the top of a controlled surface froth, while the heavier impurities sink to the bottom. Mechanical cleaning can reduce the ash content by 10 to 70 % and the sulphur content by up to 35 %. Ultra-fine grinding (micronization) of coal to an average particle size of 10 microns followed by washing has produced some coals with less than 1 % ash. Chemical cleaning methods are being investigated to further clean or beneficiate coal.

ANALYSIS AND TESTING OF SOLID FUELS

Standard analyses of solid fuels are proximate analysis, ultimate analysis, heating value, and ash fusion temperature. The *proximate* analysis gives rough information of the fuel by the content of moisture, volatile combustible matter, fixed carbon, and ash in a fuel. In Fig 2.3 there is an example of a protocol from an ultimate analysis and analysis of heating value of wood pellets. The *ultimate* analysis provides the major elemental composition (C, H, O, S, N and Cl) of the fuel, reported on a dry and ash-free basis. Moisture is determined by drying a crushed fuel sample in an oven at 105 °C to a stable weight. Carbon, hydrogen and nitrogen are determined by burning the sample in oxygen (at about 1000 °C) in a closed system and quantitatively measuring the combustion products. The carbon includes organic carbon as well as carbon from the mineral carbonates. The hydrogen includes organic hydrogen as well as any hydrogen from the moisture of the dried sample and mineral hydrates. The extraneous carbon and hydrogen are usually negligible. Sulphur is determined by burning the sample in oxygen (at a minimum temperature of 1350 °C) in a closed system and quantitatively measuring the sulphur oxides formed. Oxygen is determined by the difference between 100 and the sum of the percentages of C, H, N, and S. Chlorine, if important, should be included in the ultimate analysis. The heating value is determined in a bomb calorimeter. The bomb calorimeter gives the heating value at constant volume, i.e. the higher heating value (HHV).

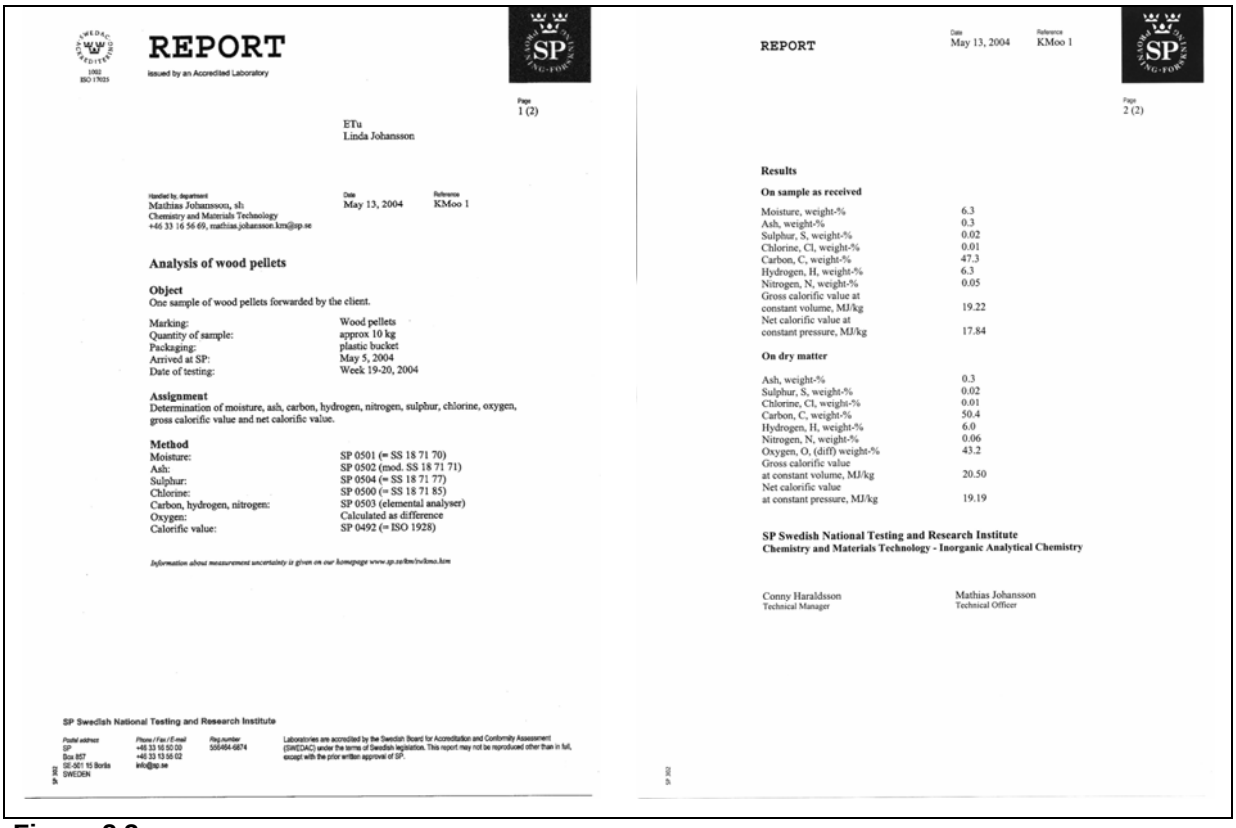

REPORT

issued by an Accredited Laboratory

Page 1 (2)

ETu
Linda Johansson

Handled by, department
Mathias Johansson, sh
Chemistry and Materials Technology
+46 33 16 56 69, mathias.johansson.kmx@sp.se

Date: May 13, 2004
Reference: KMoo 1

Analysis of wood pellets

Object
One sample of wood pellets forwarded by the client.

Marking:	Wood pellets
Quantity of sample:	approx 10 kg
Packaging:	plastic bucket
Arrived at SP:	May 5, 2004
Date of testing:	Week 19-20, 2004

Assignment
Determination of moisture, ash, carbon, hydrogen, nitrogen, sulphur, chlorine, oxygen, gross calorific value and net calorific value.

Method

Moisture:	SP 0501 (≈ SS 18 71 70)
Ash:	SP 0502 (mod. SS 18 71 71)
Sulphur:	SP 0504 (≈ SS 18 71 77)
Chlorine:	SP 0500 (≈ SS 18 71 85)
Carbon, hydrogen, nitrogen:	SP 0503 (elemental analyser)
Oxygen:	Calculated as difference
Calorific value:	SP 0492 (≈ ISO 1928)

Information about measurement uncertainty is given on our homepage www.sp.se/km/rv/kmo.htm

SP Swedish National Testing and Research Institute

Postal address: SP, Box 857, SE-501 15 Borås, SWEDEN
Phone / Fax / E-mail: +46 33 16 50 00, +46 33 13 55 02, info@sp.se
Reg.number: 556464-6874

Laboratories are accredited by the Swedish Board for Accreditation and Conformity Assessment (SWEDAC) under the terms of Swedish legislation. This report may not be reproduced other than in full, except with the prior written approval of SP.

REPORT

Date: May 13, 2004
Reference: KMoo 1

Page 2 (2)

Results

On sample as received

Moisture, weight-%	6.3
Ash, weight-%	0.3
Sulphur, S, weight-%	0.02
Chlorine, Cl, weight-%	0.01
Carbon, C, weight-%	47.3
Hydrogen, H, weight-%	6.3
Nitrogen, N, weight-%	0.05
Gross calorific value at constant volume, MJ/kg	19.22
Net calorific value at constant pressure, MJ/kg	17.84

On dry matter

Ash, weight-%	0.3
Sulphur, S, weight-%	0.02
Chlorine, Cl, weight-%	0.01
Carbon, C, weight-%	50.4
Hydrogen, H, weight-%	6.0
Nitrogen, N, weight-%	0.06
Oxygen, O, (diff) weight-%	43.2
Gross calorific value at constant volume, MJ/kg	20.50
Net calorific value at constant pressure, MJ/kg	19.19

SP Swedish National Testing and Research Institute
Chemistry and Materials Technology - Inorganic Analytical Chemistry

Conny Haraldsson
Technical Manager

Mathias Johansson
Technical Officer

Figure 2.3.
Protocol from an ultimate analysis and heat value analysis of wood pellets.

The lower heating value (LHV) is calculated from the higher heating value by subtracting for the evaporation energy of water formed from combustion of hydrogen in the fuel. The calculation of LHV from HHV is illustrated in example 2.1. All these measurement procedures are standardised according to ASTM, DIN or other standards.

EXAMPLE 2.1. A solid fuel contains 6 % hydrogen, 30 % moisture, and 10 % ash and has a higher heating value of 11.6 MJ/kg (all mass %, as-received). What is the dry, ash-free lower heating value?

Solution.

$$\text{HHV (dry, ash - free)} = 11.6 \times 10^6 / (1 - 0.30 - 0.10) = 19.4 \text{ MJ/kg}$$

Dry, ash-free fuel contains 6 / (1 -0.30 -0.10) = 10 % hydrogen, and thus,

$$\frac{m_{H_2 0}}{m_{\text{fuel}}} = \frac{0.1 \frac{kg_{H_2}}{kg_{\text{fuel}}}}{0.002 \frac{kg_{H_2}}{mole_{H_2}}} \left(1 \frac{mole_{H_2O}}{mole_{H_2}} \right) \left(0.018 \frac{kg_{H_2O}}{mole_{H_2O}} \right) = 0.90 \frac{kg_{H_2O}}{kg_{\text{fuel}}}$$

Since the latent heat of vaporization of water is 2.44 MJ/kg at 25 °C,

$$\text{LHV} = 19.4 - (0.90)(2.44) = 17.2 \text{ MJ/kg}_{\text{fuel}}$$

When ash is heated to a softened state, it has a tendency to foul boiler tubes and surfaces. The *ash fusion temperature* gives an indication on the behaviour of the ashes. Ash fusion temperatures depend on the composition of the ash. The combustion engineer should note that the ash fusion temperatures are typically below the flame temperature, and above the steam and wall temperatures, which is one of the challenges of utilizing solid fuels.

SUMMARY

Naturally occurring solid fuels include biofuel, peat, and coal. In addition to the chemical makeup of the fuel, the most important properties are higher and lower heating value (HHV and LHV) and density. The standard fuel analyses are ultimate analysis, proximate analysis (moisture, volatiles, fixed carbon, and ash), ash fusion temperature. With residual fuel oils and solid fuels, the sulphur, nitrogen, and ash content are particularly important. With biomass fuels moisture and mineral content are important factors.

REFERENCES

[1] Baxter, L., Coombes, P., Gifford, J., Guiu, G., Houmann Jakobsen, H., Koppejan, J., Livingston, W., Logie, R., Loo van, S., Nussbaumer, T., Obenberger, I., Oravainen, H., Schenkel, Y., Skreiberg, Ö., and
Tullin, C., 2002. Handbook of Biomass Combustion and Co-Firing, p 11, Twente University Press, Enschede, the Netherlands, ISBN 9036517737

[2] Lewin M. and Goldstein, I. S. Wood Structure and Composition, International Fiber Science and Technlogy, Volume 11, edited by M., Lewin and I. S., Goldstein, pp 1-14, Marcel Dekker Inc

[3] Jenkins, B.M., Baxter, L..L., Miles, T.R. Jr., Miles, T.R. Combustion properties of biomass, *Fuel Processing Technology*, 54 (1998), 17-46

[4] Miles, T. R., Miles, T. R. Jr., Baxter, L. L., Bryers, R. W., Jenkins, B. M., Oden, L. L. Alkali deposits found in biomass power plants: a preliminary investigation of their extent and nature, National Renewable Energy Laboratory, Golden, CO, 1995

[5] Johansson, L. S. Leckner, B.; Tullin, C.; Sjövall, P. Particle emissions from biomass combustion in small combustors, *Biomass and Bioenergy*, 25 (2003), 435-446

[6] Nordin, A. Chemical elemental characteristics of biomass fuels, *Biomass and Bioenergy*, 6 (1994), 339-347

[7] Borman, G. L., Ragland, K. W. Combustion Engineering, 1998, WCB/McGraw-Hill

[8] RVF Rapport 2003:12, Förbränning av avfall Utsläpp av växthusgaser jämfört med annan avfallsbehandling och annan energiproduktion

[9] Wiqvist, R., Swedish Waste Management 2003, edited by RVF – The Swedish Association of Waste Management

[10] Flyhammar, P., Åkesson, M., Hedlund, H. (1993) Karakterisering av avfallsfraktioner från källsortering (Characterisationn of waste fractions from source-seaparatedmunnicipal waste) Naturvårdsverket rapport 1993:2:4

[11] Wikström, E., Marklund, S., Combustion of an artifical municipal solid waste in a laboratory fluidised bed reactor, *Waste Management & Research*, 16 (1998), 342-350

1

The Contribution of Renewables to Society

Göran Berndes

1.1 Introduction

Stocks and flows of biomass are vital components of the biogeochemical system of the Earth. Biomass builds up the ecosystem, which contains the reservoir of genetic and species diversity and provides environmental services such as water purification, waste assimilation, soil fertility rehabilitation, water runoff regulation and flood control. Biomass is also crucial for human subsistence in other ways as it serves as food, and can be used for energy purposes and for the production of, e.g., sawn wood, paper, and various chemicals. Throughout history, human societies have ultimately depended on the management and harvest of biological (land and water) resources, and their inability to sustain their productivity have led to the end of their civilizations (Ponting, 1992).

Thus, human beings have always influenced their habitats, and still today the conversion of ecosystems to land for biomass production is perhaps the most evident alteration of the Earth. However, emissions to air and water also lead to substantial environmental impacts and a large portion of these emissions come (directly or indirectly) from other than land use activities. The industrialized society of today is unique historically in that access to biomass does not impose the ultimate limit: humans have learned to decouple industrial activities from biological productivity by exploiting fossil resources in the form of petroleum, coal and gas and this ability proved a powerful driver of societal development in the twentieth century. The role of biomass as a source

Renewables-Based Technology Edited by J. Dewulf and H. Van Langenhove

of energy has steadily declined and the global energy system is today dominated by fossil fuel use. The petrochemical industry creates synthetic materials and chemicals that successfully compete with biobased products, and also the food sector has undergone dramatic changes: most of our food still comes from agriculture, but is today produced in an intensive manner that relies on fossil fuels and petroleum-based chemicals, where synthetic nitrogen fertilizers are among the crucial causes behind the past century's transformation of world food production (Smil, 2001).

In the twentieth century, the impacts of human society on nature escalated. At the beginning of the twenty-first century, human societies have put almost half of the world's land surface to their service, and have caused extensive land degradation and loss of biodiversity worldwide (Turner II *et al*., 1990, Oldeman *et al*., 1991, Groombridge and Jenkins, 2002). Human activities influence global biogeochemical cycles, bringing about environmental effects such as eutrophication, acidification, stratospheric ozone depletion and climate change (Figure 1.1). It is clear that the substitution of biomass with fossil resources (and the intensification of agriculture) have saved large areas from deforestation and conversion to agricultural land. But at the same time, much of the environmental impacts we see today is caused by the intensified land use and the use of petroleum, coal and fossil gas. For that reason, today there are attempts to reduce our dependence on fossil resources and return to relying more on biomass and other renewable resources for our subsistence. Addressing the concerns about climate change, land degradation and other environmental impacts, while providing food, energy and materials for a growing and wealthier global population, will be a formidable challenge.

This chapter will discuss the potential role of biomass as a renewable resource in a future global industrial society. Some analysts, such as Hoffert *et al*. (2002), dismiss biomass as an important future renewable resource, especially in the context of energy system transformation and climate stabilization. Others take the opposite view and propose biomass as one of the major future renewable resources (see Berndes *et al*., 2003 for a review of 17 studies of the global bioenergy potential). There is no way to narrowly determine the potential contribution of biomass in a future global industrial society, since it depends on a range of parameters that can vary substantially in the future (Hoogwijk *et al*., 2003). The aim of this chapter is instead to provide some perspectives and point out a few potentially important issues likely to come into focus in a future of extensive use of biomass for energy and as a renewable feedstock in industry. To begin with, a short review of biomass use in society, including a comparison with other major product and resource flows, followed by an outline of the prospects for non-food crop production and agricultural residue utilization in the future – emphasizing some crucial aspects that so far have received less explicit attention in assessments. After that, the drivers behind increased demand for biomass will be described. The case will be made that the demand for climate-neutral fuels and materials (especially fuels) may lead to a dramatically expanded human biomass use, with implications for biodiversity and nature conservation, and competition for land and other resources. Illustrative outlines of possible consequences are given and discussed. Finally, multifunctional biomass production systems are described. Such systems offer a way to meet the growing biomass demand while at the same time promote environmental protection and sustainable land management, thus providing a possible strategy

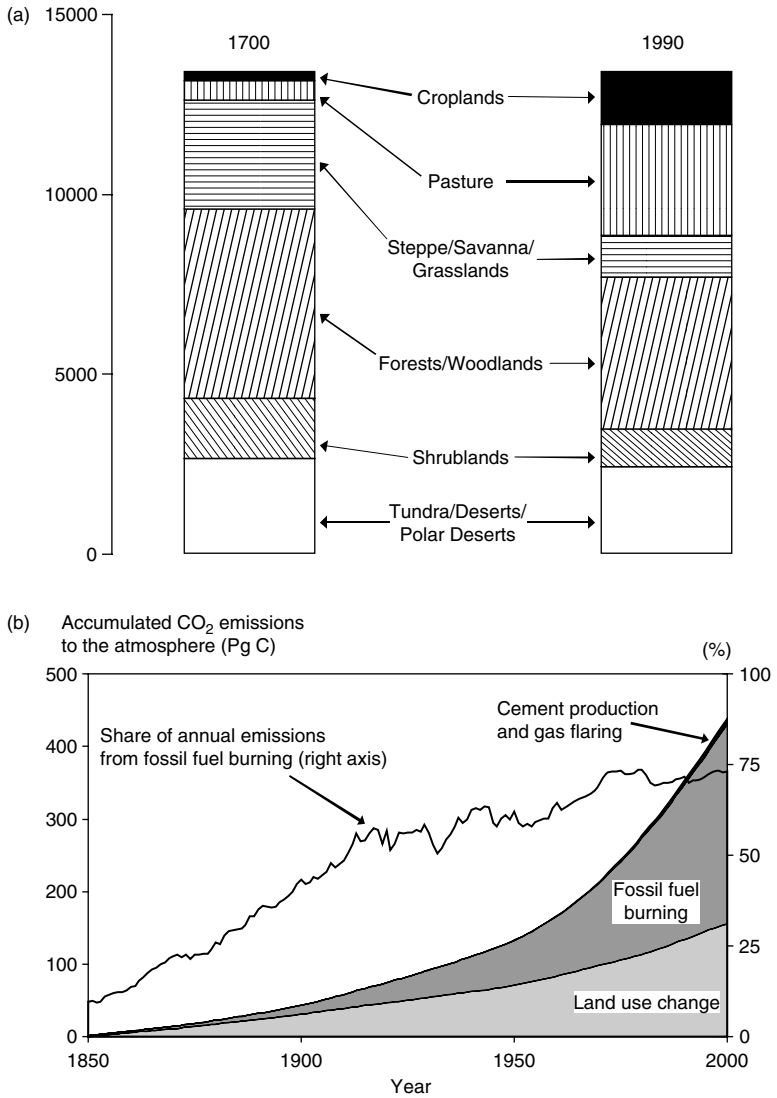

Figure 1.1 *Selected indicators of human influence on the Earth system in the past. Figure 1.1a outlines the land transformation during the past 300 years (units: million hectares). Note that this figure does not capture the far-reaching conversion within each given ecosystem type. For example, the conversion of primary natural forests to secondary production forests has resulted in the elimination of a multitude of critical habitats, leading to negative consequences for the state of biodiversity in forest ecosystems. Figure 1.1b presents the anthropogenic CO_2 emissions to the atmosphere since 1850 (expressed as carbon in CO_2). For many decades fossil fuel burning has been the major source of CO_2 emissions into the atmosphere, presently contributing close to 75% of annual emissions. But more than one-third of the accumulated emissions from 1850 to now have been caused by land use change, primarily conversion of forests to agricultural land. In cement production, fossil CO_2 is released during the calcination process where calcium carbonate is heated to yield lime. CO_2 is also released into the atmosphere when natural gas is 'flared' from petroleum reservoirs*
Source: Based on Klein Goldewijk (2000) and RIVM (2005).

to address concerns about climate change and also many other of the most pressing environmental problems of today.

1.2 Historic and Present Biomass Uses for Food, Energy and Materials in the World

Figure 1.2 presents a quantification of the biomass production for food, energy and materials. Other major product and resource flows are included for comparison. Figure 1.2 provides some insights in relation to the discussion of the prospects for biomass substituting for non-renewable resources in the future.

From Figure 1.2a, it is evident that the quantitative production of fossil resources is much larger than the biomass production in agriculture and forestry, implying that a far-reaching substitution of fossil resources with biomass would require a dramatic increase in the output from agriculture and forestry. Petroleum is to some extent used for the production of plastics and bulk chemicals, some 10–15% of the coal is used in steel production, and fossil gas (and to some extent also other fossil resources) are used for the production of synthetic fertilizers. But it is the use of fossil fuels in the energy sector that is the main source of society's exploitation of fossil resources. Clearly, the decoupling of societal energy use from biological productivity, that took place more than 100 years ago, has now brought us to energy consumption levels that make it difficult to return to a situation where the global society relies solely on biomass for energy.

The situation is different when looking at materials that are presently primarily produced based on petroleum and fossil gas, e.g., plastics, rubber and various bulk chemicals (Figure 1.2b). This production presently uses 5–10% of total annual petroleum and gas production and is small compared to the agricultural output: compare, for instance, the present global production of cereals (the major crop type in agriculture) with the plastics production in the world as presented in Figure 1.2b. It is also evident from Figure 1.2b that crop production for non-food/feed uses presently occupies a very small part of agricultural land use: the major part of society's biomass production for material purposes takes place in forestry. However, as will be shown below, agriculture can play a major future role as supplier of renewable feedstocks to industry, substituting non-renewable fossil resources, both by expanding dedicated production of non-food crops and by utilizing organic waste and residues.

The forest sector generates large amounts of biomass residues, both in the forests and at industrial sites such as sawmills and pulp/paper plants. Over the years, the forest industry has improved the wood utilization efficiency by cascading residue flows to energetic or lower value material uses. But the potential for increased residue utilization in forestry is large: increased wood extraction in connection to thinning operations and final logging may yield substantial increases in biomass output. The prospect for increased stemwood extraction by extending and/or intensifying conventional forestry operations is an issue where standpoints diverge, depending on different views regarding environmental, technical, legal and economic restrictions (Nilsson, 1996). The discussion below will focus on the agricultural sector. But several of the issues treated (e.g., the economics of biomass under an ambitious climate policy regime) are relevant also for the forest sector.

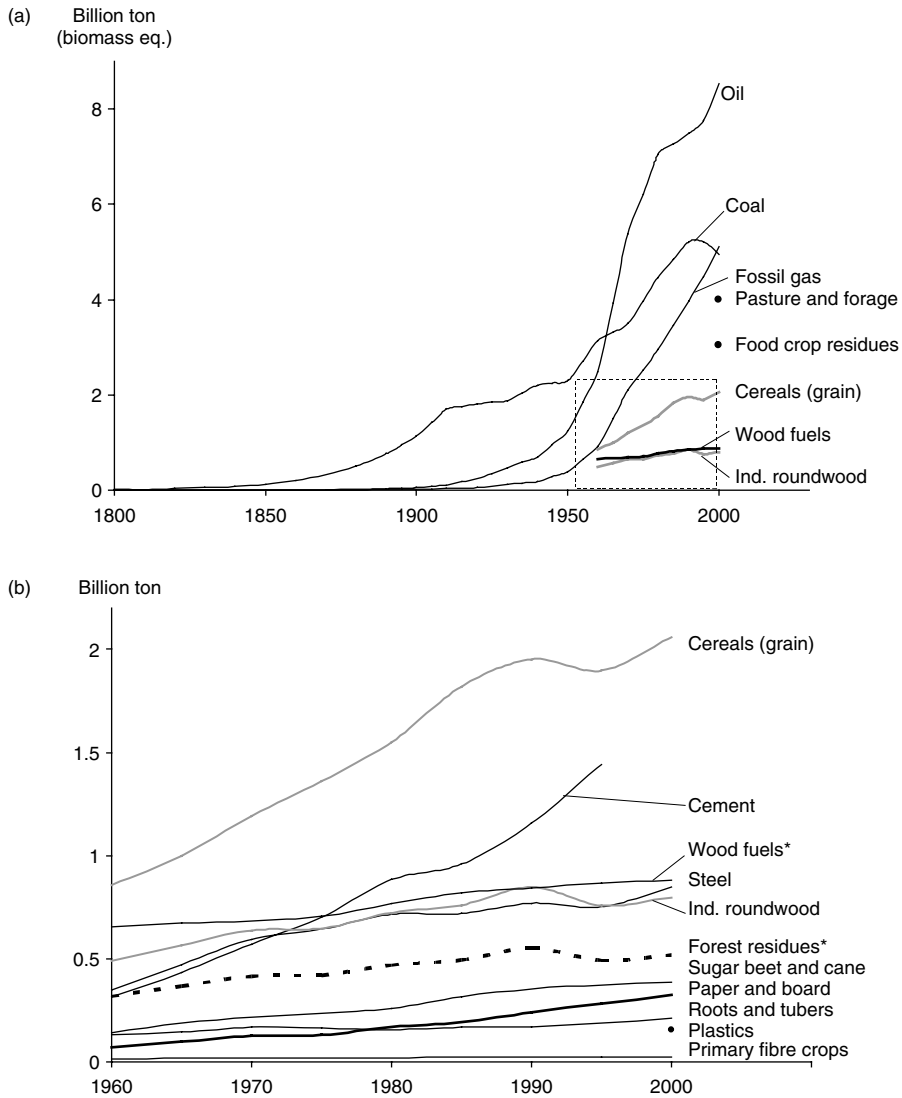

Figure 1.2 *Global annual production of major biomass types in agriculture and forestry, and of selected major products and basic resources. The fossil resources are given on a ton biomass equivalent basis (tbe) in order to facilitate a comparison with the different biomass types (conversion based on 1 ton oil equivalent 42 GJ; 1 tbe = 18 GJ). Figure 1.2b is a scaled-up segment of Figure 1.2a, including additional products. Only data for the year 2000 are presented for the three categories 'Pasture and forage', 'Food crop residues', and 'Plastics' due to lack of time series data*

Note: * 'Pasture and forage' refers to the part eaten by grazing animals. 'Forest residues' is indicative of forest biomass availability linked to industrial roundwood production, based on characteristics given in Johansson *et al*. (1993). 'Wood fuels' (FAO data) does not include all biomass uses for energy. For example, the FAO 'Wood fuels' data for year 2000 corresponds to about 15 EJ, while the global biomass use for energy is estimated at about 35–55 EJ per year (Turkenburg, 2000).

Source: Based on Marland *et al*. (2003), FAOSTAT (2005) and RIVM (2005).

1.3 Potential Availability of Agricultural Residues and Land for Non-Food Crop Production

The total food system appropriation of biological productivity is many times larger than what is finally used by humans. Wirsenius (2003a) estimated the global appropriation of terrestrial plant biomass production by the food system to be some 13 Pg (dry matter) per year in 1992–1994. Of this, about 8% ended up in food commodities eaten. Animal food systems accounted for roughly two-thirds of the total appropriation of plant biomass, whereas their contribution to the human diet was about 13% (gross energy basis). The ruminant meat systems were found to have a far greater influence than any other subsystem on the food system's biomass metabolism, primarily because of the lower feed-conversion efficiency of those systems. Based on this notion, one suspects that: (i) there are potentially major industrial (and energy) feedstocks to be found in the large pool of appropriated biomass not ending up as food; and (ii) there is scope for mitigating the long-term land use demand in the food sector by increases in efficiency (including dietary preferences). Both options are attractive in that they offer opportunities for increasing the use of biomass in industry, and in the energy sector, without imposing further conversion of natural land to agricultural uses.

In order to gain a better understanding of these opportunities, a mass and energy balanced model of the global food system was used to assess how the global biomass potential is influenced by different development paths in the food and agriculture system (Wirsenius, 2003a, 2003b; Wirsenius *et al*., 2004). The starting point for the analysis was the recent projections of global agriculture up to 2030 made by the Food and Agriculture Organization of the United Nations (FAO) (Bruinsma, 2003). In addition to the 'Reference' scenario, depicting the FAO projection, three explorative scenarios were developed: 'Increased livestock productivity' (IP); 'Ruminant meat substitution' (RS); and 'More vegetarian food and less food wastage' (VE).

The results from the scenarios indicate that if the projections made by the FAO come true, the prospects for non-food crop production will be less favourable. In the scenario depicting the FAO projection, it is estimated that total agricultural land area globally will expand from current 5.1 billion hectares to approximately 5.4 billion hectares in 2030 (Figure 1.3). This means that a major expansion of non-food crops would require even further conversion of natural to cultivated land. However, as shown in scenario IP, if livestock productivity increases faster than projected by the FAO, global land requirement for food may actually decrease to 2030. Furthermore, as shown in scenario RS and VE, if the higher livestock productivity is combined with changes in diets (a 20% substitution of ruminant meat with pig/poultry meat) and reduced food wastage, global agricultural land demand may decrease to 4.2–4.4 billion hectares (Figure 1.3). If the surplus agricultural land was targeted for non-food crop cultivation, a considerable amount of biomass could be produced without claiming land beyond what has already been appropriated.

In the IP, RS and VE scenarios, also the amount of food-system residues and by-products available for non-food purposes will be higher than in the FAO projection (Figure 1.4), mainly due to a lower use of crop residues as feed in those scenarios. In, e.g., the European regions, agricultural land demand decreases also in the Reference scenario, due to decreasing population (-8% from 1998 to 2030) and continuing rises in crop and livestock productivity. This is in contrast with the developing regions, where population growth

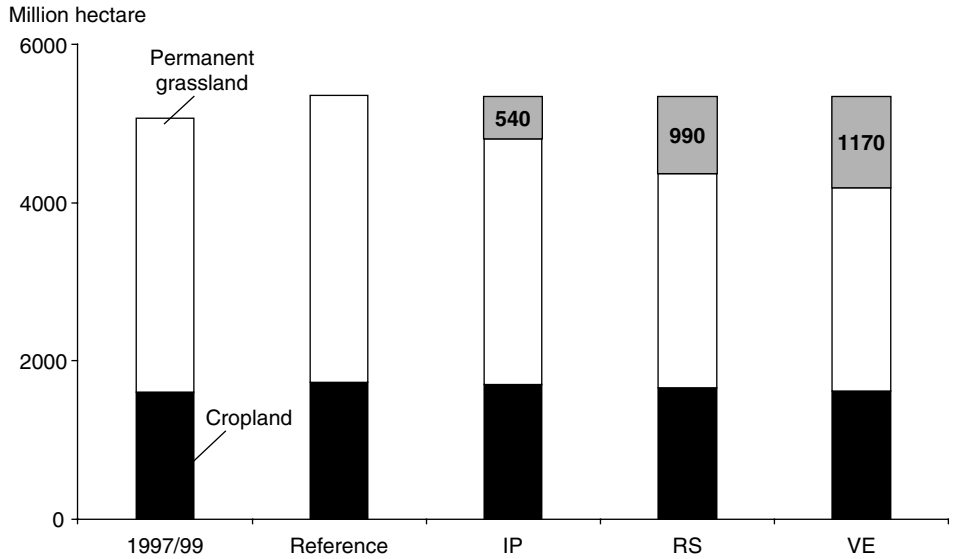

Figure 1.3 *Present and estimated future global extent of agricultural land in the scenarios. The Reference scenario depicts the FAO projection. Alternative scenarios: IP = increased livestock productivity; RS = ruminant meat substitution; and VE = more vegetarian food and less food wastage. The shaded topmost part of each alternative scenario column indicates the difference in land requirements for food production between the Reference scenario and the alternative scenario.*
Source: Based on Wirsenius *et al*. (2004). Reproduced by permission of ETA-Florence/WIP-Munich.

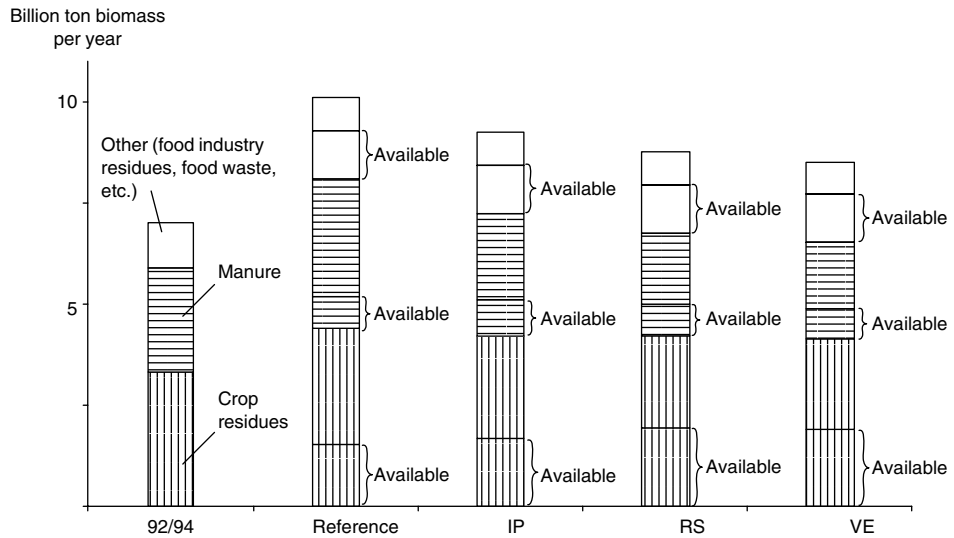

Figure 1.4 *Estimated production of by-products and residues in the global food system. The amounts possibly available for use as feedstock for industry or for energy 2030 in the scenarios are indicated*
Source: Based on Wirsenius *et al*. (2004). Reproduced by permission of ETA-Florence/WIP-Munich.

and increasing food consumption per capita add to rising land demand, as in, e.g., Latin America.

The above scenario exercise indicates that biomass from surplus cropland and from food sector residues may indeed play a large role as a renewable feedstock and help reduce the present dependence on non-renewable energy and materials. The scope for establishment of bioenergy plantations on surplus cropland may be considerable: if the food sector development follows a path similar to that in the RS/VE scenarios, a global biomass supply from plantations of the order of 3–6 billion ton per year does not seem to be impossible with regard to the land requirements of food production. Also the potential supply of biomass residues from the food system is impressive, being of the order of 3–4 billion ton per year. However, it is also clear that food sector development – and especially dietary preferences and the development of animal production efficiency – strongly influence the potential.

It is not axiomatic that the use of biomass resources is environmentally superior to the use of non-renewable resources. Both the dedicated production of feedstock crops and the collection of residues can lead to undesired environmental impacts and it is crucial that practices are found that ensure that reduction of one environmental impact does not increase another. However, if guided in sound directions, a growing biomass demand may be instrumental in promoting sustainable land management. This will be discussed further in a later section, where it will be described how biomass plantations can be located, designed and managed so as to generate environmental benefits in addition to those associated with the substitution of nonrenewable fuels or industrial feedstocks.

1.4 Drivers Behind Increasing Demand for Biomass for Energy and Materials

There are several factors behind today's interest in biomass as industrial feedstock and for the production of fuels and electricity. One early driver was the need to reduce food crop surpluses and find productive use of agricultural land in industrialized countries experiencing overproduction of food. Also, concern about high energy prices connected to the 1970s' oil crisis spurred an interest in the use of domestic energy sources to reduce dependence on foreign oil. At the same time, the insight that the industrial practices and consumption patterns of the western world seriously damage the environment stimulated a search for recyclable, biodegradable and less toxic materials. In this context, biomass was seen as a potentially important domestic, renewable resource, with the potential to meet the demand for more environmentally benign feedstocks in industry as well as for the production of fuels and electricity.

However, today's interest in biomass as a raw material for industry is not without precedents. For example, the farm chemurgy movement in the United States promoted the use of farm crops as industrial feedstocks more than half a century ago, partly due to similar concerns (Finlay, 2004). The difference is that today technology development has put us in a situation where industry can produce biofuels and bioproducts with a quality that satisfy a high consumer demand. Similar to when humans learned to use fossil feedstocks to create advanced synthetic materials with unique properties, the conversion of biomass to fuels and bioproducts continuously develops into increasingly sophisticated processes.

Modern biotechnology, material science, agricultural and process engineering today allow for a number of biobased products such as biodegradable plastics, oleochemicals, biocomposites, bulk chemicals, and biofuels.

The use of bioenergy for the production of heat and electricity has successfully increased in countries like Finland and Sweden. As the utilization has increased, the techniques and technologies to collect, transform and transport biomass have improved so as to reduce costs. Due to such developments the potential bioenergy resources have appeared to increase and there are optimistic scenarios suggesting that biofuels could also be used to replace significant parts of the fossil fuels used for transport. Stimulated by directives and regulations, first-generation liquid biofuels, such as ethanol and biodiesel based on traditional starch, sugar and oil crops, penetrate markets in, e.g., the European Union. Second-generation liquid biofuels, such as Fischer Tropsch fuels, Dimethyl Ether, lignocellulose-based ethanol and hydrogen based on gasification of biomass, are envisioned to become increasingly competitive to their fossil alternatives as technologies develop and allow production based on more abundant and potentially much cheaper lignocellulosic feedstocks.

Thus, technology development in processing biomass to fuels and materials can be expected to make possible a wide range of options for the substitution of non-renewable resources. This includes the continuation, and expansion, of 'traditional' practices such as the use of vegetable oils for lubricants and coatings, and of wood for buildings, and also new uses of established crops, such as natural fibres replacing glass fibre in composites. But it is the substitution of non-renewable (fossil) resources in the energy sector that poses the greatest challenge from the perspective of renewable resources availability (Figure 1.2). Environmental scarcities (i.e., limitations of the capacity of the ecosphere to assimilate societal emissions to air and water) rather than fossil resources scarcity determine the required extent and rate of this substitution, and the concern about human-induced climate change is possibly the most important driver for change.

Radical change of the global energy system is required if we are to reach stringent climate targets. This is a daunting challenge. For example, governments, several scientists, and environmental organizations have argued in favour of an upper limit on the increase in the global annual average surface temperature set at or around 2 °C above pre-industrial temperature levels. Such a target may require that atmospheric CO_2 concentrations are kept below 400 ppm (Azar and Rodhe, 1997), implying that total global CO_2 emissions by the year 2100 would have to drop to around 2 billion ton carbon (C) per year. Assuming a global population of 10 billion people in 2100, global average per capita emissions would then have to drop to about 0.2 ton C per capita and year by 2100. This is below the level that prevails in India today. In fact, even if a less ambitions climate target is chosen, the total global emissions would eventually have to drop to levels below 2 billion ton C per year also for these higher concentration targets (Houghton *et al*., 2001).

At the same time, global energy consumption is expected to more than double during the twenty-first century. This means that the requirements of CO_2 neutral energy may have to grow to levels several times the present global total fossil fuel use, if we are to avoid venturing into a future with a doubled, tripled or even quadrupled pre-industrial atmospheric CO_2 level.

Surveys of possible future energy sources come up with several candidates capable of supplying large amounts of CO_2-neutral energy, including solar and wind energy, bioenergy,

nuclear fission and fusion, and fossil fuels with carbon capture and sequestration (Hoffert *et al*., 2002). But bioenergy ranks as one of few technological options capable of tackling climate change already today: being a low cost renewable fuel already competitive on some markets, and near penetration into new applications as policies, markets and related technologies develop. Advanced technologies, such as nuclear fusion, may eventually satisfy safety requirements and offer abundant energy supplies, but a prudent strategy for tackling the challenge of climate change cannot rely on those to aid CO_2 stabilization during the twenty-first century. Rather than awaiting the prospective (30–50 years ahead) realization of potential silver bullet solutions, society, people and companies will have to turn to what is available closer in time – regardless of whether the estimated ultimate long-term contribution of these options correspond to 30 or 300% of the present world energy use.

Since the potential biomass supply is low compared to the required levels of CO_2 neutral energy – almost regardless of whether one is optimistic or pessimistic about the potential biomass supply – more costly CO_2-neutral energy sources will have to enter if low CO_2 targets should be reached. When such energy technologies are in place, they will most likely cost substantially more than bioenergy, and therefore bioenergy will remain very competitive even in the scenario where advanced energy technologies have come to dominate the global energy supply. The more costly carbon-free energy sources can be expected to set the energy price at a level that would lead to higher profits for the bioenergy sector. With these higher profits, farmers would get stronger economic incentives to turn to bioenergy unless food prices rise to the point where profits are as large as in the energy sector. Thus, land and food prices are likely to be pushed upwards. The implications of such a development are discussed further in the next section.

1.5 Land Use Competition

The economics of land use will be different in a world where carbon and CO_2 have a price. The value of the carbon flows that are induced by different land use practices may become similar to the value of the primary product output from the very same practices. The cost of inputs such as nitrogen fertilizers and diesel will increase, but – potentially much more important – the food and forestry sectors will also have to face increasing competition from the energy sector. Food and bioenergy interactions and competition for scarce land and biomass resources have been the subject of several studies (Azar and Berndes, 1999; Azar and Larson, 2000; McCarl and Schneider, 2001; Johansson and Azar, 2003; Sands and Leimbach, 2003). Forest sector concerns about increasing energy sector demand for biomass are expressed in, e.g., Dielen *et al*. (2000) and policies stimulating this development are even argued to induce developments towards less eco-efficient use of forest wood (Van Riet, 2003).

Azar (2005) presents detailed modelling as well as some illustrative calculations of the willingness to pay for biomass in a world striving for low emissions. Based on a survey of future energy technology costs, and that the marginal energy price will be set by advanced technologies such as solar hydrogen, it is shown that farmers could sell biomass for energy at a price that is four to five times the estimated production cost. If such a situation were to materialize, it is estimated that land values might increase by an order of magnitude, and food prices might increase by a factor of two to five.

Figure 1.5 illustrates the same prospect, but for the case of electricity generation under a carbon tax/permit price regime. The fossil options are cheapest at low carbon tax rates, but the economic performance changes with increasing tax rates and at about 40 and 110 €/ton C tax rate, biomass electricity becomes cheaper than coal and fossil gas based electricity respectively. Capture and sequestration of CO_2 from coal combustion (carbon C&S) becomes competitive with conventional coal technologies at around 75 €/ton C, and the same happens for fossil gas at about 135 €/ton C.

Figure 1.5 also illustrates the interesting cost development for biomass-based electricity generation combined with carbon C&S: the cost will drop if the plant owner gets paid for capture and sequestration of the carbon. At a 225 €/ton C carbon tax, biomass-based electricity can be produced at no cost since the revenues from the carbon C&S cover the costs of electricity generation. A plant owner running a biomass-fired power plant would obviously be willing to pay much for the biomass in a situation with such carbon taxes/permit prices. For comparison, the Swedish carbon tax on the transportation sector and on household and district heating is presently about 290 €/ton C.

The socio-economic consequences of higher land values and higher food prices, are complex and there are different views about how a large biomass demand would influence development in agriculture. On the one hand, human demand for conquering more bioproductive lands might lead to the conversion of biodiversity rich ecosystems into monocultural biomass plantations, and poor people might be evicted from their lands. On the other hand, higher land values will stimulate increased land conservation efforts on agricultural land and it might generate income for the rural poor.

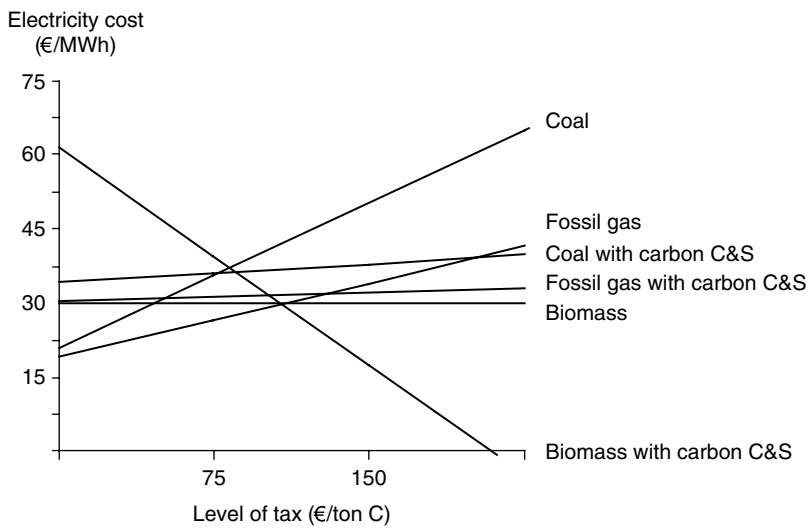

Figure 1.5 *Electricity generation cost for different feedstock and technology options under a carbon tax regime. The term 'carbon C&S' indicates that the CO_2 arising from fuel combustion is captured and sequestered in the ocean or in underground geologic repositories. Addition of carbon C&S leads to increased technology costs but much less sensitivity of electricity cost to carbon taxes. However, the electricity cost increases slowly with rising carbon taxes since not all CO_2 is captured in the C&S operations*
Source: Based on Azar *et al*. (2005), using the exchange rate 1 USD = 0.75 €. Reproduced from *Climatic Change* (in press) 2006, Azar *et al*. with kind permission from Springer Science and Business Media.

Biomass plantations can be established on degraded or otherwise marginal land, where production of food crops is not economically viable. It has been suggested that by targeting such land, farmers could restore soil organic matter and nutrient content, stabilize erosion and improve moisture conditions. In this way an increasing biomass demand could become instrumental in the reclamation of land that has been degraded from earlier over-exploitation and improper management (Hall *et al.*, 1993). However, studies indicate that biomass production on marginal/degraded land may not be the automatic outcome of increasing biomass demand (Johansson and Azar, 2003; Azar and Larson, 2000). If the allocation of land is done by profit-maximizing farmers and forestry companies, prime cropland may be targeted if the higher yields on the better soils outweigh the increased land costs. Biomass plantations may eventually be pushed to marginal/degraded land due to increasing land costs following increased competition for prime cropland, but this competition will likely also be reflected in increasing food commodity prices.

In industrialized countries, this may be less of a problem since food commodity prices only constitute a minor share of retail food prices, and the share of personal consumption expenditure spent on food is moderate. However, in developing countries where food often accounts for a very substantial part of total household consumption, the situation is different. An increase in the prices of staple food crops might cause an increased number of, or a worsened situation for, people chronically hungry and undernourished. Thus, the balance of distributional impacts is difficult to assess. Still, the risk that more people will be affected by hunger must not be disregarded. In a scenario with unequal economic development in the world, a large bioenergy demand with strong paying capacity in industrialized countries may impact food security and food availability in developing countries, creating a moral dilemma in the development of bioenergy strategies.

These potential impacts should not be taken as arguments against policies aimed at reducing CO_2 emissions. Rather, they imply that CO_2 abatement policies cannot be assessed in the absence of distributional considerations and are a clear signal of the importance of global and national efforts to advance development and reduce poverty in the world, especially in developing countries. Synergies and joint action with other multilateral environmental conventions and agreements should be sought, in order to ensure that CO_2 abatement policies do not aggravate the situation in relation to, e.g., food security, water resources and biodiversity.

In the concluding section, one possible strategy for addressing the concerns about climate change and also many other of today's most pressing environmental problems, is briefly presented.

1.6 Multifunctional Biomass Production Systems

Research carried out in Sweden and elsewhere reveals that the environmental benefits from a large-scale expansion of properly located, designed and managed biomass plantations could be substantial, as the negative environmental impacts from current agriculture practices and also municipal waste treatment could be significantly reduced (Berndes *et al.*, 2004; Berndes and Börjesson, 2004; Börjesson and Berndes, 2005; Lewandowski *et al.*, 2004).

Multifunctional biomass production systems can be defined as systems that, besides producing biomass for substitution of fossil resources, also provide additional environmental services. The potential for multifunctional biomass production systems based on Salix (Multifunctional Salix Plantations, MSPs) in Sweden has been assessed and the results are very encouraging: about 15 000 hectares are used for Salix production in Sweden today. An estimated 50 000 hectares could be dedicated to MSP systems providing environmental services having an estimated economic value exceeding the total cost of Salix production. On more than 100 000 hectares, the biomass could be produced in MSPs providing environmental services having an estimated value above, or roughly equal to, half the biomass production cost (Figure 1.6).

Thus, given that additional revenues – corresponding to the economic value of the provided environmental services – can be linked to the MSP systems, the economic performance of such biomass production can improve dramatically. Biomass supply from MSPs could bring substantial improvements in the biomass supply cost and also in other aspects of competitiveness against conventional resources. Establishment and expansion of such plantation systems would also induce development and cost reductions along the whole biomass supply chain. Thus, MSPs could become prime movers and pave the way for an expansion of low cost perennial crop production for the supply of biomass as industrial feedstock and for the production of fuels and electricity.

The production and use of biomass from multifunctional biomass production systems would not only contribute to the development towards more sustainable energy and

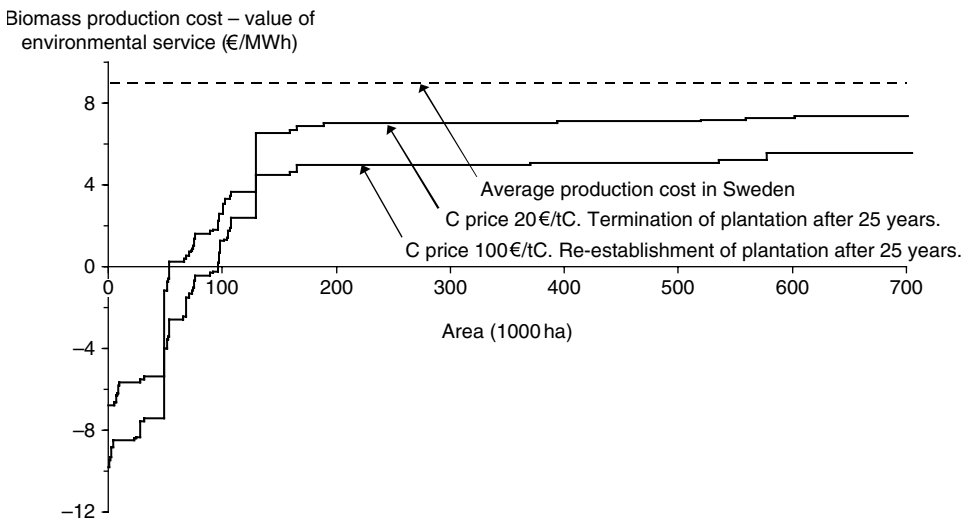

Figure 1.6 *The practical potential for multifunctional bioenergy systems in Sweden, and an illustration of the estimated value of the additional environmental services provided, as they relate to the cost of Salix production. Assessed environmental services include: reduction of nutrient leaching and soil erosion; cadmium removal from agricultural land; increased nutrient recirculation and improved treatment efficiency of nutrient-rich drainage water and pre-treated municipal wastewater and sludge; and provision of habitats and contribution to enhanced biodiversity and game potential*

Source: Based on Berndes and Börjesson (2004). Reproduced by permission of ETA-Florence/WIP-Munich.

industrial production, but also to development towards a more sustainable agriculture and to increased recirculation and efficiency in societal use of essential resources such as phosphorus and other nutrients. This way, multifunctional biomass production systems may become a valuable tool also for meeting additional great challenges such as getting the world's water cleaner and preserving the long-term quality of agricultural soils.

1.7 Summary

The use of biomass as a renewable feedstock in industry, and for the production of fuels, heat and electricity, can help reduce our dependence on non-renewable energy and materials. The question is not whether it is technically possible to supply several billion tons of biomass for energy and industry every year, but rather whether it can be done acceptably from a social and environmental point of view. A key question will be how to make sure that a large-scale expansion of biomass use for energy complies with other urgent environmental objectives, such as reduced erosion and land degradation, reduced eutrophication, good quality groundwater, a rich agricultural landscape, nature conservation and the protection of global biodiversity. These are prerequisites for bioenergy and biomaterials to be regarded as attractive options for the future.

If guided in sound directions, the growing biomass demand can be instrumental in promoting sustainable land management. The case of multifunctional Salix plantations in Sweden points the way for an expanded supply of biomass that should be systematically explored in both industrialized and developing countries. Besides estimating the potential extent and economic value of the environmental services that can be provided, a key issue will be to identify suitable mechanisms to put a premium on the environmental services provided. In some cases, actors can be identified that are willing to pay for a specific environmental service. In other situations, information campaigns and innovative government measures that credit the biomass producer may be required in order to stimulate the establishment of multifunctional biomass production systems. A challenge when implementing such measures lies in the harmonization of the different policies in the energy, environmental and agricultural fields.

Acknowledgements

This chapter builds further on earlier collaboration with Christian Azar and Stefan Wirsenius at Chalmers and Pål Börjesson at Lund University.

References

Azar, C. (2005) Emerging scarcities: Bioenergy-food competition in a carbon constrained world, in Simpson, D., Toman, M. and Ayres, R. (eds) *Scarcity and Growth in the New Millennium*, Resources for the Future Inc./Johns Hopkins University Press, Baltimore, MD.

Azar, C. and Berndes, G. (1999) The implication of CO_2-abatement policies on food prices, in Dragun, A. and Tisdell, C. (eds) *Sustainable Agriculture and Environment: Globalisation and Trade Liberalisation Impacts*, Edward Elgar: Cheltenham.

Azar, C. and Larson, E. D. (2000) Bioenergy and land-use competition in Northeast Brazil, *Energy for Sustainable Development*, **4**, 64–71.

Azar, C., Lindgren, K., Larson, E. D. and Möllersten, K. (2005) Carbon capture and storage from fossil fuels and biomass: Costs and potential role in stabilizing the atmosphere, *Climatic Change*, forthcoming.

Azar, C. and Rodhe, H. (1997) Targets for stabilization of atmospheric CO_2, *Science*, **276**, 1818–1819.

Berndes, G. and Börjesson, P. (2004) Low cost biomass produced in multifunctional plantations – the case of willow production in Sweden, in *2nd World Conference on Biomass for Energy, Industry and Climate Protection*, Rome, Italy, 10–14 May, pp. 289–292.

Berndes, G., Fredriksson, F. and Börjesson, P. (2004) Cadmium accumulation and Salix based phytoextraction on arable land in Sweden, *Agriculture, Ecosystems and Environment*, **103**, 207–223.

Berndes, G., Hoogwijk, M. and van den Broek, R. (2003) The contribution of biomass in the future global energy supply: a review of 17 studies, *Biomass and Bioenergy*, **25**, 1–28.

Börjesson, P. and Berndes, G. (2005) The prospects for willow plantations for wastewater treatment in Sweden, *Biomass and Bioenergy*, in Press.

Bruinsma, J. (ed.) (2003) *World Agriculture: Towards 2015/2030. An FAO Perspective*, Earthscan Publications Ltd, London.

Dielen, L. J. M., Guegan, S., Lacour, P.-A., Mäki, P. K., Stolp, J. A. N. and Rytkönen, A. (2000) *EU Energy Policy Impacts on the Forest-Based Industry, Part 1, Modelling Analysis of the Influence of the EC White Paper on Renewable Energy Sources on the Wood Supply to the European Forest-Based Industries*. Stichting Probos, Wageningen, The Netherlands.

FAOSTAT, *Statistical database of the FAO*, Food and Agriculture Organization of the United Nations, Rome, Italy. Available at: www.faostat.fao.org/Accessed January 2005.

Finlay, M. R. (2004) Old efforts at new uses: a brief history of Chemurgy and the American search for biobased materials, *Journal of Industrial Ecology*, **7**, 33–46.

Groombridge, B. and Jenkins, M. D. (2002) *World Atlas of Biodiversity: Earth's Living Resources in the 21st Century*, University of California Press, Berkeley, CA.

Hall, D. O., Rosillo-Calle, F., Williams, R. H. and Woods, J. (1993) Biomass for energy: supply prospects, in Johansson, T. B., Kelly, H., Reddy, A. K. N. and Williams, R. H. (eds), *Renewable Energy: Sources for Fuels and Electricity*, Island Press, Washington, DC, pp. 593–651.

Hoffert, M. I., Caldeira, K., Benford, G., Criswell, D. R., Green, C., Herzog, H., Jain, A. K., Kheshgi, H. S., Lackner, K. S., Lewis, J. S., Lightfoot, H. D., Manheimer, W., Mankins, J. C., Mauel, M. E., Perkins, L. J., Schlesinger, M. E., Volk, T. and Wigley, T. M. L. (2002) Advanced technology paths to global climate stability: energy for a greenhouse planet, *Science*, **298**, 981–987.

Hoogwijk, M., Faaij, A., van den Broek, R., Berndes, G., Gielen, D. and Turkenburg, W. (2003) Exploration of the ranges of the global potential of biomass for energy, *Biomass and Bioenergy*, **25**, 119–133.

Houghton, J. T., Ding, Y., Griggs, D. J., Noguer, M., van der Linden, P. J. and Xiaosu, D. (eds) (2001) *Climate Change 2001: The Scientific Basis. Contribution of Working Group I to the Third Assessment Report of the Intergovernmental Panel on Climate Change*, Cambridge University Press, Cambridge.

Johansson, D. and Azar, C. (2003) Analysis of land competition between food and bioenergy, *World Resources Review*, **15**, 165–175.

Johansson, T. B., Kelly, H., Reddy, A. K. N., Williams, R. H. and Burnham, L. (eds) (1993) *Renewable Energy: Sources for Fuels and Electricity*, Island Press, Washington, DC.

Klein Goldewijk, K. (2000) Estimating global land use change over the past 300 years: the HYDE database, *Global Biogeochemical Cycles*, **15**, 417–434.

Lewandowski, I., Londo, M., Schmidt, U. and Faaij, A. (2004) Biomass production in multiple land use systems: categorization of feasible land use functions and their quantification by the example of phytoremediation, paper at World Conference and Technology Exhibition on Biomass for Energy, Industry and Climate Protection, Rome, Italy.

Marland, G., Boden, T. A. and Andres, R. J. (2003) Global, regional, and national CO_2 emissions, in *Trends: A Compendium of Data on Global Change*, Carbon Dioxide Information Analysis Center, Oak Ridge National Laboratory, US Department of Energy, Oak Ridge, TN, USA.

McCarl, B. A. and Schneider, U. A. (2001) Greenhouse gas mitigation in US agriculture and forestry, *Science*, **294**, 2481–2482.

Nilsson, S. (1996) *Do We Have Enough Forests*? International Union of Forestry Research Organisations (IUFRO), Vienna.

Oldeman, L. R., Hakkeling, R. T. A. and Sombroek, W. G. (1991) *World Map of the Status of Human-Induced Soil Degradation: An Explanatory Note, October 1991*, 2nd revised edition. International Soil Reference and Information Centre (ISRIC)/United Nations Environment Programme (UNEP), Wageningen, The Netherlands.

Ponting, C. (1992) *A Green History of the World: The Environment and the Collapse of Great Civilizations*, St. Martin's Press, New York.

RIVM, History Database of the Global Environment – HYDE, National Institute of Public Health and the Environment, Bilthoven, the Netherlands. Available at: http://arch.rivm.nl/env/int/hyde/. Accessed January 2005.

Sands, R. D. and Leimbach, M. (2003) Modeling agriculture and land use in an integrated assessment framework, *Climatic Change*, **56**, 185–210.

Smil, V. (2001) *Enriching the Earth: Fritz Haber, Carl Bosch, and the Transformation of World Food Production*, MIT Press, Cambridge, MA.

Turkenburg, W. C. (2000) Renewable energy technologies, in Goldemberg, J. (ed.), *World Energy Assessment* UNDP/UN-DESA/WEC, New York.

Turner II, B. L., Clark, W. C., Kates, R. W., Richards, J. F., Mathews, J. T. and Meyer, W. B. (eds) (1990) *The Earth as Transformed by Human Action: Global and Regional Changes in the Biosphere over the Past 300 Years*, Cambridge University Press, Cambridge.

Van Riet, C. (2003) Impacts of the EU energy policy on the woodworking industries: the sound use of wood from an industries perspective, in *Strategies for the Sound Use of Wood*, Poiana Brasov, Romania.

Wirsenius, S. (2003a) The biomass metabolism of the food system: a model-based survey of the global and regional turnover of food biomass, *Journal of Industrial Ecology*, **7**, 47–80.

Wirsenius, S. (2003b) Efficiencies and biomass appropriation of food commodities on global and regional levels, *Agricultural Systems*, **77**, 219–255.

Wirsenius, S., Azar, C. and Berndes, G. (2004) Global bioenergy potentials: a new approach using a model-based assessment of biomass flows and land demand in the food and agriculture sector 2030, in *2nd World Conference on Biomass for Energy, Industry and Climate Protection*, Rome, Italy, pp. 471–474.

CHAPTER 4

PHYSICAL DATA AND HEAT AND MASS TRANSFER

GENNADI PALCHONOK, HENRIK THUNMAN

Basically, the process of solid fuel combustion can be considered as sum of elementary interactions between single fuel particles and a combustion gas. Often, the larger scale of a combustion system, the smaller size of fuel particles used:

~ 100-μm sized particles burn in dilute gas-solid suspension in Pulverised Combustors (PC) of thermal capacity ranging from 100 to 1000 MW;

~ 10-mm sized particles (chips, pellets) burn in a fixed (Grate Combustors) or fluidised bed (Bubbling or Circulating Fluidised Bed Boilers) of tens to hundreds MW thermal capacity;

~ 0.1 – 1-m sized wood logs and briquettes in small-scale home stoves and fires of 10-kW capacity range (recently, combustors for 10-mm sized pellets became available).

In general, solid fuels consist of a combustible organic part and a non- combustible mineral part (ash) and contain some moisture – free water in pores and bound moisture adsorbed on solid surfaces. Once the particle surface has reached the evaporation temperature, T_m, drying begins. Under typical combustion conditions and high moisture content in a fuel (> 30

mass % on dry basis) T_m is close to the boiling temperature of free water (100°C at 1 bar) and slightly higher for bound moisture. The organic part, when heated up above ≈ 200°C, thermally decomposes on gaseous products (carbon oxides, water vapour and light and heavy hydrocarbons) and solid char residue (mostly fixed carbon). This process is called pyrolysis (strictly, under reducing conditions) or devolatilisation (under oxidising conditions). The products of thermal decomposition are gases (CO_2, CO, H_2O, H_2, light and heavy hydrocarbons, condensable tars) and solid char residue (fixed carbon and ash).

Introduced in a hot furnace surrounding, a fuel particle first undergoes *external heat transfer* from the surrounding to the particle surface coupled with *internal transfer of heat* inside the particle. This causes a chain of more or less sequential physical and chemical transformations of the particle – heating, drying, devolatilisation and char conversion (*combustion* in the presence of oxygen or *gasification* in atmosphere of CO_2 and/or H_2O). In parallel to heat transfer, there is an external and intraparticle mass transfer of oxygen to the surface and into the particle pores and of products of conversion out from the particle. Outflow of the products reduces convective heat and mass transfer to the particle.

In general, the above conversion stages can overlap in time and space (Fig. 4.1), and their mechanisms strongly depend on the physical properties of the particle (size, density, thermal conductivity, specific heat, effective gas diffusivity, porosity, porous structure, etc.) and on the characteristics of heat and mass transfer.

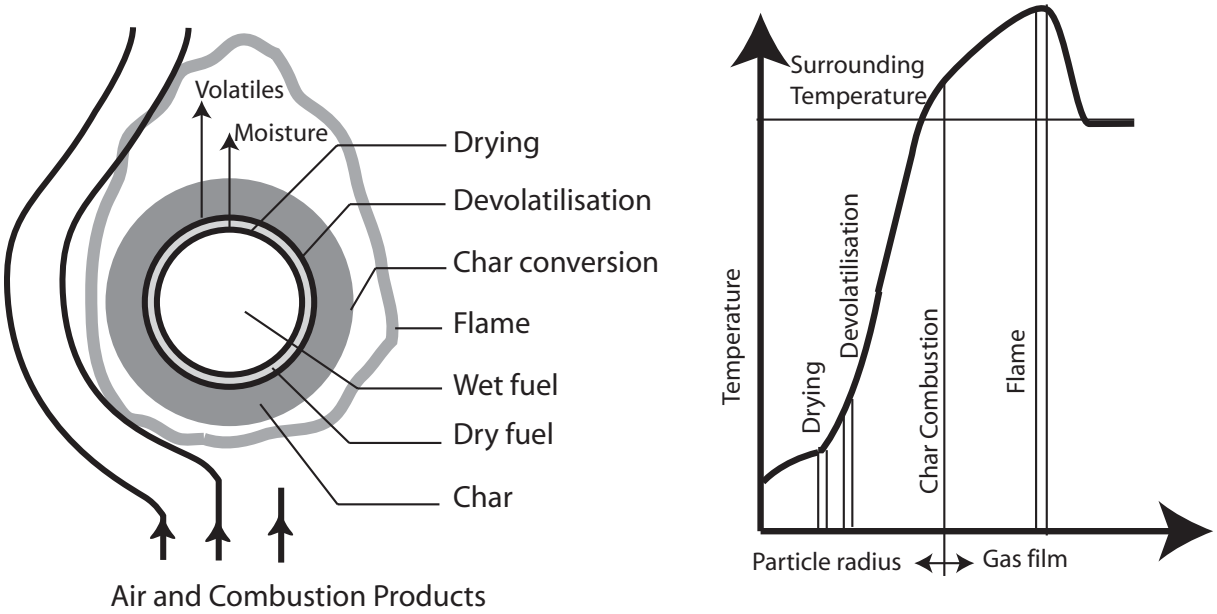

Figure 4.1
Cross-section of a large reacting fuel particle (left) and the corresponding temperature distribution (right)

INTERNAL AND EXTERNAL HEAT AND MASS TRANSFER

Thermochemical conversion of a biomass particle is basically described by partial differential equations of energy conservation

$$\frac{\partial}{\partial t}(\rho_s c_{ps} T) = r^{-n} \frac{\partial}{\partial r}\left[r^n k_{c,eff} \frac{\partial T}{\partial r} - r^n u_g \rho_g c_{pg} T \right] + H\dot{m}''' \tag{4.1}$$

and conservation of a gas species i,

$$\frac{\partial}{\partial t}(v_g \rho_g Y_i) = r^{-n} \frac{\partial}{\partial r}\left[r^n D_{eff} \rho_g \frac{\partial Y_i}{\partial r} - r^n u_g \rho_g Y_i \right] + \dot{m}_i''' \tag{4.2}$$

where $n = 2$ for a sphere, 1 for an infinite cylinder and 0 for an infinite slab, T is temperature, and Y_i is a mass fraction of the species considered.

To obtain unique solutions of Eqs (4.1) and (4.2), initial conditions are added, e.g. values of T (ambient) and Y_i (zero) at time $t = 0$, and the respective boundary conditions:

- symmetry at the centre of the particle, $r = 0$,

$$\left.\frac{\partial T}{\partial r}\right|_{r=0} = \left.\frac{\partial Y_i}{\partial r}\right|_{r=0} = 0 \tag{4.3}$$

- the "convective" boundary condition at the surface of the particle, $r = r_0$, reflecting continuity of the heat or mass flux from the surroundings to the surface and from the surface into the particle

$$-k_{c,eff}\left.\frac{\partial T}{\partial r}\right|_{r_0} = h_{eff}\left(T_{r_0} - T_\infty\right) \tag{4.4}$$

$$-D_{i,eff}\left.\frac{\partial Y_i}{\partial r}\right|_{r_0} = h_m\left(Y_{i,r_0} - Y_{i,\infty}\right) \tag{4.5}$$

Equations (4.1) and (4.2) are similar in structure. The left hand side (LHS) term corresponds to energy or mass accumulation, the first term on the right hand side (RHS) describes molecular (the first terms in square brackets) and convective heat or mass transfer with gas products of evaporation and pyrolysis, flowing out with the superficial velocity u_g (the second terms in square brackets), and the last term is source of heat or mass resulting from physico-chemical transformation of the particle (evaporation, pyrolysis and chemical reactions of fixed carbon with the pyrolysis products and oxygen supplied from ouside). All the terms in Eq (4.1) have dimensions of W/m^3 or J/(m^{3}s) and in Eq (4.2) kg/(m^{3}s).

Equations (4.1) and (4.2) imply that molecular transfer of heat and mass within the particle is described, respectively, by the Fourier law

$$q = -k_c \frac{\partial T}{\partial r} \text{ [W/m}^2 \text{ or J/(m}^2\text{s)]} \tag{4.6}$$

and by the Fick law (for simplicity, shown for binary gas mixture of gases i and j at low gradients of temperature and pressure),

$$j_i = -\rho_g D_{ij} \frac{\partial Y_i}{\partial r} \text{ [kg/(m}^2\text{s)]} \tag{4.7}$$

representing the phenomenological fact that molecular flux of heat or mass is proportional to the gradient of temperature or concentration and oppositely directed. The coefficients of proportionality are (effective) thermal conductivity k_c [W/(m s)] and diffusion coefficient (molecular diffusivity) D_{ij} [m^2/s]. For such a complicated porous structure as wood, effective thermal conductivity and diffusivity are used in Eqs (4.1) and (4.2), implying that the particle is considered as a continuum with effective properties.

In case of significant gradients of temperature and/or pressure within the particle, an extended form of the Fick law is used,

$$j_i = -\rho_g \left(D_{ij} \frac{\partial Y_i}{\partial r} + \frac{D_T}{T} \frac{\partial T}{\partial r} + \frac{D_p}{p} \frac{\partial p}{\partial r} \right) \qquad (4.7')$$

where the second and the third terms in brackets describe the effects of thermal diffusion (the Sorret effect) and barodiffusion. Usually, $D_T/D_{ij} \sim 0.1$ and $D_p/D_{ij} = Y_i Y_j (M_i - M_j)/\overline{M}$ for binary mixture of gases i and j with molar masses M_i and M_j, respectively, with $\overline{M}$ being the mean molar mass, $\overline{M} = \sum_k (X_k M_k) = 1/\sum_k (Y_k / M_k)$.

The LHS term of the boundary conditions (4.4) and (4.5) represents respectively the laws of Fourier and Fick for internal heat and mass transfer. The RHS term is the Newton law for external heat and mass transfer.

$$q = h_c (T_{r_0} - T_\infty) \qquad (4.8)$$

$$j_i = \rho_g h_m \left(Y_{i,r_0} - Y_{i,\infty} \right) \qquad (4.9)$$

The proportionality coefficients in Eqs (4.8) and (4.9) are the convective heat transfer coefficient h_c [W/(m^{2}s)] and its mass transfer analogue, the mass transfer coefficient, h_m [m/s].

The boundary layer is a zone adjacent to the surface, wherein a great deal of disturbances, caused by the presence of the particle in the gas, takes place. Due to the fact, that gas "sticks" to the particle surface, the momentum, heat and mass transfer within the boundary layer is essentially of molecular (conductive) character, and the Fourier and Fick laws are applicable as a first approximation. For a gas flow along a flat surface (Fig. 4.2), the heat flux in the gas normal to the surface reads (discretisation of the temperature gradient in finite differences is applied)

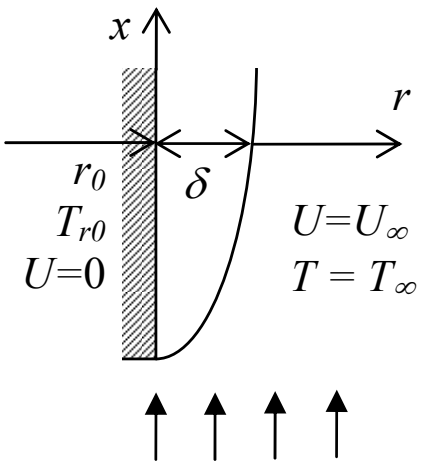

Figure 4.2
The boundary layer on a vertical surface

$$-k_{c,g}\left.\frac{\partial T}{\partial r}\right|_{r_0} \approx \frac{k_{c,g}\left(T_{r_0}-T_\infty\right)}{\delta} = h_c\left(T_{r_0}-T_\infty\right) \tag{4.10}$$

δ is the boundary layer thickness, which decreases with the rise of the gas velocity, rises along the surface and depends on the physical properties of the gas. Analogically, the background of the mass transfer coefficient can be illustrated.

Strictly, the Newton law holds only under steady-state conditions, because the heat and mass transfer coefficients vary along the surface and change with the surface temperature, Luikov (1968). However, the boundary conditions (4.4) and (4.5) are usually applied to transient problems as a reasonable approximation, with h_c and h_m assumed to be constant (averaged) over the surface and independent on its temperature. Furthermore, the Newton law describes the convective heat transfer, whereas in hot furnace surroundings the fuel particle is also exposed to thermal radiation, Fig. 4.3. This is taken into account by introducing the effective heat transfer coefficient in the boundary condition (4.4)

$$h_{eff} = \left(h_{rad} + h_c\right) \tag{4.11}$$

which includes also the radiative constituent, obtained by linearisation of the Stefan-Boltzmann law for thermal radiation

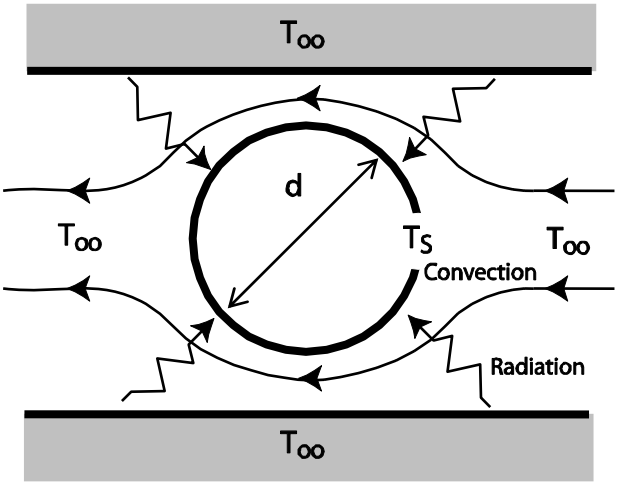

Figure 4.3
A particle with a characteristic diameter *d* exposed to convective and radiative heat transfer

$$h_{rad} = \frac{q_{rad}}{(T_{r_0} - T_\infty)} = \frac{\varepsilon\sigma(T^4_{r_0} - T^4_\infty)}{(T_{r_0} - T_\infty)} = \varepsilon\sigma(T^2_{r_0} + T^2_\infty)(T_{r_0} + T_\infty) \qquad (4.12)$$

Strictly, h_{rad} depends on the particle temperature and optical properties, which makes it applicable only to steady-state conditions. But, often its contribution is small compared to that of h_c, and it is acceptable to use its mean value over the temperature range considered.

Introducing dimensionless parameters, length $\xi = r/r_0$, temperature $\theta = (T - T_\infty)/(T_0 - T_\infty)$, and mass fraction of oxygen $\psi = Y_i / Y_{i,\infty}$, one can represent the boundary conditions (4.4) and (4.5) in non-dimensional form

$$-\left.\frac{\partial\theta}{\partial\xi}\right|_1 = \mathrm{Bi}_t\,\theta \qquad (4.4')$$

$$-\left.\frac{\partial\psi}{\partial\xi}\right|_1 = \mathrm{Bi}_m\,\psi \qquad (4.5')$$

where the thermal and diffusion Biot numbers appear, being the ratios of internal to external resistances to the transfer process

$$\mathrm{Bi}_t \equiv \frac{r_0 h_{eff}}{k_{c,eff}} = \frac{r_0 / k_{c,eff}}{1/h_{eff}} \tag{4.13}$$

$$\mathrm{Bi}_m \equiv \frac{r_0 h_m}{D_{i,eff}} = \frac{r_0 / D_{i,eff}}{1/h_m} \tag{4.14}$$

A large Biot number $\mathrm{Bi}_{t(m)} >> 1$ implies that the internal resistance to the heat (mass) transfer is much higher then the external one. This results in a temperature (species concentration) wave that propagates from the surface of the particle to its centre, determining the overall rate of the conversion. Due to a low external resistance, the surface is at nearly the same temperature (concentration) as that of the surroundings. In such a case the particle is called "thermally (diffusionally)" thick. If the Biot number is instead small, $\mathrm{Bi}_{t(m)} << 1$, there is practically no temperature (concentration) gradient within the "thermally (diffusionally)" thin particle, with the overall conversion rate being controlled by the transport of heat or matter to the surface of the particle.

Introducing similar dimensionless parameters in Eq (4.10) and in an analogous equation for external mass transfer, one obtains very important non-dimensional groups, the Nusselt number (in this case the characteristic length d is used instead of r_0, e.g. $d = 2r_0$)

$$\mathrm{Nu} \equiv \frac{h_c d}{k_{c,g}} \tag{4.15}$$

(note that Nu includes the *convective* heat transfer coefficient) and the Sherwood number

$$\mathrm{Sh} \equiv \frac{h_m d}{D_{ij}} \tag{4.16}$$

The Nusselt and Sherwood numbers are usually evaluated for convective flow from dimensionless semi-empirical correlations of the following type,

$$\mathrm{Nu} = c\,\mathrm{Re}^m\,\mathrm{Pr}^n \tag{4.17}$$

$$\mathrm{Sh} = c\,\mathrm{Re}^{m}\,\mathrm{Sc}^{n} \qquad (4.18)$$

where $\mathrm{Re} \equiv U_\infty d/\nu$ is the Reynolds number, $\nu = \mu_g/\rho_g$ the kinematic viscosity of the gas [m^2/s], μ_g the dynamic viscosity of the gas [Pa·s], $\mathrm{Pr} \equiv \nu/a$ the Prandtl number, $a = k_g/(c_{pg}\cdot\rho_g)$ the thermal gas diffusivity [m^2/s], and $\mathrm{Sc} \equiv \nu/D_{ij}$ the Schmidt number. The factors c, m and n are empirically proven constants (at least, for a certain range of Re-values), depending on the gas flow regime and geometric configurations.

In Eqs (4.17) and (4.18) Re^m represents the effect of the gas velocity on the boundary layer thickness, $\delta \sim \mathrm{Re}^{-(1-m)}$, and the last terms define the thickness ratio between the thermal and fluid dynamic boundary layers (Pr^n), diffusion and fluid dynamic boundary layers (Sc^n), and altogether they describe the effect of the gas properties on the heat and mass transfer coefficients. Bearing in mind the similar structure of Eqs (4.17) and (4.18), one can conclude that at Pr=Sc=1 there is an analogy between the convective transfer of heat and mass. Expressed by Chilton and Colburn (refined Reynolds analogy), the analogy between heat, mass and momentum transfer reads,

$$\mathrm{St}\cdot\mathrm{Pr}^{2/3} = \mathrm{St_m}\cdot\mathrm{Sc}^{2/3} = C_f/2 \qquad (4.19)$$

which implies n=1/3, where $\mathrm{St} \equiv \mathrm{Nu}/(\mathrm{Re}\cdot\mathrm{Pr})$ and $\mathrm{St_m} \equiv \mathrm{Sh}/(\mathrm{Re}\cdot\mathrm{Sh})$ are the Stanton numbers for the heat and mass transfer, respectively, and C_f the friction coefficient. Variations of n between 0.3 and 0.5 in available empirical correlations for gases (Pr ≈ Sc ≈ 0.7) do not affect the result significantly.

The Reynolds number expresses the ratio between inertial forces, dominant in turbulent flows, and viscous forces, dominant in laminar flows. For laminar (viscous) gas flow along a flat surface, as shown in Fig. 4.2, the local heat transfer coefficient at a longitudinal position x is described by Eq (4.17) with $d \equiv x$ and c = 0.33, m = 1/2 and n = 1/3 ($\mathrm{Re_x} < 10^4$). It follows from Eqs (4.17) and (4.18) that at x = 0 $h_c \rightarrow \infty$ and $h_m \rightarrow \infty$ due to the boundary layer thickness δ = 0 (Fig. 4.2). The integral-average heat transfer coefficient over the surface length x_0 ($d \equiv x_0$) is evaluated from the same expression with c = 0.66. Transition to turbulent flow regime ($\mathrm{Re_x} > 6\cdot10^4$) leads to m = 0.8 and c = 0.02. Equations (4.17) and (4.18) also hold for a gas cross-flow past a long horizontal cylinder. The parameters recommended in Russian

Table 4.1. Parameters of Eqns (17) and (18) for a horizontal cylinder, Zukauskas (1982)

Parameter	Re			
	< 40	40 to 100	100 to $2 \cdot 10^5$	> $2 \cdot 10^5$
c	0.76	0.52	0.26	0.023
m	0.4	0.5	0.6	0.8
n	0.37	0.37	0.37	0.40

literature for the surface-average heat and mass transfer are shown in Table 4.1 (characteristic size is the cylinder diameter).

The above configurations and Eqs (4.17), (4.18) are typical for wood chips and cylindrical biomass pellets and briquettes.

Somewhat special is the description of external heat and mass to a sphere, the shape which is often used in three-dimensional practical calculations. There is a theoretical lower limit for the Nusselt and Sherwood numbers at vanishing low gas velocities, motivated by the following analysis.

Consider a spherical particle at ambient temperature surrounded by a slightly hotter stagnant gas (to exclude the effects of natural convection and thermal radiation), Fig. 4.4. Under steady state condition heat transfer through the boundary layer by molecular thermal conduction ($k_{c,g}$ = const.) is governed by the energy equation

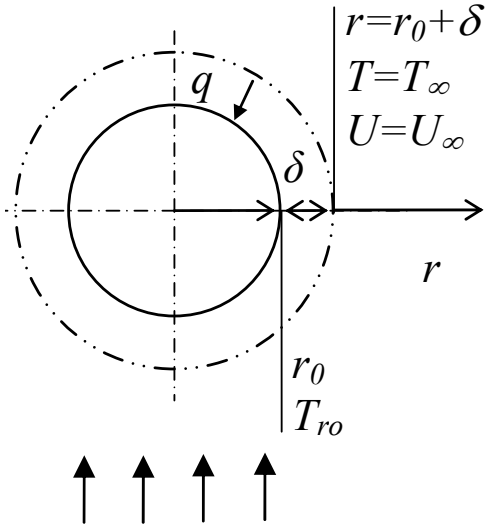

Figure 4.4
Convective heat transfer to a spherical particle

$$\frac{1}{r^2}\frac{d}{dr}\left(r^2\frac{dT}{dr}\right)=0 \tag{4.20}$$

with the boundary conditions on the surface

$$r_1 = r_0,\ T = T_{\mathrm{ro}} \tag{4.21}$$

and on the outer surface of the boundary layer

$$r_2 = r_0 + \delta,\ T = T_\infty \tag{4.22}$$

The first integration of Eq (4.20) from r_1 to r_2 gives

$$\frac{dT}{dr}=\frac{c_1}{r^2} \tag{4.23}$$

and the second one gives the general solution of Eq (4.20)

$$T = c_2 - \frac{c_1}{r} \tag{4.24}$$

The integration constants are evaluated from the boundary conditions,

$$c_1 = \frac{T_\infty - T_{r_0}}{\dfrac{1}{r_0}-\dfrac{1}{r_0+\delta}},\quad c_2 = T_{r_0} + \frac{T_\infty - T_{r_0}}{\dfrac{1}{r_0}-\dfrac{1}{r_0+\delta}}\frac{1}{r_0} \tag{4.25}$$

which, together with Eq (4.24), gives a hyperbolic temperature distribution within the spherical boundary layer.

Applying the Fourier law to Eq (4.23) together with the above value for c_1, one obtains the external heat flux on the surface (r=r_0),

$$q = -k_{c,g}\left.\frac{dT}{dr}\right|_{r_0} = -k_{c,g}\frac{T_\infty - T_{r_0}}{r_0^{\,2}\left(\frac{1}{r_0} - \frac{1}{r_0+\delta}\right)} \tag{4.26}$$

which, on the other hand, can be expressed through the Newton law

$$q = h_c\left(T_{r_0} - T_\infty\right) \tag{4.27}$$

Equating the RHS parts of Eqs (4.26) and (4.27) yields

$$\mathrm{Nu} \equiv \frac{h_c d}{k_{c,g}} = 2 + \frac{d}{\delta} \tag{4.28}$$

From Eq (4.28) the thermal boundary layer thickness becomes (in the analogous expression for the diffusional boundary layer Sh substitutes Nu)

$$\delta = \frac{d}{\mathrm{Nu} - 2} \tag{4.29}$$

In completely stagnant gas ($U_\infty \rightarrow 0$, $\delta \rightarrow \infty$) the sphere Nusselt number trends to its minimum value, following from Eq (4.28),

$$\mathrm{Nu}_{\min} = 2 \tag{4.30}$$

and, by the analogy,

$$\mathrm{Sh}_{\min} = 2 \tag{4.31}$$

In Eq (4.28) the last term on the RHS implicitly accounts for the effect of the gas velocity on the heat transfer coefficient: the higher U_∞ and Re, the thinner δ and the higher h_c. Applying dimensional analysis to this term, similar to that behind the expressions (4.17) and (4.18), one comes to the following expressions for the external heat transfer coefficient

$$\mathrm{Nu}_{mm} = 2 + c\,\mathrm{Re}^m\,\mathrm{Pr}^n \tag{4.32}$$

and, by the analogy, for the mass transfer coefficient

$$\mathrm{Sh} = 2 + c\,\mathrm{Re}^m\,\mathrm{Sc}^n \tag{4.33}$$

The parameters c, m and n have been determined experimentally by Frössling (1937) for Eq (4.33) and Ranz and Marschall (1952) for Eq (4.32). In presently rounded form the coefficients are c = 0.6, m = 1/2 and n = 1/3, Kunii and Levenspiel (1991)

Equations (4.32) and (4.33) also hold in a fixed bed of large spherical particles (Re > 80), with the only different parameter c=1.8 adopted from data of Ranz (1952). Strictly, the values of $\mathrm{Nu}_{\min}$ and $\mathrm{Sh}_{\min}$ should be corrected to account for the presence of neighbour particles, which partly block the heat and mass exchange surface. Often, a product $2v_g$ is used instead of 2, where v_g is a void fraction of the bed.

For evaluation of the convective heat and mass transfer coefficients from Eqs (4.17), (4.18), (4.32) and (4.33), the particle film temperature is used:

$$\overline{T} = (T_{r_0} + T_\infty)/2 \tag{4.34}$$

For a spherical particle suspended in gas, e.g. in a pneumo-conveying flow during pulverised combustion (PC) or in fluidised bed combustion (FBC) of more or less isometric (single-sized) particles, the Reynolds number should include the slip gas velocity U_∞, which can be evaluated from the following expression

$$\mathrm{Re} = \frac{\nu_g^{4.75}\,\mathrm{Ar}}{18 + 0.6\sqrt{\nu_g^{4.75}\,\mathrm{Ar}}} \tag{4.35}$$

where ν_g is a void fraction of the gas-solid suspension (≈ 1 in a PC and ≈ 0.4 in a FBC) and Ar is the Archimedes number

$$\mathrm{Ar} = \frac{gd^3}{\nu^2}\frac{\rho_s - \rho_g}{\rho_g} \tag{4.36}$$

with g being the gravity acceleration and ρ_s the solids density.

In fluidised bed, fuel particles are incorporated in the matrix of chemically inert bed particles (sand, ash). In general, the fuel and inert particles are different in sizes and density. The overall heat transfer coefficient is represented as the additive sum of a particle-convective, a gas-convective and a radiative components. Under such conditions the analogy between heat and mass transfer only holds for the gas-convective constituent. The slip gas velocity U_∞ is evaluated from the Archimedes number of inert particles. The Nusselt and Sherwood numbers are described by rearranged correlations of the type of Eqs (4.32) and (4.33). An example of such correlations is presented in Palchonok (1998) [9] and further adopted in the appendix of Thunman et al. [10].

The convective heat and mass transfer coefficients, defined by Eqs (4.17), (4.18), (4.32) and (4.33) (marked below with index 0), need to be corrected for gases flowing out from the particle with the superficial velocity u_g, see Eqs (4.1) and (4.2). The correction factors can be analytically obtained from a steady state problem of combined diffusive and convective transfer of heat and species across the boundary layer of a sphere, an infinite cylinder and an infinite slab. The corrected heat and mass transfer coefficients h_c and h_m read

$$\frac{h_c}{h_{c0}} = \frac{\rho_g u_g c_p / h_{c0}}{\exp\left(\rho_g u_g c_p / h_{c0}\right) - 1} \tag{4.37}$$

$$\frac{h_m}{h_{m0}} = \frac{u_g / h_{m0}}{\exp\left(u_g / h_{m0}\right) - 1} \tag{4.38}$$

In fluidised bed Eq (4.37) concerns only the gas-convective constituent of the heat transfer coefficient. The correction factor may vary from 0.6 to 1 during drying and devolatilisation depending on the moisture content and volatile release rate, and is about 0.9 for char combustion.

The gas flow inside the particle along a co-ordinate x is caused by the pressure gradient, which is often described by Darcy's law

$$u_g = -\frac{s_g}{\mu_g}\frac{\partial P}{\partial x} \tag{4.39}$$

where the proportionality coefficient is the permeability s_g [m^2] divided by the dynamic viscosity. Due to specifics of wood structure, the permeability as well as the effective gas diffusivity, is direction dependent.

The pressure field is calculated from the gas concentration C by the gas law,

$$P = C\Re T \tag{4.40}$$

where C [mole/m^3] is the molar concentration in the gas filling the void of the porous structure and $\Re$ the gas constant, 8.314 J/mole K.

PHYSICAL PROPERTIES

The combustible part of wood consists of around 50 mass % carbon, 6 mass % hydrogen and 40 mass % oxygen, see Table 4.2. Wood is characterised by a high content of moisture (unless specially pre-treated, e.g. pelletised) and volatile matter. This makes drying and devolatilisation critical stages for the overall combustion process. In densified biofuel (pellets, briquettes) the moisture content is less than 10 wt% as delivered. The ash content is small in both solid and densified wood and somewhat higher in refuse derived fuel (RDF).

Table 4.2. Proximate and elemental analyses of typical biofuels

	Solid wood		Pelletised biofuel		
	pine	birch	wood	paper	RDF
Density, kg/m^3 as delivered	760	970	1200	730	1250
Proximate analyses					
Moisture, mass % as delivered	50	50	8	3	8
Volatile matter, mass % d.b.*	87.6	90.4	78.4	90.5	72.5
Fixed carbon , mass % d.b.	12.3	9.4	20.8	6.1	13.2
Ash, mass % d.b.	0.1	0.2	0.8	3.4	14.3
Ultimate analyses (main elements)					
C, mass % d.a.f.**	46.9	47.1	51.7	53.5	56.0
H, mass % d.a.f.	6.3	6.2	6.3	7.8	8.1
O, mass % d.a.f.	46.7	46.6	41.9	38.5	35.7

* d.b. – dry basis,
** d.a.f. – dry, ash free basis

The structure of stem wood, Fig. 4.5, consists of parallel tube-like fibers (smaller diameters) and vessels (large diameters), with the walls consisting of cellulose and hemicellulose bound together by lignin. Softwood (conifers: pine, fir), which normally is used as fuel, has more regular and uniform structure, than hardwood (birch, ash). Due to such a structure, wood transfer properties with respect to heat, gas and liquid are presumably different in directions parallel to fibers (higher) and perpendicular to fibers (lower). This is referred as *anisotropy* of transfer properties.

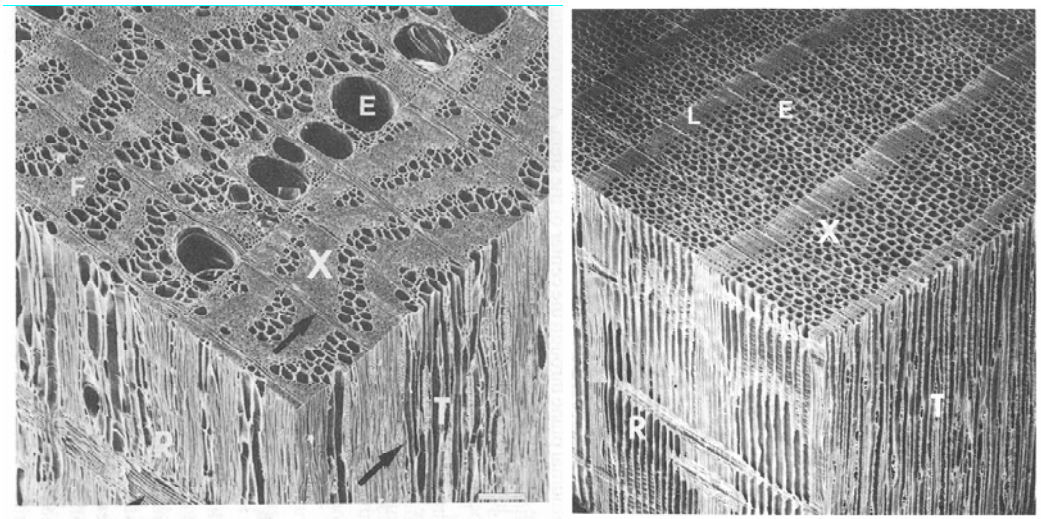

Figure 4.5
Hardwood (left) and softwood (right) structure shown in cross-sectional (X), radial (R) and tangential (T) views

Sometimes wood is ground, dried and compressed (pelletised or briquetted) to improve storage, transportation and combustion efficiency. In this case the small wood grains (~1 mm) are nearly randomly oriented, which results in *isotropic* transfer properties.

The physical data depend on temperature and degree of conversion. The effect of temperature on the solid properties is not as well known as on those of gas. As the conversion progresses, the particle size normally decreases, and so does the particle mass due to gasification of the solid phase. As a result, the particle density, thermal conductivity, gas voidage, and other properties change in a rather complicated way. During the conversion process of a wood particle, its properties change from those of wet wood (as delivered, subscript *0*) through states of dry wood (sub-*df*) and char (sub-*C*) to final properties of ash (sub-*a*). As a reasonable simplification, it can be recommended to use averaged physical data in each conversion stage of the solid phase, assuming a linear relation between two adjacent stages of conversion 1 and 2, expressed as,

$$\begin{aligned}\chi &= Y_m\chi_0 + (Y_v - Y_m)\chi_{df} + (Y_C - Y_v)\chi_C + (1 - Y_C)\chi_a = \\ &= Y_m(\chi_0 - \chi_{df}) + Y_v(\chi_{df} - \chi_C) + Y_C(\chi_C - \chi_a) + \chi_a\end{aligned} \tag{4.41}$$

where χ is the physical property of interest and Y_i is a relative mass fraction of each constituent *i*, (mass of component *i*)/(initial mass of component *i*), moisture, sub-*m*, volatile matter, sub-*v*, char, sub-*C*.

The physical property is averaged over the temperature range between T_1 and T_2

$$\chi = \int_{T_1}^{T_2} \chi[T]\, dT /(T_1 - T_2) \tag{4.42}$$

Reasonable temperature ranges for the moist fuel extend from ambient temperature to boiling temperature. For dry wood the range may be from boiling temperature to mean devolatilisation temperature, for char from devolatilisation temperature to temperature of the surroundings, and for ash the temperature of the surroundings. Properties needed for the boundary conditions can be taken at the temperature of the surroundings. The radiation

emissivity of wood can be assumed to be 0.5 for wet wood, 0.6 for dry wood, and 0.9 for char and ash.

PARTICLE SHRINKAGE

During conversion a biomass particles shrink in size, but more or less retain their shapes, especially pellets. Simultaneously, the particle mass and density, as well as voidage (porosity), change due to release of moisture, volatiles and char. The shrinkage process is described by the following parameters (Fig. 4.6):

- **The shrinkage factor**, (current particle volume, V)/(initial particle volume, V_0)

$$\theta = \frac{V}{V_0} \tag{4.43}$$

Given that the shrinkage is linearly dependent on the release of the each constituent, a current value of the overall shrinkage coefficient, θ, can be calculated as

$$\begin{aligned} \theta &= Y_m + (Y_v - Y_m)\theta_m + (Y_C - Y_v)\theta_v\theta_m + (1 - Y_C)\theta_C\theta_v\theta_m = \\ &= Y_m(1-\theta_m) + Y_v(\theta_m - \theta_v\theta_m) + Y_C(\theta_v\theta_m - \theta_C\theta_v\theta_m) + \theta_C\theta_v\theta_m \end{aligned} \tag{4.44}$$

where Y_i is the relative mass fraction of each constituent, θ_i – volume shrinkage over complete yield of the i-th constituent, i = moisture, sub-m, volatile matter, sub-v, char, sub-C.

- **The relative volume of the solid (condensed) phase** in the particle, $\omega = \frac{V_s}{V_0}$

$$\omega = Y_m\left(\frac{Y_{m0}}{1-Y_{m0}}\frac{\rho_{df}}{\rho_m}\right) + Y_v\left(\frac{Y_{v0}\rho_{df}}{\rho_v}\right) + Y_C\left(\frac{Y_{C0}\rho_{df}}{\rho_C}\right) + Y_a\left(\frac{Y_{a0}\rho_{df}}{\rho_a}\right) \tag{4.45}$$

where index *0* indicates the initial mass fraction of moisture (as recived), and volatiles, fixed carbon and ash (on dry basis) given from the proximate analysis. The indexes to the densities are as follows: *df*, dry fuel, *m* moisture (water), *C* char, *a* ash, and *v* volatile matter, defined as

$$\rho_v = \left(\rho_{df} - Y_{C0}\rho_C - Y_{a0}\rho_a\right)/Y_{v0}$$

- **The relative volume of the gas phase and the void fraction (porosity)**

$$\zeta = \frac{V_0}{V_g} = \frac{V_0}{V - V_s} = \frac{1}{V/V_0 - V_s/V_0} = \frac{1}{\theta - \omega} \tag{4.46}$$

$$v_g = \frac{V_g}{V} = \frac{1}{\zeta\theta} \tag{4.47}$$

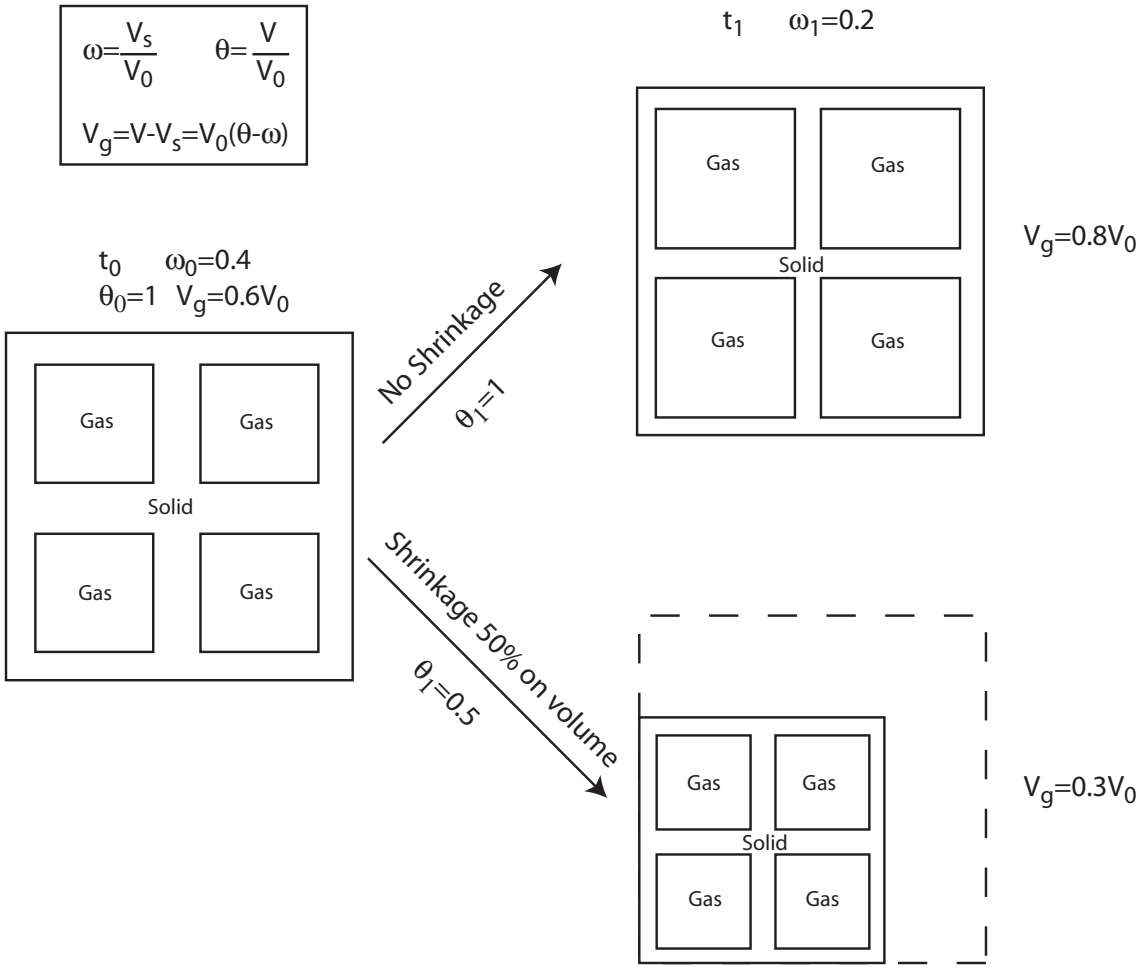

Figure 4.6
Relation between the particle shrinkage θ, by the solid fraction ω and the gas void at initial time t0 and time t1 when part of the solid material has left the particle.

Table 4.3. Shrinkage factors for size, volume mass and density of 10-mm wood pellets (unpublished material)

T_∞, °C	Length, L/L_o	Diameter, d/d_o	Volume, V/V_o	Mass, m/m_o	Density, ρ/ρ_o
600	0,86	0,78	0,51	0,156	0,30
”	0,88	0,83	0,61	0,17	0,27
700	0,86	0,78	0,51	0,150	0,29
”	0,87	0,84	0,61	0,15	0,24
800	0,86	0,78	0,52	0,143	0,28
”	0,87	0,84	0,62	0,14	0,23
900	0,87	0,83	0,59	0,135	0,23
1000	0,87	0,83	0,59	0,125	0,21

Unshaded rows – in cross flow of air
Shaded rows – in air-fluidised bed of 0.52-mm sand particles

A rough guideline for the volume shrinkage of a wood particle during different conversion stages can be formulated as:

- Initial particle state (fuel as received) $V = V_0$, $Y_i = 1$, the overall shrinkage coefficient $\theta = V/V_0 = 1$;
- 10-% volume shrinkage during drying (for moisture >15% of mass as received), θ_m = (dry fuel volume, V_{df})/(initial fuel volume, V_0) = 0.9, $\theta = \theta_m$;
- 50-% volume shrinkage during devolatilisation, θ_v = (initial volume of char, V_C)/(volume of dry particle, V_{df}) = 0.5, $\theta = V_C/V_0 = \theta_m\theta_v = 0.45$;
- 95-% volume shrinkage during char combustion, θ_C = (volume of ash, V_a)/(initial volume of char, V_C) = 0.05, $\theta = V_a/V_0 = \theta_m\theta_v\theta_C = 0.0225$

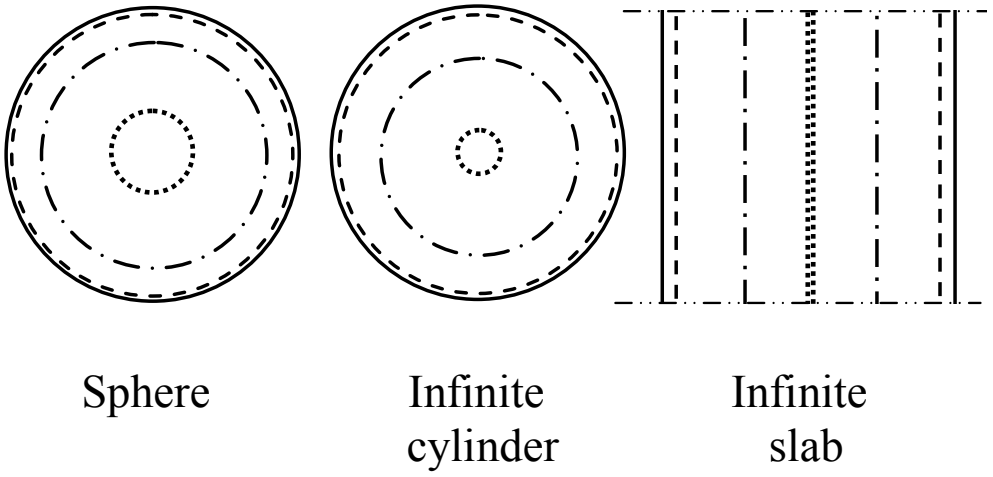

Figure 4.7
Shrinkage of different geometric forms during drying (dashed lines), devolatilisation (dashed and dotted lines) and char combustion (dotted lines)

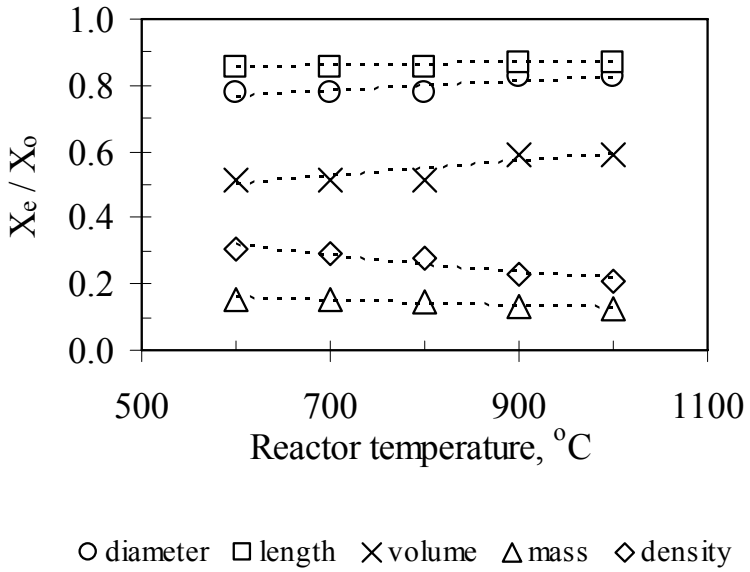

Figure 4.8
The effect of temperature on pellet shrinkage in cross-flow of air (unpublished material)

Figure 4.7 illustrates the shrinkage of a sphere ($V = 4\pi r^3/3$), an infinite cylinder ($V = \pi r^2$) and an infinite slab (V=2r) of the same initial characteristic size r during drying, devolatilisation and char combustion. Experimental data for the shrinkage of a single wood pellet during drying + devolatilisation in cross-flow of air and in an air-fluidised bed are shown in Table 4.3 and Fig. 4.8.

Table 4.3 shows that the higher the heating rate (in fluidised bed compared to one-phase air flow) the less the pellet shrinkage, especially at lower temperatures. The relative size and volume of a pellet decrease with the increase of temperature, whereas the char yield and the relative pellet density decrease, Fig. 4.8.

THERMAL CONDUCTIVITY OF WOOD

The change of the thermal conductivity with density and temperature can be modelled in a sufficiently accurate way. For ambient conditions, in the direction perpendicular to the fibers the thermal conductivity as function of density and moisture content is given by the correlation of MacLean (1941).

$$Y_{m,0} < 0.3,\ k^o{}_{c,per} = 23.7\times10^{-3} + 0.2\times10^{-3}\rho_{df}\left(1.0 + 2.0\times Y_{m,0}/\left(1 - Y_{m,0}\right)\right)$$

$$Y_{m,0} \geq 0.3,\ k^o{}_{c,per} = 23.7\times10^{-3} + 0.2\times10^{-3}\rho_{df}\left(1.0 + 2.5\times Y_{m,0}/\left(1 - Y_{m,0}\right)\right) \qquad (4.48)$$

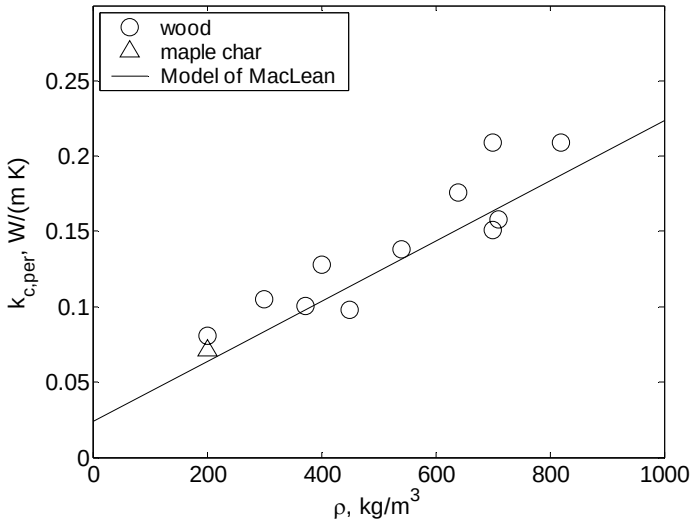

Figure 4.9. Effective thermal conductivity of dry wood across the fibers at ambient conditions. Symbols – experimental data, solid line – Eqn (4.48)

Based on his numerous data, MacLean concluded that the thermal conductivity parallel with the fibres $k^o_{c,par}$ is ≈2.5 times higher than across the fibres. However, Grønli's (1996) compilation of the literature data for dry woods shows that $k^o_{c,par} / k^o_{c,per} =$ 1.6 to 2.6. This data is shown in Fig. 4.9, where the only experimental point corresponding to wood char is in excellent agreement with Eq (4.48). As reasonable approximation, Eq (4.48) can be applied to char.

At elevated temperatures, which are characteristic for char, the effect of thermal radiation and the dependence of the thermal conductivity of gas on temperature should be included in Eq (4.48) as follows

$$k^o_{c,per} = k^o_{c,per} - 0.0237 + \nu_g k_{cg}(T) + \nu_{g,macro} k_{rad} \qquad (4.\ 49)$$

The term 0.0237 allows for gas conductivity under ambient conditions, and is replaced by the temperature-dependent thermal conductivity of gas $k_{cg}(T)$ related to the gas void fraction v_g, whereas the radiative thermal conductivity k_{rad} is associated with the void fraction of larger pores $v_{g,macro}$ and estimated by a Damköhler-type of expression

$$k_{rad} = 4\sigma\varepsilon d_{p,macro} T^3 \qquad (4.50)$$

where $d_{p,macro}$ is the average diameter of larger pores. For wood char $v_{macro} \approx 0.60$ and $d_{p,macro} \approx 3.5 \cdot 10^{-4}$ m (20-700 μm). Data on mercury porosimetry for the wood pellet char are available, $v_{macro} \approx 0.48$ and $d_{p,macro} \approx 2 \cdot 10^{-4}$ m (90-340 μm). The emissivity of char cells is assumed to be $\varepsilon = 0.9$.

For the direction along the fibres, the last term in Eq (4.49) responsible for the radiative conductivity reads

$$k_{rad} = 4\sigma d_{p,macro} T^3 / \left[1 + 2(d_p / L_p)(1/\varepsilon - 1)\right] \qquad (4.51)$$

where the pore diameter to length ratio $d_p/L_p \approx 0.01$. In typical temperature range for dry wood, 100 to 400°C, the contribution of radiation in the effective thermal conductivity is negligibly small.

To allow for the conversion transformations, the thermal conductivity can also be modelled from the fibre structure in wood. The model assumes that the thickness of the fiber walls can be calculated from the density and that the free moisture stays in an even layer on the inside of the fibre walls, see Fig 4.10.

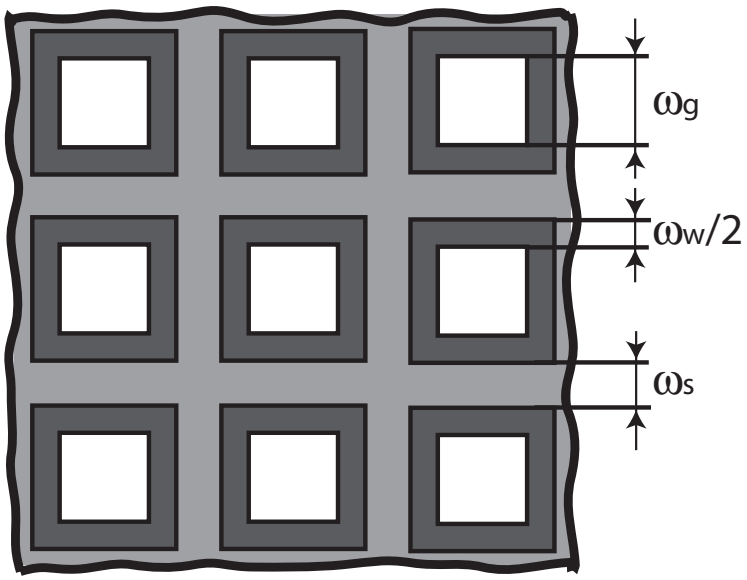

Figure 4.10
Model of fiber structure of wet wood. ω_s is width of solid, ω_w width of moisture layer and ω_g width of gas

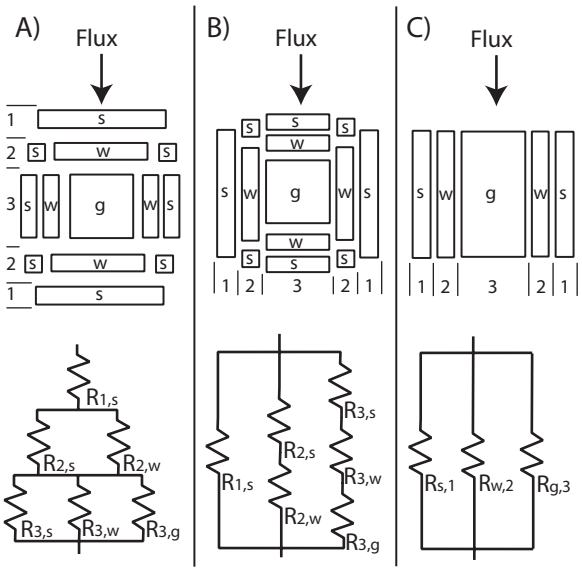

Figure 4.11
The paths perpendicular to the fiber derived as resistances combined in serial (A) and parallel (B) paths, and the path parallel to the fiber derived as parallel paths (C)

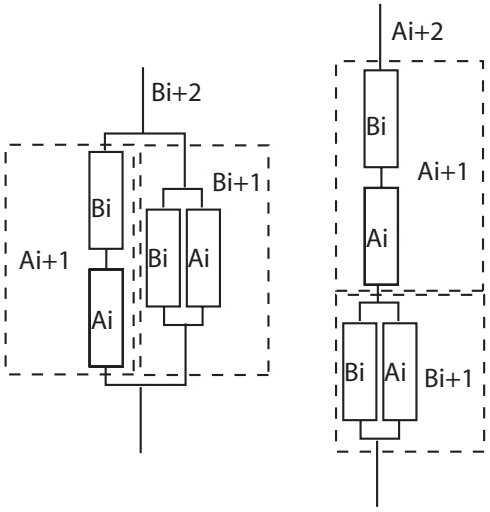

Figure 4.12
Combination of the resistance paths A and B to get the correct resistance

The heat resistance through the fiber structure can be derived according to different paths, Fig 4.11. As shown in Fig 4.11 there are two ways to derive the path perpendicular to the fiber, dependent on the one is used the result differs slightly. However, the right conductivity is somewhere between the two cases and this can be calculated by combining the two paths (A) and (B) of Fig 4.11 according to Fig 4.12. The thermal conductivity, perpendicular and

parallel to the fiber direction, is calculated from the conductivities and densities of dry fuel, liquid water, fiber wall, and the solid part of the char. The densities of moisture and solid phase are related to density of the dry unconverted fuel. The fibre structure in the wood and the char is given an equivalent structure of quadratic tubes. The equivalent thicknesses of wall fiber, ω_s, moisture layer, ω_w, and gas layer are calculated from the dry density of the fuel, the shrinkage factor and the relative volume of the gas void,

$$\omega_g = (\zeta\theta)^{-1/2} \tag{4.52}$$

$$\omega_s = \left(\omega_g^2 + \frac{Y_m Y_{m,0}}{1 - Y_{m,0}} \frac{\rho_{df}}{\theta \rho_m} \right)^{1/2} \tag{4.53}$$

$$\omega_w = 1 - \omega_s - \omega_g \tag{4.54}$$

According to Fig. 4.12, to obtain the correct effective thermal conductivity perpendicular to the fiber direction, its minimum value is calculated for each conversion stage for the path (A), Fig. 4.11,

$$k_{c,per,A1} = \omega_s k_{c,s} + \omega_w \left(\frac{\omega_s}{k_{c,s}} + \frac{(1-\omega_s)}{k_{c,m}} \right)^{-1} + \omega_g \left(\frac{\omega_s}{k_{c,s}} + \frac{\omega_w}{k_{c,m}} + \frac{\omega_g}{(k_{c,g} + k_{rad})} \right)^{-1} \tag{4.55}$$

and the maximum value for the path (B), Fig. 4.11

$$k_{c,per,B1} = \left(\frac{\omega_s}{k_{c,s}} + \frac{\omega_w}{\omega_s k_{c,s} + (1-\omega_s) k_{c,m}} + \frac{\omega_g}{\omega_s k_{c,s} + \omega_w k_{c,m} + \omega_g (k_{c,g} + k_{rad})} \right)^{-1} \tag{4.56}$$

The minimum Eq (4.55) and maximum Eq (4.56) thermal conductivities, (i = 1), are combined in serial and parallel paths according to Fig. 4.12,

$$\begin{aligned} k_{c,per,Ai+1} &= \left(k_{c,per,Ai} + k_{c,per,Bi} \right) / 2 \\ k_{c,per,Ai+1} &= 2 / \left(1/k_{c,per,Ai} + 1/k_{c,per,Bi} \right) \end{aligned} \tag{4.57}$$

Table 4.4. Physical properties for modelling the effective thermal conductivity

Property = a_1+a_2T	a_1	a_2
$k_{c,s,wood}$ [W/mK] per / par*	0.52 / 0.73	-
$k_{,c,m}$ [W/mK]	0.278	$1.11\cdot10^{-3}$
$k_{c,s,char}$ [W/mK]**	1.47	$1.1\cdot10^{-3}$
$\rho_{df,wood}$ [kg/m^3]*	1480	-
ρ_m [kg/m^3]	1000	-
$\rho_{df,char}$ [kg/m^3]**	1950	-

* The thermal conductivity and specific density of cell wall of dry wood
** The thermal conductivity and density of cell wall of char

which gives the effective thermal conductivity at $i = 2$ after combination of those at $i = 1$, where i is a counter. As i approaches infinity the two values converge and a correct effective thermal conductivity is obtained which is in good agreement with the MacLeans correlation.

$$i \to \infty \quad ; \quad k_{c,per} = k_{c,per,A\infty} = k_{c,per,B\infty} \tag{4.58}$$

Along the fibre, pipes placed next to each other represent the wood structure. The effective thermal conductivity can be modelled by a parallel path (C), Fig. 4.11.

$$k_{c,par} = \left(1-\left(1-\omega_s\right)\right)^2 k_{c,s} + \left(\left(1-\omega_s\right)^2 - \omega_g^2\right)k_{c,m} + \omega_g^2 (k_{c,g} + k_{rad}) \tag{4.59}$$

The recommended thermal conductivities and densities of the water, gas, fibre wall and the solid part of the char are given in Table 4.4.

The density of pelletised wood is increased as a result of compression. This affects both $k^o{}_{c,per}$ and $k^o{}_{c,par}$, but, as follows from the models of heat conduction of wood, the former increases more than the latter. The ratio $k^o{}_{c,par} / k^o{}_{c,per}$ for solid wood at ambient temperature decreases from approximately 2 to 1.7 as the apparent wood density increases from 400 kg/m^3, typical for solid softwood, to 1200 kg/m^3, typical for wood pellets, see Fig. 4.13. For char, this ratio is practically constant, $k^o{}_{c,par} / k^o{}_{c,per} \approx 1.6$, over the density range of interest, 100 to 400 kg/m^3. Given that the wood grains forming the pellet are randomly oriented, the

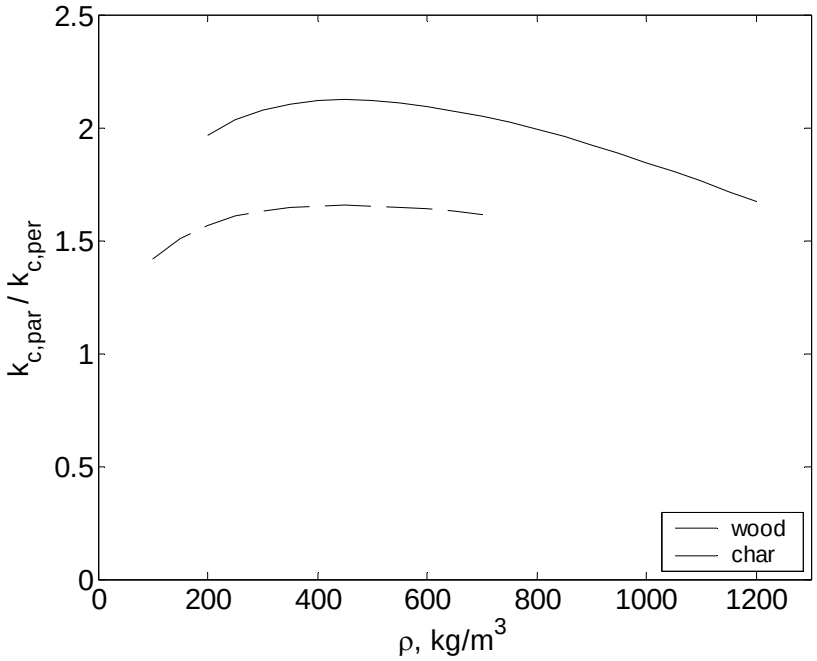

Figure 4.13
The ratio of parallel to perpendicular effective thermal conductivity of dry wood and wood char at ambient conditions vs density, calculated from 4.58 and 4.59

effective thermal conductivity of pellets and pellet char is the same in all directions and can be estimated as

$$k^o = k^o{}_{c,par}/3 + 2\,k^o{}_{c,per}/3 \qquad (4.60)$$

Together with the above estimates of the $k^o{}_{c,par}/k^o{}_{c,per}$ ratio this leads to $k^o{}_c \approx 1.2\,k^o{}_{c,per}$ for both pellets and pellet char. Bearing in mind the approximate character of the above considerations, the use of the isotropic effective thermal conductivity $k^o = k^o{}_{c,per}$ is reasonable for treatment of pellets.

SPECIFIC HEAT

The specific heat of wood is dependent on temperature. It can be represented by empirical correlations from the literature Thunman et al., e.g. for dry wood (i), (ii) (a mean value of six reported correlations), (iii),

Table 4.5. Specific heat of various gas species, $c_{pi} = a_1 + a_2T + a_3T^2 + a_4T^3 + a_5T^4$ Thunman et al.

Species	a_1	a_2 ($\times 10^3$)	a_3 ($\times 10^6$)	a_4 ($\times 10^9$)	a_5 ($\times 10^{12}$)
[(a)] O_2	811	411	-175	37.5	-2.97
[(a)] N_2	939	302	-81.0	8.23	-0.150
[(a)] H_2O	1612	740	-8.24	-38.5	4.84
[(a)] H_2	14400	-369	1620	-467	41.3
[(b)] CO	982	139	138	-96.1	15.9
[(b)] CO_2	508	1390	-899	274	-31.5
[(b)] $C_{1.16}H_4$ (c_p for CH_4)	1086	3820	159	-682	141.2
[(b)] $C_nH_mO_k$ (c_p for C_6H_6)	-9.31	2290	-763	112	-4.01
[(b)] Char (c_p for graphite)	-334	4410	-3160	1010	-119

Correlations valid in the range [(a)] 273-4000K, [(b)] 273-3000K, error less than ±2%

$$\begin{aligned} c_{p,wood} &= 4.2T - 38 \qquad (i) \\ c_{p,wood} &= 4.6T - 133 \qquad (ii) \\ c_{p,wood} &= 3.9T + 103 \qquad (iii) \end{aligned} \tag{4.61}$$

All of these correlations are close to each other. The correlations are established at temperatures below 100 °C. However, there are other investigations indicating that the linear increase continues until devolatilisation starts. Small differences between different woods can be expected, as they consist of different amounts of cellulose, hemicellulose and lignin. The heat capacity of pure cellulose is similar to the specific heat of wood, but has slightly higher temperature dependence. Moist wood has a greater specific heat than what would be expected from the simple law of mixtures, as a result of the energy absorbed by the wood-water bonds. This is represented by a correction term to the dry substance and the specific heat of the wet wood is, Siau,

$$\begin{aligned} c_{p,wet} &= \left(c_{p,wood} + 4190Y_{moist}/\left(1-Y_{moist}\right)\right)/\left(1+Y_{moist}/\left(1-Y_{moist}\right)\right) + A \\ A &= \left(23.55T - 1320Y_{moist}/\left(1-Y_{moist}\right) - 6191\right)Y_{moist}/\left(1-Y_{moist}\right) \end{aligned} \tag{4.62}$$

The specific heat for char can be assumed to be the same as the one for graphite. The specific heat of graphite is somewhat special in the lower temperature range, but in the temperature range of char conversion it gives reasonable values. Due to the low ash content, the contribution of the ash is here included in the char. For fuels with a high ash content better values must be taken forward.

For gas species the specific heat is known and can easily be found. In Table 4.5 correlations for some species are given. The effective properties of gas mixtures are calculated as the mass average, $\chi = \sum Y_i \chi_i$.

EFFECTIVE DIFFUSIVITY AND PERMEABILITY IN WOOD

The effective diffusivity of a species *i* is expressed through the multicomponent diffusion coefficient of this species in the mixture of the other components D_i^m, gas void fraction v_g, and tortuosity τ, which is the ratio of the real diffusion path length in tortuous porous structure to the straightforward path along a co-ordinate *x*.

$$D_{i,eff} = \frac{v_g D_i^m}{\tau} \tag{4.63}$$

The diffusion coefficient for species *i* into the mixture of the other species is calculated from the binary diffusion coefficients of the mixture species.

$$D_i^m = \frac{1 - Y_i}{\sum_{j \neq i}^{N} \frac{X_j}{D_{ij}}} \tag{4.64}$$

The effect of temperature on the binary diffusion coefficients is described by a polynomial function,

$$\ln D_{ij} = \sum_{n=1}^{4} a_n \left(\ln T\right)^{n-1} \tag{4.65}$$

with the coefficients a_n shown in Table 4.6. The binary diffusion coefficients are inversely proportional to pressure.

In case of char combustion it is often sufficient to consider binary diffusion of oxygen in nitrogen.

Table 4.6. Polynomial coefficients for Eq (4.65) at $P=1.01\cdot10^5$ Pa, Kee et al. (1991)

Species	a_0	a_1	a_2	a_3
N2 - N2	-0.149E+02	0.323E+01	-0.206E+00	0.895E-02
CH4 - N2	-0.160E+02	0.368E+01	-0.262E+00	0.113E-01
CH4 - CH4	-0.170E+02	0.404E+01	-0.307E+00	0.131E-01
O2 - N2	-0.152E+02	0.334E+01	-0.221E+00	0.960E-02
O2 - CH4	-0.163E+02	0.378E+01	-0.275E+00	0.118E-01
O2 - O2	-0.155E+02	0.344E+01	-0.232E+00	0.101E-01
CO - N2	-0.150E+02	0.323E+01	-0.206E+00	0.898E-02
CO - CH4	-0.161E+02	0.368E+01	-0.263E+00	0.114E-01
CO - O2	-0.153E+02	0.335E+01	-0.222E+00	0.964E-02
CO - CO	-0.150E+02	0.324E+01	-0.207E+00	0.901E-02
H2 - N2	-0.119E+02	0.254E+01	-0.117E+00	0.511E-02
H2 - CH4	-0.125E+02	0.279E+01	-0.151E+00	0.662E-02
H2 - O2	-0.119E+02	0.257E+01	-0.121E+00	0.529E-02
H2 - CO	-0.119E+02	0.255E+01	-0.117E+00	0.514E-02
H2 - H2	-0.978E+01	0.196E+01	-0.407E-01	0.183E-02
CO2 - N2	-0.178E+02	0.422E+01	-0.327E+00	0.139E-01
CO2 - CH4	-0.189E+02	0.463E+01	-0.375E+00	0.157E-01
CO2 - O2	-0.182E+02	0.433E+01	-0.341E+00	0.145E-01
CO2 - CO	-0.179E+02	0.422E+01	-0.328E+00	0.139E-01
CO2 - H2	-0.148E+02	0.366E+01	-0.265E+00	0.116E-01
CO2 - CO2	-0.206E+02	0.505E+01	-0.420E+00	0.173E-01
H2O - N2	-0.203E+02	0.517E+01	-0.430E+00	0.176E-01
H2O - CH4	-0.206E+02	0.524E+01	-0.428E+00	0.170E-01
H2O - O2	-0.204E+02	0.520E+01	-0.430E+00	0.175E-01
H2O - CO	-0.203E+02	0.519E+01	-0.432E+00	0.176E-01
H2O - H2	-0.176E+02	0.477E+01	-0.397E+00	0.169E-01
H2O - CO2	-0.199E+02	0.463E+01	-0.324E+00	0.116E-01
H2O - H2O	-0.139E+02	0.181E+01	0.110E+00	-0.939E-02
C6H6 - N2	-0.200E+02	0.479E+01	-0.390E+00	0.162E-01
C6H6 - CH4	-0.202E+02	0.480E+01	-0.379E+00	0.152E-01
C6H6 - O2	-0.203E+02	0.486E+01	-0.397E+00	0.164E-01
C6H6 – CO	-0.201E+02	0.479E+01	-0.391E+00	0.162E-01
C6H6 - H2	-0.182E+02	0.478E+01	-0.407E+00	0.177E-01
C6H6 - CO2	-0.215E+02	0.502E+01	-0.397E+00	0.156E-01
C6H6 - H2O	-0.184E+02	0.369E+01	-0.184E+00	0.500E-02
C6H6 - C6H6	-0.223E+02	0.498E+01	-0.375E+00	0.140E-01

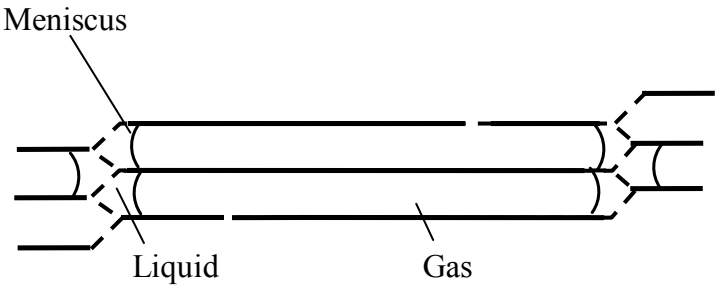

Figure 4.14
Wood fibres with pits and meniscus between the gas and liquid

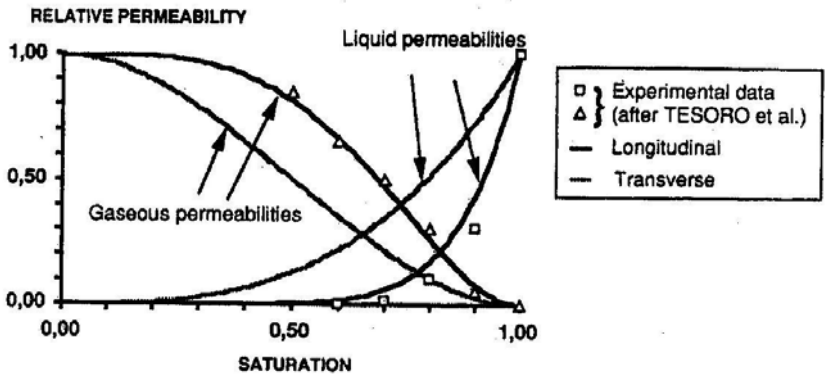

Figure 4.15
Relative permeability vs the water saturation

The tortuosity of wood and char in different directions can be estimated from the schematic wood fiber structure, Fig. 4.14. The fibres have perforated ends and a very few pits in side walls. That is why in case of diffusion parallel to the fibres $\tau \approx 1$, whereas perpendicular to the fibers τ ~ (pore length, L_p)/(pore diameter, d_p) ~ 100. This results in the ratio $D_{i,eff,par}/D_{i,eff,per} \sim 100$.

The above estimate of the parallel to perpendicular diffusivity ratio is qualitatively consistent with the range of the corresponding gas permeability ratio in dry wood, between 500 and 10^5 reported in the literature. However, in wet wood the presence of liquid water in the fiber ends prevents gas flow, Fig. 4.14. At the water saturation point the entire void structure is filled with water, which results in maximum liquid permeability and zero gas permeability. As wood dries, the gas permeability increases and the liquid permeability decreases. To describe these phenomena, the permeability is represented as a product of the intrinsic (maximum) s_g permeability and relative permeability $s_{g,rel}$ varying from 0 to 1 as the water saturation S increases from 0 to 1, Fig. 4.15.

$$s = s_g s_{g,rel} \tag{4.66}$$

Typical literature values of the intrinsic permeability for softwood are $s_{g,\,par} \approx 2\cdot10^{-14}$ m^2 and $s_{g,\,pear} \approx 3\cdot10^{-18}$ m^2. Perre et al. (1993) derived the following expressions for the relative permeabilities of softwood,

$$s_{g,rel,par} = 1+(4S-5)S^4, \quad s_{g,rel,per} = 1+(2S-5)S^2 \tag{4.67}$$

where S is the water saturation

$$S = \frac{M - M_{fsp}}{M_{sat} - M_{fsp}}, \quad M = \frac{Y_m}{1 - Y_m} \tag{4.68}$$

and the fibre saturation point M_{fsp} depends on temperature as follows (M_{fsp} = 0.3 at T=298 K).

$$M_{fsp} = (0.3 + 0.298) - 0.001T \tag{4.69}$$

The water saturation moisture content (on dry basis) M_{sat} should be calculated for the entire gas void $\nu_{g0} V_0$ of the particle to be filled with water, $\rho_m = 1000\, kg/m^3$.

SUMMARY

An overview is presented of the basic principles and descriptions of heat and mass transfer, as well as physical properties of biomass fuel, relevant to thermo-chemical conversion of a single fuel particle. Biomass fuel, in particular wood, is characterised by a high content of moisture and volatile matter, which makes the physical data dependent on degree of conversion. As the conversion progresses, the particle size decreases, and so does the particle mass due to transformations of the solid phase in gas. As a result, particle density, thermal conductivity, gas voidage, and other properties change in a rather complicated way. Due to the anisotropic structure of wood, its transfer properties with respect to heat, gas and liquid are also dependent on direction. Guidelines and models are recommended in order to account for the above phenomena when evaluating the transfer characteristics and effective properties for each conversion stage. One should be careful when applying the expressions recommended for external heat and mass transfer to fuel particles of irregular shapes. For instance, the corner effects can not be interpreted in the framework of a concept of equivalent spherical particle.

REFERENCES

1. Luikov, A.V. (1968) Analytical heat diffusion theory, ed J.P. Hartnett, Academic Press, New York, 1968.
2. Middleman, S. (1997) An introduction to mass and heat transfer: principles of analysis and design. John Wiley & Sons, New York.

3. Zukauskas A.A. (1982) Convective transfer in heat exchangers. Nauka Publishing House, Moscow (in Russian).
4. Kunii, D. and Levenspiel, O. (1991) Fluidization Engineering. Butterworth-Heine mann, Boston.
5. Bird, R.B., Stewart, W.E. and Lightfoot, E.N. (1960) Transport phenomena, John Wiley & Sons Inc., New York.
6. Pomerantsev, V.V., ed. (1986) Fundamentals of applied combustion theory, Energoatomizdat Publishing House, Leningrad. (in Russian).
7. Warnatz, J., Maas, U. and Dibble, R.W. (1996) Combustion: physical and chemical fundamentals, modeling and simulation, experiments, pollutant formation, Springer-Verlag, Berlin.
8. MacLean, J.D. (1941) Thermal conductivity of wood, Transactions Amarican Society of Heating and Ventilating Engineers, 47, 323-354.
9. Palchonok G.I. Heat and mass transfer to a single particle in fluidized bed. Ph.D. thesis, Chalmers University of Technology, Göteborg, Sweden, 1998.
10. Thunman, H., Leckner, B., Niklasson, F. and Johnsson, F. (2002) Combustion of wood particles - a model for Eulerian calculations, Combustion and Flames, 129, 30-46.
11. Thunman, H. and Leckner, B. (2002) Thermal conductivity of wood - models for different stages of combustion, Biomass & Bioenergy, 23, 47-54.
12. Thunman, H. and Leckner, B. (2004) Influence of size and density of fuel on combustion in a packed bed, Proceedings of the Combustion Institute.
13. Thunman, H. and Leckner, B. (2002) Modelling of the combustion front in a downdraft fuel converter, Proceedings of the Combustion Institute, 29, 511-518.
14. Thunman, H. and Leckner, B. (2003) Co-current and counter-current fixed bed combustion of biofuel - a comparison, Fuel, 82, 275-283.
15. Koch, P. (1969) Specific heat of ovendry spruce pine wood and bark, Wood Science, 1, 203-214.
16. Grønli, M. (1996) A theoretical and experimental study of the thermal degradation of biomass. Ph.D. thesis, Norwegian University of of Science and Technology, Trondheim, Norway.
17. Larfeld, J., Leckner, B. and Melaaen, MC. (2000) Modelling and measurements of heat transfer in charcoal from pyrolysis of large wood particles. Biomass & Bioenergy, 18, 507-514.

18. Siau, J.F.,'Transport Processes in Wood', Sprngler-Verlag, Berlin, ISBN 3-540-12574-4, 1984.

CHAPTER 5

DRYING AND DEVOLATILISATION OF THERMALLY SMALL PARTICLES

The three main types of combustion systems for firing solid fuels are combustion in fixed-bed, suspension, and fluidised-bed. The basic behaviour of these combustion systems is related to the behaviour of a single fuel particle. Here, a single fuel particle, e.g. wood or coal, in a hot surrounding with gas flowing around the particle, is discussed.

SOLID FUEL COMBUSTION MECHANISMS

The fuel size ranges from pulverised fuels to larger sizes such as crushed, chipped, or shredded fuels, or logs. Investigation on the behaviour of individual solid fuel particles provides insight into the design and performance of furnaces and boilers.

When a solid fuel particle is exposed to a hot flowing gas stream, it undergoes three stages of mass loss: drying, devolatilisation and char combustion or drying, pyrolysis and char gasification, depending on the composition of the surrounding gas. The relative significance of each of these three processes is indicated by the proximate analysis of the fuel. For example, wood has relatively much moisture, more volatiles, and less fixed carbon (char) than coal, see Chapter 2. For pulverised fuel particles, drying, devolatilisation, and char conversion occur sequentially. The burning or gasification period of the char lasts much longer than the devolatilisation and drying stages. The principle phases of conversion of a small solid fuel particle in a hot surrounding are seen in Fig 5.1. The fuel particle is first heated to evaporation temperature and then the temperature is constant during evaporation of the moisture due to the endothermic process.

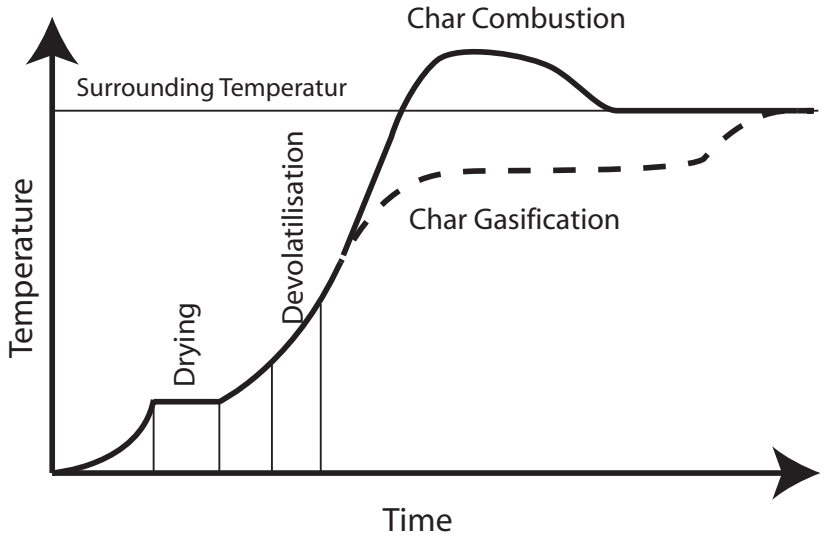

Figure 5.1.
Principle stages of conversion of a small solid fuel particle in a hot surrounding versus particle temperature and time. The extension of drying and devolatilisation are marked with thin lines.

After all moisture is gone, the temperature again rises, and at a certain temperature the volatiles are released, whereas the temperature still increases. As all volatiles are released, the conversion of the char starts, resulting in a higher particle temperature than that of the surrounding if the surrounding gas contains oxygen, char combustion, or a lower temperature than that of the surrounding if the surrounding gas contains carbon monoxide or water vapour but no oxygen, char gasification.

For larger particles, drying, devolatilisation, and char conversion occur simultaneously in different locations in the particle. However, locally the processes take place sequentially in the same way as for a small particle. It is rather simple to determine if a particle is large or small from a thermal point of view, because this judgement can be based on the thermal Biot number (the derivation is given in Chapter 4), Bi_t,

$$Bi_t = \frac{r_{car} h_{c,eff}}{k_{cs}} \qquad (5.1)$$

where r_{car} is a characteristic length, $h_{c,eff}$ the effective heat transfer coefficient ($h_{c,eff} = h_c + h_{rad}$, where h_c is convective heat transfer coefficient calculated from the Nu number, $Nu = h_c d / k_c$, h_{rad} is the heat transfer coefficient for radiation Eq 5.15 and k_{cs} is the thermal conductivity of the particle. The

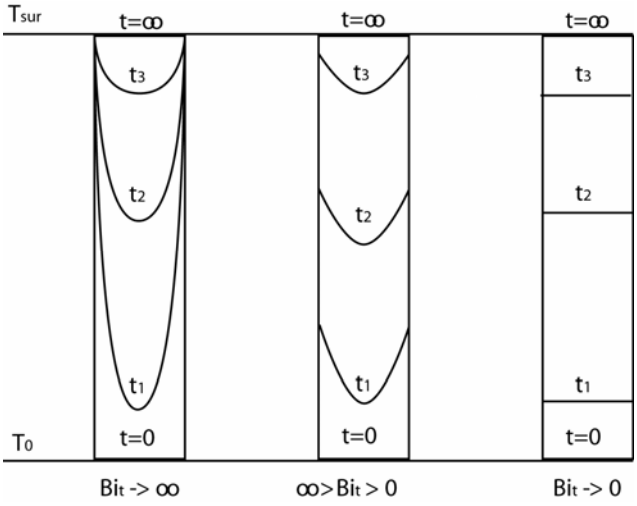

Figure 5.2.
Temperature distribution inside a heated particle for various times and Biot numbers, for particle of temperature T_0 at time t=0 suddenly exposed to a temperature T_∞.

temperature distribution at various times and Bi_t is shown in Fig 5.2 showing a slab at temperature T_0 suddenly exposed to a gas of temperature T_∞. A large Biot number $Bi_t >> 1$ implies that the heat transfer to the surface of the particle is faster than the heat flow into the particle. This results in a temperature wave that propagates from the surface of the particle to the centre, determining the rate of drying and devolatilisation of the particle. If the Biot number is instead small, $Bi_t << 1$, the whole particle will adopt the same temperature (isotherm) while the particle is gradually heated: The heating of the particle is controlled by the heat transfer to the surface of the particle. In many cases the Bi_t ends up in the intermediate area, where it is not obvious if the drying and devolatilisation are sequential or overlapping. In this area the Drying number *Dr* will give this information. This number relates the kinetic rate of devolatilisation to the rate of evaporation, the later being controlled by heat transfer to the evaporation front. The treatment is intended

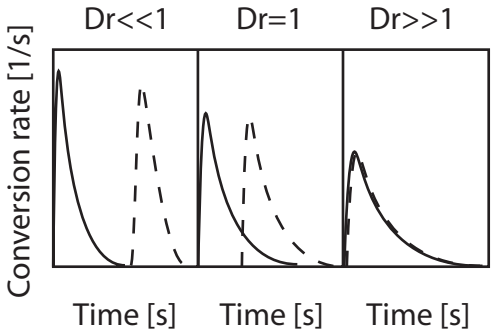

Figure 5.3.
Qualitative illustration of the characteristic conversion behaviour at various drying numbers during conversion of a fuel particle in a thermal converter. The rate of evaporation of moisture (solid line) and the devolatilisation rate (dashed line) are plotted versus time.

for fuels entering an environment having a considerably higher temperature than the saturation temperature of the moisture. The expected relation between the drying and devolatilisation processes for various Drying numbers is illustrated by Fig. 5.3. Such a Drying number gives information on the choice of models. If the drying number is less than 0.1 the processes can be modelled as sequential and if it is above 100 the devolatilisation can be modelled as it is released at the same rate as the moisture. All these cases $Dr < 0.1$, $0.1 < Dr < 100$ and $Dr > 100$ will be treated here, where we start in this chapter with the thermally small particles together with the description of basic processes of drying and devolatilisation. After this the case where the Drying number is high (> 100) is treated. The intermediate region ($0.1 < Dr < 100$) can for most engineering situations be treated similar to the high drying numbers, but in some situations the conversion need to be described by a more general description. This will be done in detail after the basic description of all the conversion stages, drying, devolatilisation and char conversion, of a solid fuel particle. The Drying number relates the rate of drying in the end of the drying process R_m with the rate of devolatilisation close to the surface R_v,

$$\mathrm{Dr}_{X_m} \equiv R_v / R_m \qquad (5.2)$$

The rate of moisture R_m is defined as the mass release of moisture in the end of the drying period divided by the initial mass of moisture. The rate of devolatilisation R_v is defined as the mass release of volatiles close to the surface of the particle divided by the initial mass of volatiles. If the rate of devolatilisation at the end of the drying period is larger than the rate of drying it means that considerable amount of volatiles has left the fuel before the drying is completed and consequently the processes are overlapped within the fuel particle. On the other hand, if the rate of devolatilisation is smaller then the rate of drying, nearly no volatiles have left the particle before all the moisture has left. To use the analysis one has to decide the time for which the Drying number is to be calculated. One suggestion is to chose the time when 10 % of the initial moisture remains, $X_m = 0.1$. This corresponds to a relative position, ξ_m, of the drying front in the particle, which can then be calculated from the geometry of the particle. For particles described as spheres (n = 2), a three-dimensional shape, infinite cylinders (n = 1), a two-dimensional shape or infinite plates (n = 0), a one-dimensional shape the relative position of the drying front is given by

$$\xi_m = X_m^{1/(n+1)} \tag{5.3}$$

If a steady state temperature profile is assumed to be established in each time step of the conversion, the rate of the drying is given by the heat transported from the surrounding through the boundary layer and the dry material into the drying front. This heat transport is obtained from the steady state solution of the conservation equation for energy, $1/r^n \partial/\partial r(r^n \partial T/\partial r) = 0$, with the boundary condition at the particle surface $k_c \partial T/\partial r = h_{c,eff}(T - T_\infty)$, and at the evaporation front $T = T_m$, T_m is the temperature of evaporation. This gives the rate of drying

$$R_m = -\frac{(n+1)}{r_0^2}\frac{(1-Y_m)}{Y_m}\frac{c_{ps}}{c_{pg}} a_s \alpha\beta \tag{5.4}$$

r_0 is the initial particle radius, Y_m initial mass fraction of moisture, a_s thermal diffusivity c_{pg} specific heat of the gas (in this case water vapour), c_{ps} specific heat of the solid, α is a dimensionless number relating the shape of the particle and the heat needed to heat up the escaping gases to the heat of evaporation,

$$\alpha = \xi_m^n c_{pg}(T_\infty - T_m)/H_m \tag{5.5}$$

and β is the dimensionless temperature gradient at the drying front

$$\beta = \left.\frac{\partial\theta}{\partial\xi}\right|_{\xi_m} \tag{5.6}$$

Table 5.1. The dimensionless temperature gradient and the dimension less surface temperature $\theta_{\xi=1}$ obtainde from the solution of the conservation equation for energy. $\Gamma[\xi] = (1-\xi)$ when n = 0 (plate), $\Gamma[\xi] = -\ln(\xi)$ when n = 1 (Cylinder), $\Gamma[\xi] = (1/\xi - 1)$ when n = 2 (sphere)

Dimensionless temperature gradient	$\beta = -\dfrac{\mathrm{Bi}_{\mathrm{th}}}{\xi_m^n\left(1+\mathrm{Bi}_{\mathrm{th}}\Gamma\left[\xi_m\right]\right)}$	(5.7)
Dimensionless temperature at surface of the particle	$\theta_{\xi=1} = \dfrac{1}{1+\mathrm{Bi}_{\mathrm{th}}\Gamma\left[\xi_m\right]}$	(5.8)

H_m is the latent heat of vaporisation per unit mass of water. The full derivation of rate of evaporation is given below in the next chapter under the section 'An analytic model for simultaneous drying and devolatilisation of large particles'. The dimensionless temperature gradient at the drying front of the three general particle shapes is found in Table 5.1 as function of the thermal Biot number. The rate of devolatilisation is expressed by an Arrhenius form of equation.

$$R_v = k_{rv,0}\exp\left(-E/(\Re(\theta_{\xi=1}T_m + \left(1-\theta_{\xi=1}\right)T_\infty))\right) \qquad (5.9)$$

The temperature used to estimate the rate of devolatilisation is that of particle surface in dimensionless form, $\theta_{\xi=1}$, the evaporation temperature T_m and the surrounding temperature T_∞. The dimensionless temperature of the surface of the particle is written in Table 5.1 for three general shapes: sphere, infinite cylinder and infinite plate.

DRYING OF SOLID FUELS

Moisture in solid fuels can exist in two forms; as free water within the pores of the fuel including surface moisture, and as bound water, which is adsorbed in the interior pore structure of the fuel. Wood, being rather porous, contains both free and bound water, while bituminous coals have relatively small pores and contain only a few percent of water, mostly as bound water.

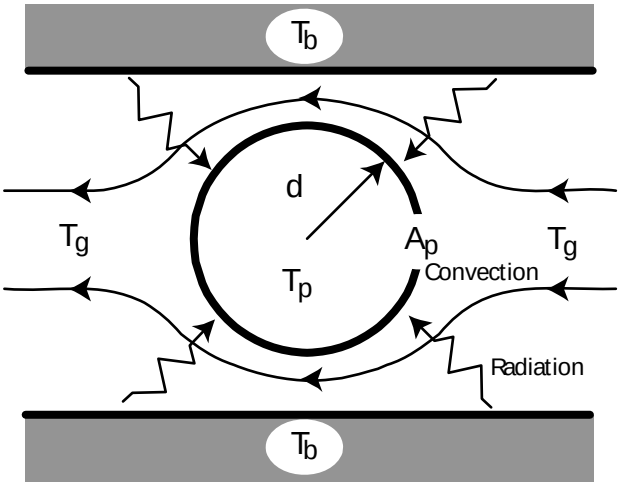

Figure 5.4
A particle with a characteristic diameter *d* exposed to convective and radiative heat transfer.

Consider a pulverised wood or coal particle, $Bi_{th} < 0.1$, which is introduced into a furnace. Upon entry into the gas stream, se Fig 5.4, heat is convected and radiated to the particle's surface and conducted into the particle. For a pulverised particle (say, 100 µm in size), which has a very small drying number, the water is vaporised and forced out of the particle rapidly before the volatiles are released. There is no temperature gradient in the particle. The drying time of a small pulverised particle is the time required to heat up the particle to the vaporisation point, t_1, and drive off the water, t_2. The time to heat up the particle from the initial temperature, T_0, to the evaporation temperature, T_e, is given by the heating rate of the particle resulting from the specific heat, c_p, times the mass, m, of the dry fuel, subscript *df*, and the moisture, subscript *m*, divided by the heat transported to the particle surface, q,

$$t_1 = \int_{T_0}^{T_e} \frac{m_m c_{pm} + m_{df} c_{pf}}{q} dT \qquad (5.10)$$

When the particle has reached the evaporation temperature all heat transported to the particle surface is used to evaporate the moisture, and the time of evaporation can be calculated

$$t_2 = \frac{m_m H_m}{q} \qquad (5.11)$$

The heat flow to the particle, q, depends on the background furnace temperature T_b, and the surrounding gas temperature T_g, see Fig 5.4. The heat is assumed to be transferred to the particle by grey body radiation with emissivity ε_{rad}, a view factor of 1, and a convective film coefficient:

$$q = \varepsilon_{rad} \sigma A\left(T_b^4 - T^4\right) + h_c^* A\left(T_g - T\right) \qquad (5.12)$$

h^*_c is the convective heat transfer coefficient corrected for gases flowing out from the particle, Bird [1],

$$\frac{h_c^*}{h_c} = \frac{\rho_g u_g c_p / h_c}{\exp\left(\rho_g u_g c_p / h_c\right) - 1} \tag{5.13}$$

u_g is the velocity of the gas flowing out. By expressing also the radiation by a heat transfer coefficient and assuming that the background temperature is the same as the gas temperature $T_g = T_b = T_\infty$ and neglecting the effect of the gases flowing out from the particle, Eq (5.12) can be simplified

$$q = A\left(h_{rad} + h_c\right)\left(T_\infty - T\right) = A h_{c,eff}\left(T_\infty - T\right) \tag{5.14}$$

where the radiative heat transfer coefficient is

$$h_{rad} = \varepsilon_{rad}\sigma\left(T_\infty^4 - T^4\right)/\left(T_\infty - T\right) = \varepsilon_{rad}\sigma\left(T_\infty^2 + T^2\right)\left(T_\infty + T\right) \tag{5.15}$$

Assuming that the effective heat transfer coefficient is constant and that the surface temperature is equal to the evaporation temperature T_e, the time to heat up of the fuel particle can be obtained by integrating Eq (5.10). The total drying time is then given by

$$\begin{aligned} t_{dry} &= t_1 + t_2 = \\ &= -\frac{\left(m_m c_{pm} + m_{df} c_{pf}\right)}{A h_{c,eff}} \ln\left(\frac{T_\infty - T_e}{T_\infty - T_0}\right) + \frac{m_m H_m / \left(T_\infty - T_e\right)}{A h_{c,eff}} \end{aligned} \tag{5.16}$$

where m_m is the initial mass of moisture in the particle. The differential heat of wetting (i.e., the heat required to release the absorbed water from the surface) is about 70 kJ/kg dry solid and is neglected compared with the heat of vaporisation of water of 2400 kJ/kg of water. For evaluation of the convective heat transfer coefficient, the particle film temperature is used:

$$\overline{T} = \frac{T_e + T_g}{2} \tag{5.17}$$

along with a Nusselt number correlation giving the convective heat transfer coefficient, for example,

$$\mathrm{Nu} = \frac{h_{c0} d_{car}}{k_{cg}} = 2 + 0.6\,\mathrm{Re}^{1/2}\, Sc^{1/3} \tag{5.18}$$

EXAMPLE 5.1. A 100-μm oak particle which contains 40% moisture (dry basis) is injected into a 1500-K furnace. The oak particle was initially at 300 K and had a dry density of 690 kg/m^3. Find the drying time.

Solution. The convective heat transfer coefficient is calculated from the thermal conductivity of the gas (air) at a film temperature of ≈900 K is k_{cg} = 0.0625 W/mK, the particle diameter and the Nusselt number, which here is assumed to be 2.0 as the particle most likely follows the gas,

$$h_{c0} = \frac{2k_{cg}}{d} = \frac{(2.0)(0.0625\ \mathrm{W/mK})}{100\times10^{-6}\ \mathrm{m}} = 1250\ \mathrm{W/m^2K}$$

The radiative heat transfer coefficient is, where the emissivity of wood is assumed to be ε = 0.90 and the average temperature of the surface is assumed to be close to the evaporation temperature,

$$h_{rad} = 0.9\times5.67\times10^{-8}\left(1500^2+373^2\right)(1500+373) = 230\ \mathrm{W/m^2}K$$

The effective heat transfer coefficient is then

$$h_{c,eff} = h_{c0} + h_{rad} = 1250 + 230 = 1480\ \mathrm{W/m^2K}$$

The specific heat of dry wood is c_{pdf} = 1000 J/kgK, and for water c_{pw} = 4180 J/kgK. The heat of vaporisation is 2400 kJ/kg. The masses of dry wood and water are

$$m_{df} = \frac{\pi d^3}{6}\rho_p = \frac{\pi\left(100\times10^{-6}\right)^3 690}{6} = 3.61\times10^{-10}$$
$$m_m = 0.4\times3.61\times10^{-10} = 1.44\times10^{-10}$$

and the surface area of the particle is

$$A = \pi\times\left(100\times10^{-6}\right)^2 = 3.14\times10^{-8}$$

Evaluating Eq. 5.16 for the drying time,

$$t_{dry} = t_1 + t_2 = 1.3\times10^{-3} + 6.6\times10^{-3} = 7.9\times10^{-3}$$

so that t_{dry} = 7.9 ms

While 7.9 ms may seem to be a relatively short time, but if, for example, an oil-fired burner is converted to a burner using sawdust, the distance traveled while drying before ignition would be 7.9 cm if the velocity is 10 m/s. This could create difficulties in trying to stabilize the flame, and thus the fuel should be dried before being fed to the burner.

DEVOLATILISATION OF SOLID FUELS

When the drying of a small fuel particle or a zone within a large particle is completed, the temperature rises and the solid fuel begins to decompose, releasing volatiles. This decomposition is called pyrolysis if oxygen is absent and devolatilisation if oxygen is present

in the surrounding. Since the volatiles flow out of the solid through the pores, external oxygen cannot penetrate into the particle, and hence the devolatilisation is often referred to as the pyrolysis stage. The rate of devolatilisation and the formation of pyrolysis products depend on the temperature and the type of fuel. The pyrolysis products ignite and form an attached flame around the particle while oxygen diffuses into the products. This consumes all oxygen before it reaches the particle surface and prohibit char combustion. The flame in its turn heats the particle, causing enhanced devolatilisation.

For wood, the hemicellulose pyrolyses at 225-325°C, the cellulose at 325- 375°C, and the lignin at 300-500°C. Certain extractives such as terpenes, which amount to only a few percent of the wood, escape at less than 225°C. Various hydrocarbon vapours, liquids (if condensed), and tars (if condensed) and water are formed and quickly broken down under combustion conditions provided that the temperature is sufficiently high so that the pyrolysis products in a combustion environment may be considered to be short-chained hydrocarbons, carbon dioxide, carbon monoxide, hydrogen, and water vapour. The exact composition is a function of the heating rate. A model, which can be used to estimate the composition of the volatile products, is presented below in the section 'composition of volatile gases leaving during devolatilisation'.

For lignite coals, pyrolysis begins at 300-400°C releasing CO and CO_2. Ignition of the volatiles occurs at 400-600°C. Carbon monoxide, carbon dioxide, water, hydrocarbon vapours, tars, and hydrogen are produced rapidly as the temperature reaches 700-900°C. Above 900°C pyrolysis is essentially complete, and char (fixed carbon) and ash remain.

The devolatilisation of bituminous coal proceeds differently from lignite because bituminous coal contains less oxygen than lignite. First the bituminous coal becomes plastic and some of coals swell markedly. Pressure within the particle builds up, and tars are squeezed out of the particle. Fracture of the coal particle into several pieces may occur due to the internal pressure. Meanwhile, pyrolysis proceeds, releasing carbon monoxide, hydrocarbons, and soot, which burn in an attached diffusion flame around the particle.

The simplest way to approximate the rate of devolatilisation of a solid fuel is by a first order global reaction:

$$\frac{dm_v}{dt} = -m_v R_v \qquad (5.19)$$

where the rate "constant" is $R_v = k_{rv,0} \exp(-E/\Re T_p)$, and where v refers to volatiles and $m_v = m - m_c - m_a$ (i.e., the mass of the volatiles equals the mass of the dry particle minus the masses of the char and ash). Equation 5.19 implies that a single chemical reaction converts the solid fuel to pyrolysis products. In reality, solid fuels, such as wood and coal are complex compounds, which undergo many reactions when they are heated and they should consequently be represented by a number of rate equations with there respective m_v and $k_{rv,0}$. Some of these reactions are endothermic and some are exothermic, and they proceed at different rates. Nevertheless, the net heat of devolatilisation is thought to be near zero. Despite the simplicity of Eq 5.19 it gives a useful approximate global pyrolysis rate, where the two constants used must be determined experimentally for specific combustion conditions and fuel type. Representative values of these constants are given for various fuels in Table 5.2.

For pulverised wood fuels with a low heating rate compared to the rate of devolatilisation, the Biot number is small, $Bi_{th} << 1$. This means that the temperature raise of these small particles controls the rate of the devolatilisation. For wood more or less all volatiles are released before 500°C. The heating of the particle is described by the heat

transferred from the surroundings to the surface of the particle and the heat needed for the devolatilisation, H_v, is a small value, often put to zero.

Table 5.2. Representative one-equation pyrolysis parameters for three solid fuels.

Fuel	$k_{rv,0}$ (1/s)	$E/\Re$ (K)
Bituminous coal	**280**	**5940**
Lignite	**700**	**5690**
Wood	**1.9×10^{12}**	**21500**

$$\frac{\partial\left(m_v c_{pv} + m_c c_{pc} + m_a c_{pa}\right)T}{\partial t} = Ah_{c,eff}\left(T_\infty - T\right) + \frac{dm_v}{dt} H_v \qquad (5.20)$$

The amount of char remaining after devolatilisation depends on fuel and heating rate. The volatile content of the fuel analysis is the quantity obtained under standard conditions of the analysis and this could differ slightly from what is actually obtained in an actual application. However, significantly higher volatiles yield, than the one given by the standard analysis, is obtained for fuels exposed for high heating rates, such as in pulverised flames. Volatile yields of 90% for pulverised wood and 50% for pulverised coal are typical. To evaluate if the devolatilisation is limited by heating of the particle or by kinetics a dimensionless number is used, the Damköler number Da, also referred to as the external pyrolysis number Py. This number compares the heating rate with the rate of the kinetics and is defined as

$$\frac{1}{Da} = Py = \frac{Ah_{c,eff}}{V\rho_{df} c_{pdf}} \frac{1}{k_{rv,0}\exp(-E/(\Re T_\infty))} \qquad (5.21)$$

where the effective heat transfer coefficient is calculated for a surface temperature equal to the evaporation temperature and the rate of devolatilisation is calculated for the surrounding temperature T_∞. If Da << 1 the process is controlled by the kinetics and if Da >> 1 it is controlled by the heating rate. If the kinetics limits the rate of pyrolysis Da << 1, as often is the case for coal powder, the particle attains the surrounding temperature before the major part of the volatiles has left the particle. Then the kinetic rate can be estimated by the rate corresponding to the temperature of the surroundings and the time needed for the pyrolysis is obtained by integrating Eq. 9.11 for a constant rate.

$$t_v = -\ln\left[\frac{m - m_c - m_a}{m_{df} - m_c - m_a}\right] / R_v \qquad (5.22)$$

where m without subscript is the mass of the converting particle. If the time of devolatilisation is limited by the heating rate, Da >> 1, it can be estimated as the time required to heat the particle to a given devolatilisation temperature T_v by integrating Eq (5.20)

$$t_v \approx -\frac{m_{df} c_{pdf}}{A h_{c,eff}} \ln\left(\frac{T_\infty - T_v}{T_\infty - T_0}\right) \qquad (5.23)$$

The devolatilisation temperature T_v can be estimated as the temperature when the Damköler number is unity, which means that the heating rate is equal to the rate of devolatilisation

$$T_v \approx \left(-\ln\left(\frac{A h_{c,eff}}{V \rho_{df} c_{pdf} k_{rv,0}}\right)\frac{\Re}{E}\right)^{-1} \qquad (5.24)$$

EXAMPLE 5.2. The oak particle in example 5.1 is devolatilised in the same surrounding (1500 K). Compare the time needed for heating of the particle with the time to release 99% of the volatile mass due to the kinetic rate.

Solution.
Assuming that the effective heat coefficient, as well as all ingoing properties is same as the one in example 5.1:

Effective heat transfer coefficient: 1480 W/m^{2}K
Specific heat of particle: 1000 J/kg K
Surface area of particle: 3.14×10^{-8} m^2
Dry mass of particle: 3.61×10^{-10} kg
Devolatilisation temperature

$$T_v \approx \left(-\ln\left(\frac{3.14\times10^{-8}\times1480}{3.61\times10^{-10}\times1000\times1.9\times10^{12}}\right)\frac{1}{21500}\right)^{-1} = 918 \text{ K}$$

The time to heat up the particle to 645°C or 918 K is then

$$t_v \approx -\frac{3.61\times10^{-10}\times1000}{3.14\times10^{-8}\times1480}\times\ln\left(\frac{1500-918}{1500-373}\right) = 4 \text{ ms}$$

The corresponding time of devolatilisation if the devolatilisation is limited by the kinetics is:
From Table 9.1, $k_{rv0} = 1.9\times10^{12}$ s^{-1} and $E / \Re = 21500$ K. Thus,

$$R_v = 1.9\times10^{12} \exp\left[-\frac{21500}{1500}\right] = 1.13\times10^{6}\ s^{-1}$$

From Eq. 9.14,

$$t_v = \frac{-\ln(1-0.99)}{1.13\times10^{6}} = 4\times10^{-6}\ s$$

$t_v \approx 0.004$ ms

This shows that in present case the heating of the particle is limiting the rate of devolatilisation. At a lower surrounding temperature and for coal the result may be the opposite.

COMPOSITION OF GASES LEAVING DURING DEVOLATILISATION

Devolatilisation is a complex thermal process; breaking the solid fuel down thermally into a large number of different species, see Fig 5.5, which in their turn break down further by cracking of long hydrocarbons to an even greater number of species. This is difficult to model, as the formation and release of a great number of species have to be described, together with the heating of the particle, the structural change within the particle, as well as the gas flow and the reactions of the pyrolysis gases within the particle. The degree of complexity of devolatilization makes it very time consuming to obtain a solution from a model, which includes all effects described above, even if the model concerns only a single particle. In a large combustion system a refined

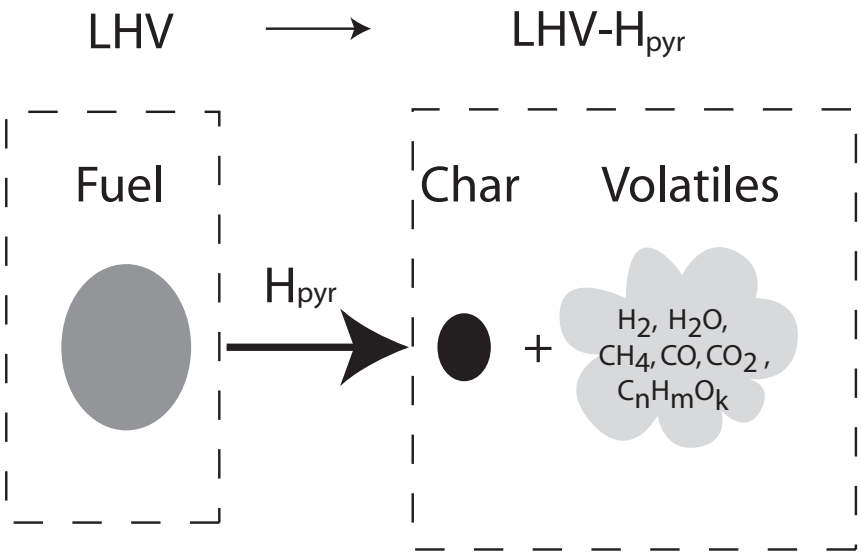

Figure 5.5.
Devolatilisation of a fuel particle

description of the release of volatile species is more or less impossible, as a great number of particles have to be considered simultaneously, and the description of the devolatilisation is only one of many submodels. Therefore, considerable simplifications have to be made to get around the complexity of the problem. One solution presented by Thunman et al. Energy & Fuels 2001. 15:1488-1497 is to locate the system boundary of the model at the surface of the particle. By doing so, the processes inside the particle are treated as a black box, only the gases flowing out from the particle have to be estimated, and this can be done from energy, mass and species balances over the particle, where the conservation equations are reduced to the source terms related to the reactions.

The combustible part of a fuel consists mainly of carbon, hydrogen and oxygen. For example, the combustible part of wood typically consists of 50% C, 44 % O_2 and 6% H_2.The lower heating value of dry wood is around 18.5 MJ/kg and the ash content around 0.5%, which makes the lower heating value of the combustible part of the dry fuel to be around 18.6 MJ/kg_{wood}. In combustion systems, the char residue from wood is around 20% (on dry ash-free basis), consisting of nearly pure carbon. The heating value of this char is around 33 MJ/kg char. To devolatilize the fuel, approximately 0.2 MJ/kg is needed (heat of pyrolysis). The heating value of the pyrolysis gases can thereby be calculated,

$$H_{vol} = \frac{(18.6 - 0.2 - 0.2 \times 33)}{1 - 0.2} = 14.75\ MJ / kg\ volatiles \quad (5.25)$$

The pyrolysis gases contain 6 main species or groups of species; carbon monoxide, carbon dioxide, water, hydrogen, light and heavy hydrocarbons. Light hydrocarbons are defined as non-condensable hydrocarbons at ambient temperature. These hydrocarbons are mainly methane and ethylene; with approximately 3 times more methane than ethylene. This results in an equivalent light hydrocarbon molecule $C_{1.15}H_4$ with a heating value of 49.4 MJ/kg. The heavy hydrocarbons, those condensed to tar or liquids at ambient temperature, are cracked to more stable hydrocarbons, such as benzene, naphthalene and toluene at the temperatures of a combustion system. A rough estimate used, here, of the composition of the heavy hydrocarbons can be expressed as $C_6H_{6.2}O_{0.2}$, with a lower heating value of 37 MJ/kg. This value corresponds to the longer hydrocarbons leaving in a high temperature surrounding.

If the devolatilisation occurs at a lower temperature more oxygen will be present and the heating value drops and can in extreme be as low as 24 MJ/kg. With the assumptions made above, the energy balance of the volatiles reads,

$$Y_{CO}H_{CO} + Y_{CO_2}H_{CO_2} + Y_{H_2O}H_{H_2O} + Y_{H_2}H_{H_2} + \\ + Y_{C_iH_j}H_{C_iH_j} + Y_{C_mH_nO_n}H_{C_mH_nO_k} = H_{vol} \tag{5.25}$$

or with the values presented above

$$Y_{CO}10.25 + 0 + 0 + Y_{H_2}120 + Y_{C_iH_j}49.4 + Y_{C_mH_nO_k}37 = 14.75 \tag{5.26}$$

where

$$Y_{CO} + Y_{CO_2} + Y_{H_2O} + Y_{H_2} + Y_{C_iH_j} + Y_{C_mH_nO_k} = 1 \tag{5.27}$$

Species balances can be made for C, H_2 and O_2.

For elemental carbon C, this is the sum of the carbon in the volatile species and in the char residue,

$$Y_{CO}\frac{M_C}{M_{CO}} + Y_{CO_2}\frac{M_C}{M_{CO_2}} + \\ + Y_{C_iH_j}\frac{M_{C_i}}{M_{C_iH_j}} + Y_{C_mH_nO_k}\frac{M_{C_m}}{M_{C_mH_nO_k}} = \frac{Y_{C,0} - Y_{char}}{1 - Y_{char}} \tag{5.28}$$

or

$$Y_{CO}0.429 + Y_{CO_2}0.273 + Y_{C_iH_j}0.775 + Y_{C_mH_nO_k}0.885 = \frac{0.5 - 0.2}{1 - 0.2} \tag{5.29}$$

for elemental hydrogen H_2

$$Y_{H_2O}\frac{M_{H_2}}{M_{H_2O}} + Y_{H_2} + Y_{C_iH_j}\frac{M_{H_j}}{M_{C_iH_j}} + Y_{C_mH_nO_k}\frac{M_{H_n}}{M_{C_mH_nO_k}} = \frac{Y_{H_2,0}}{1 - Y_{char}} \tag{5.30}$$

or

$$Y_{H_2O}0.111 + Y_{H_2} + Y_{C_iH_j}0.225 + Y_{C_mH_nO_k}0.076 = 0.075 \tag{5.31}$$

and for elemental oxygen O_2

$$Y_{CO}\frac{M_O}{M_{CO}} + Y_{CO_2}\frac{M_{O_2}}{M_{CO_2}} + Y_{H_2O}\frac{M_O}{M_{H_2O}} + Y_{C_mH_nO_k}\frac{M_{O_k}}{M_{C_mH_nO_k}} = \frac{Y_{O_2,0}}{1 - Y_{char}} \tag{5.32}$$

or

$$Y_{CO}\,0.571 + Y_{CO_2}\,0.727 + Y_{H_2O}\,0.889 + Y_{C_mH_nO_k}\,0.04 = 0.55 \tag{5.33}$$

The balances provide four equations, but there are six unknowns. This means that there is a need for two additional equations to solve for the composition of the system. Measurements with conventional gas analysers make it possible to derive these two equations as the ratios of CO to CO_2 and C_iH_j to CO_2. From measurements in a laboratory fluidized bed at 850°C, with an inert atmosphere, the molecular ratio of CO to CO_2 is around 3 and of C_iH_j to CO_2 is around 1.5. These ratios are to be taken as an example, because they were obtained under specific conditions. The two additional equations then become,

$$Y_{CO} - Y_{CO_2}\,3\frac{M_{CO}}{M_{CO_2}} = 0 \tag{5.34}$$

and

$$Y_{C_iH_j} - Y_{CO_2}\,1.5\frac{M_{C_iH_j}}{M_{CO_2}} = 0 \tag{5.35}$$

The system of equations can be summarised in a matrix form

$$\begin{bmatrix} 10.25 & 0 & 0 & 120 & 49.4 & 37 \\ 0.429 & 0.273 & 0 & 0 & 0.775 & 0.885 \\ 0 & 0 & 0.111 & 1 & 0.225 & 0.075 \\ 0.571 & 0.727 & 0.889 & 0 & 0 & 0.04 \\ 1 & -1.9 & 0 & 0 & 0 & 0 \\ 0 & -0.61 & 0 & 0 & 1 & 0 \end{bmatrix} \begin{bmatrix} Y_{CO} \\ Y_{CO_2} \\ Y_{H_2O} \\ Y_{H_2} \\ Y_{C_iH_j} \\ Y_{C_nH_mO_k} \end{bmatrix} = \begin{bmatrix} 14.75 \\ 0.375 \\ 0.075 \\ 0.55 \\ 0 \\ 0 \end{bmatrix} \tag{5.36}$$

The solution of the system of equations for the given example, a wood with a typical composition inserted into a fluidised bed at 850°C, gives the following composition of the volatiles,

$$\begin{aligned} Y_{CO} &= 0.361 \\ Y_{CO_2} &= 0.190 \\ Y_{H_2O} &= 0.227 \\ Y_{H_2} &= 0.017 \\ Y_{C_iH_j} &= 0.116 \\ Y_{C_nH_mO_k} &= 0.089 \end{aligned} \tag{5.37}$$

This derivation is an example of a zero-order model that can be useful in combustion models for solid fuels, even if there is a weakness in the present formulation in the sense that the two empirical coefficients are not known for more than one combustion situation.

SUMMARY

Solid fuel particles (pulverised, crushed, chipped, or cut) in a combustion environment undergo drying, devolatilisation, and char combustion. The rate of these processes depends on fuel type, fuel moisture content, size, and heat and mass transfer to the particle. For small particles, drying, devolatilisation, and char combustion occur in sequence, whereas for large particles these processes occur simultaneously but in different locations in the particle. For small particles drying is the fastest step, and char combustion takes much longer time than devolatilisation. For large fuel entities such as logs, char combustion is the rate-limiting step. Devolatilisation is a kinetic process which is often modelled as a first-order reaction in simplified representations to be included in comprehensive models. The volatiles contain H_2, CO, CO_2, H_2O, hydrocarbon gases, and condensable hydrocarbons (tar) which mix with oxygen and burn out in the gas phase.

REFERENCES

1. Bird, R.B., Stewart, W.E., and Lightfoot, E.N., "Transport Phenomena", John Wiley & Sons Inc., New York, 1960.

CHAPTER 6

DRYING AND DEVOLATILISATION OF THERMALLY LARGE PARTICLES

SIMULTANEOUS DRYING AND DEVOLATILISATION

For relatively large fuel particles, with drying number around unity or higher, such as for coal and wood chips used on a grate, the whole particle will not attain the same temperature in each time step. Instead a temperature gradient will be present within the particle; moisture is evolved from the inside of the particle, while volatiles are being driven off near the outer shell of the particle. Due to the high pressure in the fuel's pores during devolatilisation of the outer layer of the particle, some of the moisture is forced toward the centre of the particle where it condenses while the pressure builds up throughout the particle. Hence, drying of large solid fuel particles initially involves inward migration of water vapour as well as an outward flow. A pyrolysis layer starts at the outer edge of the particle and gradually moves inwards, releasing volatiles and forming char. The release of moisture reduces the heat and mass transfer from the surrounding to the surface of the particle so that the mass loss of the particle (the burning rate) is reduced. While the moisture and volatile release is reduced, the char surface begins to react. For even larger fuel particles, such as a wood log burning in a campfire, a fireplace, or a fixed bed, drying, pyrolysis, and char conversion occur simultaneously until most of the mass is consumed, at which point only char remains. Figure 6.1 shows the three zones of a partially reacted log. The outside char layer is black and porous. The pyrolysis zone is a thin brown layer, and the interior portion of the log is white, moist wood with a temperature of less than 100°C even though the outside of the log is very

hot. The moisture impedes the inward conduction of heat, and some moisture is retained during almost the entire conversion. For short wood logs, some moisture escapes out of the ends of the log during combustion, while for long logs some moisture remains until 99% of the initial mass of the log is consumed.

For engineering applications the time of drying and devolatilisation of these larger pieces of fuel is often given by a simple empirical correlation with two constants a_1 and a_2, which are fitted to experimental results, together with the characteristic diameter of the fuel particle

$$t = a_1 d_{car}^{a_2} \tag{6.1}$$

The constants have some physical meaning as can be seen from the derivation of the time of drying and devolatilisation of thermally small particles above, and from the derivation of thermally large particles below. The first constant, a_1, is related to the specific fuel and the second constant, a_2, is related to the physical process. From the analysis of thermally small particles it can be seen that a_2 approaches unity if the process is limited by the thermal process ($t \propto V / A \propto d$). If on the other hand the process is controlled by the kinetics of the devolatilisation a_2 approaches zero and the time for devolatilisation is calculated by integrating Eq 5.19. For thermally large particles a_2 approaches two as will be shown below. These numbers are approximate because other processes are also present such as swelling or shrinkage of the particles, temperature dependence of the physical data and convective flows within the fuel particles. However, for most fuels in combustion or gasification devices the constant a_2 ends up in the region 1.5 to 2.

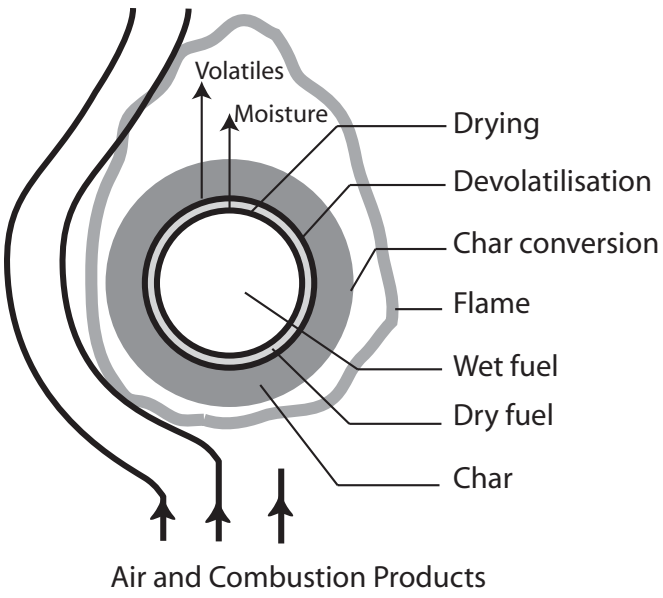

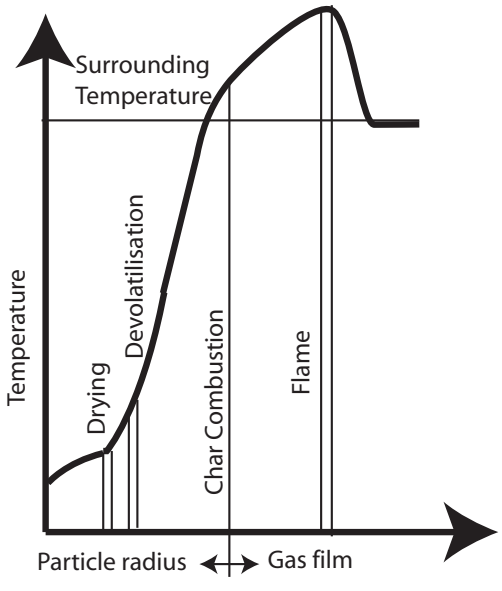

Figure 6.1.
Cross section of reacting log showing char, pyrolysis, and undisturbed wood regions

In most practical application the volatile gases leaving a fuel particle ignite, if oxygen is present, and form a flame around the fuel particle during devolatilisation. However, if the heating of the particle is slow or if oxygen is absent, ignition will not occur. The fixed carbon (char) on the surface of the fuel can also ignite. Which mechanism actually occurs first depends on the rate of convective and radiative heat transfer to the particle. If the radiative heat transfer is high so that the surface quickly heats up to the ignition temperature of the carbon, or if the rate of convective heating is high so that the surface rapidly heats up but the volatiles are swept away before a combustible mixture can accumulate, the ignition will occur first at the surface. On the other hand, if surface heating is low, then the volatiles may ignite first, since they have a lower ignition temperature than carbon. If the purpose is to gasify the solid fuel, and not to complete the combustion, such as in a gasifiers (or devolatilisers), then only enough oxygen is provided to generate the heat needed for drying and pyrolysis of the particle by exothermic reactions.

Ignition temperatures of various fuels are shown in Table 6.1. Note that char has a much lower ignition temperature than graphite. This implies that char is not pure carbon, and in fact char contains some hydrogen as well as carbon. Pyrolysis under the usual combustion conditions does not drive off all of the hydrogen. Note that wood char ignites at a lower temperature than coal char. Similarly, volatiles from wood ignite at a lower temperature than volatiles from coal. The temperature of the flame formed around the particle depends on the heating value of the gas leaving the particle. Consequently, the flame temperature is lower and the flame weaker as long as water vapour from the drying is flowing out of the pores. Once all the moisture is driven off from the particle, the flame temperature will rise.

Table 6.1. Typical ignition temperature of selected solid fuels.

Fuel	Ignition Temperature (K)
Graphite	1090
Bituminous coal char	680
Bituminous coal volatiles	620
Wood char	610
Wood volatiles	530
Peat	500

AN ANALYTIC MODEL FOR SIMULTANEOUS DRYING AND DEVOLATILISATION OF LARGE PARTICLES

For a large particle in a hot surrounding, having a high drying number, the time of drying and devolatilisation can be estimated by a simplified analytical solution. The analysis presented below is carried out for one-dimensional geometries where the thermal conductivity is assumed to be the same for the dry fuel as for the char. However, the analysis can be expanded to two or three dimensions and for different thermal conductivities in different zones, as well as in different directions. In the present case the temperature of the particle surface can be assumed to attain the evaporation temperature as soon as it enters the combustor or gasifier. With this assumption the rate of evaporation, based on mass flow $\dot{m}_g$, is determined by the rate at which heat is transported to the evaporation front within the particle:

$$\dot{m}_g = \frac{c_1 r_m^n k_c}{H_{m,eff}} \left.\frac{\partial T}{\partial r}\right|_{r_m} \tag{6.2}$$

where r_m is the position of the evaporation front, $c_1 r^n$ area of a shell at the co-ordinate r and particle shape n ($c_1 = 1$ and $n = 0$ for a infinite plate per unit area, $c_1 = 2\pi$ and $n = 1$ for an infinite cylinder per unit length and, $c_1 = 4\pi$ and $n = 2$ for a sphere), k_c is the thermal conductivity of the dry solid, $H_{m,eff}$ is here the heat of vaporisation plus the energy needed to heat up the moist particle from the initial temperature to the evaporation temperature per unit mass of moisture, and T is temperature. The position of the evaporation front r_m, the size of the wet core, can be evaluated from the geometry of the particle

$$r_m = X_m^{1/(1+n)} r_0 \tag{6.3}$$

where r_0 is the radius or thickness of the particle and X_m is the remaining moisture content divided by the initial moisture content. For a comparison of the rate of evaporation with the rate of devolatilisation, it is preferable to write the rate of evaporation as the relative release rate

$$R_m = \dot{m}_g / m_{m0} = \dot{m}_g /(Y_m V_0 \rho_{df} /(1 - Y_m)) \tag{6.4}$$

where m_{m0} is the initial mass of moisture in the particle, Y_m is the mass fraction of moisture in the fuel as received, ρ_{df} the dry density of the fuel and V_0 is the initial volume. The initial volume of the particle is

$$V_0 = \int_0^{r_0} c_1 r^n \, dr = c_1 r_0^{n+1} /(n+1) \tag{6.5}$$

To determine the rate of evaporation, the temperature gradient at the evaporation front (Eq. 6.2) is needed. Evaporation is very endothermic and the temperature profile between the evaporation front and the surface of the particle is therefore close to steady state at all times in a moist particle. For a fuel particle with lower moisture content it become somewhat less steep. If the moisture content of the fuel is very low the heat of evaporation is of the same magnitude as the energy needed to heat up the fuel particles. The present analysis is not applicable when ($Y_m H_{m,eff}$ / (c_{pdf}(T_m - T_0)) < 1 as the evaporation does not dominate the heating of the particle (T_m is the evaporation temperature, T_0 initial temperature and c_{pdf} is the specific heat of the solid). In the general case, the steady state solution gives the highest possible surface temperature and the largest possible temperature gradient at the evaporation front. The steady state temperature profile between the evaporation front and the surface of the particle is obtained from the heat transfer equation:

$$\frac{1}{r^n}\frac{\partial}{\partial r}\left(r^n k_c \frac{\partial T}{\partial r}\right) - \frac{1}{r^n}\frac{\partial}{\partial r}\left(r^n u_g \rho_g c_{pg} T\right) = 0 \tag{6.6}$$

where T is temperature, with the boundary condition at the surface, $r = r_0$,

$$-k_c \left.\frac{\partial T}{\partial r}\right|_{r_0} = h_{eff}\left(T_{r_0} - T_\infty\right) \tag{6.7}$$

and at the evaporation front, $r = r_m$,

$$T\big|_{r_m} = T_m \tag{6.8}$$

where u_g is the flow-rate of vapour leaving the particle, ρ_g the density of the vapour, c_{pg} the specific heat of the vapour, h_{eff} the effective heat transfer coefficient and T_∞ the ambient temperature. The temperature at which evaporation occurs is the equilibrium temperature of the vapour at the evaporation front. This temperature can be determined from a simultaneous solution of the mass and heat transfer equations, analogous to the description of evaporation of a liquid droplet. However, at surrounding temperatures which are considerably above the saturation temperature (373 K at ambient conditions), the evaporation temperature approaches the saturation temperature. In moist fuels most of the water is free, but water can also be bound in the structure of the fuel. In most cases the bound water is released at a temperature slightly above the saturation temperature. If the moisture in the fuel is known to be bound, an evaporation temperature that is higher than the saturation temperature can be introduced into the analysis.

The convective mass flow of vapour outwards through the particle per unit area in Eq. (6.6) can be expressed by the rate of evaporation based on mass, Eq. (6.2),

$$r^n u_g \rho_g = \frac{r_m^n k_c}{H_{m,eff}} \frac{\partial T}{\partial r}\bigg|_{r_m} \tag{6.9}$$

Inserting Eq. (6.9) into Eq. (6.6), introducing a dimensionless length $\xi = r / r_0$ and a dimensionless temperature $\theta = (T - T_\infty)/(T_m - T_\infty)$, and defining a dimensionless position of the evaporation front, $\xi_m = X_m^{1/(1+n)}$, Eq. (6.6) can be rewritten as:

$$\frac{1}{\xi^n}\frac{\partial}{\partial \xi}\left(\xi^n \frac{\partial \theta}{\partial x}\right) + \frac{\xi_m^n c_{pg}\left(T_\infty - T_m\right)}{H_{m,eff}} \frac{\partial \theta}{\partial \xi}\bigg|_{\xi_m} \frac{1}{\xi^n}\frac{\partial \theta}{\partial \xi} = 0 \tag{6.10}$$

To make the representation more concise two constants are introduced: α is basically the ratio of the enthalpy required to rise the temperature of the water vapour from the evaporation temperature to the ambient temperature and the heat of evaporation; β expresses the dimensionless temperature gradient at the evaporation front,

$$\alpha = \xi_m^n c_{pg} \left(T_\infty - T_m\right) / H_{m,eff} \tag{6.11}$$

$$\beta = \left.\frac{\partial\theta}{\partial\xi}\right|_{\xi_m} \tag{6.12}$$

Inserting these expressions into Eq. (6.10) yields

$$\frac{1}{\xi^n}\frac{\partial}{\partial\xi}\left(\xi^n \frac{\partial\theta}{\partial\xi}\right) + \alpha\beta \frac{1}{\xi^n}\frac{\partial\theta}{\partial\xi} = 0 \tag{6.13}$$

This equation, the final form of Eq. (6.6), should be solved together with the dimensionless boundary conditions (from Eqs. (6.7) and (6.8)) at the particle's surface, $\xi = 1$,

$$-\left.\frac{\partial\theta}{\partial\xi}\right|_1 = \mathrm{Bi_t}\,\theta|_1 \tag{6.14}$$

and at the evaporation front, $\xi = \xi_m$,

$$\theta|_{\xi_m} = 1 \tag{6.15}$$

where $\mathrm{Bi_t}$ is the thermal Biot number ($h_{eff}\, r_0 / k_c$). The general analytical solution of Eq. (6.13) and its boundary conditions are shown as Eq. (6.16) in Table 6.2, together with the dimensionless temperature gradient at the evaporation front, Eq. (6.17), and the dimensionless surface temperature, Eq. (6.18). The special case when the thermal influence of the volatile gases leaving the particle is small, $\alpha\beta \to 0$ in Eq (6.13), Eqs. (6.19-6.21), is also given in Table 6.2. The simplified formulation of $\alpha\beta \to 0$ in Eq. (6.13), if it can be used, facilitates the analysis significantly, since no iterative calculation is needed to determine the dimensionless temperature gradient.

The rate of evaporation, Eq. (6.4), can now be expressed in dimensionless quantities,

$$R_m = -\frac{(n+1)}{r_0^2}\frac{(1-Y_m)}{Y_m}\frac{c_{ps}}{c_{pg}} a_s \alpha\beta \tag{6.22}$$

Table 6.2. Solution of Eq. (6.13) with the boundary conditions Eqs. (6.14) and (6.15). $\Gamma[\xi] = (1-\xi)$ when n = 0 (plate), $\Gamma[\xi] = -\ln(\xi)$ when n = 1 (cylinder), $\Gamma[\xi] = (1/\xi - 1)$ when n = 2 (sphere)

General solution		Solution when $\alpha\beta \to 0$ in Eq. (6.13)	
$\theta = \dfrac{\alpha\beta + \mathrm{Bi_t}\left(\exp(\alpha\beta\Gamma[\xi]) - 1\right)}{\alpha\beta + \mathrm{Bi_t}\left(\exp(\alpha\beta\Gamma[\xi_m]) - 1\right)}$	(6.16)	$\theta = \dfrac{1 + \mathrm{Bi_t}\Gamma[\xi]}{1 + \mathrm{Bi_t}\Gamma[\xi_m]}$	(6.19)
Temperature gradient at evaporation front			
$\beta = -\dfrac{\alpha\beta\,\mathrm{Bi_t}\exp(\alpha\beta\,\Gamma[\xi_e])}{\xi_m^n\left(\alpha\beta + \mathrm{Bi_t}\left(\exp(\alpha\beta\,\Gamma[\xi_m]) - 1\right)\right)}$	(6.17)	$\beta = -\dfrac{\mathrm{Bi_t}}{\xi_m^n\left(1 + \mathrm{Bi}_t\Gamma[\xi_m]\right)}$	(6.20)
Surface temperature			
$\theta_{\xi=1} = \dfrac{\alpha\beta}{\alpha\beta + \mathrm{Bi_t}\left(\exp(\alpha\beta\,\Gamma[\xi_m]) - 1\right)}$	(6.18)	$\theta_{\xi=1} = \dfrac{1}{1 + \mathrm{Bi_t}\Gamma[\xi_m]}$	(6.21)

where a_s is the thermal diffusivity.

By integrating the rate of evaporation Eq. (6.4) the time to dry the particle from initial, $X_m = 1$, to a specified, $X_m = X_{m0}$, moisture content is obtained

$$t = \int_1^{X_{m0}} -R_m^{-1} dX_m \tag{6.23}$$

If the effect of the outflow of gases is negligible and average data are given for the physical properties, including the effective heat transfer coefficient Eqs (6.19)-(6.21) can be used. The drying time, Eq 6.23, is then given by an analytical solution

$$t = \tau\, f[X_{m0}] \tag{6.24}$$

where τ is the time constant for the fuel particle extracted from Eq. (6.22)

$$\tau = \frac{Y_m}{1 - Y_m} r_0^2 \frac{\rho_{df}}{k_{c,df}} \frac{H_{m,eff}}{(T_\infty - T_m)} \tag{6.25}$$

and the function $f[X_m]$ is the dimensionless time, which is the solution of Eq (6.23) divided by the time constant Eq (6.25)

Table 6.4 a_1 and a_2 in Eq (6.26) for different shapes

Particle shape	a_1	a_2
Infinite plate n = 0	$2(1+Bi)$	$-X_m{}^2$
Infinite cylinder n = 1	$(2+Bi)$	$-2X_m \ln(X_m^{1/2})$
Sphere n = 2	$2(1-Bi)$	$3X_m^{2/3}$

$$f[X_m] = \frac{2 + Bi_t - (a_1 X_m + a_2 Bi_t)}{2(n+1)Bi_t} \tag{6.26}$$

where a_1 and a_2 contain the information for the three general geometries as shown in Table 6.4. When all moisture is released from the particle $X_m \to 0$ the dimensionless time for the particle shapes considered become,

$$f(X_m \to 0) \to \frac{2 + Bi_t}{2(n+1)Bi_t} \tag{6.27}$$

This implies, as said before, that physical data are constant.

Looking at Eq 6.27, one can see that the dimensionless time will be a direct function of the Biot number, which is the same number as defining if the particle is thermally large or small. A relevant question, here, is how the derived model would work for thermally small particles? To investigate this we investigate Eq 6.24 when $X_m \to 0$

$$t = \tau f[X_{m0} \to 0] = \frac{Y_m}{1-Y_m} r_0^2 \frac{\rho_{df}}{k_{c,df}} \frac{H_{m,eff}}{(T_\infty - T_m)} \frac{2 + Bi_t}{2(n+1)Bi_t} \tag{6.28}$$

for the case when r $\to$ 0, which means that $Bi_t \to 0$. Start by replacing the Biot number with its physical properties

$$t[r \to 0] = \frac{Y_m}{1-Y_m} r_0^2 \frac{\rho_{df}}{k_{c,df}} \frac{H_{m,eff}}{T_\infty - T_m} \frac{\overbrace{2 + r_0 h_{c,eff}/k_{c,df}}^{\approx 2 \, when \, r \to 0}}{2(n+1) r_0 h_{c,eff}/k_{c,df}} \tag{6.29}$$

This can be rewritten as

$$t[r \to 0] = \frac{Y_m}{1-Y_m} \rho_{df} H_{m,eff} \frac{r_0}{(n+1)} \frac{1}{h_{c,eff}(T_\infty - T_m)} \tag{6.30}$$

where, $r_0/(n+1)$ is identified as V/A

$$t[r \to 0] = \frac{Y_m}{1-Y_m} \rho_{df} V H_{m,eff} \frac{1}{A h_{c,eff}(T_\infty - T_m)} \tag{6.31}$$

The equation is now reduced down to two parts where the first represent heat needed to evaporate the moisture and the second represent the Heat transported to the particle for the evaporation.

$$t[r \to 0] = \frac{\frac{Y_m}{1-Y_m} \rho_{df} V H_{m,eff}}{A h_{c,eff}(T_\infty - T_m)} = \frac{m_m H_{m,eff}}{q} \tag{6.32}$$

The final result is then the same as 5.11 derived for a thermally small particle in Chapter 5. The heating of the moisture to the temperature of evaporisation is included in the effective heat of evaporation. This means that the model is valid for all particle sizes for drying and devolatilisation, if the time for devolatilisation is much shorter than the time for drying, i.e. have a moisture content above ~ 10 %.

From the model the time dependent release of volatiles can be given. The bases for the analysis is based on a situation where the surrounding temperature is much higher than the evaporation temperature, which means that the devolatilisation is likely to start before the drying is completed. Due to the very endothermic drying process it is reasonable to assume that the rate of devolatilisation is limited by the propagation of the drying front. If we now assume that the thermal conductivity of the char is approximately the same as the one of the dry fuel and that all volatiles remaining at the end of drying is rapidly released as soon as the drying is completed and no heat sink remains. It is further assumed that the devolatilisation takes place in a narrow front analogous to the drying and that the heat of devolatilisation is negligible. Of course, the devolatilisation takes place in a wider temperature range than the drying front, but this range is narrow enough for the present analysis. However, the temperature of devolatilisation will be found in a temperature range and not at a given temperature as for drying. To estimate the temperature of which devolatilisation starts at the

surface of the particle, we assume that this temperature correspond to the temperature when the rate of devolatilisation Eq. (5.19) is the same as the rate of evaporation Eq. (6.22).

$$R_m = R_v$$

$$-\frac{(n+1)}{r_0^2}\frac{(1-Y_m)}{Y_m}\frac{c_{ps}}{c_{pg}} a_s \alpha\beta = k_{rv0} \exp\left(-E/(\Re(\theta_{\xi=1}T_m + (1-\theta_{\xi=1})T_\infty))\right) \tag{6.33}$$

or

$$-\frac{(n+1)X_m^{n/(1+n)}}{\tau}\beta = k_{rv0} \exp\left(-E/(\Re(\theta_{\xi=1}T_m + (1-\theta_{\xi=1})T_\infty))\right) \tag{6.34}$$

When this condition is fulfilled, the devolatilisation temperature, θ_{Xv}, can be calculated together with the position of the drying front x_e. The time when the drying arrives to this position is evaluated from Eq (6.24). As the devolatilisation has started, the devolatilisation front propagates into the particle and its position can be estimated from the dimensionless temperature obtained when the rate of drying is equal to the rate of devolatilisation

$$-\frac{(n+1)X_m^{n/(1+n)}}{\tau}\beta = k_{rv0} \exp\left(-E/(\Re(\theta_{X_v}T_m + (1-\theta_{X_v})T_\infty))\right) \tag{6.35}$$

The corresponding position can be calculated from Eq (6.19).

Two alternative methods to determine the time dependent release of volatiles can be considered one simpler and one slightly more complicated, but more physically correct. Fisrt we consider a simpler approach, which is to define the position of the devolatilisation front by using a single dimensionless temperature determined by Eq (6.33). The second approach, which is slightly more complicated, but physically correct approach, is to calculate the propagation of the devolatilisation front directly from the rate of devolatilisation. In the later case the propagation of the devolatilisation front has to be solved from the ordinary differential equation

$$-\frac{\partial X_v}{\partial t} = k_{rv} \exp\left(-E/(\Re(\theta_{X_v}T_m + (1-\theta_{X_v})T_\infty))\right) \tag{6.36}$$

with the initial condition $X_v = 1$. The dimensionless devolatilisation temperature, θ_{X_v}, is a function of X_v and X_m, the latter calculated in each time step from Eq (6.24).

Example 6.1
Wood particles are fed into a fluidised bed. The wood particles can be estimated as infinitely long cylinders with a diameter of 10 mm, having a dry density of 500 kg/m^3, a moisture content of 30% (as received), a thermal conductivity of 0.12 W/mK and a specific heat of the dry fuel of 1000 J/kgK. The effective heat transfer coefficient is estimated to be 600 W/m^{2}K. The temperature of the bed is 850°C. Calculate the time of drying and devolatilisation, and give the relative position of the drying and devolatilisation front, as well as the rate of the two processes as a function of time.

Solution:
The time constant τ

$$\tau = \frac{Y_m}{1-Y_m} r_0^2 \frac{\rho_{df}}{k_{c,df}} \frac{H_{m,eff}}{T_\infty - T_m}$$
$$= \frac{0.3}{1-0.3}(0.01/2)^2 \frac{500}{0.12} \frac{2400\times10^3 + (4180+1000/0.3)(100-25)}{850-100} = 176\ s$$

thermal Biot number

$$Bi_t = \frac{h_{c,eff} r_0}{k_{c,eff}} = \frac{600\times 0.01/2}{0.12} = 25$$

dimensionless drying time (n = 1 for cylinder, n = 2 for sphere)

$$f(X_m) \rightarrow \frac{2+Bi_t}{2(n+1)Bi_t} = \frac{2+25}{2(1+1)25} = 0.27$$

the drying time

$$t_{dry} = 176\times 0.27 = 47.5\ s$$

(This result can be compared with the resulting time for a spherical particle with the same diameter 47.5×2/3 = 32 s)

The time before the start of devolatilisation is given from

$$\frac{(n+1)}{\tau} \frac{\mathrm{Bi_t}}{(1+\mathrm{Bi}_t \Gamma[x_m])} = k_{rv0} \exp\left(-E/\Re / \left(\frac{1}{1+\mathrm{Bi_t}\Gamma[x_m]} T_m + \left(1 - \frac{1}{1+\mathrm{Bi_t}\Gamma[x_m]}\right) T_\infty \right)\right)$$

the constants for the rate of devolatilisation is taken from Table 5.2, k_{rv0} = 1.9×10^{12} [1/s] and E/$\Re$ = 21500 [K]. (Remember to give the temperatures in Kelvin, when using the rate expression). For a cylinder $\Gamma[\xi]$ = - ln(ξ_m)). The position of the drying front at the start of devolatilisation is obtained from a graphical or an iterative calculation. A graphical solution of the problem, shown in Fig 6.2, gives the dimensionless drying position ξ_m = 0.967, which correspond to a remaining moisture content of

$$X_m = \xi_m^{(n+1)} = 0.967^2 = 0.94$$

and temperature of the devolatilisation 440°C. The time before the start of devolatilisation is calculated from Eq (6.22), where the time constant is already determined. The dimensionless time becomes

$$f\left[X_m\right] = \frac{2 + Bi_t - \left(a_1 X_m + a_2 Bi_t\right)}{2(n+1)Bi_t}$$

where $a_1 = \left(2 + Bi\right)$ and $a_2 = -2X_m \ln(X_m^{1/2})$

$$f\left[X_m\right] = \frac{2 + 25 - \left(27 \times 0.94 + 0.058 \times 25\right)}{2(1+1) \times 25} = 1.7 \times 10^{-3}$$

The time before devolatilisation starts, which is assumed to be equal to the ignition time t_{ign}, is then

$$t_{ign} = 176 \times 1.7 \times 10^{-3} = 0.3\ s$$

The propagation of the drying front is given directly from Eq (6.22) and the mass fraction of the remaining volatiles can be determined by three different methods:

Method 1: The mass fraction of the remaining volatiles is determined from Eq (6.33) by an iterative procedure

$$-\frac{(n+1)X_m^{n/(1+n)}}{\tau}\beta = k_{rv0} \exp\left(-E/(\Re(\theta_{X_v} T_m + \left(1-\theta_{X_v}\right)T_\infty))\right)$$

where

$$\theta_{X_v} = \frac{1 + \mathrm{Bi_t}\Gamma\left[X_v^{1/2}\right]}{1 + \mathrm{Bi_t}\Gamma\left[X_m^{1/2}\right]}$$

Inserting the dimensionless temperature gradient and the dimensionless temperature into the equation and solving,

$$\frac{(n+1)}{\tau}\frac{\mathrm{Bi_t}}{\left(1 + \mathrm{Bi}_t\Gamma\left[X_m^{1/2}\right]\right)} = k_{rv0} \exp\left(-E/\Re/\left(\frac{1 + \mathrm{Bi_t}\Gamma\left[X_v^{1/2}\right]}{1 + \mathrm{Bi_t}\Gamma\left[X_m^{1/2}\right]}T_m + \left(1 - \frac{1 + \mathrm{Bi_t}\Gamma\left[X_v^{1/2}\right]}{1 + \mathrm{Bi_t}\Gamma\left[X_m^{1/2}\right]}\right)T_\infty\right)\right)$$

for each time step. The rate of evaporation results from the left side of the equation above and the rate of devolatilisation is derived from the resulting propagation of the devolatilisation front.

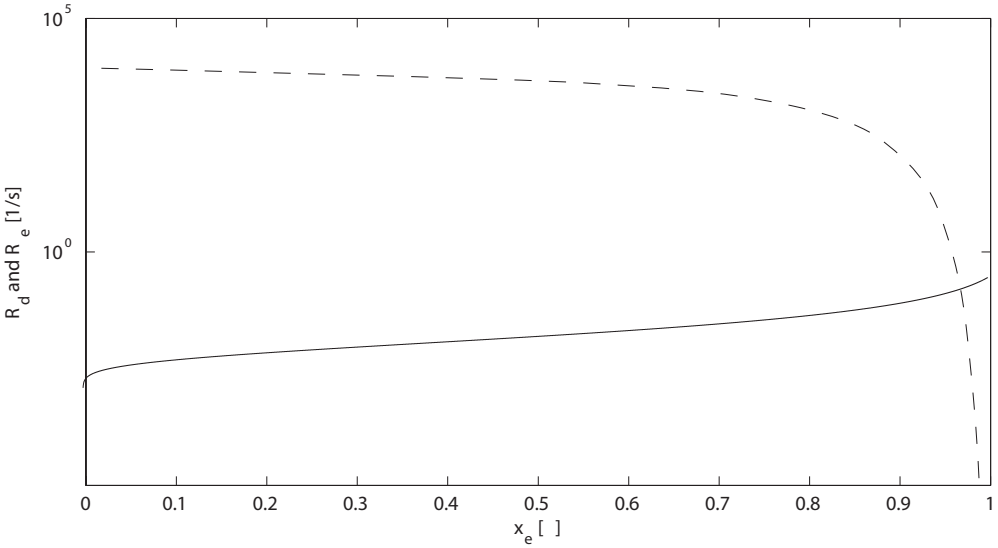

Figure 6.2.
Rate of devolatilisation at the surface of the particle (dashed line) and rate of evaporation (solid line) as a function of the position of the drying front.

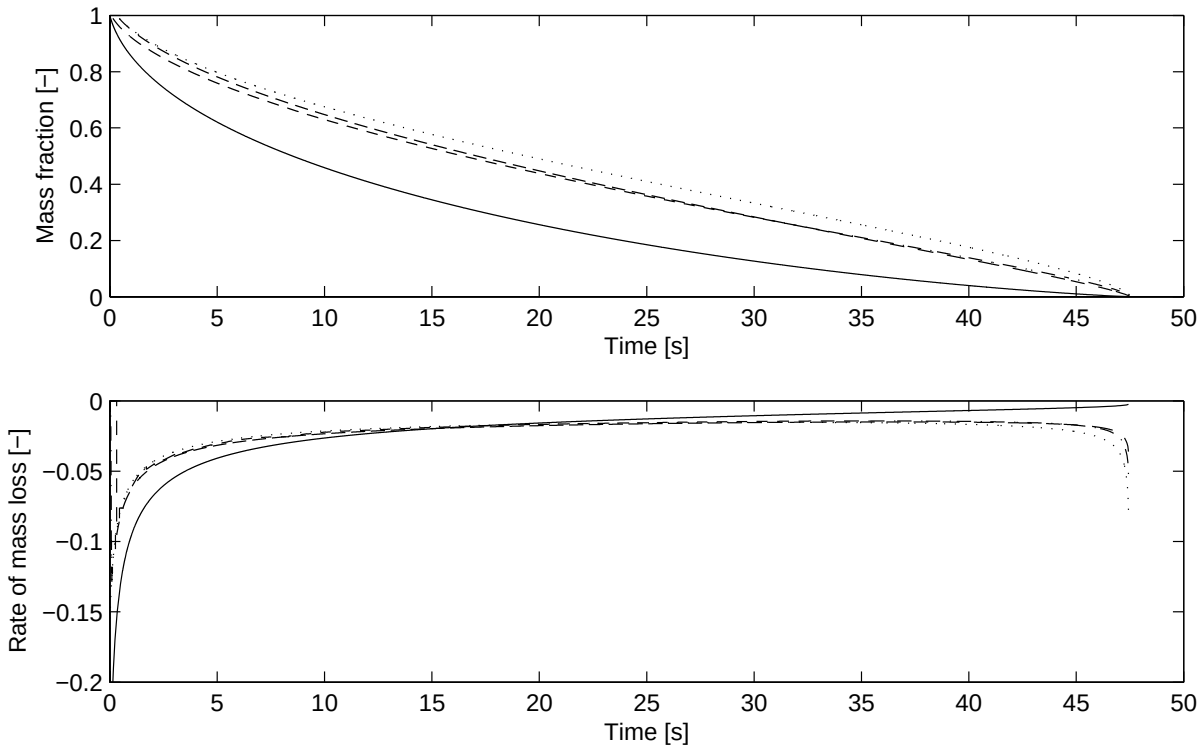

Figure 6.3.
Upper figure: Remaining mass fraction of moisture (solid line) and volatiles (method 1 dashed line, method 2 dotted line, method 3 dashed dotted line) as a function of time. Lower figure: release rate of moisture and volatiles.

Method 2: If the devolatilisation front is defined by a single devolatilisation temperature the analysis become simpler because the position of the front can be calculated from Eq (6.19) without any iterative procedure. The devolatilisation temperature can be selected as the temperature giving the start of devolatilisation, which in this case is 440°C, $\theta = 0.55$. The rate of the devolatilisation is calculated as in method 1.

Method 3: The position of the devolatilisation front and the rate of devolatilisation are calculated from Eq (6.36).

As seen from Fig 6.3 the three methods to calculate the remaining mass fraction of volatiles and rate of devolatilisation yield almost identical results, even if the volatiles are released a little later in method 2 then in the other two. This is a consequence of deriving the temperature of devolatilisation from the highest heating rate. If the devolatilisation temperature would have been chosen from the average release rate of moisture it is likely that the agreement would have been even better.

CHAPTER 7

CHAR COMBUSTION AND GASIFICATION

HENRIK THUNMAN

CHAR COMBUSTION

The final step in the solid fuel combustion process is char combustion or generally spoken, conversion, if gasification is to be regarded as well. When devolatilisation is completed highly porous char remains. The porosity of wood char is about 0.9 (90% gas voidage), while coal char tends to have a porosity of about 0.7, although this value can vary widely. The internal surface area is on the order of 300 m^2/g for wood char and 100 m^2/g for coal char. No volatiles are escaping from the char at this time, and since the char is porous, oxygen can diffuse through the external boundary layer and into the char particle. The conversion rate of the char depends on both the chemical rates of the reactions carbon-oxygen

$$C + ½\ O_2 \rightarrow CO \qquad (a)$$
$$C+O_2 \rightarrow CO_2$$

carbon- carbon dioxide

$$C + CO_2 \rightarrow 2CO \qquad (b)$$

and carbon-water vapour

$$C + H_2O \rightarrow CO + H_2 \qquad (c)$$

and the mass transfer of the reactant through the external boundary layer and into the reactive region within the particle. The first reaction (a) is the combustion reaction, which is one to two order of magnitude faster then the other two reactions (b and c), which are referred to as the gasification reactions. Primarily product of the char conversion is CO. In a combustion situation some of the CO will react further to CO_2 within the particle or in the external boundary layer depending on the temperature and availability of oxygen. The combustion reaction and the CO oxidation within the particle may raise the temperature of the char 100-200°C above the temperature of the surroundings. On the other hand, for a gasification

situation the temperature of the particle will be lower than the surroundings. The chemical reaction rates can be treated in different ways dependent on the reactivity. The simplest way is to relate the reaction rate to the external surface area and the kinetics are then refereed global surface kinetics. More correct is to use the area within porous structure on which the reactions take place referred to the intrinsic area, which will change with conversion. The intrinsic area should be connected to a reaction rate, a kinetic intrinsic rate, evaluated from the same experiments as the intrinsic area.

The temperature of the particle can be estimated from a steady-state energy balance, which equates heat generation or consumption in the particle to heat loss or gain by convection and radiation, related to the temperature difference between the particle and the surroundings, external surface area and effective heat transfer coefficient Eq (5.14):

$$\frac{dm_C}{dt} H_C = h_{c,eff} A\left(T_g - T_p\right) \qquad (7.1)$$

The heat generation or consumption is given by the burning rate dm_c/dt and the heating value of the reaction H_C. The particle temperature is determined for a specific case in the following example.

EXAMPLE 7.1. Determine the char particle temperature due to combustion of C to CO at the char surface for the following conditions: burning rate based on the particle surface 0.07 kg/m^{2}s, particle size 100 μm, gas temperature and background temperature is 1500 K, particle emissivity 0.9.

Solution. For the C-CO reaction, the heat of reaction is 9.2×10^6 J/kg coal. The convective heat transfer coefficient is calculated from Nu = 2 (given for a sphere in stagnant surrounding, see derivation in Chapter 4), using a gas conductivity for air,

$$h_{c0} = \frac{2k_g}{d} = \frac{2\times0.105}{100\times10^{-6}} = 2100\, W/m^2K$$

For the radiative heat transfer coefficient the particle temperature is assumed to be 100 K higher than the surrounding, and the emissivity is assumed to be equal to 1.

$$h_{rad} = 1\times5.67\times10^{-8}\left(1600^2+1500^2\right)\left(1600+1500\right) = 850\ \mathrm{W/m^2K}$$

The effective heat transfer coefficient is then

$$h_{c,eff} \approx 2100+850 \approx 2950\ \mathrm{W/m^2K}$$

Dividing Eq 7.1 with *A* yields

$$0.07\times9.2\times10^6 = 2950\times\left(T_p - 1500\right) \quad \left[\mathrm{W/m^2}\right]$$

which give the surface temperature, T = 1720 K, which is 220 K above the gas temperature. From the assumption made, the radiative heat transfer coefficient is underestimated with around 10 %, which leads to an underestimation of the effective heat transfer coefficient with 3 % or an overestimation of the particle temperature with 7 K. This is well below the accuracy of the estimation.

The burning rate, *dm*/*dt*, of the char depends on the oxygen concentration, gas temperature, Reynolds number, particle size and porosity of the char. The conversion of the char can schematically occur according to three simplified cases, see Fig 7.1: The first case is called shrinking density. This case assumes that the mass transport of the reactants from the surrounding to the surface of the particle and further into the particle is much faster than the consumption of the reactants within the particle, resulting in a constant concentration of the reactant throughout the fuel particle and a constant conversion rate in the entire particle. This means that the mass gradually decreases in the whole particle at the same time and if the particle keeps its size, only the density changes. Therefore the name of this case: constant diameter model.

The second case is called shrinking sphere or constant density case. This case assumes that the reactant transported from the surroundings into the surface of the particle reacts at the surface of the particle and that no ash layer builds up around the particle. This situation occur under two conditions, the temperature of the particle is so high that all reactants transported to the surface are immediately consumed, and/or, the porosity of the particle is close to zero, which does not allow any reactant to be transported further into the particle.

The third and last case, shrinking core, is similar to the second case, with the difference that an ash layer is built up around a shrinking core of combustible material. This shrinking core corresponds to the shrinking particle in the second case. From a modelling point of view the difference between the two cases is that the mass transfer resistance through the external gas film must be complemented with an additional resistance through the ash layer that builds up around the shrinking core.

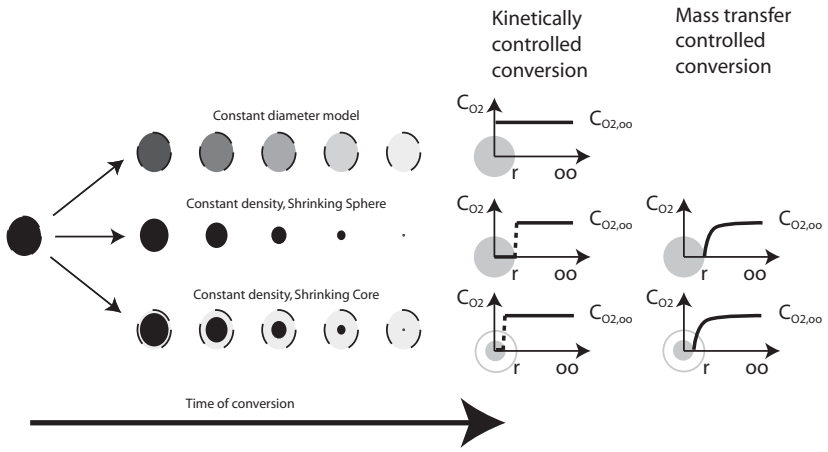

Figure 7.1.
Char conversion with time for three simplified cases, where the darkness indicates density.

Which of these three simplified cases is applicable to a given practical problem? If the conversion should be described by a shrinking density case or shrinking core / shrinking sphere case can be determined by means of the Thiele modulus and this module is derived below. The Thiele modulus is a dimensionless Damköhler number which relates the mass transport of the reactant into the particle with the reaction rate and gives a measure of the distribution of the reactant within the particle. The Thiele modulus is defined

$$Th = r_0 \sqrt{\frac{R_{C,O2}}{D_{AB,eff}}} \qquad (7.2)$$

where r_0 is the particle radius, $R_{C,O2}$ intrinsic reaction rate constant for a first order reaction and $D_{AB,eff}$ effective molecular diffusion inside the fuel particle. The derivation of the Thiele modulus follows below. The intrinsic reaction rate is related to the particle intrinsic area (considering the pore structure and given as internal surface are per unit volume of the particle [m^2/m^3]) of the particle, A_{int}, and reaction rate $k_{r,C}$

$$R_{C,O2} = A_{\text{int}} k_{rC} \qquad (7.3)$$

The effective diffusion coefficient $D_{AB,eff}$ includes the molecular diffusion D_{AB} of the gas pair A in B, and the relation between the molecular diffusion inside and outside of the porous structure of char particles. When evaluating the binary diffusion coefficient (for combustion in air), it is recommended to use the molecular diffusion coefficient for oxygen in nitrogen. A widely used approximation is to relate the reduction of the diffusivity due to the voidage, ε_{por}, as follows,

$$D_{AB,eff} = \varepsilon_{por}^2 D_{AB} \qquad (7.4)$$

The diffusivity is reduced further due to the extra distance of the diffusion caused by the wrinkled path in the porous structure, which is approximated by a quantity that is about equal to the voidage, thereof the voidage squared in Eq (7.4). A high Thiele modulus value indicates that the reactant is consumed close to the particle's surface (the shrinking sphere or shrinking core case) and a low Thiele modulus indicates that the reactant penetrates into the particle (shrinking density case). This can be seen in Fig 7.2, where dimensionless concentration of oxygen (C_{O2} / $C_{O2\infty}$) is shown versus dimensionless radius (r / r_0) for Thiele modulus between 0.1 and 100.

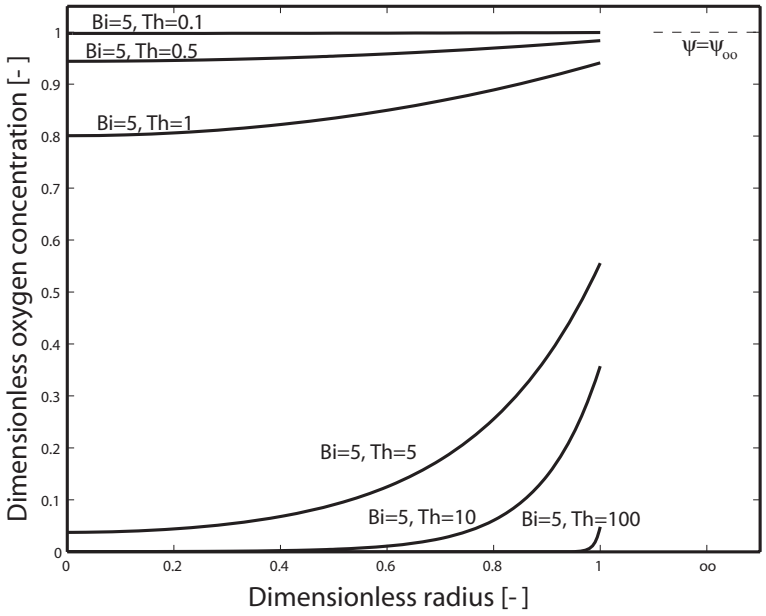

Figure 7.2
Dimensionless concentration of oxygen (C_{O2} / $C_{O2\infty}$) versus dimensionless radius (r / r_0) for Thiele modulus between 0.1 and 100.

Experience on how the ash builds up on a special fuel under special conditions indicates if the conversion is to be characterized as shrinking core or a shrinking sphere. In a fluidised bed the ash layer is most likely removed as soon as it is formed, due to attrition caused by collisions between fuel and bed particles. For conversion in fixed beds or in suspensions there is no such general recommendation to be given.

The conversion of the char can be described by the local reaction rate of order n, which for char conversion with respect to oxygen is given by

$$\frac{dm_C}{dt} = -\Omega V A_{\text{int}} k_{rC} C_{O2s}^{n} M_C \qquad (7.5)$$

where Ω is the stoichiometric ratio of moles of carbon per mole of oxygen (which is 2 for reaction (a), A_{int} reactive intrinsic surface area [m^2/m^3], k_{rC} kinetic intrinsic rate constant [m/s], C_{O2} local oxygen concentration, and n is the order of reaction. The reaction rate of Eq (7.5) can be used directly in the first simplified case of char conversion, the constant diameter case, where the oxygen concentration in the fuel particle is almost equal to that of the surroundings. This case is associated with low temperatures and high porous particles. The intrinsic reaction rates should be used. However, the intrinsic rates are often not straight-forward as they often are connected to a model describing the evolution of reactive intrinsic area. As a first estimate global surface kinetic data (Table 7.1) can be used for the reaction rate and the external area related to this rate is replaced by an intrinsic area. The global reaction rate is formulated in terms of rate of reaction of the char mass per unit external surface area and per unit oxygen concentration on the surface. As with all global reactions, the results should be verified experimentally over the range of application. If the intrinsic area is assumed to decrease linearly with the conversion of the char, the conversion rate of the char combustion in this first case becomes

$$\frac{dm_C}{dt} = -\Omega \left(m_C / m_{C0}\right) V A_{\text{int}} k_C C_{O2,\infty}^{n} M_C \qquad (7.6)$$

and the conversion time is obtained by integrating Eq. 7.6

$$t_C = -\frac{m_{C,0}}{\Omega V A_{\text{int}} k_{rC} C_{O2,\infty}^{n} M_C} \ln\left(\frac{m_C}{m_{C,0}}\right) \qquad (7.7)$$

The time is then a function of the degree of conversion. A conversion of 95 or 99% can be used for comparison.

If the Thiele modulus is high, all oxygen is consumed in a narrow region close to the surface of the particle, a case associated with high temperature and large particles. This means that the density of the unreacted char is constant, and instead the volume of the unreacted char decreases. The area of reaction is then the surface area of the particle instead of the intrinsic area, and Eq (7.5) becomes

$$\rho_C \frac{dV}{dt} = -\Omega A k_{rC} C_{O2}^{n} M_C \qquad (7.8)$$

The conversion rate of the char given by Eq 7.8 requires the local concentration of the reactant. However, the concentration of the reactant is not known at the particle's surface, but it can be estimated by equating the reactant, in the present example the oxygen is consumed by the char where the oxygen diffuse across the particle boundary layer. Since, a simplification occurs when the reaction order is 1 (n=1), we consider only this case (and this is also a very common assumption in the literature). Then,

$$Ak_C C_{O2,s} M_{O2} = Ah_m \left(C_{O2,\infty} - C_{O2,s}\right) M_{O2} \qquad (7.9)$$

Solving Eq 7.9 for the oxygen concentration at the surface,

Table 7.2. Representative global char coal conversion surface rate constants. $k_{rc,0}$ = 10^(0.2×10^{-4} E + 2) (m/s)

Fuel	E_1 (J/mol) $C+O_2 \rightarrow CO_2$	E_2 (J/mol) $C+½O_2 \rightarrow CO$
Char coal (char from wood)	75000 - 84000	1.1×E_1
Peat	84000	1.1×E_1
Lignite	92000 - 105000	1.1×E_1
Bituminous coal	117000 - 134000	1.1×E_1
Fuel	E_3 (J/mol) $C+CO_2 \rightarrow 2CO$	E_4 (J/mol) $C+H_2O \rightarrow CO+H_2$
Char coal (char from wood)	2.2×E_1	1.6×E_1
Peat	2.2×E_1	1.6×E_1
Lignite	2.2×E_1	1.6×E_1
Bituminous coal	2.2×E_1	1.6×E_1

$$C_{O2,s} = \left(\frac{h_m}{k_{rC} + h_m}\right) C_{O2,\infty} \qquad (7.10)$$

Hence, Eq. 7.8 becomes

$$\rho_C \frac{dV}{dt} = -\Omega A k_{rC,eff} C_{O2,\infty} M_C \qquad (7.11)$$

where the effective rate constant $k_{rC,eff}$ includes both kinetics and diffusion:

$$k_{rC,eff} = \frac{k_{rC} h_m}{k_{rC} + h_m} \qquad (7.12)$$

The burning rate to be used in Eq (7.5) become $dm_C/dt = \rho_C \, dV / dt$. The kinetic rate constant related to oxygen concentration is calculated from the Arrhenius relation

$$k_{rC} = k_{rC,0} \exp\left(-E / \Re T\right) \qquad (7.13)$$

Global kinetic parameters for surface reactions for several chars of different origin are given in Table 7.2.

The mass transfer coefficient h_m (m/s) is obtained from the Sherwood number (Sh = $h_m d/D_{AB}$). For low flows around a spherical particle, Sh = 2, but when the particle Reynolds number is in the order of 1, or greater the Frössling correlation may be used:

$$Sh = \left(2 + 0.6\,\mathrm{Re}^{1/2}\,Sc^{1/3}\right)\phi \qquad (7.14)$$

The Schmidt number Sc is typically 0.73 for gas at standard conditions. Also, a mass transfer correction factor ϕ is introduced to account for rapid outward flow of combustion products, which can be estimated with Eq 5.13, where $\rho_g u_g c_p/h_c$ is replaced by $u_g D_{AB}/h_m$. ϕ may vary from 0.6 to 1 during drying and devolatilisation depending on the moisture and volatile release rate, and is about 0.9 for char combustion. If the particle is modelled as a shrinking core the mass transfer coefficient has to be compensated for the resistance of the mass flow through the ash layer, which builds up outside the reacting core.

For a shrinking sphere an analytical solution of Eq (7.8) can be found for two conditions $k_{rC} >> h_m$ and $k_{rC} << h_m$. The first condition, $k_{rC} >> h_m$, is the common condition for large particles in a hot surrounding, while the second condition represents a char with a very low porosity in low temperature environment. For spherical particles (the same derivation can be done for other geometrical shapes) and where oxidation of the char takes place close to the surface of the particle and $k_{rC} >> h_m$, Eq. 7.8 can be written,

$$\begin{aligned} &\rho_C \frac{\pi}{6}\frac{dd^3}{dt} = \rho_C \frac{\pi}{6} 3d^2 \frac{dd}{dt} = -\Omega \pi d^2 h_m C_{O2,\infty} M_C \Rightarrow \\ &\frac{dd}{dt} = -2\Omega \frac{h_m}{\rho_C} C_{O2,\infty} M_C \end{aligned} \qquad (7.15)$$

(Eq 7.15 is also applicable for the shrinking core case) Assuming that Sh=2, which for a shrinking particle makes $h_m = 2\,D_{AB}\,/\,d$, the char burnout time is obtained by integrating Eq. 7.15 from the initial fuel diameter to zero:

$$t_C = \frac{\rho_C d_i^2}{8\Omega D_{AB} C_{O2,\infty} M_C} \qquad (7.16)$$

For the second condition $k_{rC} << h_m$ the oxidation still takes place close to the surface, but is restricted by the reaction rate on the surface. Eq (7.8) can then be rewritten as

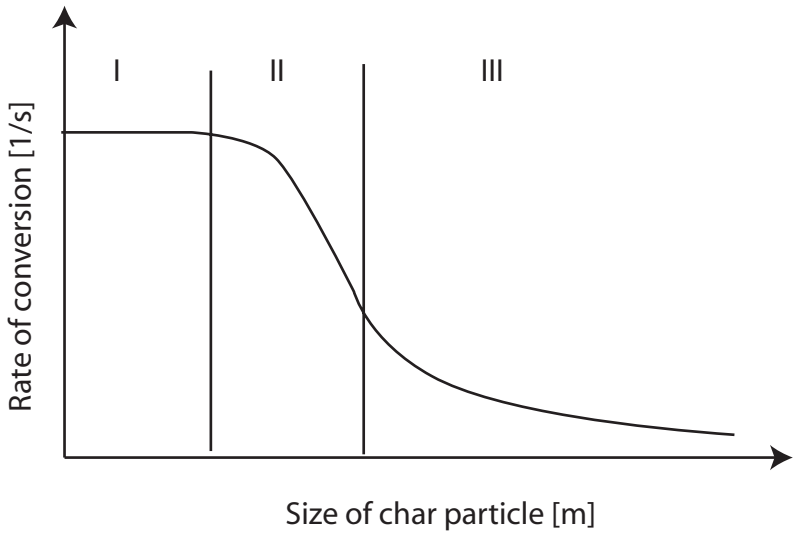

Figure 7.3.
Rate of char combustion as a function of particle size. Regime I kinetically controlled conversion, Regime II intermediate region, Regime III mass transfer controlled conversion. The curve in the diagram is affected by temperature and other parameters.

$$\rho_C \frac{\pi}{6}\frac{dd^3}{dt} = \rho_C \frac{\pi}{6} 3d^2 \frac{dd}{dt} = -\Omega \pi d^2 R_C C_{O2,\infty} M_C \Rightarrow$$
$$\frac{dd}{dt} = -2\Omega \frac{k_{rC}}{\rho_C} C_{O2,\infty} M_C \qquad (7.17a)$$

The char burnout time is obtained by integrating Eq. 7.17a from the initial fuel diameter to zero and is the same for both shrinking sphere and shrinking core

$$t_C = \frac{\rho_C d_i}{2\Omega k_{rC} C_{O2,\infty} M_C} \qquad (7.17b)$$

From these simplified cases it can be seen that for small particles the conversion time, Eq (7.7), becomes independent of particle size, as $m_{C0}/V = \rho_{C0}$, and consequently also the conversion rate is independent of the particle size. For large particles, on the other hand, the conversion time, Eq (7.17b), is proportional to the surface area of the particle, which for a spherical particle is equal to the square of the particle diameter. The rate of conversion is then proportional to one divided by the square of the diameter. Often this is presented as different regimes of char combustion; regime I corresponds to kinetically controlled conversion according to the shrinking density case, regime III to mass transfer controlled conversion according to the shrinking particle or shrinking core and regime II is the intermediate region, see Fig 7.3.

ASH FORMATION

The type and extent of mineral matter in the solid fuel can influence the reaction rate. Mineral matter in biomass is less than a few percent, while in coal it can range from a few percent to

50% or more for very low-grade coals when the char burns, the minerals, which are dispersed in the form of ions and submicron particles in the fuel, are converted to a layer of ash on the char surface. In high-temperature pulverised coal combustion, the ash tends to form spheres called cenospheres. At lower temperatures the ash remains softer. The ash layer can have a significant effect on the heat capacity, radiative heat transfer, catalytic surface reactions, and can also result in increased diffusive resistance to oxygen, especially late in the char combustion stage. In combustion systems, the ash which is formed from the mineral matter can form slag on radiant heat transfer surfaces and deposit on convective heat transfer surfaces if the temperature of the particle is too high. The size and composition of the particulate emissions are influenced by the nature of the mineral matter and time-temperature history of the combustion.

DERIVATION OF MASS TRANSFER COEFFICIENT IN STAGNANT AIR AND ZERO GRAVITY, THIELE MODULUS AND BIOT NUMBER

The use of dimensionless numbers is a way to categorise the different combustion situations, and to allow comparison between them. The dimensionless numbers also reveal the most important phenomena and thereby support the choice of simplified models. To demonstrate this we will show why Sh = 2 in stagnant air and zero gravity and derive dimensionless numbers that can be used to select an appropriate char combustion model.

For low-speed flows around a spherical particle, the Sherwood number is equal to 2 by the following reasoning. Consider a spherical char particle surrounded by stagnant air in a zero gravity field. Diffusion of oxygen to the surface is governed by the steady state diffusion equation, which is analogous to the heat conduction equation:

$$\frac{d}{dr}\left(r^2 \frac{dX_{O_2}}{dr} \right) = 0 \qquad (7.18)$$

Integrating twice,

$$X_{O2} = \frac{-c_1}{r} + c_2 \qquad (7.19)$$

The boundary conditions are as follows: for r large, $X_{O2} = X_{O2}\infty$; and at the particle surface ($r = d/2$), it is assumed that all of the oxygen is consumed (X_{O2},s = 0). Hence, Eq. 7.19 becomes

$$X_{O2} = X_{O2,\infty}\left(1-\frac{d}{2r}\right) \tag{7.20}$$

Differentiating Eq. 7.20, the flux of oxygen to the surface is

$$D_{AB}A\frac{dX_{O2}}{dr}\bigg|_{r=d/2} = \frac{2D_{AB}AX_{O2,\infty}}{d} \tag{7.21}$$

Also, by definition of the mass transfer coefficient, the oxygen flow to the surface is given by

$$D_{AB}A\frac{dX_{O2}}{dr}\bigg|_{r=d/2} = h_m A\left(X_{O2,\infty} - X_{O2,S}\right) \tag{7.22}$$

Equating Eqs. 7.21 and 7.22, and letting the oxygen concentration approach zero at the surface of the particle, $X_{O2,S} \to 0$, yields

$$h_m d/D_{AB} = Sh = 2 \tag{7.23}$$

If the particle is exposed to convection constituent const×Re^a×Pr^b is added and Eq (7.14) is obtained. The coefficients have been determined by experiments. The dimensionless number, allowing selection of char combustion model is the Thiele modulus. This number is derived from the conversion of a char particle, which is described for isothermal particles by the conservation of species in spherical coordinates for oxygen, formulated for the region inside or outside a particle,

$$\frac{\partial}{\partial t}\left(\nu\rho_g Y_{O_2}\right)+\frac{1}{r^2}\frac{\partial}{\partial r}\left(r^2\nu\rho_g u Y_{O_2}\right)= \frac{1}{r^2}\frac{\partial}{\partial r}\left(r^2\rho_g D_{AB,eff}\frac{\partial Y_{O_2}}{\partial r}\right)+\dot{m}_i''' \tag{7.24}$$

where ν is the voidage and $D_{AB,eff}$ the effective diffusion coefficient. The effective diffusion coefficient outside the particle is the one of the gas pair A and B ($D_{AB,eff} = D_{AB}$), and the

relation between the molecular diffusion inside and outside of the porous structure for char particles can be estimated from the voidage, as already been described above Eq (7.4),

$$D_{AB,eff} = \nu^2 D_{AB} \tag{7.25}$$

Assume that the system is in quasi steady-state, (steady state reached in every time step) and that the carbon is converted to CO_2. The later assumption (which is a simplification, since primarily carbon also can be converted to CO) makes the reaction equimolar and no gas flow is therefore present inside or outside the char particle. The equation to be solved is then reduced to,

$$0 = \frac{1}{r^2}\frac{\partial}{\partial r}\left(r^2 \rho_g D_{AB,eff} \frac{\partial Y_{O_2}}{\partial r} \right) + \dot{m}_i''' \tag{7.26}$$

If we now restrict the equation to be valid inside the particle, the source term can be written as,

$$\dot{m}''' = -R_{C,O2}\rho_g Y_{O_2} \left(= -A_{\text{int}} R_C \rho_g Y_{O_2} \right) \tag{7.27}$$

where R_C has the unit [1/s]. Introducing dimensionless quantities for the co-ordinate r and for the mass fraction of oxygen Y_{O2}:

$$\xi = \frac{r}{r_0} \tag{7.28}$$

and

$$\psi = \frac{Y_{O_2}}{Y_{O_2\infty}} \tag{7.29}$$

where r_0 is the external particle radius and $Y_{O2\infty}$ is the oxygen concentration far outside the boundary layer. With the dimensionless numbers and the source term, together with some manipulations, the conservation equation becomes

$$0 = \frac{1}{\xi^2}\frac{\partial}{r_0 \partial \xi}\left(\xi^2 D_{AB,eff}\,\frac{Y_{O_2\infty}\partial\psi}{r_0\partial\xi}\right) - R_{C,O_2} Y_{O_2\infty}\psi \tag{7.30}$$

which can be rewritten as

$$0 = \frac{1}{\xi^2}\frac{\partial}{\partial \xi}\left(\xi^2 \frac{\partial\psi}{\partial\xi}\right) - Th^2\psi \quad ; \quad Th = r_0\sqrt{\frac{R_{C,O_2}}{D_{AB,eff}}} \tag{7.31}$$

where *Th* is a dimensionless number, the Thiele modulus. The Thiele modulus indicates where the reaction takes place inside the particles. If the Thiele modulus is large (>>1), the conversion of the char particle takes place in a narrow area close to the particle's surface. In the opposite case when the Thiele modulus is small (<<1), the conversion takes place within the entire particle. With the introduction of the Thiele modulus the general solution of Eq. (7.31) is,

$$\psi = \frac{1}{\xi}\left(c_1 \exp(Th\xi) + c_2 \exp(-Th\xi)\right) \tag{7.32}$$

The constants c_1 and c_2 are evaluated from the boundary condition of the problem. The boundary condition in the centre of the particle is symmetry, which means that the first derivative is equal to zero,

$$\frac{\partial\psi}{\partial\xi} = 0 \tag{7.33}$$

The surface boundary condition is that the molar flow of oxygen through the boundary layer is equal to the diffusion of oxygen from the surroundings to the surface of the particle,

$$-AD_{AB,eff}\left.\frac{\partial Y_{O_2}}{\partial r}\right|_{Surface} = Ah_m\left(Y_{O_2} - Y_{O_2\infty}\right) \tag{7.34}$$

where *A* is the external particle surface area and h_m is the mass transfer coefficient. Dividing the equation with the surface area and including the dimensionless quantities yields,

$$-D_{AB,eff}\frac{Y_{O_2\infty}\partial\psi}{r_0\partial\xi}=h_m\left(Y_{O_2\infty}\psi-Y_{O_2\infty}\right) \tag{7.35}$$

which becomes,

$$-\frac{\partial\psi}{\partial\xi}=\frac{r_0h_m}{D_{AB,eff}}(\psi-1)=Bi_m(\psi-1) \tag{7.36}$$

$Bi_m = r_0h_m/D_{AB,eff}$. is the diffusional Biot number for the mass transport. The Biot modulus compares the external and the internal mass transport resistances. This Biot number is of the same form as the Sherwood number,

$$Sh=\frac{2r_0h_m}{D_{AB}}=2+0.6\,\mathrm{Re}^{1/2}\,Sc^{1/3} \tag{7.37}$$

but in contrast to the Biot modulus *Sh* considers the condition external to the particle, and is a measure of the thickness of the boundary layer, through which the molecules have to diffuse to reach the particle. The difference between the Biot and the Sherwood number lies in the characteristic length scale, conventionally chosen 2*r* and *r*, and in the diffusion coefficient.

The symmetry condition at the particle's centre gives,

$$0=-c_1-c_2\Rightarrow c_1=-c_2 \tag{7.38}$$

After substituting c_1 with $-c_2$, deriving Eq 7.32, and inserting the result into the boundary condition at the surface of the particle, the constant c_1 become,

$$c_1=\frac{Bi_m}{(Bi_m+Th-1)\exp(Th)+(Th+1-Bi_m)\exp(-Th)}=-c_2 \tag{7.39}$$

The dimensionless oxygen concentration can now be plotted for various Thiele and Biot numbers in order to investigate the behaviour of the char combustion. To better visualise the influence of different parameters, the Biot number is rewritten as,

$$Bi_m = \frac{r_0}{D_{AB,eff}} \frac{D_{AB}\left(2 + 0.6\,\mathrm{Re}^{1/2}\,Sc^{1/3}\right)}{2r_0} = \frac{\left(1 + 0.3\,\mathrm{Re}^{1/2}\,Sc^{1/3}\right)}{\nu^2} \tag{7.30}$$

where

$$\mathrm{Re} = \frac{2r_0 u\rho}{\mu} \quad \text{and} \quad Sc = \frac{\mu}{\rho D_{AB}} \tag{7.31}$$

This reveals that the Biot number (related to mass transport) must always be above 1. For porous particles, typically different types of chars, the porosity is in many cases high 0.9, which give minimum of the Biot number of around 1.2.

In Fig 7.4 the dimensionless mass fraction of oxygen is plotted against the dimensionless particle radius for different Biot number. As can be seen in the figure, the Biot number influences the mass fraction of oxygen inside the particle. This is an expected result, since high Bi_m implies no external diffusion resistance; the mass transfer of oxygen from the surrounding to the surface of the particle is much higher than the mass transfer of oxygen into the interior of the particle.

In Fig 7.5, once more the dimensionless mass fraction of oxygen is plotted against the dimensionless particle radius, but this time for various Thiele numbers. The result from the variation of the Thiele modulus is more interesting; it visualises the conditions under which the simplified char combustion models can be used; different approaches of the simplified char combustion models are discussed above and illustrated in Fig 7.1. A low value on *Th* gives that the concentration of oxygen is constant throughout the particle, indicating that the reaction takes place in the entire particle. For a large *Th* the concentration of oxygen goes rapidly tends towards zero close to the particle surface, which indicates that the combustion takes place on the particle surface. A simplified model for char combustion is the shrinking sphere model, or if an ash layer is built up outside of the reacting core, the char burns like a shrinking core. The assumption for the shrinking sphere or the shrinking core model is that the reactions take place in a narrow area close to what is defined as the reaction surface. Fig 7.4 shows that this is valid for high Thiele numbers (above 10). The alternative simplified model, the shrinking density model, assumes that the reaction takes place uniformly inside the char particle, which can be seen (Fig 7.5) to be valid for low Thiele numbers (below 1).

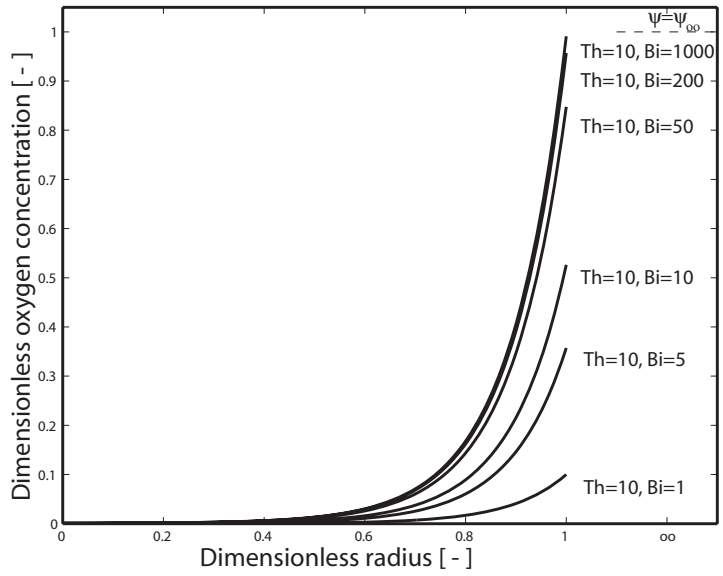

Figure 7.4
Dimensionless mass fraction as a function of dimension-less radius for different Bi_m numbers.

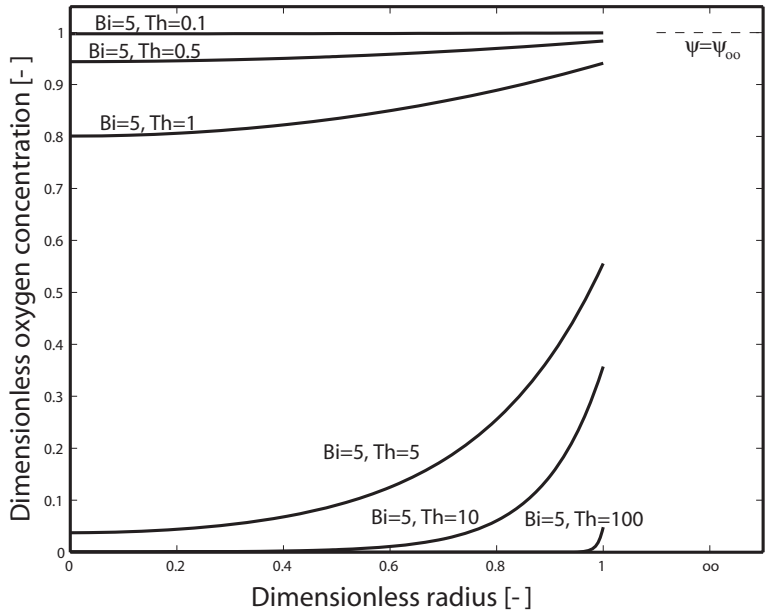

Figure 7.5.
Dimensionless mass fraction as a function of dimensionless radius for different Th numbers.

SUMMARY

Char is a porous carbon matrix with a small amount of hydrogen interspersed with inorganic compounds. Char combustion involves diffusion of oxygen to the surface of the char and chemical reaction at the surface. An effective global rate constant was formulated which includes both diffusion and chemical kinetics (Eq. 7.12). Constant-density ($Th>>1$) and constant-diameter ($Th<<1$) char burnout models have been presented, see Eqs. 7.7, 7.16 and 7.17. Due to the surface reaction, the char surface is hotter than the surrounding gas. As the

char burns, the tiny inorganic particles build up on the surface of the char, and ash particulates are formed.

QUESTIONS

7.1 A char particle is burned in a fluidised bed with a temperature of 850°C and a bed voidage (porosity) of 0.5. The initial diameter of the char particle is 5 mm and the particle is assumed to have the same temperature as the surrounding. Will the combustion take place only close to the surface of the particles or within the entire particle?

For the char particle the following is given

Reaction rate $R_C = k_{rC,0} \exp[-E/\Re T]$

Pre-exponential factor 254×10^{11} 1/s

Activation energy 179.5 kJ/mole

Porosity $\nu = 0.6$

7.2 When designing a new cyclone for a fluidised bed one wishes to know the smallest particle size circulated in order to assure burnout before reaching the cyclone again. The combustion chamber is 40 m high, the gas velocity is 5 m/s, the temperature in the combustor chamber is 850ºC and the average oxygen concentration is 8% on mass. The reaction is controlled by diffusion and it takes place on the surface of the particle. The reaction rate of the char is

$$\dot{m}'' = 84T \exp\left[-18000/T\right] Y_{O_2} \rho_g \ [\mathrm{kg_C/m^2 s}]$$

How small fuel particles must be recirculated, if one assumes that the fuel particle attains the same velocity and temperature as the gas? No combustion takes place outside the combustion chamber. Assume that the density of the char is 1500 $\mathrm{kg/m^3}$, and that the char consists of pure carbon.

7.3 What temperature will a 10 mm char particle attain if it burns under diffusion control in a stationary surroundings of 1400°C and an average oxygen concentration of 5% on mass? Assume that the effective emissivity between the particle and the surrounding equals one and the lower heating value of the char is about 30 MJ/kg.

Answers

7.1 Th=104 => reactions only close to the surface

7.2 2.7 μm

7.3 1408°C

CHAPTER 8

DETAILED MODELLING OF THE CONVERSION OF A SINGLE FUEL PARTICLE

The simplified consideration of the conversion processes of a single fuel particle made in previous chapters can be used for approximations in most engineering situations. However, most simplified analyses do not give any information on the local phenomena. To better understand the processes involved, a more detailed description must be given and the fundamental equations for heat and mass transfer need to be solved. Here, the aim is to formulate such a model that describes the conversion process in detail. The complexity of the model is reduced to allow formulation in a reasonable time. The structure of the model is, however, of general validity and can be refined to catch more details if needed. The structure of the model and the order in which various submodels are included into the model and validated are presented below. The first steps can be carried out rather easily, but the complexity of the model increases for each submodel that is included, and if the model is not properly structured and validated step by step, the implementation of the model may fail. The structure and implementation steps of the model are given in Table 8.1. The first step is to model heating of the particle by conduction of heat from the surroundings to the centre of the particle. This step can be validated by comparison with analytical solutions, derived for constant physical properties and heat transfer coefficient. The second step is to include the drying and devolatilisation processes. These processes are functions of the local temperature. Already after this second step the model can simulate drying and devolatilisation of fuel particles heated in an inert atmosphere, as is often done in experiments. The model is comparable to the simplified analytical model given above for simultaneous drying and

devolatilisation. From thereon, the submodels included in the model structure (Steps 3-8) can be considered as refinements of the description, where more phenomena occurring during the conversion process are taken into account, and more details can be investigated. The first refinement introduced to the model is a one-dimensional convective flow, Step 3. This step is rather simple and offers an opportunity to investigate the influence of the convective heat flow in one dimension, especially important for wood particles, since the gas flow inside a wood particle is dominated by the flow along the fibres. Step 4 and 5 are related to shrinkage, first in one and then in two dimensions. After Step 5 the model is more or less a state-of-the-art model for drying and devolatilisation and better than most models published at present. In Step 6 the pressure distribution is included into the model. Then it becomes possible to describe the flow in n dimensions for one single gas component. Already in this step the complexity of the model is high, and it may be difficult to have a clear overview of it. Further improvements of the model require a good structure, and a strategy on how to validate the model is necessary. In the next step, Step 7, the model is expanded to account for n species also when the flow is in n dimension. In this step, the change of various species is limited to the gas production and convective flow. In Step 8 the diffusion of species is included. This allows oxygen to be transported into the fuel particle, thereby making it possible to model char combustion. The last step introduces heterogeneous reactions and describes the rate of char conversion.

TRANSIENT HEATING OF A SINGLE SOLID FUEL PARTICLE DURING CONVERSION

(Formulation of the basic equation (Step 0))

The initial step of modelling the conversion of a single solid fuel particle is to describe the heating process, since both drying and devolatilisation are thermally controlled processes. The energy conservation equation, derived from the balance shown in Figure 8.1, needs to be solved (here given in one-dimensional Cartesian co-ordinates)

$$\frac{\partial \rho c_p T}{\partial t} + \frac{\partial \rho u c_p T}{\partial x} = \frac{\partial}{\partial x}\left(k_c \frac{\partial T}{\partial x}\right) + \dot{m}''' H \qquad (8.1)$$

Table 8.1 Structure of the model. The boxes indicate the submodels implemented as functions, supplying the variables to the right of the boxes. The number in front of each variable indicates in which step the variable is to be included into the model, following the suggested step by step procedure.

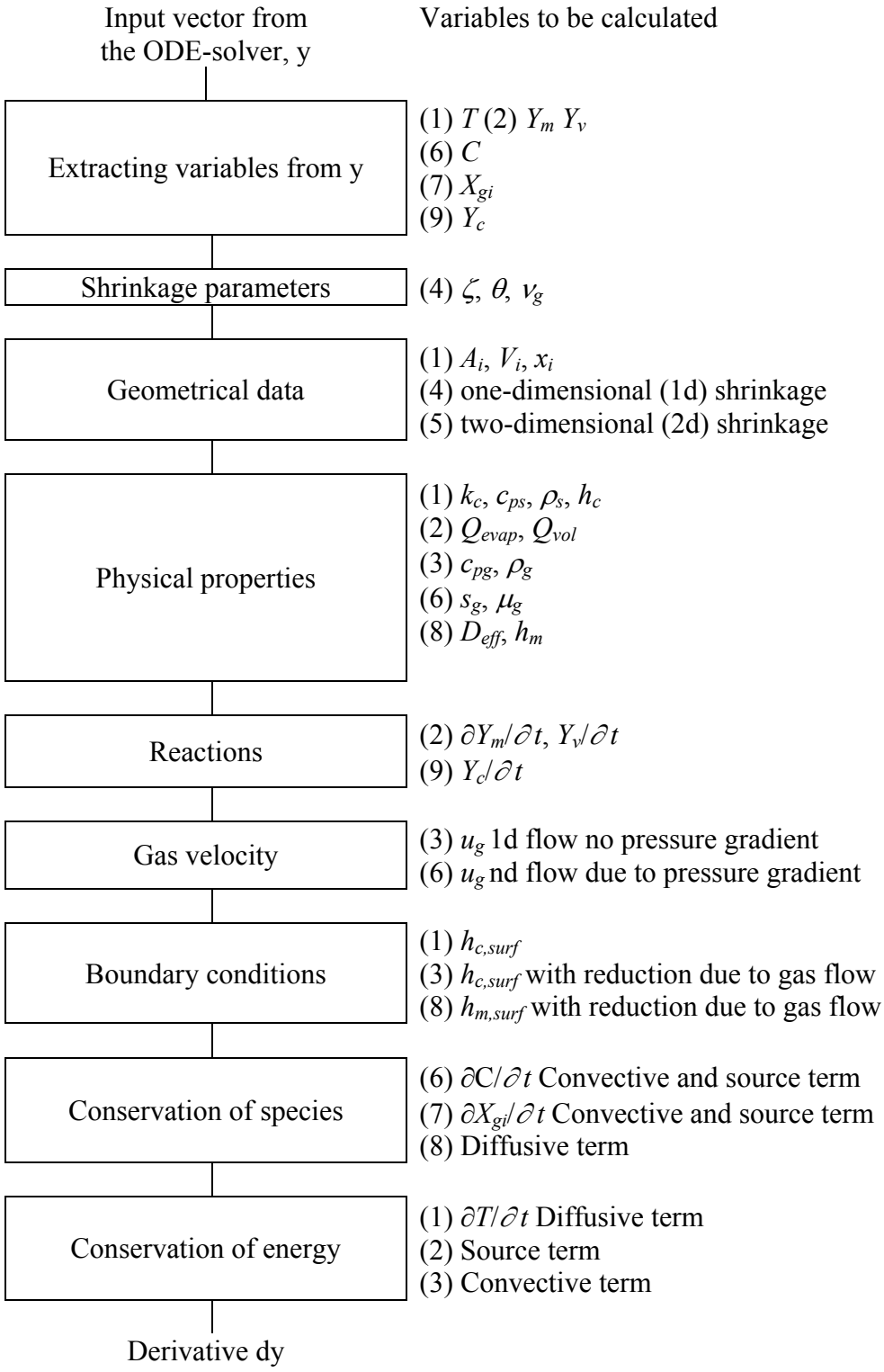

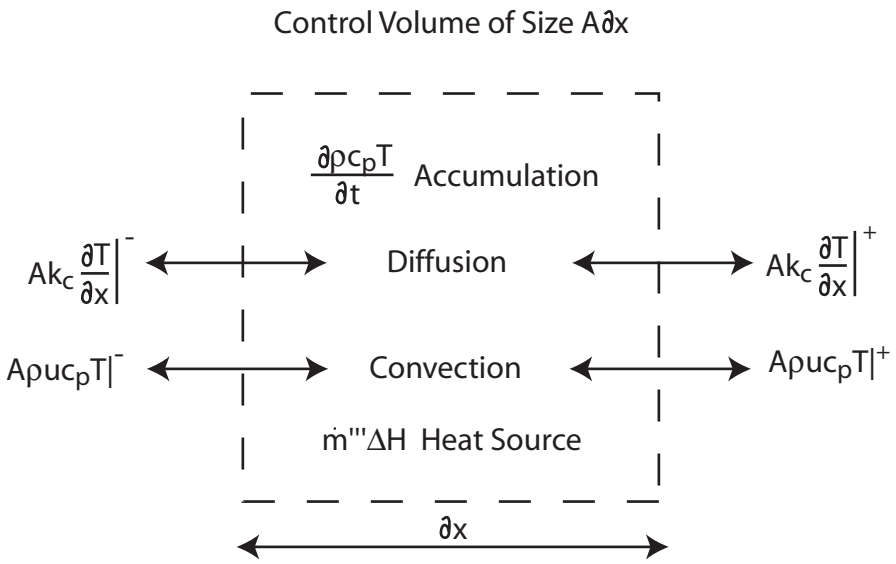

Figure 8.1.
Heat balance on a one-dimensional control volume of size *A∂x*

where ρ is density, c_p specific heat, k_c thermal conductivity of the particle and T temperature, t time, u velocity, x co-ordinate, and $\dot{m}'''\,\Delta H$ is a heat source. In a solid fuel particle there are two phases, a solid and a gas phase. Since the intrinsic surface area is large, the two phases attain the same temperature at all times (after a short initial transient). However, the velocities of the two phases differ, and the equation must therefore be expanded

$$\frac{\partial \rho_s c_{ps} T}{\partial t} + \frac{\partial \rho_g c_{pg} T}{\partial t} + \frac{\partial \rho_s u_s c_{ps} T}{\partial x} + \frac{\partial \rho_g u_g c_{pg} T}{\partial x} = \frac{\partial}{\partial x}(k_c \frac{\partial T}{\partial x}) + \dot{m}''' H \tag{8.2}$$

This form is often further expanded in order to simplify the calculation

$$\begin{aligned} &\rho_s \frac{\partial c_{ps} T}{\partial t} + c_{ps} T \frac{\partial \rho_s}{\partial t} + c_{ps} T \frac{\partial \rho_s u_s}{\partial x} + \rho_s u_s \frac{\partial c_{ps} T}{\partial x} + \\ &+ \rho_g \frac{\partial c_{pg} T}{\partial t} + c_{pg} T \frac{\partial \rho_g}{\partial t} + c_{pg} T \frac{\partial \rho_g u_g}{\partial x} + \rho_g u_g \frac{\partial c_{pg} T}{\partial x} = \frac{\partial}{\partial x}\left(k_c \frac{\partial T}{\partial x} \right) + \dot{m}''' H \end{aligned} \tag{8.3}$$

applying the continuity equation

$$\frac{\partial \rho_s}{\partial t} + \frac{\partial \rho_s u_s}{\partial x} + \frac{\partial \rho_g}{\partial t} + \frac{\partial \rho_g u_g}{\partial x} = 0 \tag{8.4}$$

where the mass transferred between the two phases, *R*, is given by

$$R = \frac{\partial \rho_s}{\partial t} + \frac{\partial \rho_s u_s}{\partial x} = -\left(\frac{\partial \rho_g}{\partial t} + \frac{\partial \rho_g u_g}{\partial x} \right) \tag{8.5}$$

With these expressions the energy equation is reduced to

$$\begin{aligned} &\rho_s \frac{\partial c_{ps} T}{\partial t} + \rho_s u_s \frac{\partial c_{ps} T}{\partial x} + \left(c_{ps} - c_{pg}\right) TR + \\ &+ \rho_g \frac{\partial c_{pg} T}{\partial t} + \rho_g u_g \frac{\partial c_{pg} T}{\partial x} = \frac{\partial}{\partial x}(k_c \frac{\partial T}{\partial x}) + \dot{m}''' H \end{aligned} \tag{8.6}$$

This equation can be further reduced by moving the term $\left(c_{ps} - c_{pg}\right) TR$ into the source term $\dot{m}''' H$, which at this stage is not defined. The density of the solid phase is always several orders of magnitude higher than the density of the gaseous phase, whereas the specific heat is in the same order. This means that

$$\rho_s \frac{\partial c_{ps} T}{\partial t} >> \rho_g \frac{\partial c_{pg} T}{\partial t} \tag{8.7}$$

and it is possible to reduce the equation neglecting the heat stored in the gaseous phase

$$\rho_s \frac{\partial c_{ps} T}{\partial t} + \rho_s u_s \frac{\partial c_{ps} T}{\partial x} + \rho_g u_g \frac{\partial c_{pg} T}{\partial x} = \frac{\partial}{\partial x}(k_c \frac{\partial T}{\partial x}) + \dot{m}''' H \tag{8.8}$$

In many models one step further is taken and the time derivative of the temperature is defined in order to solve for the temperature immediately without any additional computation. This is done by partially derivating the time derivative term

$$\rho_s c_{ps} \frac{\partial T}{\partial t} + \rho_s T \frac{\partial c_{ps}}{\partial t} + \rho_s u_s \frac{\partial c_{ps} T}{\partial x} + \rho_g u_g \frac{\partial c_{pg} T}{\partial x} = \frac{\partial}{\partial x}(k_c \frac{\partial T}{\partial x}) + \dot{m}''' H \tag{8.9}$$

When this is done, one usually assumes that the specific heat is constant. This makes the term $\rho_s T \partial c_{ps} / \partial t$ equal to zero, otherwise this term has to be partially derivated as well

$$\rho_s T \frac{\partial c_{ps}}{\partial t} = \rho_s T \left(\frac{\partial c_{ps}}{\partial T} \frac{\partial T}{\partial t} + \frac{\partial c_{ps}}{\partial Y_{is}} \frac{\partial Y_{is}}{\partial t} \right) \tag{8.10}$$

The dependence of the specific heat on the temperature and composition of the solid phase is known from the input data. The change of composition of the solid with time is given by the source term. If we assume constant specific heat and that the fuel particle retains its shape and size at all times (solid flow $u_s = 0$), one obtains the form that is often used to describe the heating process during drying and devolatilisation

$$\rho_s c_{ps} \frac{\partial T}{\partial t} + \rho_g u_g \frac{\partial c_{pg} T}{\partial x} = \frac{\partial}{\partial x} (k_c \frac{\partial T}{\partial x}) + \dot{m}''' H \tag{8.11}$$

In most cases there is no advantage to simplify the energy conservation equation this much, and from here on the only simplification made is

$$\frac{\partial \rho_s c_{ps} T}{\partial t} >> \frac{\partial \rho_g c_{pg} T}{\partial t} \tag{8.12}$$

The equation to solve finally becomes

$$\frac{\partial \rho_s c_{ps} T}{\partial t} + \frac{\partial \left(\rho_s u_s c_{ps} + \rho_g u_g c_{pg} \right) T}{\partial x} = \frac{\partial}{\partial x} (k_c \frac{\partial T}{\partial x}) + \dot{m}''' H \tag{8.13}$$

which is expanded

$$\begin{aligned} &\rho_s c_{ps} \frac{\partial T}{\partial t} + c_{ps} T \frac{\partial \rho_s}{\partial t} + \rho_s T \frac{\partial c_{ps}}{\partial t} + \frac{\partial \left(\rho_s u_s c_{ps} + \rho_g u_g c_{pg} \right) T}{\partial x} \\ &\quad = \frac{\partial}{\partial x} (k_c \frac{\partial T}{\partial x}) + \dot{m}''' H \end{aligned} \tag{8.14}$$

The terms $c_{ps}T\partial\rho_s/\partial t$ and $\rho_s T\partial c_{ps}/\partial t$ describe change of density and specific heat with time related to mass release (the specific heat also changes with temperature, but this change is not well known for the solid material during conversion, and it is smaller than the change due to mass release of moisture and volatiles).

HEATING BY HEAT TRANSFER TO THE SURFACE OF AND CONDUCTION OF HEAT WITHIN A SOLID PARTICLE (STEP 1)

The first step is to model the conductive heat transport into the particle. This process is described by the first term on the right hand side of the energy conservation equation

$$\frac{\partial}{\partial x}\left(k_c \frac{\partial T}{\partial x}\right) \tag{8.15}$$

The term can be rewritten, because the energy flows through the surface A of the volume element $\partial V = A\partial x$,

$$\frac{\partial}{A\partial x}\left(Ak_c \frac{\partial T}{\partial x}\right) \text{ or } \frac{\partial x}{\partial V}\frac{\partial}{\partial x}\left(Ak_c \frac{\partial T}{\partial x}\right) \text{ or } \frac{\partial}{\partial V}\left(Ak_c \frac{\partial T}{\partial x}\right) \tag{8.16}$$

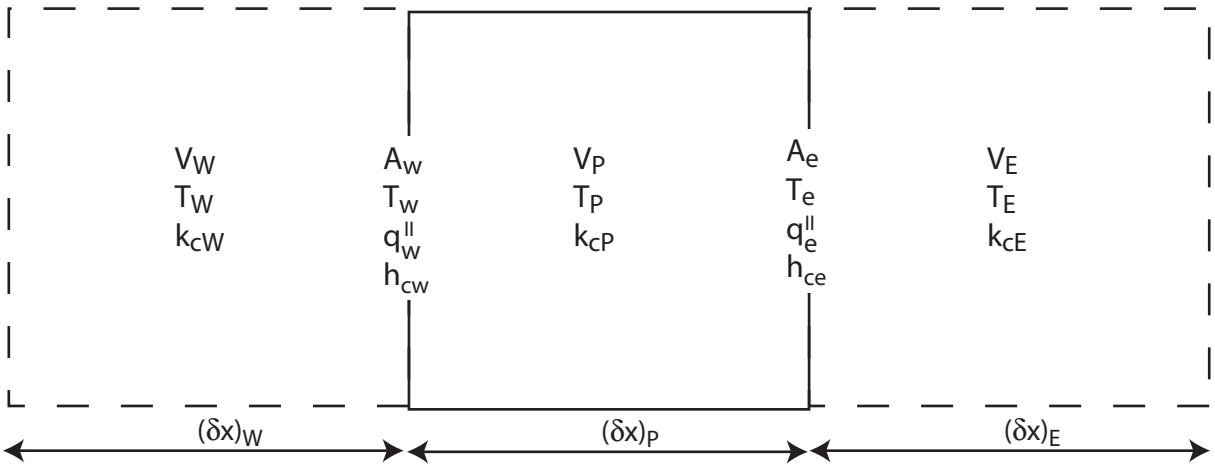

Figure 8.2.
Variables included in the discrete form of the diffusive term in the energy equation, related to the active cell P, the cell to the east, E, the cell to the west, W, the boundary to the east, e, and the boundary to the west, w.

or in discrete form (Figure 8.2)

$$\frac{1}{V_P}\left(\frac{A_e k_{cP}\left(T_e - T_P\right) - A_w k_{cP}\left(T_P - T_w\right)}{\left(\delta x\right)_P / 2}\right) = \frac{\left(q_e^{II} - q_w^{II}\right)}{V_P} \tag{8.17}$$

where q_{ij}^{II} is the diffusive heat flow and the indices indicate the discrete cells seen in Fig 8.2. The energy equation Eq (8.17) corresponds to a heat balance across a control volume, where the entering minus the exiting heat flow is divided by the volume. In this way computational volumes of any geometrical shape can be considered, as long as the heat or mass flows in and out of the volume can be defined. The formulation was made for a one-dimensional case. In the general three-dimensional case the heat flux in the second or third dimensions (y,z) of the equation can easily be expressed in the same way

$$q''' = \frac{(q_e^{II} - q_w^{II}) + (q_n^{II} - q_s^{II}) + (q_b^{II} - q_t^{II})}{V_P} \tag{8.18}$$

where the indices n, s, b, t indicate the boundaries to the north, south, bottom and top of cell P. Computational difficulties to treat large matrixes and time restrictions in practical applications often result in one-dimensional descriptions of the fuel particle, in order to get a sufficient resolution to capture local phenomena taking place in the fuel particle. For example, assume that the memory of a computer limits the calculation to 1 million cells. In a one-dimensional description of a sphere with a diameter of 1 m the width of each cell in the cell becomes 0.5 μm ($d/2/n_{cells}$). A two-dimensional cylinder with length and diameter equal to 1 m, would require cells with width and length of 0.7 mm ($d/2\times(n_{cells}/2)^{0.5}$). Finally, in a three-dimensional case of a cubic box with the side length of 1 m, the width of the cells becomes 10 mm.

The areas and volumes of the computational elements are calculated in relation to the shape of the particle. A one-dimensional representation can be formulated for five different shapes, which can be categorized into two groups:

1. sphere, infinite cylinder and infinite plate
2. finite cylinder and parallelepipeds (boxes)

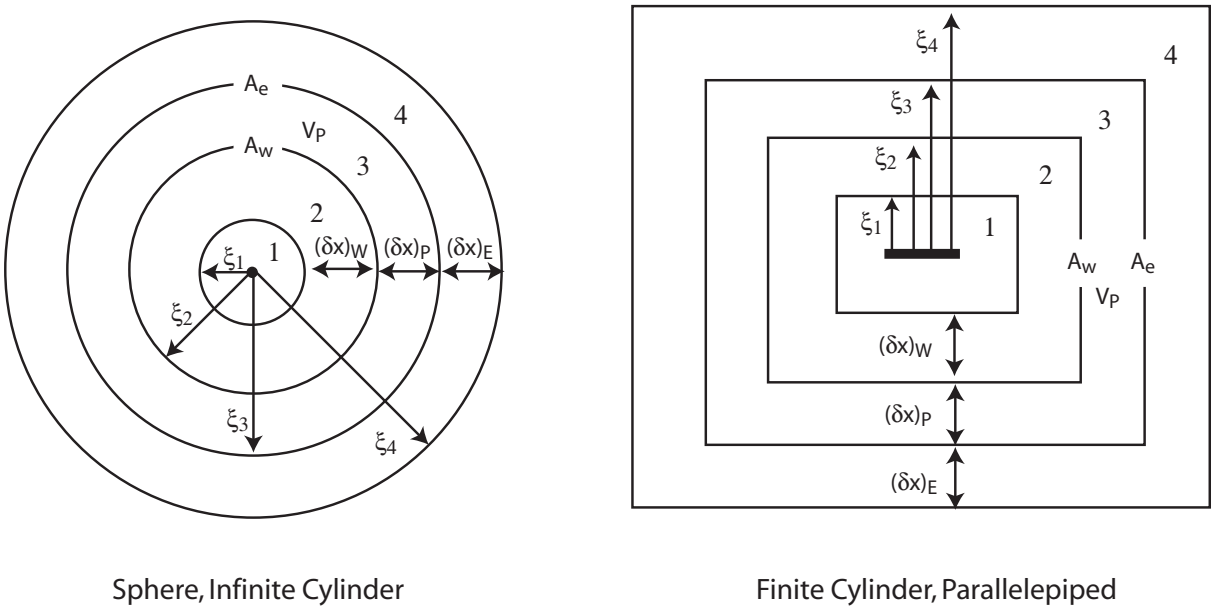

Figure 8.3.
Division of cells for sphere, infinite cylinder, finite cylinder and parallelepiped. (In the figure only a central cell, an external boundary cell and an interior cell surrounded by an eastern and a western cell are shown. In an actual calculation there may be more internal cells).

A uniform mass and heat transport is assumed for all shapes, and uniform physical properties are given across a surface at an equal distance to the closest particle surface, such as indicated in Fig 8.3. For the first group, this can be achieved from a geometrical point of view, but for the second group one needs to assume that the corner effects, as well as the physical data, can be averaged across the derived surface. Corner effects are always present in the second group of shapes and for most biofuels anisotropy (different properties of the physical data in different directions) may be considerable. Because of the corner effect a mathematical error always occurs in the treatment of the second group of shapes.

The surface area between two cells and the volume of a cell can be calculated for shapes represented in one dimension as follows

$$A_{i,i+1} = f_A[\xi_i] \text{ and } V_i = f_V[\xi_i] - f_V[\xi_{i-1}] \text{ where } \xi = \sum_{j=0}^{i} (\delta x)_j \qquad (8.19)$$

The functions *f*, representing areas and volumes, are given in Table 8.2. Note that the shapes of a finite cylinder and a parallelepiped result in the more conventional shapes (infinite cylinders, infinite plate) for extreme conditions. For example, a finite cylinder is the same as an infinitely long cylinder if $L/d \to \infty$ and an infinite plate if $L/d \to 0$.

How is then the heat flow between two computational cells described? See the example in Fig 8.3, where a cylindrical particle is divided into four volumes. Here Cell 2 has been given the cell index *P* and the neighbouring Cell 1 and 3 are given the index *E* and *W*. The heat transported between cell *P* and *E* through the boundary with index *e*, q_e^{II}, is equal to the heat flow from the centre of cell *E* to boundary *e*, which in its turn is equal to the heat flow from the boundary e to the centre of cell *P*. If the heat transport within each cell is dominated by the heat conducted in the normal direction to the boundary, the heat flow is given by the temperature difference between temperature of the centre of the cell (T_P or T_E) and the temperature of the boundary (T_e). This gives that the conductive heat flow across the boundary *e* is equal to (assuming constant physical properties)

Table 8.2. Geometrical functions of shapes that can be treated in one-dimension, together with area and volume of a cell included in a cylinder described in two dimensions.

Shape	$f_A[\xi]$ (area)	$f_V[\xi]$ (volume)
Sphere $\xi \in (0, d/2)$	$4\pi\xi^2$	$4\pi\xi^3/3$
Infinite cylinder $\xi \in (0, d/2)$	$2\pi\xi$	$\pi\xi^2$
Infinite plate $\xi \in (0, l/2)$	1	ξ
Finite cylinder $\xi \in (\xi_0, d/2)$ $\xi\|_0 = \max[-(L-d)/2, 0]$	$2\pi\left(3\xi^2 + \xi(L-d)\right)$	$2\pi\left(\xi^3 + \xi^2(L-d)/2\right)$
Parallelepiped $\xi \in (0, L_1/2)$ $L_1 < L_2 < L_3$	$24\xi^2 + 8\xi\left((L_2-L_1)+(L_3-L_1)\right)$ $+ 2(L_2-L_1)(L_3-L_1)$	$8\xi^3 + 4\xi^2\left((L_2-L_1)+(L_3-L_1)\right)$ $+ 2\xi(L_2-L_1)(L_3-L_1)$
Cylinder in 2-d	$A_{j_a j_r}$	$V_{j_a j_r}$
Axial direction, index a	$2\pi(\xi^2_{rj_a j_r} - \xi^2_{rj_a j_r-1})$	$2\pi(\xi^2_{rj_a j_r} - \xi^2_{rj_a j_r-1})(\xi_{aj_a j_r} - \xi_{aj_a-1 j_r})$
Radial direction, index r	$2\pi\xi_{rj_r}(\xi_{aj_a j_r} - \xi_{aj_a-1 j_r})$	

$$q_e^{II} = A_e k_{cE} \frac{(T_E - T_e)}{(\delta x)_E/2} = A_e k_{cP} \frac{(T_e - T_P)}{(\delta x)_P/2} \tag{8.20}$$

From the heat flows given by Eq 8.20 the temperature at the boundary T_e can be extracted:

$$T_e = \frac{\frac{k_{cE}}{(\delta x)_E/2} T_E + \frac{k_{cP}}{(\delta x)_P/2} T_P}{\frac{k_{cE}}{(\delta x)_E/2} + \frac{k_{cP}}{(\delta x)_P/2}} \tag{8.21}$$

The heat transport across boundary *e* can now be calculated from known temperature and physical properties in cell *P* and *E*,

$$\begin{aligned}
&q_e^{II} = \frac{A_e k_{cE}}{(\delta x)_E/2}\left(T_E - \frac{\frac{k_{cE}}{(\delta x)_E/2} T_E + \frac{k_{cP}}{(\delta x)_P/2} T_P}{\frac{k_{cE}}{(\delta x)_E/2} + \frac{k_{cP}}{(\delta x)_P/2}} \right) = \\
&A_e\left(\frac{\frac{k_{cE}}{(\delta x)_E/2}\left(\frac{k_{cE}}{(\delta x)_E/2} + \frac{k_{cP}}{(\delta x)_P/2} \right) T_E - \frac{k_{cE}}{(\delta x)_E/2}\left(\frac{k_{cE}}{(\delta x)_E/2} T_E + \frac{k_{cP}}{(\delta x)_P/2} T_P \right)}{\frac{k_{cE}}{(\delta x)_E/2} + \frac{k_{cP}}{(\delta x)_P/2}} \right) = \\
&A_e\left(\frac{\frac{k_{cE}}{(\delta x)_E/2}\frac{k_{cP}}{(\delta x)_P/2} T_E - \frac{k_{cE}}{(\delta x)_E/2}\frac{k_{cP}}{(\delta x)_P/2} T_P}{\frac{k_{cE}}{(\delta x)_E/2} + \frac{k_{cP}}{(\delta x)_P/2}} \right) = \\
&A_e \frac{2k_{cE}/(\delta x)_E \times k_{cP}/(\delta x)_P}{(k_{cE}/(\delta x)_E + k_{cP}/(\delta x)_P)} (T_E - T_P) = A_e h_{ce} (T_E - T_P)
\end{aligned} \tag{8.22}$$

where h_{ce} is an effective coefficient for heat transfer between cell *P* and *E*

$$h_{ce} = \frac{2k_{cE}/(\delta x)_E \times k_{cP}/(\delta x)_P}{(k_{cE}/(\delta x)_E + k_{cP}/(\delta x)_P)} \tag{8.23}$$

The heat flow through the boundary *w* is derived in the same way and the final result is

$$q_w^{II} = A_w h_{cw}\left(T_P - T_W\right) \tag{8.24}$$

Across the boundaries in directions *n*, *s*, *b* and *t* (two or three dimensions) the heat flows are

$$\begin{aligned} &q_s^{II} = A_s h_{cs}\left(T_P - T_S\right),\ q_n^{II} = A_n h_{cn}\left(T_N - T_P\right), \\ &q_b^{II} = A_b h_{cb}\left(T_P - T_B\right),\ q_t^{II} = A_t h_{ct}\left(T_T - T_P\right) \end{aligned} \tag{8.25}$$

With Eqs 8.22, 8.24 and 8.25 the conductive heat flows are given for all cells except for the cell in the centre, Cell 1 in Fig 8.3, and the cell at the surface of the particle, Cell 4 in Fig 8.3, which are connected to the "external" boundary conditions. Starting by selecting Cell 1, in Fig 8.3, as the active cell *P*, the conductive heat flow to the east is given by Eq 8.24 as for all cells except for the cell next to the surface of the fuel particle. To the west we have a boundary along a symmetry line and the symmetry condition gives that no heat is transported across this line; q_w^{II} is consequently 0 in this cell. If we then regard Cell 4 in Fig 8.3 to be the active cell *P*, the conductive heat flow to the west is given by Eq 8.22 as for all other cells except for the cell in the centre of the particle. The boundary to the east represents the surface of the particle, and the heat flow to the particle's surface is given by an external heat transfer coefficient h_{cS}, consisting of a convective h_c and a radiative h_{rad} term,

$$h_{cS} = h_c + h_{rad} \tag{8.26}$$

The convective term is derived from the Nusselt number, Nu, which is a function of the Reynolds and Prandtl numbers. For a spherical particle, exposed to a gas stream with velocity *u*, the Nusselt and Reynolds number can be estimated from

$$Nu = \frac{h_c d_{car}}{k_{cg}} = 2 + 0.6\,\mathrm{Re}^{1/2}\,\mathrm{Pr}^{1/3} \qquad \mathrm{Re} = \frac{u d_{car}}{\mu_g / \rho_g} \tag{8.27}$$

where μ is dynamic viscosity, k_g thermal conductivity of gas and d_{car} is the characteristic diameter, defined as the diameter of a sphere with the same surface area as the fuel particle,

$$d_{car} = V_{part}/(6A_{surf}) \tag{8.28}$$

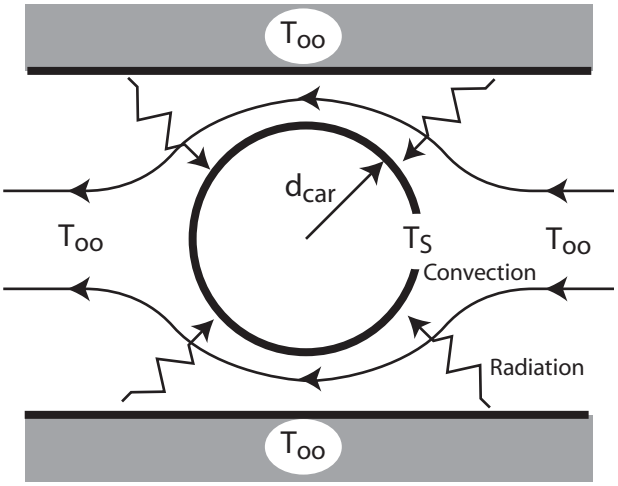

Figure 8.4.
A particle with a characteristic diameter d_{car} exposed to convective and radiative heat transfer.

Eq 8.27 is the most commonly used correlation for a single particle situated in a free gas flow. If the fuel particle is immersed in a fluidised bed the correlation is described by similar, but slightly different, correletion (an example of such correlation is found in the appendix of Thunman et al. [1]).

The radiative heat transfer coefficient is derived from the radiative heat transfer between two bodies,

$$h_{rad} = \frac{\varepsilon\sigma\left(T_\infty^4 - T_{surf}^4\right)}{\left(T_\infty - T_{surf}\right)} = \frac{\varepsilon\sigma\left(T_\infty^2 + T_{surf}^2\right)\left(T_\infty + T_{surf}\right)\left(T_\infty - T_{surf}\right)}{\left(T_\infty - T_{surf}\right)} = \varepsilon\sigma\left(T_\infty^2 + T_{surf}^2\right)\left(T_\infty + T_{surf}\right) \tag{8.29}$$

where ε is the emissivity, σ Stefan Boltzmann's constant, T_{surf} is the surface temperature of the particle and T_∞ is the temperature of the surroundings. For the east boundary of the cell the effective heat transfer coefficient can be derived in the same way as for the effective heat transfer coefficient between cells, Eq (8.22),

$$h_{c,surf} = \frac{2h_c k_{cP}/(\delta x)_P}{\left(h_c + 2k_{cP}/(\delta x)_P\right)} \tag{8.30}$$

This representation of the effective heat transfer coefficient at the boundary, representing the surface of the particle, has some limitations, primarily when it comes to radiation. The radiative heat transfer coefficient is not linear; it is proportional to the third power of the surface temperature. Also the convective part of the heat transfer coefficient is dependent on the surface temperature, since the gas properties depend on temperature, but not as much as the radiative part. Due to the influence of the surface temperature on the heat transfer through the outer boundary layer, the computation of the effective heat transfer coefficient by Eq 8.30 is not straightforward. Basically, there are three approaches; the first is to calculate the surface temperature of the particle by solving the heat balance over the surface by an iterative computation. This can be done in each time step, even if it is complicated to implement. The solution of the surface temperature also becomes sensitive to disturbances, and in most cases it results in a tremendous increase in the time of calculation and sometimes in numerical problems. The second approach is to use the temperature of the cell, whose boundary represents the surface of the particle, to estimate the coefficient of heat transfer (both radiative and convective heat transfer) between the particle and the surroundings. The third option, which is the one mostly used, is the same as the second, except that the heat transfer between the surface and the centre of the first cell is not considered, and the effective heat transfer coefficient through the boundary representing the surface is assumed to be equal to the external heat transfer coefficient, $h_{c,surf} = h_c$.

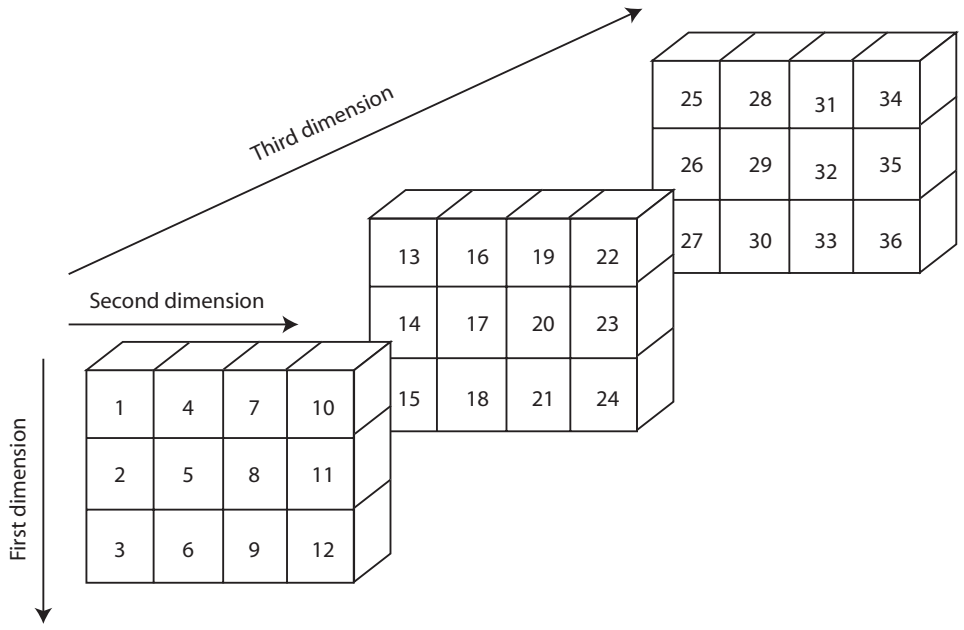

Figure 8.5.
Indices of the cells of a three-dimensional particle divided into 3x4x3 cells

Now the conductive heat transport is defined in all cells from the centre to the surrounding gas and can be included in into the conservation equation of energy Eq (8.14). At present, the source term and the convective term are zero, density and specific heat are kept constant. This makes it possible to describe the transient heating of each and every cell described by

$$\frac{\partial T_P}{\partial t} = \left(\frac{(q_e^{II} - q_w^{II}) + (q_n^{II} - q_s^{II}) + (q_t^{II} - q_b^{II})}{V_P} \right) / \rho_{sP} c_{psP} \qquad (8.31)$$

The initial condition is that the temperature of each cell is equal to the initial fuel temperature.

The set of ordinary differential equations to be solved is

$$\begin{aligned} \frac{\partial T_1}{\partial t} &= Eq\ 8.31 \\ \frac{\partial T_2}{\partial t} &= Eq\ 8.31 \\ &\vdots \\ \frac{\partial T_j}{\partial t} &= Eq\ 8.31 \end{aligned} \qquad (8.32)$$

where j is the number of cells used in the calculation. The index of the cells is trivial for one-dimensional shapes as the first cell indicates the cell in the centre of the particle and the j^{th} cell is the surface. For two or three dimensions the indices of the cells are shown in Fig 8.5

Implementation and validation strategy of Step 1

Calculate the heating of a particle due to diffusive heat transport and validate the model by an analytic solution of the same problem. An analytic solution can be obtained if radiation is excluded and the physical data are constant, see for example Incropera and DeWitt [2]. Carry out this validation for a plate, infinite cylinder, sphere and a two-dimensional cylinder and estimate the mathematical error arising due to the one-dimensional representation of finite cylinders and parallelepipeds.

DRYING (STEP 2)

Now, when the temperature of the particle is described as a function of time it is possible to include the thermal processes of drying and devolatilisation. We start with the drying. The

simplest way is to describe the rate of drying by an Arrhenius equation assuming that the fuel moisture is released at a certain temperature

$$-\frac{\partial Y_m}{\partial t} = Y_m k_{rm0} \exp(-E/T) \qquad (8.33)$$

Y_m is the mass fraction of moisture in the fuel at time t related to the initial moisture content. According to this definition the initial mass fraction is unity. The constants k_{rm0} and E have to be chosen so that the water is released at the physical correct temperature, that is, close to 100°C at an ambient pressure of 100 kPa. The values of 1×10^{27} and 25000 of these constants yield good results for most sizes and biofuels. These values give a release of moisture in a very narrow temperature range around 100°C, and may result in an on-off behaviour of the drying as the drying front goes from one cell to the next. To smoothen out the overall drying rate one can choose a lower value of E. However, if E is changed, also k_{rm0} needs to be changed to keep the drying at the right temperature. For E in the range of 10000 to 30000 a useful value for k_{rm0} can be estimated from

$$k_{rm0} = \exp(-3.15 + E/380) \qquad (8.34)$$

To improve the convergence and speed up the calculation, it is sometimes better to carry out the integration in time using the logarithm of the mass fraction instead of the mass fraction directly, because then the mass fraction does not become negative, a case which may cause numerical problems,

$$-\frac{\partial \log(Y_m)}{\partial t} = k_{rm0} \exp(-E/T) \qquad (8.35)$$

The initial condition for this case is the logarithm of unity, which is zero.

In this way the drying process is described as a one-way process where liquid water evaporates to water vapour. However, the process can also go in the other direction, especially in large particles, where water vapour can be transported from the evaporation front into the cold interior of the particle condensing back to liquid water. A model that allows re-condensation of water vapour transported to the wet core is described later in this chapter.

DEVOLATILISATION (STEP 2)

The simplest way is to model devolatilisation by a single Arrhenius equation similar to the treatment of drying:

$$-\frac{\partial Y_v}{\partial t} = Y_v k_{rv0} \exp(-E/T) \qquad (8.36)$$

Y_v is the mass fraction of volatiles: the content of volatiles in the fuel particle at time t related to the initial content of volatiles. Hence, the initial mass fraction of the volatiles is unity. Appropriate values of the constants k_{rv0} and E for wood are 1.9×10^{12} and 21500 [3]. These values of the constants result in a release of the volatiles in the temperature range of 350 to 450°C. Also for the description of the volatiles it is an advantage to integrate the logarithm of the mass fraction in time instead of the mass fraction directly

$$-\frac{\partial \log(Y_v)}{\partial t} = k_{rv0} \exp(-E/T) \qquad (8.37)$$

In this model the char yield and the corresponding initial content of volatiles have to be given, which is a drawback, since the char and volatile yields actually depend somewhat on heating rate, particle size and final temperature. It is not yet well established how to describe the formation of char, but there are some attempts, and a description is given later in this chapter.

SOURCE TERMS (STEP 2)

With the rates of drying and devolatilisation, the source term in the energy equation can be calculated. The mass releases of moisture and volatiles are

$$R_m = -\frac{Y_{0,m}}{1-Y_{0,m}} \rho_{sd} \frac{\partial Y_m}{\partial t} \qquad (8.38)$$

$$R_v = -Y_{0,v} \rho_{sd} \frac{\partial Y_v}{\partial t} \qquad (8.39)$$

where the initial moisture content of the fuel $Y_{0,\mathrm{m}}$ is based on fuel received and the initial volatile content $Y_{0,\mathrm{v}}$ is based on dry fuel. The heat needed for the processes are given by the mass release times the heat of reaction.

$$S_m = -R_m\left(H_m + \int_{T_{ref}}^{T_P} \left(c_{psm} - c_{pgm}\right)dT \right) \tag{8.40}$$

$$S_v = -R_v\left(H_v + \int_{T_{ref}}^{T_P} \left(c_{psv} - c_{pgv}\right)dT \right) \tag{8.41}$$

where H_m and H_v is the heat of reaction at reference temperature T_{ref}. The sum of the two terms is equal to the source term in the energy equation

$$q_P^{III} = \dot{m}'''H = S_{mP} + S_{vP} \tag{8.42}$$

THE CONSERVATION EQUATION OF ENERGY IN DISCRETE FORM WITH NO CONVECTIVE TERM (STEP 2)

All gases are assumed to leave the particle immediately, without exchanging any heat with the particle, see Fig 8.6. With this assumption, the convective term in the energy equation can be excluded, and the equations to be solved for every cell in the computational domain are

$$\frac{\partial T_P}{\partial t} = \left(\left(q_P^{III} + \frac{(q_e^{II} - q_w^{II}) + (q_n^{II} - q_s^{II}) + (q_t^{II} - q_b^{II})}{V_P} \right) - \rho_{sP} T_P \frac{\partial c_{psP}}{\partial t} \right) / \rho_{sP} c_{psP} \tag{8.43}$$

where the term describing the density change in equation 8.14 disappears due to continuity,

$$\frac{\partial \rho_{sP}}{\partial t} + \frac{\partial u_g \rho_{sP}}{\partial x} = 0 \Rightarrow -\frac{\partial \rho_{sP}}{\partial t} = \frac{\partial u_g \rho_{sP}}{\partial x} = R\,, \tag{8.43a}$$

which give

$$c_{psP} T_P \frac{\partial \rho_{sP}}{\partial t} + c_{pgP} T_P \frac{\partial u_g \rho_{sP}}{\partial x} = \left(c_{psP} T_P - c_{pgP} T_P\right) R\,, \tag{8.43b}$$

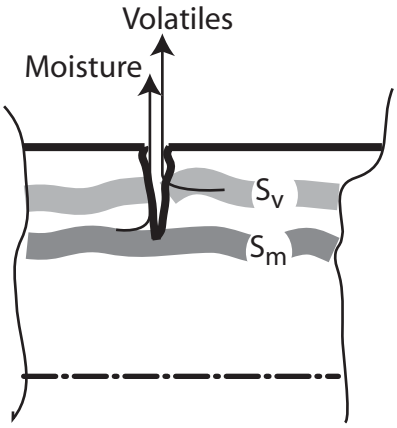

Figure 8.6.
Release of produced gases through cracks.

This term is included in Eqs 8.40 and 8.41 and describes the extra contribution to the heat of reaction.

$$\rho_{sP} T_P \frac{\partial c_{psP}}{\partial t} = \rho_{sP} T_P \left(\frac{\partial c_{psP}}{\partial Y_v} \frac{\partial Y_v}{\partial t} + \frac{\partial c_{psP}}{\partial Y_m} \frac{\partial Y_m}{\partial t} \right) \tag{8.44}$$

$$-\frac{\partial \log(Y_{mP})}{\partial t} = k_{rm0} \exp\left(-E / T_P\right) \tag{8.45}$$

$$-\frac{\partial \log(Y_{vP})}{\partial t} = k_{rv0} \exp\left(-E / T_P\right) \tag{8.46}$$

The set of ordinary differential equation to be solved are expanded with two: one for the fraction of moisture and one for the fraction of volatiles remaining in the fuel particle,

$$\frac{\partial T_1}{\partial t} = Eq\ 8.44$$
$$\frac{\partial T_2}{\partial t} = Eq\ 8.44$$
$$\vdots$$
$$\frac{\partial T_j}{\partial t} = Eq\ 8.44$$
$$\frac{\partial \log(Y_m)_1}{\partial t} = Eq\ 8.45$$
$$\frac{\partial \log(Y_m)_2}{\partial t} = Eq\ 8.45$$
$$\vdots$$
$$\frac{\partial \log(Y_m)_j}{\partial t} = Eq\ 8.45$$
$$\frac{\partial \log(Y_v)_1}{\partial t} = Eq\ 8.46$$
$$\frac{\partial \log(Y_v)_2}{\partial t} = Eq\ 8.46$$
$$\vdots$$
$$\frac{\partial \log(Y_v)_j}{\partial t} = Eq\ 8.46 \qquad (8.47)$$

Implementation and validation strategy of Step 2

Assume that all gases, produced during drying and devolatilisation, leave the particle immediately through cracks and, thereby, do not cause any convective heat transfer within the fuel particle. Formulate the source term and calculate the mass loss due to drying and devolatilisation for all particle shapes. Simulate the drying and devolatilisation of the measured fuel particles and compare the mass loss with the mass loss obtained from measured fuel particles.

CONVECTIVE TERM IN THE ENERGY EQUATION (STEP 3)

During the heating of the particle gas is produced and then transported from the interior of the particle to the surroundings. This causes a convective heat flow, described by the second term on the left hand side of the conservation equation, Eq 8.1

$$\frac{\partial \rho_g u_g c_{pg} T}{\partial x} \qquad (8.48)$$

This term can be rewritten as

$$\frac{\partial A \rho_g u_g c_{pg} T}{A \partial x} \text{ or } \frac{\partial A \rho_g u_g c_{pg} T}{\partial V} \qquad (8.49)$$

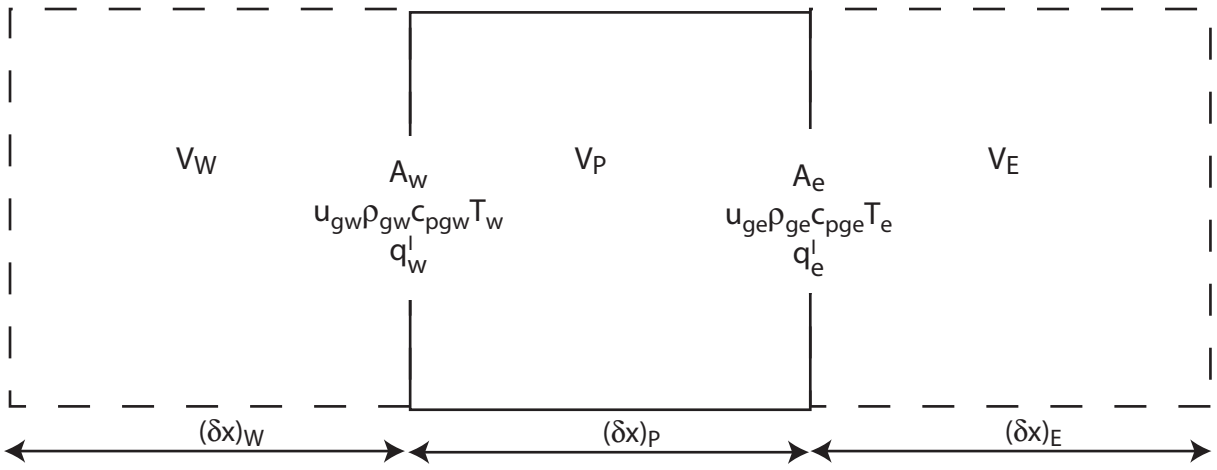

Figure 8.7.
Variables included in the discrete form of the convective term in the energy equation.

or in discrete form

$$\frac{\Delta\left(A\rho_g u_g c_{pg} T\right)}{V_P} = \frac{\left(q_e^I - q_w^I\right)}{V_P} \tag{8.50}$$

The total convective flow is expressed by two terms: one for the gas flow and one for the flow of solid. The solid flow is due to shrinkage or swelling of the particle. These processes of the solid material are, however, slow and usually handled by changing the volume of the computational cell instead of describing the flow of the solid. By doing so, the derivation is simplified:

- the surface area of the particle is defined by the surface area of the initial set of computational cells in all time steps.
- the velocity of the solid phase does not have to be calculated, a complicated calculation, because the velocity is affected by nearly all cells in the computational domain.

The heat transported between cell P and E, q_e^I, for a shrinking or swelling computational cell follows from eq (8.50)

$$q_e^I = A_e u_{ge} \rho_{ge} c_{pge} T_e \tag{8.51}$$

This leaves gas velocity, density and specific heat at the boundary to be determined. The gas velocity is given by the pressure gradient, density and specific heat in the condition on the boundary. In a simplified case, where the specific heat is kept constant, this is no problem, as the density is obtained from the temperature at the boundary. However, in a more exact description of the problem complications occur. For example, the temperature and the concentration of the gases at the boundary are shifted from some average value to one of the values at the centre of the cells on either side of the boundary due to the convective flow. Is this then a problem? The answer is that, in the case of the temperature, the convective term does not have a great influence, as seen from the thermal Peclet number that relates heat transported by convection to that transported by conduction,

$$Pe_{th} = \frac{u_{ge} c_{pge} \rho_{ge}}{h_{ce}} \tag{8.52}$$

At the cell sizes needed for the description of the processes within the fuel particles this number is close to zero, the influence of the convective term is negligible, and the average temperature given by Eq (8.21) is the temperature to use at the boundary. For the gas composition the result is not so clear, because the convective term is often larger than the diffusive one, as can be seen from the Peclet number related to transport of mass

$$Pe_m = \frac{u_{ge}}{h_{me}} \tag{8.53}$$

where h_{me} is the effective mass transfer coefficient at boundary e, to be defined below, Eq 8.102. The molar fraction X of each species i at the boundary is calculated from the Peclet number as

$$X_{ie} = X_{iP}(1-\Phi) + X_{iE}\Phi \tag{8.54}$$

where Φ is the split factor between the molar fraction in cell E and P, which is given by the steady state solution of the conservation equation of species without any source term at the boundary e

$$\Phi = \frac{\exp(\mathrm{Pe}\,(\delta x)_P / 2) - 1}{\exp(\mathrm{Pe}) - 1} \tag{8.55}$$

Now the density and specific heat can be calculated at the boundary. If the cells are kept reasonably large and the convective heat flow is defined according to Eq (8.51) a rather large numerical error will result due to the temperature gradient and the change of the gas composition within the computational cell, caused by the gas production within the cell. The way around this problem is to define the convective heat transported across the boundary by integrating the heat flow from the reference temperature T_{ref} to the temperature at the boundary T_e,

$$q_e^I = A_e \sum_i u_{ge} \rho_{ie} \int_{T_{ref}}^{T_e} c_{pgi}\, dT \tag{8.56}$$

where

$$\rho_{ie} = X_{ie} C_e / M_i \tag{8.57}$$

When the convective term is defined in this way, the source terms (Eq 8.40 and 41) must be modified in order not to account for the heat leaving with the gas twice. The resulting source terms become,

$$S_m = -R_m \left(H_m + \int_{T_{ref}}^{T_P} c_{ps} dT \right) \tag{8.58}$$

$$S_v = -R_v \left(H_v + \int_{T_{ref}}^{T_P} c_{ps} dT \right) \tag{8.59}$$

When gas flows out from the particle, the convective heat transfer from the surroundings to the surface of the particle is reduced. Denoting the convective heat transfer coefficient that is not compensated for the gases leaving the particle by h_{c0}, and the convective heat transfer coefficient compensated for this gas flow by h_c, the ratio of these two can be calculated according to[Bird],

$$\frac{h_c}{h_{c0}} = \frac{\rho_g u_g c_{pg} / h_{c0}}{\exp\left(\rho_g u_g c_{pg} / h_{c0}\right) - 1} \tag{8.60}$$

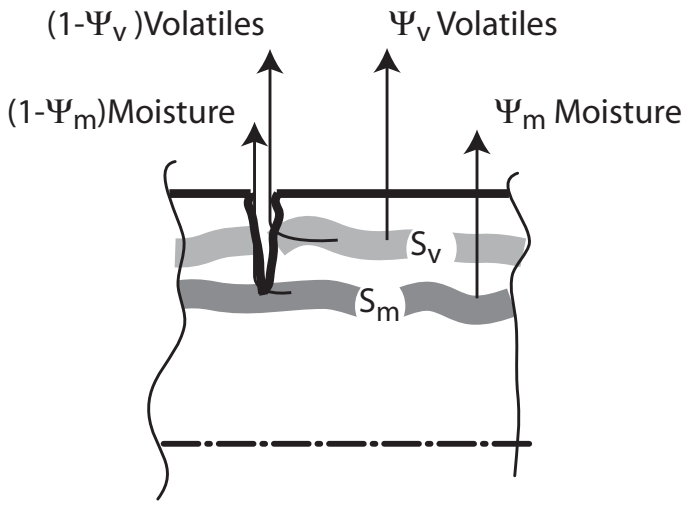

Figure 8.8
Release of produced gases through cracks and through the porous structure.

In the general case, only part of the gas passes through the solid matrix. Here Ψ represents this mass fraction and $(1-\Psi)$ represents the rest of the produced gas, the part leaving through the cracks, see Fig 8.8. Most biofuel particles form cracks, through which the gas easily can escape without having any contact with the solids between the position of its release and the surface of the particle. It is not known how to treat this factor, and it therefore, remains uncertain when comparing model results with measurements. Of course, some estimation can be made from investigation of the amount of cracks in dried and devolatilised particles. The part of the gas flow that does not pass through the porous structure is excluded from the convective flow, and must therefore be included in the source terms

$$S_m = -R_m\left(H_m + \int_{T_{ref}}^{T_P} \left(c_{psm} - (1-\Psi_m)c_{pgm}\right)dT \right) \tag{8.61}$$

$$S_v = -R_v\left(H_v + \int_{T_{ref}}^{T_P} \left(c_{psv} - (1-\Psi_v)c_{pgv}\right)dT \right) \tag{8.62}$$

In a particle with one-dimensional convective gas flow, the convective flow leaving one cell for the next can be described by the mass release integrated from the particle's centre to the outer boundary of the cell P in the direction of the flow. If cell P is the j^{th} cell from the centre, the heat flow through its east boundary would be

$$q_e^I = A_e \sum_i u_{ge} \rho_{ie} \int_{T_{ref}}^{T_e} c_{pgi}\, dT = \sum_{k=1}^{j} \left(\sum_i \left(V_k \left(\psi_{mk} R_{mk} Y_{mi} + \psi_{vk} R_{vk} Y_{vi} \right) \int_{T_{ref}}^{T_e} c_{pgi}\, dT \right) \right) \quad (8.63)$$

This simple representation of the convective flow assumes that all gas produced is immediately transported to the surface of the particle and, therefore, no pressure is built up inside the particle, and no re-condensation of water or hydrocarbons takes place inside the particle. For a particle with a two-dimensional convective flow this simplification is applicable, since the gas flows in the different directions are given by the local pressure distribution, together with the permeability of the flow in the different directions inside the fuel particle. However, the permeability of a wood particle is much larger along the fibre than perpendicular to the fibres. This means that nearly all gas will be transported in one dimension (along the fibres) and Eq (8.63) becomes applicable even in two- and three-dimensional computations of wood particles.

CONSERVATION EQUATION OF ENERGY IN DISCRETE FORM (STEP 3)

All of the terms in the energy equation are now described, and the equation to be solved for the temperature in every cell of the computational domain is

$$\frac{\partial T_P}{\partial t} = \left(\left(q_P^{III} + \frac{(q_e^{II} - q_e^I - q_w^{II} + q_w^I) + (q_n^{II} - q_n^I - q_s^{II} + q_s^I) + (q_t^{II} - q_t^I - q_b^{II} + q_b^I)}{V_P} \right) - \rho_{sP} T_P \frac{\partial c_{psP}}{\partial t} \right) / \rho_{sP} c_{psP} \quad (8.64)$$

$$\rho_{sP} T_P \frac{\partial c_{psP}}{\partial t} = \rho_{sP} T_P \left(\frac{\partial c_{psP}}{\partial Y_C} \frac{\partial Y_C}{\partial t} + \frac{\partial c_{psP}}{\partial Y_v} \frac{\partial Y_v}{\partial t} + \frac{\partial c_{psP}}{\partial Y_m} \frac{\partial Y_m}{\partial t} \right) \quad (8.65)$$

So far the convective flow is only described for a one-dimensional gas flow. The same set of ordinary differential equations as before (Eq 8.47) are to be solved, however, the temperature derivative is given by Eq 8.64 instead of Eq. 8.44.

Implementation and validation strategy of Step 3

Introduce the convective flow into your model and validate the result by a heat and mass balance over the particle. Calculate the mass loss due to drying and devolatilisation and

compare mass release from the model with experimental data of mass release. For this comparison, use the shape of a one- and two-dimensional finite cylinder and a sphere. Assume that a particle of any shape can be characterised by the conversion of a sphere that has the same area-volume ratio as the initial area-volume ratio of the particles used in the measurements. Investigate how the convective flow influences the heating process of the fuel particle (change the fraction of gas that escapes through cracks) and control that the condition when all gas go through cracks correspond to the result obtained by the model after step 2.

PARTICLE TRANSFORMATION IN ONE DIMENSION (STEP 4)

An important factor, which is not always considered, is the transformation of particle size during conversion. For example, wood, which is of main interest here, shrinks in size but more or less retains its shape. A guideline for wood is that the volume of a fuel particle shrinks with 10% during drying, expressed by a shrinkage coefficient, θ_m, (dry fuel volume/ initial volume), if the particle is initially wet (moisture >15% of mass as received). During devolatilisation the shrinkage is around 50%, θ_v, (volume of char/ volume of dry particle). During char combustion the particle is consumed and the volume is reduced by 95%, θ_C, (volume of ash/ volume of char). Assuming that the shrinkage is linearly dependent on the release of the each constituent, moisture, volatile and char, the relative volume θ (volume/ initial volume) can be calculated from the relative mass fraction of each constituent Y_i (massof component *i*/ initial mass of component *i*),

$$\begin{aligned}\theta &= Y_m + (Y_v - Y_m)\theta_m + (Y_C - Y_v)\theta_v\theta_m + (1 - Y_C)\theta_C\theta_v\theta_m = \\ &= Y_m(1-\theta_m) + Y_v(\theta_m - \theta_v\theta_m) + Y_C(\theta_v\theta_m - \theta_C\theta_v\theta_m) + \theta_C\theta_v\theta_m\end{aligned} \tag{8.66}$$

It is complex to handle the shrinkage of the particle, although there are a number of approaches available. For shapes treated in one dimension there is, however, no problem, since the shrinkage can only occur in the direction of the co-ordinate. The height of the computational cell in such case can be calculated from the initial volume of the cell and the relative shrinkage. If the active cell *P* is the j^{th} cell from the centre of the particle, the co-ordinate of its east boundary is given by the inverse function, $f_\xi[V]$, of $f_V[\xi]$ (listed in Table 8.2) defining the volume from the centre of the particle to the same boundary,

$$\sum_{k=1}^{ji} V_{k0}\theta_k = f_V[\xi]$$

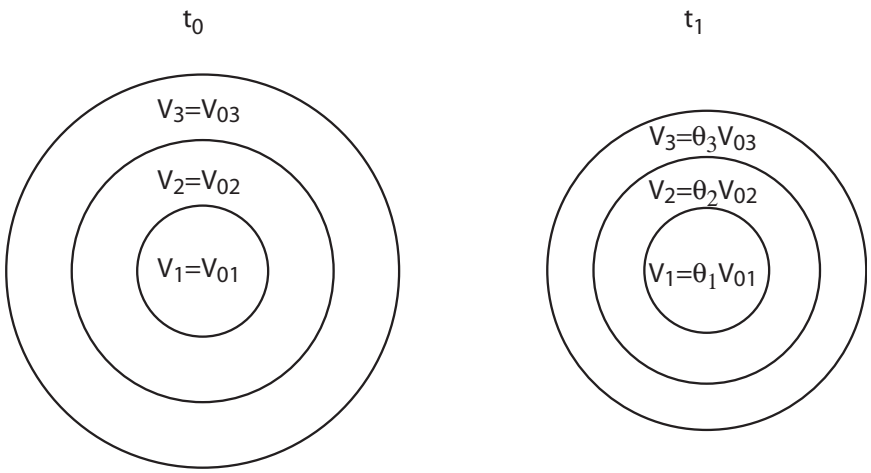

Figure 8.9
The volume of cells at initial time t_0 and at time t_1.

Table 8.3 The inverse functions of the volume give the co-ordinate of the east boundary of each cell.

Shape	$f_\xi[V]$
Sphere	$\left((3/4)V/\pi\right)^{1/3}$
Infinite cylinder	$\left(V/\pi\right)^{1/2}$
Infinite plate	V
Finite cylinder	$\left(\left(-2a+2^{2/3}W\right)/6+2^{4/3}a^2/W\right)/6$
where	$W=\left(-2a^3+27V^*+\sqrt{V^*\left(729V^*-108a^3\right)}\right)^{1/3}$
	$a=\left(L-d\right)/2\,,\qquad V^*=V/(2\pi)$
Parallelepiped, $L_1\le L_2\le L_3$	$\left(-a_1+2^{1/3}\left(a_1^2-3a_2\right)/W+2^{-1/3}W\right)/6$
where	$W=\left(9a_1a_2-2a_1^3+27V+\sqrt{4\left(3a_2-a_1^2\right)^3+\left(9a_1a_2-2a_1\right.}\right.$
	$a_1=(L_2-L_1)+(L_3-L_1),\qquad a_2=(L_2-L_1)(L_3-L_1)$

The coordinate ξ is obtained from

$$\xi = f_{\xi}\left[\sum_{k=1}^{j} V_{k0}\theta_k\right] \tag{8.67}$$

The expressions of the inverse function, $f_{\xi}[V]$, are summarised for various shapes in Table 8.3. The expressions are simple for the three conventional shapes (sphere, infinite cylinder and infinite plate), but rather complicated for the other two (finite cylinder and parallelepiped). This is, however, not a problem, because they are easily expressed in the numerical code, making the calculation simple and fast to perform. The new size of the cells are calculated from the co-ordinates of the boundaries

$$(\delta x)_P = \xi_e - \xi_w \tag{8.68}$$

Because of the roots, the expressions for finite cylinder and parallelepiped may result in a real part and a very small imaginary part. Such an imaginary part is due to truncation errors in the computation (error due to numerical precision of the computer). It is important to make the number real by removing the imaginary part, because the imaginary part may result in unexpected errors in other parts of the computation.

CONSERVATION EQUATION OF ENERGY IN DISCRETE FORM ACCOUNTING FOR SHRINKAGE (STEP 4)

All of the terms in the energy equation are now described, and the equation to be solved for the temperature in every cell of the computational domain is

$$\frac{\partial T_P}{\partial t} = \left(\left(q_P^{III} + \frac{(q_e^{II} - q_e^{I} - q_w^{II} + q_w^{I}) + (q_n^{II} - q_n^{I} - q_s^{II} + q_s^{I}) + (q_t^{II} - q_t^{I} - q_b^{II} + q_b^{I})}{V_{P,0}}\right) - \rho_{sP}^0 T_P \frac{\partial c_{psP}}{\partial t}\right) / \rho_{sP}^0 c_{psP} \tag{8.69}$$

$$\rho_{sP}^0 T_P \frac{\partial c_{psP}}{\partial t} = \rho_{sP}^0 T_P \left(\frac{\partial c_{psP}}{\partial Y_C}\frac{\partial Y_C}{\partial t} + \frac{\partial c_{psP}}{\partial Y_v}\frac{\partial Y_v}{\partial t} + \frac{\partial c_{psP}}{\partial Y_m}\frac{\partial Y_m}{\partial t}\right) \tag{8.70}$$

where we use an apparent density indicated by the superscript 0 and the initial volume of the cell. The apparent density is defined

$$\rho_{sP}^{0} V_{P,0} = \rho_{sP} V_P = m_P \tag{8.71}$$

The source terms included in q_P^{III}, given by Eqs (8.33) and (8.36), are related to the initial cell volume and therefore follow the formulation of Eq (8.69). On the other hand, the diffusive and convective terms (q^{II}, q^{I}) are affected, and the new geometrical and new physical data for the new cell volume resulting from the shrinkage must be considered. When the convective flow is described in one dimension by Eq (8.63), the flow results from the gas production and the initial volume of the cell should be used. No compensation for shrinkage has to be made. If cell P is the j^{th} cell from the centre, the heat flow through its east boundary would be

$$q_e^I = \sum_{k=1}^{j} \left(\sum_i \left(V_{k,0} \left(\psi_{mk} R_{mk} Y_{mi} + \psi_{vk} R_{vk} Y_{vi} \right) \int_{T_{ref}}^{T_e} c_{pgi}\, dT \right) \right) \tag{8.72}$$

The set of ordinary differential equations is the same as in the previous step, with the difference that the temperature derivatives are calculated according to Eq (8.69) instead of Eq (8.64).

Implementation and validation strategy of Step 4

Introduce shrinkage in the case of one-dimensional shapes and investigate the influence of the shrinkage. Remember to change the physical data as you change shrinkage parameters. Investigate how the shrinkage influences the drying and devolatilisation times by changing the relative shrinkage of the different stages and the moisture and volatile contents of the fuel. Compare the result from the finite cylinder shape with measurement data.

PARTICLE TRANSFORMATION IN A TWO-DIMENSIONAL CASE (STEP 5)

The treatment of shrinkage is not as straightforward for a two-dimensional cylinder as for the shapes represented in one-dimension. Here, a simple model will be presented. The model assumes that the shrinkage can be decomposed in two directions, shrinkage along the symmetry line, θ_{par}, can be described in the same way as it is done for the infinite plate and in

the perpendicular direction, θ_{per}, as done for the infinite cylinder. The two-dimensional shrinkage factor then becomes

$$\theta_{par}\theta_{per}^2 = \theta \tag{8.73}$$

The relation between the shrinkage in the two directions is assumed to be constant, given by a factor φ, where φ is defined

$$\varphi = \frac{1-\theta_{par}}{1-\theta_{per}} \tag{8.74}$$

This means that the shrinkage along the fibres can be expressed by the shrinkage in the perpendicular direction,

$$\theta_{par} = 1-\varphi(1-\theta_{per}) \tag{8.75}$$

It becomes simple to extract the shrinkage parameters in the two directions from Eq (8.73) if $\varphi = 1$, since then $\theta_{par} = \theta_{per} = \theta^{1/3}$. If $\varphi \neq 1$ the extraction is somewhat more complicated, as derived from 8.73 and 8.75

$$\theta_r = \left((\varphi\text{-}1)+\left(2^{-2/3}\left(1+(-3)^{1/2}\right)(\varphi\text{-}1)^2\right)W^{-1} + 2^{-4/3}\left(1-(-3)^{1/2}\right)W\right)/(3\varphi) \tag{8.76}$$

where

$$W = \left(2 + (6 - 27\theta)\varphi^2 - 2\varphi^3 + 3\varphi\left(-2 + \sqrt{3\theta\left(-4 + 12\varphi + 3(9\theta - 4)\varphi^2 + 4\varphi^3\right)}\right)\right)^{1/3} \tag{8.77}$$

and θ_a is calculated from Eq (8.75). Eq 8.76 will give a small imaginary part, due to the limitation of the numerical resolution of the computer. It is important to make the number real by removing the imaginary part of the number, because as mentioned before the imaginary part may result in unexpected errors in other parts of the computation. The co-ordinates of the east and the top boundary of the active cell P situated j_a cells from the perpendicular

symmetry plane and j_r cells from the axial symmetry line are calculated from the initial size of the cells

$$\xi_{aj_a j_r} = \sum_{k=1}^{j_a} \theta_{akj_r} (\delta x)_{akj_r,0} \qquad (\delta x)_{aj_a j_r} = \theta_{aj_a j_r} (\delta x)_{aj_a j_r,0} \qquad (8.78)$$

$$\xi_{r_{j_a} j_r} = \left(\sum_{k=1}^{j_r} \theta^2_{rj_a k} \left((\delta x)_{rj_a k,0} - (\delta x)_{rj_a k-1,0} \right) \right)^{1/2} \qquad (\delta x)_{rj_a j_r} = \xi_{rj_a j_r} - \xi_{rj_a j_r-1} \qquad (8.79)$$

The change of the shape of the cells is demonstrated in Fig 8.10.

Implementation and validation strategy of Step 5
Introduce shrinkage in the two-dimensional description. Validate the result and compare simulations of the mass release from particles with measured mass release. If you have reached this step you have a model describing drying and devolatilisation of a single wood particle, which is state of the art and better than most models published at present.

PRESSURE DISTRIBUTION AND GAS VELOCITY IN N-DIMENSIONS (STEP 6)

So far the description of the convective flow within the fuel particles is simplified and can only account for a one-dimensional flow. No gas pressure was allowed to be built up during the conversion. In order to describe the flow in more than one dimension the pressure field has to be introduced in the modelling. This can be calculated from the gas concentration C by the gas law.

$$P = C\Re T \qquad (8.80)$$

where the gas concentration is the concentration within the gas filling the void of the porous structure. In the calculation it is an advantage to relate the concentration of the gas to the initial volume of the cell C^0. This is done by introducing a relative gas volume ζ as the ratio of the initial volume of the computational cell, V_0, to the volume of gas in the shrunk or swelled computational volume,

$$C = \zeta C^0 \qquad (8.81)$$

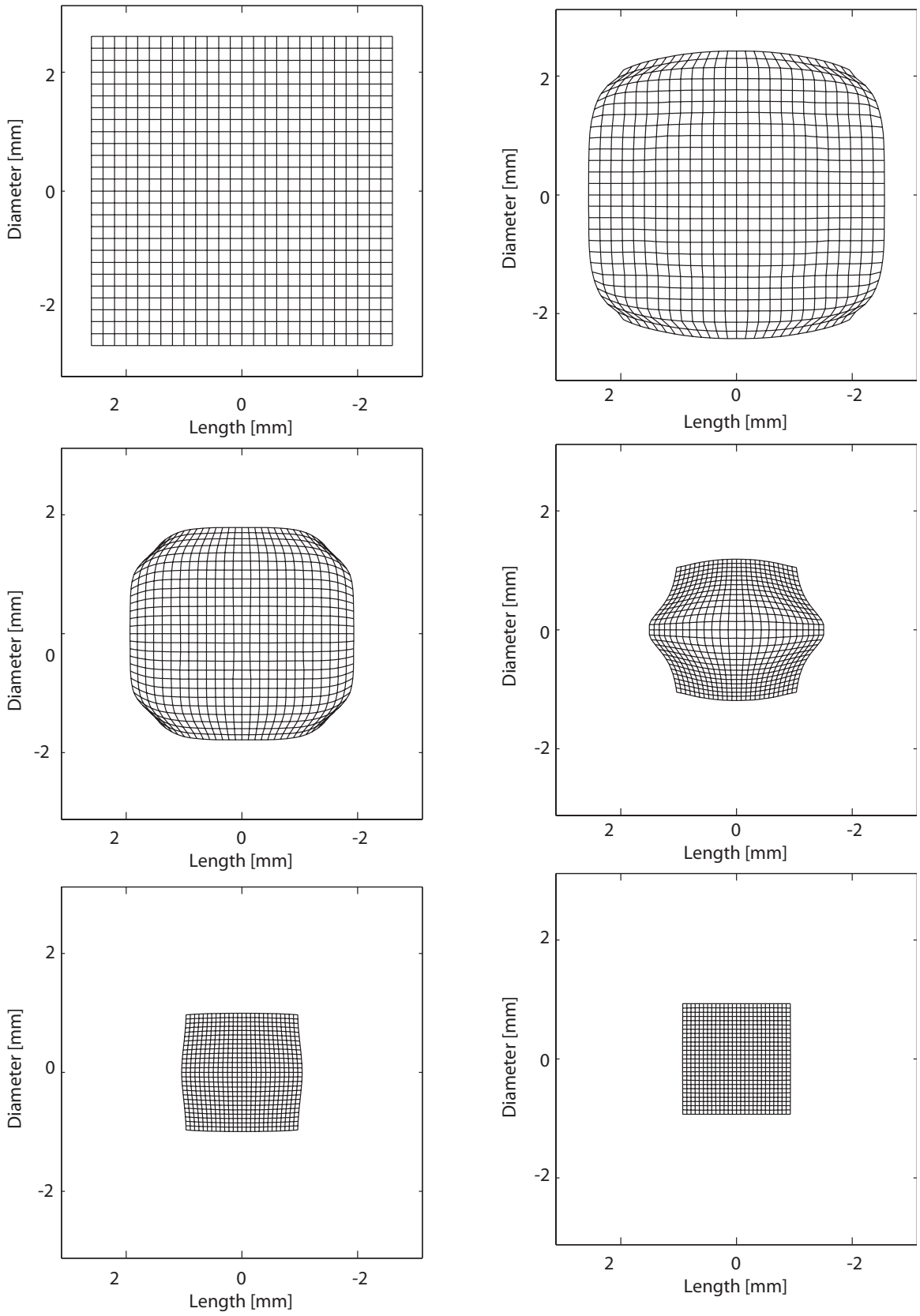

Figure 8.10.
The geometrical change of a cylindrical particle at different times. In the end of combustion (bottom right figure) when only ash remains the cylinder has shrunk with 97%.

The relative volume of the gas void in one cell is calculated

$$\zeta = \frac{V_0}{V_g} = \frac{V_0}{V - V_s} = \frac{1}{V/V_0 - V_s/V_0} = \frac{1}{\theta - \omega} \tag{8.82}$$

where θ is the shrinkage factor, as above, and ω is relative volume of the solid phase, which changes due to the release of moisture, m, volatiles, v, and char, c.

$$\omega = Y_m\left(\frac{Y_{m0}}{1-Y_{m0}}\frac{\rho_{df}}{\rho_m}\right) + Y_v\left(\frac{Y_{v0}\rho_{df}}{\rho_v}\right) + Y_C\left(\frac{Y_{C0}\rho_{df}}{\rho_C}\right) + Y_a\left(\frac{Y_{a0}\rho_{sd}}{\rho_a}\right) \tag{8.83}$$

The index to the densities are as follows: *df*, dry fraction, *m* moisture (water), *v* density of the volatile part of the solid structure in the porous particle, defined

$$\rho_v = \left(\rho_{s0} - Y_{C0}\rho_C - Y_{a0}\rho_a\right)/Y_{v0} \tag{8.84}$$

The indices *c* and *a* are the density of char and ash parts of the solid structure in the porous particle. Index *0* indicate the initial mass fraction of moisture (as recived), volatiles, fixed carbon and ash given from the proximate analysis. The gas void can be calculated from the relative volume of the gas void and the shrinkage,

$$\nu_g = \left(\zeta\theta\right)^{-1} \tag{8.85}$$

The change of porosity (gas voidage) related to the shrinkage and the escape of solid material is illustrated in Fig 8.11. Once the pressure field is known, the gas flow in the various directions can be calculated. Darcy's law is a widely used model describing the average gas flow through a surface with a given area caused by the pressure distribution

$$u_g = -\frac{s_g}{\mu_g}\frac{\partial P}{\partial x} \tag{8.86}$$

s_g is the permeability, and P is pressure. If we assume that the pressure P represents the pressure in the centre of a cell, the gas flow can be calculated analogously to the conductive heat transfer, Eq (8.22),

$$u_{ge} = -\frac{s_{gE}}{\mu_{gE}} \frac{2(P_e - P_E)}{(\delta x)_E} = -\frac{s_{gP}}{\mu_{gP}} \frac{2(P_P - P_e)}{(\delta x)_P} \qquad (8.87)$$

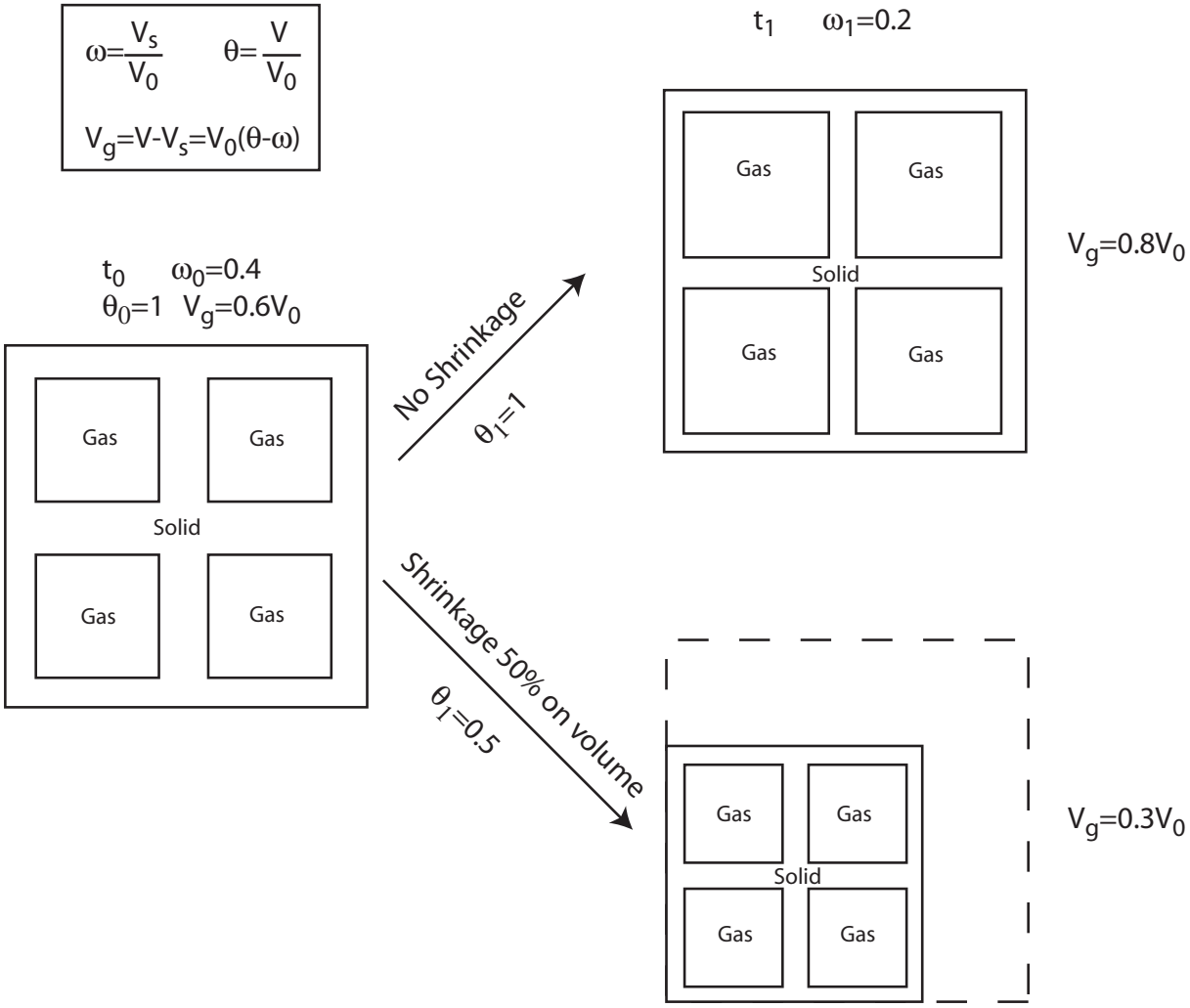

Figure 8.11.
Relation between the gas void and the initial volume as the particle shrinks, shrinkage is charcterised by θ and solid material leaving the particle is expressed by the solid fraction ω, at initial time t_0 and time t_1 when part of the solid material has left the particle.

$$u_{ge} = \vartheta_e \left(P_E - P_P \right) \tag{8.88}$$

$$\vartheta_e = \frac{2\left(s_{gE} / (\mu_{gE} (\delta x)_E) \right)\left(s_{gP} / (\mu_{gP} (\delta x)_P) \right)}{\left(s_{gE} / (\mu_{gE} (\delta x)_E) \right) + \left(s_{gP} / (\mu_{gP} (\delta x)_P) \right)} \tag{8.89}$$

To apply this law we must assume that the gas behaves like an ideal gas obeying the gas law. The boundary conditions are that the pressure at the surface of the particle is the equal to the ambient pressure and that there is no pressure gradient across symmetry lines or symmetry planes in the particle. The initial condition is that the ambient pressure prevails in the entire particle.

The pressure is given by the gas concentration in the particle. The change of gas concentration must be included in the model. The change in concentration is due to the gas flow between cells and gas production within the cells

$$\frac{\partial C_P^0}{\partial t} = -\frac{n_e^I - n_w^I}{V_{P,0}} + \frac{R}{M} \tag{8.90}$$

The molar flow between the cells is given by

$$n_e^I = A_e u_{ge} C_e \tag{8.91}$$

where the gas concentration at the boundary can be calculated from the temperature, Eq (8.21), and the pressure at the boundary from Eqs (8.87) and (8.88)

$$C_e = \frac{P_e}{\Re T_e} \tag{8.92}$$

The molar flow through the boundaries in the other directions, west, north, south, top, bottom, are calculated in the same way.

To obtain the pressure field and the gas flows in n directions the set of ordinary differential equation need to be expanded by one variable, the gas concentration.

$$
\begin{aligned}
\frac{\partial T_1}{\partial t} &= Eq\ 8.69 \\
\frac{\partial T_2}{\partial t} &= Eq\ 8.69 \\
&\vdots \\
\frac{\partial T_j}{\partial t} &= Eq\ 8.69 \\
\frac{\partial \log(Y_m)_1}{\partial t} &= Eq\ 8.45 \\
\frac{\partial \log(Y_m)_2}{\partial t} &= Eq\ 8.45 \\
&\vdots \\
\frac{\partial \log(Y_m)_j}{\partial t} &= Eq\ 8.45 \\
\frac{\partial \log(Y_v)_1}{\partial t} &= Eq\ 8.46 \\
\frac{\partial \log(Y_v)_2}{\partial t} &= Eq\ 8.46 \\
&\vdots \\
\frac{\partial \log(Y_v)_j}{\partial t} &= Eq\ 8.46 \\
\frac{\partial C_1^0}{\partial t} &= Eq\ 8.90 \\
\frac{\partial C_2^0}{\partial t} &= Eq\ 8.90 \\
&\vdots \\
\frac{\partial C_j^0}{\partial t} &= Eq\ 8.90
\end{aligned}
\qquad (8.93)
$$

Implementation and validation strategy of Step 6
Introduce the change of the gas concentration into the model. In this step, give all gases the same average molar mass and specific heat. Investigate the change of pressure during the process. It is important to validate this step numerically to assure that the mass leaving the particle in the form of gas is correct before going to the next step.

CHANGE IN SPECIES CONCENTRATION DUE TO CONVECTIVE FLOW (STEP 7)

In the previous step the gas was assumed to consist of a single species In the real case, however, several species have to be considered. This may not be critical for the drying and the devolatilisation processes, but it is so for the char combustion. In order not to go to fast forward we start by expanding Eq (8.90) for species *i*, considering the changes of the molar fractions of the individual species only due to the convective flow

$$\frac{\partial C_P^0 X_{iP}}{\partial t} = -\frac{n_e^I X_{ie} - n_w^I X_{iw}}{V_{P,0}} + \frac{R_i}{M_i} \tag{8.94}$$

which can be rewritten as

$$\frac{\partial X_{iP}}{\partial t} = \left(-\frac{n_e^I X_{ie} - n_w^I X_{iw}}{V_{P,0}} + \frac{R_{iP}}{M_i} - X_{iP} \frac{\partial C_P^0}{\partial t} \right) / C_P^0 \tag{8.95}$$

or in all dimensions

$$\frac{\partial X_{iP}}{\partial t} = \left(-\frac{n_{ie}^I - n_{iw}^I + n_{in}^I - n_{is}^I + n_{it}^I - n_{ib}^I}{V_{P,0}} + \frac{R_{iP}}{M_i} - X_{iP} \frac{\partial C_P^0}{\partial t} \right) / C_P^0 \tag{8.96}$$

where

$$n_{ie}^I = n_e^I X_{ie} \text{ and } n_{iw}^I = n_w^I X_{iw} \tag{8.97}$$

The concentration at the boundary X_{ie} is expressed by Eq (8.54) and the concentration on the other boundaries is calculated in the same way. By definition, the sum of the all molar fractions is unity,

$$\sum_j X_i = 1, \tag{8.98}$$

which makes it possible to calculate only n-1 species. During the development of the model it is, however, suggested to include all species in the calculation and use this condition for the validation of the model.

The boundary condition is that the flow across the symmetry line or plane is zero. The initial condition is that the gas composition inside the particle is the same as the gas composition in the surroundings.

Each species included into the model needs its own set of equation to be solved and the set of differential equations given by Eq (8.93) should be expanded as follows

$$
\begin{aligned}
&Eq\ 8.90 \\
&\frac{\partial X_{11}}{\partial t} = Eq\ 8.96 \\
&\frac{\partial X_{21}}{\partial t} = Eq\ 8.96 \\
&\quad\vdots \\
&\frac{\partial X_{j1}}{\partial t} = Eq\ 8.96 \\
&\frac{\partial X_{12}}{\partial t} = Eq\ 8.96 \\
&\frac{\partial X_{22}}{\partial t} = Eq\ 8.96 \\
&\quad\vdots \\
&\frac{\partial X_{j2}}{\partial t} = Eq\ 8.96 \\
&\quad\vdots \\
&\quad\vdots \\
&\frac{\partial X_{1i}}{\partial t} = Eq\ 8.96 \\
&\frac{\partial X_{2i}}{\partial t} = Eq\ 8.96 \\
&\quad\vdots \\
&\frac{\partial X_{ji}}{\partial t} = Eq\ 8.96
\end{aligned}
\tag{8.99}
$$

where j is the number of the cells and i is the number of species.

Implementation and validation strategy of Step 7
Introduce three species, water, volatiles, and air, and introduce the change of the molar fractions of these species with time within the particle, caused by the convective flow. Use the condition that the sum of the molar fractions should be equal to unity at all time.

DIFFUSION OF GASES WITHIN A FUEL PARTICLE (STEP 8)

The diffusive term describes the transport of, for example, oxygen from the surroundings into the particle for char combustion. This term corresponds to the term describing conduction of heat in the energy equation Eq (8.18), and it is expressed in the same way but for mass instead of temperature.

$$
\frac{(n_{ie}^{II} - n_{iw}^{II}) + (n_{in}^{II} - n_{is}^{II}) + (n_{it}^{II} - n_{ib}^{II})}{V_{P,0}} \tag{8.100}
$$

where

$$n_{ie}^{II} = A_e h_{me} C_e \left(X_E - X_P \right) \tag{8.101}$$

The effective mass transfer coefficient h_{me} between cell P and E is derived analogously to the effective heat transfer coefficient h_{ce}, Eq (8.23)

$$h_{me} = \frac{2(D_{AB,effP} / x_P)(D_{AB,effE} / x_E)}{(D_{AB,effP} / x_P) + (D_{AB,effE} / x_E)} \tag{8.102}$$

where the heat conductivity is replaced by the effective diffusivity (molecular diffusivity compensated for the porous structure). By including the diffusive term into Eq (8.96) the final form of the conservation equation of species is obtained

$$\frac{\partial X_{iP}}{\partial t} = \left(\frac{n_{ie}^{II} - n_{ie}^{I} - n_{iw}^{II} + n_{iw}^{I} + n_{in}^{II} - n_{in}^{I} - n_{is}^{II} + n_{is}^{I} + n_{ib}^{II} - n_{ib}^{I} - n_{it}^{II} + n_{it}^{I}}{V_{P,0}} + \frac{R_{iP}}{M_i} - X_{iP} \frac{\partial C_P^0}{\partial t} \right) / C_P^0 \tag{8.103}$$

As the gas species have different specific heats the convective term in the energy equation has to be compensated for the corresponding diffusive flow. This is made by considering the convective flow as a sum of the flow of each individual species through the boundary of the cell as described in Eq (8.56)

$$q_e^I = A_e \sum_i u_{ge} \rho_{ie} \int_{T_{ref}}^{T_e} c_{pgi}\, dT = \sum_i (n_{ie}^{II} - n_{ie}^{I}) M_i \int_{T_{ref}}^{T_e} c_{pgi}\, dT \tag{8.104}$$

The first boundary condition along the symmetry line or plane as well as the initial condition is already given above. The second boundary, at the surface of the particle, has a condition that is analogous to that of convective heat transfer, but in the present case the mass transfer coefficient h_m is used instead of the heat transfer coefficient

$$-D_{AB,eff}\left.\frac{\partial X_i}{\partial x}\right|_{surf} = h_m\left(X_{isurf} - X_{i\infty}\right) \tag{8.105}$$

In the discrete form the mass transfer from boundary to centre of the cell is assumed to be negligible, and the diffusive mass flow through the boundary representing the surface of the particle is given by

$$n_e^{II} = A_e C_e h_m\left(X_{iP} - X_{i\infty}\right) \tag{8.106}$$

The concentration at this boundary is

$$C_e = P_\infty / (\Re T_P) \tag{8.107}$$

The mass transfer coefficient is evaluated from

$$Sh = \frac{h_{m0} d}{D_{AB}} \tag{8.108}$$

There is an analogy between mass and (non-radiative) heat transfer, and Sh ≈ Nu. The mass transfer coefficient must be compensated for the gases flowing out from the particle in the same way as done for the heat transfer coefficient, Eq (8.60)

$$\frac{h_m}{h_{m0}} = \frac{u_g / h_{m0}}{\exp\left(u_g / h_{m0}\right) - 1} \tag{8.110}$$

The same set of ordinary differential equations as in the previous step, Eq (8.96), needs to be solved. The only difference is that the change of the molar fractions of each species should be given by Eq (8.103) instead of Eq (8.96)

Implementation and validation strategy of Step 8
Introduce the diffusive term into the calculation and validate the result, first for three species then for the eight species that characterise the main chemistry of a solid fuel particle (O_2,CO, CO_2, H_2, H_2O, C_iH_j, $C_nH_mO_k$, N_2). This is preferably done by letting all gases, produced inside the particle, leave through cracks (Ψ = 0) and change the concentration in the surrounding atmosphere stepwise.

COMBUSTION OR GASIFICATION OF CHAR (STEP 9)

The final step in the conversion process of a solid fuel particle is the char conversion. The char conversion is due to heterogeneous reactions between gas and solid phase. The conversion of the char takes place as follows; the gas phase reactant or reactants (O_2, H_2O and CO_2) are transported from the surroundings through the outer boundary layer of the particle and into the porous structure of the char, see Fig 8.12. The reactant then reacts with the char inside the porous structure and the products produced (CO, CO_2 and H_2) are transported out through the porous structure and the outer boundary layer of the particle to the surrounding. The mass transport of species in and out of the particle is dominated by the diffusive flow described in Step 8, even if a small convective flow can arise because some of the heterogeneous reactions produce more molecules than they consume. The most interesting global reactions in combustion and gasification applications are the combustion reaction between oxygen and char, which is an exothermic reaction, and the one to two orders of magnitude slower gasification reactions between water vapour and char or carbon dioxide and char, which are endothermic reactions. The conversion rate of the char is related to the reactive intrinsic surface area of the char $A[Y_C]$, which can be seen as the "concentration" of char surface analogous to concentration of gas. The rate also depends on the local concentration of the reactant C_i up to the exponent n, the reaction order. The temperature dependence is usually given by an Arrhenius form of equation $k_{rC,j}\exp(-E_j/T)$, even if other correlations also are common to describe heterogeneous reaction. A common assumption is

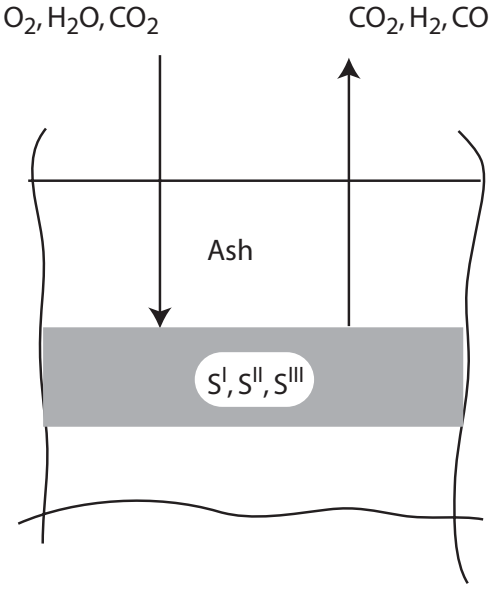

Figure 8.12.
Diffusive flow of reactant from the surroundings to the reacting char within the fuel particle

that char consists of pure carbon. This is more or less true if the final temperature for a produced char is high, typically above 700°C. If the char is produced at lower temperatures the amount of oxygen and hydrogen in the char are not negligible and must be included into the global reaction expressions. If we assume the char to consist of pure carbon, the oxygen - char reaction forms carbon monoxide and carbon dioxide; the primary split between them is not known. However, in general it is assumed that the primary product is carbon monoxide, which in the gas void reacts further to carbon dioxide. In order to simplify the modelling of the processes a fixed split factor or a correlation for the split factor based on experiments is given. Here, the split factor is included in the stoichiometric coefficient of the reaction $\Omega_{C/O2}$ defined as

$$\Omega_{C/O2} C + O_2 \rightarrow 2(\Omega_{C/O2} - 1)CO + (2 - \Omega_{C/O2})CO_2 \tag{8.111}$$

In the present formulation all variables are related to the initial volume and the char to the initial amount of char, analogous to the moisture and volatiles. The reaction rate is then given

$$-\frac{\partial Y_C}{\partial t} = \frac{\Lambda[Y_c]\Omega_{C/O2} C_{O2}^n k_{rC0} \exp(-E/RT) M_C/\zeta}{\rho_{df} Y_{0c}} = \frac{M_C}{\zeta \rho_{df} Y_{0c}} \Omega_{C/O2} R^i \tag{8.112}$$

where the C_{O2} oxygen concentration is defined

$$C_{O2} = C\zeta X_{O_2} \tag{8.113}$$

and R^i is the reaction rate. The unit of reactive intrinsic surface area of the char, $\Lambda[Y_C]$, related to the unit of the constant k_{rC0} in the Arrhenius equation. In this presentation the rates of the heterogeneous reactions are given in m/s and the unit of $\Lambda[Y_C]$ is m^2/m^3. This area is not constant during the conversion process, and there are various approaches on how to express the variation of the intrinsic surface area with conversion. However, this complication is left for more advanced exercises, and here the active area is related to the relative mass fraction with some exponent β,

$$\Lambda[Y_C] = A_{\text{int}} Y_C^{\beta} \tag{8.114}$$

The order of the reaction and the exponent β are not easy to extract from experiments because both terms are strongly connected to each other. Therefore, the simplest case is presented here, reactions of the first order (n = 1) and the exponent β is assumed to be to unity. The rate of the oxygen-char reaction is then

$$R^i = Y_C A_{\text{int}} C_{O2} k_{rC0i} \exp\left(-E_i / RT\right) / \zeta \tag{8.115}$$

One may question why the concentration is multiplied by relative volume of the gas void, ζ, and the reaction rate is divided by ζ. The answer is that the reaction should always be calculated at the actual concentration, because in a general formulation the reaction order can differ from unity.

The source terms in the conservation equation for all species involved in the reaction between char and oxygen are calculated from the reaction rate of Eq (8.115)

$$R_{O2} = -R^i M_{O2} \tag{8.116}$$

$$R_{CO} = 2\left(\Omega_{C/O2} - 1\right) R^i M_{CO} \tag{8.117}$$

$$R_{CO2} = \left(2 - \Omega_{C/O2}\right) R^i M_{CO2} \tag{8.118}$$

The heat released by the reaction is derived in analogy to the source term for the drying and devolatilisation equation 8.58 and 8.59. The difference is that in the heterogeneous reactions one of the gas components is consumed together with solid phase, which adds an extra term. For the char – oxygen reaction a reduction of the heating value must also be included for the char due to the fact that not all carbon forms CO_2

$$\begin{aligned} S^i = {} & H_C\left(R_{CO} / M_{CO} + R_{CO2} / M_{CO2}\right) M_C - H_{CO} R_{CO} \\ & + R^i M_{O2} \int_{T_{ref}}^{T} c_{pO2} dT + \Omega_{C/O2} R^i M_C \int_{T_{ref}}^{T} c_{pC} dT \end{aligned} \tag{8.119}$$

So far the reaction rate in Eq (8.112) is only defined for the combustion reaction, but it can easily be modified to include also the gasification reactions

$$-\frac{\partial Y_C}{\partial t} = \frac{M_C}{\zeta \rho_{df} Y_{0C}} \sum_j \left(\Omega_j R^j \right) \tag{8.120}$$

where j represents the various reactions. In the gasification reactions the rates and source terms describing the heat release and changes in species concentration are given in the same form as for the char – oxygen reaction. The reaction with water vapour, R^{ii} is

$$C + H_2O \rightarrow CO + H_2 \tag{8.121}$$

$$R^{ii} = Y_C A_{\text{int}} C_{H2O} k_{rC0ii} \exp\left(-E_{ii} / RT\right) / \zeta \tag{8.122}$$

and the reaction with carbon dioxide, R^{iii} is

$$C + CO_2 \rightarrow 2CO \tag{8.123}$$

$$R^{iii} = Y_C A_{\text{int}} C_{CO2} k_{rC0iii} \exp\left(-E_{iii} / RT\right) / \zeta \tag{8.124}$$

The overall source term expressing the conservation of species includes all three reactions

$$R_{O2} = -R^i M_{O2} \tag{8.125}$$

$$R_{CO} = \left(2\left(\Omega_{C/O2} - 1\right)R^i + R^{ii} + 2R^{iii}\right)M_{CO} \tag{8.126}$$

$$R_{CO2} = \left(\left(2 - \Omega_{C/O2}\right)R^i - R^{iii}\right)M_{CO2} \tag{8.127}$$

$$R_{H2} = R^{ii} M_{H2} \tag{8.128}$$

$$R_{H2O} = -R^{ii} M_{H2O} \tag{8.129}$$

and the complementing source terms expressing the conservation of energy in relation to the two gasification reactions are

$$S^{ii} = R^{ii}\left(H_C M_C - H_{H2} M_{H2} - H_{CO} M_{CO}\right) + \\ + R^{ii} M_{H2O} \int_{T_{ref}}^{T} c_{pH2O} dT + \Omega_{C/H2O} R^{ii} M_C \int_{T_{ref}}^{T} c_{pC} dT \tag{8.130}$$

$$S^{iii} = R^{iii}\left(H_C M_C - 2H_{CO} M_{CO}\right) + \\ + R^{iii} M_{CO2} \int_{T_{ref}}^{T} c_{pCO2} dT + \Omega_{C/CO2} R^{iii} M_C \int_{T_{ref}}^{T} c_{pC} dT \tag{8.131}$$

When char combustion is included the one additional variable describing the consumption of char has to be introduced into the set of ordinary differential equation that must be solved. This variable is preferably placed after the variable describing the mass decrease of the volatiles in Eq (8.99).

$$\begin{array}{l} \vdots \\ \vdots \\ \dfrac{\partial \log(Y_v)_1}{\partial t} = Eq\ 8.46 \\ \dfrac{\partial \log(Y_v)_2}{\partial t} = Eq\ 8.46 \\ \vdots \\ \dfrac{\partial \log(Y_v)_j}{\partial t} = Eq\ 8.46 \\ \dfrac{\partial Y_{C1}}{\partial t} = Eq\ 8.120 \\ \dfrac{\partial Y_{C2}}{\partial t} = Eq\ 8.120 \\ \vdots \\ \dfrac{\partial Y_{Cj}}{\partial t} = Eq\ 8.120 \\ \dfrac{\partial C_1^0}{\partial t} = Eq\ 8.90 \\ \dfrac{\partial C_2^0}{\partial t} = Eq\ 8.90 \\ \vdots \\ \dfrac{\partial C_j^0}{\partial t} = Eq\ 8.90 \\ \vdots \\ \vdots \end{array} \tag{8.132}$$

Implementation and validation strategy of Step 9
Introduce the heterogeneous reactions and validate your model. Compare the model with measurements of char combustion. How well does the model agree with measurements? For which temperatures would a simple shrinking sphere model be appropriate?

FINAL REMARKS

If you have managed to formulate and validate all these steps you have obtain a model that is sufficient for most practical applications. With minor adjustments in the fuel-related properties you can model the conversion of nearly all kind of solid fuels. Of course, details can be improved, and below two improvements, which can easily be implemented, are given, as well as an outline on how to model the char yield and how to consider a porous bed instead of a porous particle. It is highly recommended to improve your model with these additional models elements for drying, and homogeneous reactions.

A DRYING MODEL ALLOWING RE-CONDENSATION

Drying is not only a one-way process. Evaporated moisture is transported, not only outwards, but also into the centre of the particle and condenses back to water, as seen in Fig 8.13. To take this into account, one needs to determine the rate of the vaporisation and condensation process. The simplest way to do this is by assuming that the saturation point of water is reached with some time lag in each position within the cell. To formulate this we need to calculate the rate of the vaporisation, R_m, which replace the rate in Arrhenius form used in Eq (8.35),

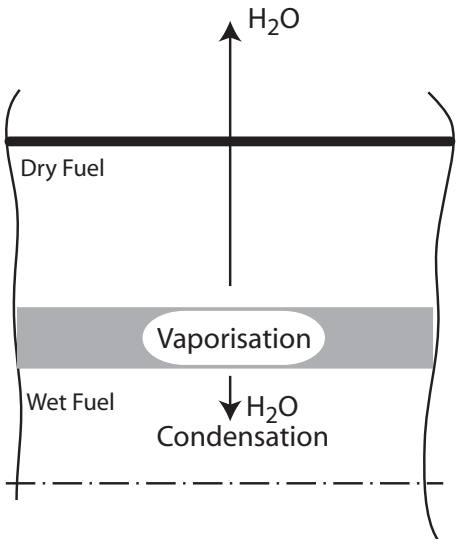

Figure 8.13.
Transport of water vapour inside a fuel particle.

$$\frac{\partial R_m}{\partial t} = \left(X^*_{H2O} - X_{H2O}\right) k_1 Y_m \tag{8.133}$$

where k_1 is an empirical constant representing the time lag, which is given an arbitrary value. The saturation molar fraction at a given temperature is determined by the partial pressure of saturation divided by the local pressure

$$X^*_{H2O} = 2.21 \times 10^{10} \exp(-4193/(T-32))/P \tag{8.134}$$

The correlation for the partial pressure at saturation is derived from steam tables. The drying rate is calculated in the same way as above

$$-\frac{\partial \log(Y_m)}{\partial t} = R_m \text{ and } -\frac{\partial Y_m}{\partial t} = R_m Y_m \tag{8.135}$$

HOMOGENEOUS REACTIONS

Not only heterogeneous reactions (reactions between solid and gas) are present within the particles but homogeneous reactions (gas reactions) can also take place. In this type of models the reactions are usually described by global reactions and global reaction rates given by an Arrhenius form of equation

$$R_j = C_A^a C_B^b \cdots C_Z^z A_j \exp(-E_j/\Re T)/\zeta \tag{8.136}$$

Indices *A* to *Z* represent all species included in the model and *a* to *z* represent the exponent for the species in the given reaction. The source terms to the conservation equation of species is expressed by

$$R_i = M_i \sum_j \Omega_{ji} R_j \tag{8.137}$$

where *j* is the number of the reaction and Ω_{ji} is the stoichiometric factor for species *i* in reaction *j*. The species not included in the reaction are given the exponent zero. The source term in the conservation equation of energy is

$$S = R_j H_j M_j + \sum_i \sum_j \left(\min(\Omega_{ji}, 0) R_j \int_{T_{ref}}^{T} c_{pi} M_i dT \right) \tag{8.138}$$

where M_j is the molar mass of the species for which the heating value is given. The first term in Eq (8.138) give the heat of reaction at reference temperature and the second term compensate the heat of reaction for the temperature difference between temperature at which the reaction occur and the reference temperature.

DEVOLATILISATION MODEL WHERE THE CHAR YIELD IS ESTIMATED

Char yield is one of the unknown parameters; therefore, it is given as an input to the model. It is, however, known how the char yield depends on rate of devolatilisation, final temperature and particle size. The general behaviour is that the char yield and the mass fractions of oxygen and hydrogen decrease with increasing heating rate and final temperature, which can be described by a distribution of reaction rates describing the thermal break down of the fuel. The char yield also increase in the char yield with increasing particle size, which are due to reactions involving long hydrocarbons, which form secondary char. One idea on the outline of a model, which can be used to describe composition of the paralysis gas and char yield are as followed:

1. The rate of devolatilisation is complemented by a term that limit the char yield as a function of temperature for example:

$$-\frac{\partial Y_v}{\partial t} = \left(Y_v - Y_C[T]\right) k_{rv0} \exp\left(-E_v / T\right) \tag{8.139}$$

   where the char yield is a function of temperature.
2. Introduce a new variable that describes the secondary char, which is produced from reactions with long hydrocarbons.

$$\frac{\partial m_{c2}}{\partial t} = C_{tar} k_{rC0} \exp\left(-E/(\Re T)\right) \tag{8.140}$$

3. Introduce one variable, which instead of counting down the mass fraction from a given initial amount of char as is done in Step 9, keeps track of the released char.
4. Assume that the ratio between oxygen and hydrogen in the released volatiles is constant, but the ratio between oxygen and carbon changes and this ratio has to be accounted for by one additional variable. The composition of the gases is calculated from a heat and mass balance as described in Chapter 5.

This model idea, which includes three additional variables compared to a single rate model with an assumed char yield, is most likely the minimum requirement, if one wants to describe this process in a sufficient way.

POROUS BED

With some modifications the model presented here can describe a porous bed. Below the basic changes to the model will be presented, but not in such a detail way as the presentation of the conversion of the porous particle and the derivation is not complete. The changes needed to describe the combustion of a batch are:

1. The gas velocity should be calculated from the Ergun equation instead of Darcy's law.
2. An apparent reaction rate, which accounts for the reaction rate and the mass transfer to the particle surface, should be used for the conversion.
3. Effective diffusivity and heat conductivity of the gas need to be adapted for the porous medium.
4. A gas flow should be introduced into the medium at least at one of the boundaries.
5. Boundary condition for the conservation equations for energy and species must be adapted for the new case.
6. Account should be taken for mixing in the homogenous reactions.
7. Shrinkage occurs only in the direction of the gravity

The gas velocity should be calculated from the Ergun equation for rough surfaces

$$-\frac{\partial P}{\partial x} = u_g \left(\frac{180 \mu_g (1-\nu_g)}{d_{car}^2 \nu_g^3} + \frac{4 \rho_g |u_g| (1-\nu_g)}{d_{car} \nu_g^3} \right) \tag{8.141}$$

Here, the voidage, ν_g, is equal to the gas voidage of the porous bed. The apparent reaction rate for the char reaction is given by (compare with Eq (8.120))

$$-\rho_{df} Y_{0C} \frac{\partial Y_C}{\partial t} = \Lambda[Y_c] M_C / \zeta \sum_i \left(\Omega_i C_i \frac{R h_{m,surf}}{R + h_{m,surf}} \right) \tag{8.142}$$

where $\Lambda[Y_C]$ gives the active surface for the reactions, which, if one assumes the char conversion occur like a shrinking core case, can be approximated as the core surface of char per unit initial volume, R is the reaction rate

$$R = C_{O2}^n k_{rC0} \exp(-E/RT) / C_{O2}^{n-1} \tag{8.143}$$

and $h_{m,surf}$ is the mass transfer coefficient to surface of the particles in the bed calculated from Wakao [4]

$$Sh = 2 + 1.1 \mathrm{Re}^{0.6} \mathrm{Sc}^{1/3} = h_{m0,surf} d_{car} / D_{AB} \tag{8.144}$$

compensated for the gas outflow from the particles $u_{g,surf}$ by Bird [5].

$$\frac{h_{m,surf}}{h_{m0,surf}} = \frac{u_{g,surf} / h_{m0,surf}}{\exp(u_{g,surf} / h_{m0,surf}) - 1} \tag{8.145}$$

The effective molecular diffusivity and the thermal conductivity of the gas can be estimated by from the axial properties given by Wakao [4].

$$D_{AB,eff} = 0.8 D_{AB} + 0.5 d_{car} u_g / \nu \tag{8.146}$$

$$k_{cg,eff} = 0.8 k_{cg} + 0.5 d_{car} c_{pg} \rho_g u_g / \nu \tag{8.147}$$

and the effective conductivity of the bed is calculated in analogy to the conductivity of wood Thunman and Leckner [6]

$$k_{c1,1} = (1 - \nu_g) k_{cs} + \nu_g k_{cg,eff} \tag{8.148}$$

$$k_{c2,1} = \frac{\nu_g (1-\nu_g) k_{cs} k_{cg,eff}}{(1-\nu_g) k_{cs} + \nu_g k_{cg,eff}} \tag{8.149}$$

$$k_{c1,i+1} = 0.5 k_{c1,i} + 0.5 k_{c2,i} \tag{8.150}$$

$$k_{c2,i+1} = \frac{2 k_{c1,i} k_{c2,i}}{k_{c1,i} + k_{c1,i}} \tag{8.151}$$

$$k_{c,eff} = k_{c1,\infty} + k_{c,rad} = k_{c2,\infty} + k_{c,rad} \tag{8.152}$$

where index i is a counter and the radiative conductivity for cylindrical cavities can be estimated from Gennadij [7]

$$k_{c,rad} = 2\pi \frac{\nu}{2-\nu} \sigma d_{car} T^3 \tag{8.153}$$

At the gas inlet the boundary conditions of the conservation equations are

$$n^I = n_{in} \tag{8.154}$$

$$n_i^I = n_{in} X_{i,in} \tag{8.155}$$

$$n_i^{II} = 0 \tag{8.156}$$

$$q^I = n_{in} \sum_i \left(X_{i,in} / M_i \int_{T_{ref}}^{T_{in}} c_{pi} dT \right) \tag{8.157}$$

$$q^{II} = 0 \tag{8.158}$$

at adiabatic walls

$$n^{I} = 0 \tag{8.159}$$

$$n_i^{I} = 0 \tag{8.160}$$

$$n_i^{II} = 0 \tag{8.161}$$

$$q^{I} = 0 \tag{8.162}$$

$$q^{II} = 0 \tag{8.163}$$

at gas outlet

$$n_i^{II} = 0 \tag{8.164}$$

$$q^{II} = 0 \tag{8.165}$$

Between the particles in the bed the gas is not immediately mixed and the rate of the homogenous reactions must be compensated for mixing. The rate of the mixing in a porous fuel bed can be estimated by, Thunman and Leckner [8]

$$R_{mix} = 0.63\left(\frac{1.75u_g(1-\nu)}{\nu d_{car}}\right)\min\left(\frac{C_{i,reak}}{\Omega_i}\right) \tag{8.166}$$

The resulting reaction rate is the slowest one of the mixing and the kinetic rates.

If there is a flow of solid phase, equations for the apparent density of moisture, volatiles, char, and ash analogous to conservation equation of species Eq (8.103) need to be formulated. The apparent density is the density of the mass of the fraction of one constituent in a discrete volume related to the initial volume of the discrete volume. If we have a Cartesian co-ordinate system in tree dimension the change of the apparent density in an active cell P is

$$\frac{\partial \rho_P^0}{\partial t} = \frac{m_e^{II} - m_e^{I} - m_w^{II} + m_w^{I} + m_n^{II} - m_n^{I} - m_s^{II} + m_s^{I} + m_t^{II} - m_t^{I} - m_b^{II} + m_b^{I}}{V_{P,0}} + R \tag{8.167}$$

The diffusive flow is represented by the dispersion coefficient D_s at the east boundary of the active cell P,

$$m_{ie}^{II} = A_e h_{de}\left(\rho_E^0 / \theta_E - \rho_P^0 / \theta_P\right) \tag{8.168}$$

where h_{de} is

$$h_{de} = \frac{2(D_{sP}/(\delta x)_P)(D_{sE}/(\delta x)_E)}{(D_{sP}/(\delta x)_P)+(D_{sE}/(\delta x)_E)} \tag{8.169}$$

The convective flow given for the east boundary,

$$m_{ie}^{I} = A_e^0\left(\max(u_{se}^0,0)\rho_{iP}^0 + \min(u_{se}^0,0)\rho_{iE}^0\right) \tag{8.170}$$

where A_e^0 is the initial area of the cell wall to the east and u_{se}^0 is the velocity of the solid related to the initial cell width in the direction of the flow. By also calculating the apparent density of the ash the accumulation and the release of particles from a cell can be accounted for if the ash, is assumed to stick onto the particle and the bed voidage is assumed constant during the whole combustion process. Then the shrinkage term has to be compensated for the difference in the inflow and outflow of particles

$$\theta = \frac{\theta^0 \rho_{as}^0}{\rho_{as,0}^0} \tag{8.171}$$

where θ^0 is the volume shrinkage due to combustion, ρ_{as}^0 apparent density of ash at time t and $\rho_{as,0}^0$ is the initial apparent density of ash. As there is a flow of solid there will be one additional convective flow added to the conservation equation

$$\frac{\partial T_P}{\partial t} = q_P^{III} + \frac{(q_e^{II} - q_e^I - q_{es}^I - q_w^{II} + q_w^I + q_{ws}^I) + (q_n^{II} - q_n^I - q_{ns}^I - q_s^{II} + q_s^I + q_{ss}^I)}{V_{P,0}} + \frac{(q_t^{II} - q_t^I - q_{ts}^I - q_b^{II} + q_b^I + q_{bs}^I)}{V_{P,0}} - c_{psP} T_P \frac{\partial \rho_{sP}^0}{\partial t} - \rho_{sP}^0 T_P \frac{\partial c_{psP}}{\partial t} \Bigg) / \rho_{sP}^0 c_{psP} \tag{8.172}$$

where the solid convective and diffusive term given for the east boundary is

$$q_{es}^I = \sum_i (m_{ie}^{II} - m_{ie}^I) \int_{T_{ref}}^{T_e} c_{psi}\, dT \tag{8.173}$$

The boundary conditions to the solid phase are: at the fuel inlet:

$$m_i^I = m_{i,in}^I \tag{8.174}$$

$$m_i^{II} = 0 \tag{8.175}$$

$$q_s^I = m_{i,in}^I \int_{T_{ref}}^{T_{in}} c_{psi}\, dT \tag{8.176}$$

at walls

$$m_i^I = 0 \tag{8.177}$$

$$m_i^{II} = 0 \tag{8.178}$$

$$q_s^I = 0 \tag{8.179}$$

at ash outlet

$$m_i^{II} = 0 \tag{8.180}$$

This bed model assumes that the temperature of the solid and the gaseous phase are the same at all times, which is true for small particles. As the particle size increases, a temperature difference between the two phases becomes visible, and it is necessary to represent the

gaseous and the solid phase by two instead of one energy equations. If the particles are even larger, a temperature gradient will be present even within the single particles and a submodel describing these needs to be implemented. An example of such a model is presented by Thunman and Leckner [9,10].

REFERENCES

1. H., Thunman, B., Leckner, F., Niklasson, F., Johnsson, "Combustion of wood particles - a model for Eulerian calculations", Combustion and Flames 2002, 129, 30-46.
2. F.P. Incropera, D.P. DeWitt, Fundamentals of Heat and Mass Transfer, Fourth edition, John Wiley & Sons Inc., New York, 1996.
3. K.O. Davidsson, J.B.C. Pettersson, M. Bellais, T. Liliedahl, K. Sjöström, Progress in Thermochemical Biomass Conversion, (A.V.Bridgwater, Ed.), MPG Books, Great Britain, 2001, 1129.
4. Wakao, N., and Kaguei, S., "Heat and Mass Transfer In Packed Beds", Gordon and Breach, New York, 1982.
5. Bird, R.B., Stewart, W.E., and Lightfoot, E.N., "Transport Phenomena", John Wiley & Sons Inc., New York, 1960.
6. H., Thunman, B., Leckner, 'Thermal conductivity of wood - models for different stages of combustion', Biomass & Bioenergy 2002, 23, 47-54.
7. G.I. Palchonok, Heat and Mass Transfer to a Single Particle in Fluidized Bed, Doctoral dissertation, Chalmers University of Technology, Sweden, 1998.
8. H., Thunman, B., Leckner, 'Influence of Size and Density of Fuel on Combustion in a Packed Bed', Proceedings of the Combustion Institute 2004.
9. H., Thunman, B., Leckner, 'Modelling of the Combustion Front in a Downdraft Fuel Converter', Proceedings of the Combustion Institute 2002, 29, 511-518.
10. H., Thunman, B., Leckner, 'Co-Current and counter-current fixed bed combustion of biofuel - a comparison', Fuel 2003,82, 275-283.

CHAPTER 9
BOILERS AND FURNACES

BO LECKNER

INTRODUCTION

There are many types of boilers and furnaces burning organic fuels for a wide variety of purposes. As far as possible only the general aspects of the subject will be considered here, with a clear emphasis on boilers (pannor) for the production of heat for space heating and for electric power.

CONDITIONS FOR OPERATION OF BOILERS

The most commonly used thermodynamic cycle for power production is the Rankine cycle for steam/water. This cycle is shown in Fig. 9.1. Water is pumped up to a high pressure, ab. Heat is added from a heat source (a boiler), bc, to raise the temperature of the water, to convert the water into steam (the horizontal part of the curve), and finally to superheat the steam.

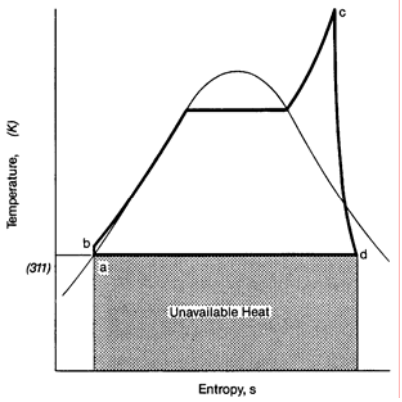

Figure 9.1.
Rankine cycle for a thermal power station (värmekraftverk, kondenskraftverk), shown in a temperature-entropy diagram (Ts-diagram).

The steam is expanded through a steam turbine, cd, and cooled in a condensor, da, by the ambient air or water at a temperature, corresponding to a sufficiently low steam pressure (below atmospheric conditions). In this case we have a thermal power station (värmekraftverk). If the expansion in the steam turbine is interrupted at a higher pressure (at about atmospheric pressure), the temperature in the condenser has a higher temperature (100 to 200 ^{o}C) and the heat removed can be used for an industrial process or for district heating. In such a case the power station is a combined heat and power plant (kraftvärmeverk), common in Northern Europe.

The most efficient thermodynamic cycle is the ideal Carnot process whose efficiency is

$$\eta_{ca} = (T-T_o)/T \qquad (9.1)$$

Heat is supplied at a temperature level T and removed at T_o. The efficiency of real cycles is lower than that of the Carnot cycle, because of losses and other imperfections. This is the case with the Rankine cycle, where the heat is supplied at varying temperatures (bc), and not only at the highest one (c). Nevertheless, the upper temperature level of the cycle is important for the efficiency, and a qualitative discussion about any thermodynamic cycle can be based on Eq (9.1).

If an organic fuel is fired in air, a typical adiabatic temperature achieved is 2400 K (if oxygen is used instead of air, the adiabatic temperature would exceed 3000 K). The top temperature of a Rankine cycle based on water is around 900 K, set by heat transfer and material limitations. 900 K corresponds to a maximum possible efficiency for electricity production of 60%. Considering the less efficient Rankine cycle and other losses, the real value of maximum attainable efficiency would be in the order of 50%. (Existing power stations have efficiencies between 30 and 40%). The situation is different in a combined heat and power process whose thermal efficiency is always close to 100%, since the heat removed in the condenser is not wasted to the environment but used for heating. In such a process the maximum temperature is still important; it determines the amount of electric power that can be produced for a given demand of heat power.

Obviously there is a gap between the maximum possible temperature of the combustion gas and the maximum temperature of the Rankine cycle. This gap could be reduced by the selection of another process medium than water. In theory there are many possibilities for improvement. Many thermodynamic cycles and other solutions have been proposed. The most applicable solution during the next decades would be to add another thermodynamic cycle (the Brayton cycle Fig 9.2) on top of

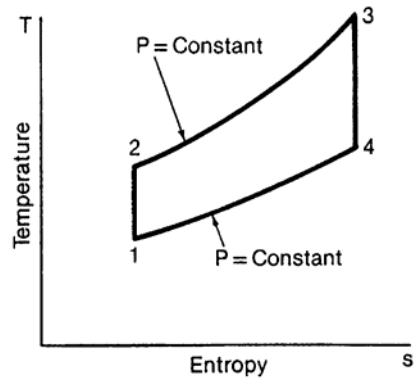

Figure 9.2.
Gas turbine or Brayton cycle. 12 compression of air, 23 supply of heat to the combustion chamber, 34 expansion in the turbine.

the Rankine cycle to increase the upper temperature, using the exhaust gas from the gas turbine of the Brayton cycle to supply heat to the Rankine cycle. This is called a **combined cycle** and an example is shown in Fig. 9.3**.** The Brayton cycle is also limited by temperature, by the gas temperature at the entrance to the turbine (3 in Fig. 9.2), but in this case the temperature is already above 1000° C. In future applications 1500° C might be attained.

In the combined cycle the efficiency may reach higher values than in the single cycles, but the very high temperatures that could be generated by combustion are not utilised in any thermodynamic cycle proposed at present.

Conclusion. The adiabatic combustion temperatures of dry organic fuels are high in comparison to the temperature levels of available thermodynamic cycles for power production, and there is an essential loss of exergy in the transfer of energy from combustion to the working media of the cycles. The limits are set by the working media of the thermodynamic processes or by materials (turbine blading and boiler steam tubes).

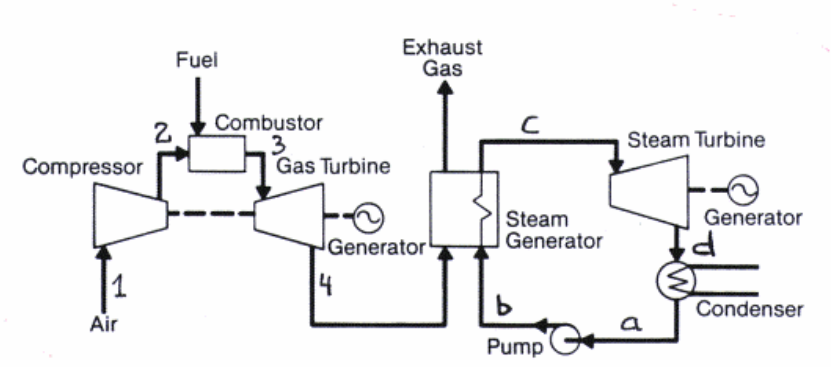

Figure. 9.3.
Simple combined cycle plant. Numbers refer to Fig. 9.2, letters to Fig. 9.1.

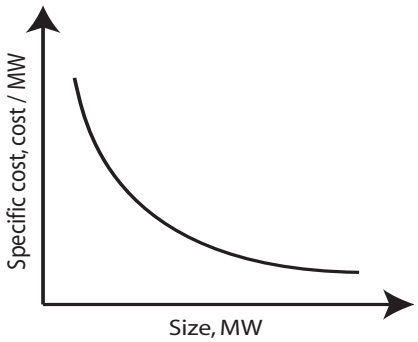

Figure 9.4.
Influence of plant size on specific cost.

In some cases, such as for wet or extremely high-ash fuels, the adiabatic temperature may be in the same range or even below the process requirement of the boilers (in the latter case, of course, even some additional supply of energy in the form of admixture of high quality fuel could be needed). Also, for the purpose of avoiding formation of thermal nitrogen oxides, moderate flame temperatures may be desired.

SIZE OF THE BOILER

The size and design of a combustor for heat and power production is determined by the conditions of economy of scale, illustrated in Fig. 9.4. There is usually a logarithmic relationship between the cost of a unit of power (a MW) and the size of the power plant: a unit of power becomes cheaper in a large plant than in a small one. Therefore, the plants tend to be as large as is permitted by the energy supply system. In large national power systems there are no system limitations. Instead the plant size is chosen to be as large as technical feasibility permits. The size-limiting components in a plant are usually not the combustors but rather the steam turbine or the electric generator. Presently, the maximum size of a power station is about 1000 MW electric power, which corresponds to almost 3000 MW fuel. In some cases the size is limited by the energy demand (the energy system). The combustor is intended to supply heat to an industry or to a community, whose size will determine the size of the plant, including the scope for electricity production in combination with the heat production. The most obvious lower limit of size is that of a boiler serving a single house or a stove for occasional use.

Also fuel supply can be a limiting factor for size. This is so in the case of biofuels like wood (for instance, wood-chips) that have to be collected over large areas of forest and which are seven times as voluminous as coal per unit of energy; transportation becomes a limiting factor for plant size.

For small size plants, competing with large plants, the economy of scale leads to relatively high costs per unit of power and consequently impedes a number of methods for energy conversion to be applied in small scale plants. Advanced plants become expensive and may not be built in small scale even though the technology could be available. The large plants, on the other hand, represent very large investments per unit, and in order not to risk the performance of a plant the choice of technology tends to be conservative. In addition, the design of boilers is subject to severe optimisation, and only the recent environmental restrictions have made refined developments necessary.

In contrast to consumers' goods, such as refrigerators and cars, the many special conditions of application and the small series of production make the equipment sensitive to scale economic effects and require individual design of equipment. If large series of similar equipment could be produced a cost reduction could be achieved.

In addition to the electrical plants that have been referred to here, furnaces of different kinds are used in industry: in the pulp and paper industry, refineries, glass and metallurgical industries. Moreover, incineration of wastes is becoming increasingly important.

BOILERS

The combustion chamber of a boiler serves two purposes:

1) it accommodates the combustion process with the aim of achieving complete combustion under the condition of minimising harmful emissions,

2) it receives some of the heat released from combustion by heat transfer to the heat carrier (steam/water) and cools the combustion gases to a temperature which is sufficiently low for the ashes to have solidified before leaving the combustion chamber.

The gases are then further cooled in a set of convection heat exchangers down to the exit flue-gas temperature.

In addition to the combustion chamber and its adjacent flue-gas passes, a boiler consists of a number of subsystems for control, alarm and safety, systems for fuel feed and fuel preparation etc., which will not be treated here; we focus attention on the combustion aspect.

The following figures show some examples of boilers.

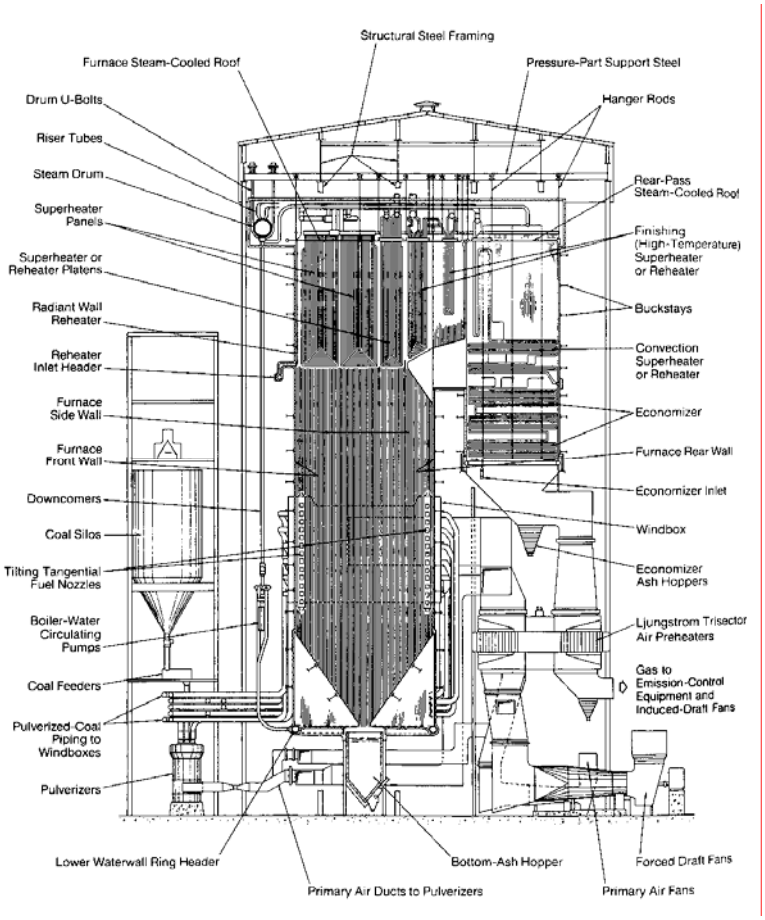

Figure 9.5.
Pulverised coal-fired boiler for a power station.

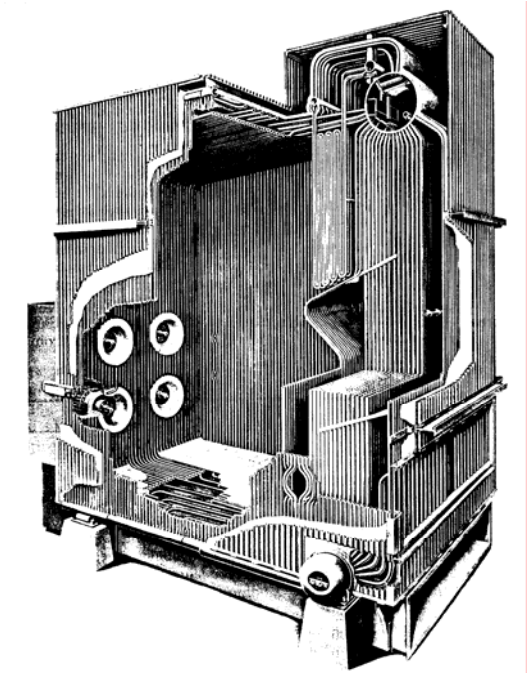

Figure 9.6.
Oil-fired steam boiler for industrial use.

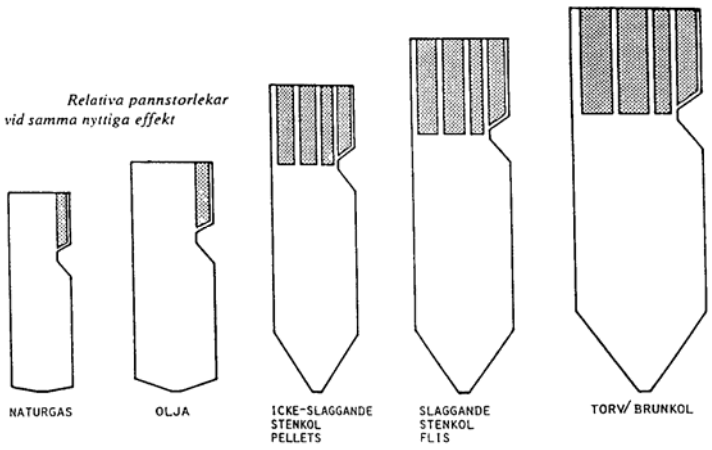

Figure 9.7.
Combustion chambers for a boiler of the same thermal power fired with different fuels.

Kværner Pulping

Steam capacity:

Bark, sludge	**300,000 lb/h**	**136 t/h**
Bark + Gas	**500,000 lb/h**	**227 t/h**
Gas	**600,000 lb/hr**	**272 t/h**
Steam pressure	**1070 psig**	**8.7 MPa(a)**
Steam temperature	**900 °F**	**482°C**

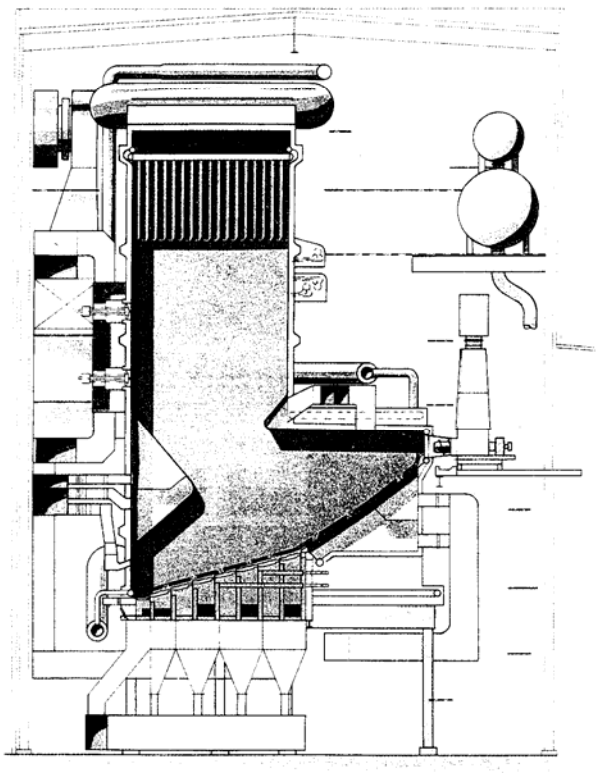

Figure 9.8. Industrial steam boiler for bark (Kvaerner) Bark, sludge 136 t/h. Bark+gas 227 t/h. Gas 272 t/h. Steam pressure and temperature 8.7 Mpa (a) and 482 ^{o}C.

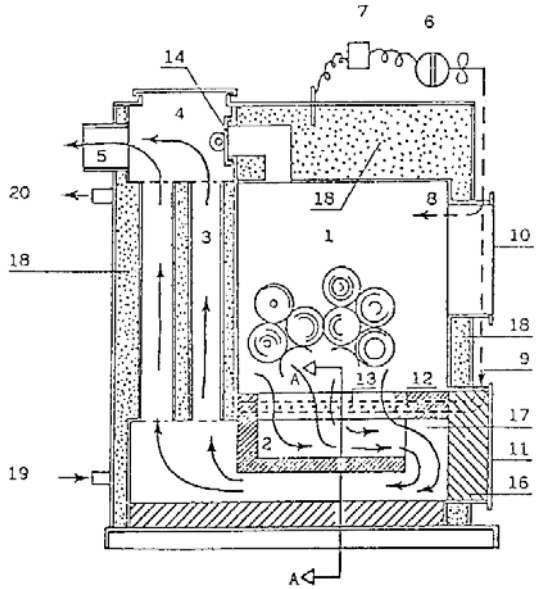

Snit A - A

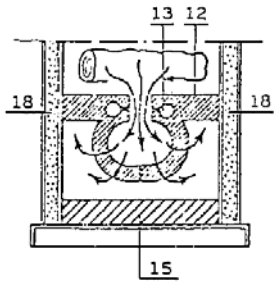

1 Brændselsmagasin
2 Ildkanal
3 Konvektionszone
4 Røgkasse
5 Røgstuds
6 Ventilator
7 Termostat
8 Primærluft
9 Sekundærluft
10 Indfyringslåge
11 Askelåge
12 Fyrboksbund
13 Kanal f. sek.luft
14 By-pass-spjæld
15 Ildfast sten - bund
16 Endestykke
17 Vendekammer
18 Vandkammer
19 Returløb
20 Fremløb

Figure 9.9.
Wood log boiler for house heating.

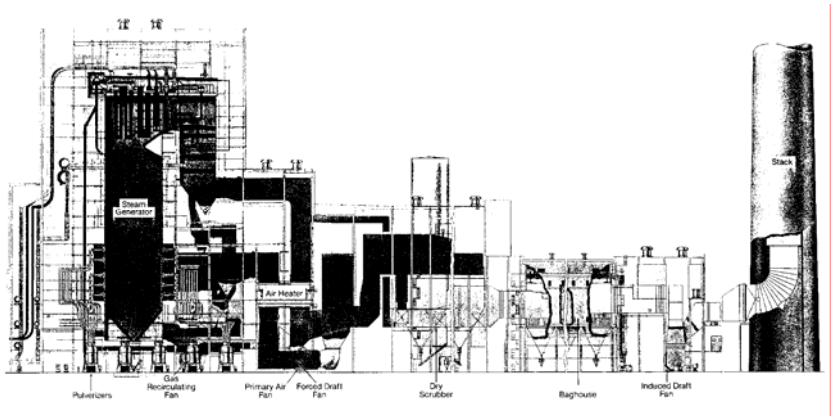

Figure 9.10.
Boiler plant showing the flue-gas pass including cleaning equipment.

Figure 9.5 shows a large pulverised coal-fired boiler for a power station. The coal is pulverised in a number of mills to a size of <100 μm and injected through the burners seen in the corners of the furnace. The furnace walls consist of steam/water tubes welded together to form a membrane surrounding the combustion space. The heat transfer from the flames in the combustion chamber to the membrane-tube walls is almost entirely due to radiation. At the exit of the combustion chamber, superheater tube bundles are seen in Fig. 9.5. The tube bundles hang from the roof. Convective heat exchangers are located in the flue gas path: the economiser for heating of the boiler water and the Ljungström regenerative air preheater (a rotating heat exchanger bringing the heat from the flue gas to the air duct just downstream of the air fans). The entire 30 to 40 m high boiler hangs in a steel framework. This arrangement allows the boiler structure to expand freely downwards when heated.

Figure 9.6 shows an oil-fired steam boiler, resting on a bottom support, for industrial use. The features of the combustion chamber and the flue-gas duct are similar to the previous figure (and to boilers in general). The outside, also like other boilers, covered by corrugated metal sheets, is insulated from the hot (in the order of 500^{o}C) boiler tubes by a layer of insulating material (white on the figure). The burnup of fuel requires less space in oil or gas-fired boilers, and the combustion chamber is smaller than for solid fuels of similar output, as illustrated on Fig. 9.7.

Figure 9.8 shows an industrial steam boiler fired with bark and sludge on a grate. The fuel enters through a screw-feeder on the right-hand side. Two (or perhaps four) oil-burners are also installed.

Finally, just to emphasise the variety of types of boilers, a small down-draft fired wood-log boiler for house heating is shown on Fig. 9.9.

Environmental concern gives rise to arrangements for reducing harmful emissions in the combustion chamber itself **(primary measures),** and in the exiting flue-gas stream downstream of the heat exchangers **(secondary measures**). A view of such installations (secondary measures) is given by Fig. 9.10. In addition to the equipment shown, in many countries the environmental restrictions are such that desox (for sulphur capture) and denox equipment for reduction of nitrogen oxides are needed; usually consisting of a catalytic flue gas cleaner.

THE SHAPE OF A COMBUSTION CHAMBER

There are some useful criteria for estimation of the shape and size of a combustion chamber:

- cross-sectional surface loading $Q_c = Q_{fuel}/A_c$ [MW/m^2]
- volumetric loading $Q_v = Q_{fuel}/V$ [MW/m^3]

where

A_c cross-sectional area of the furnace [m^2]

V volume of furnace [m^3]

Q_{fuel} fuel power in MW. Fuel power is related to electrcal power Q_e by

$$Q_e = Q_{fuel} \ \eta_{boiler} \ \eta_{cycle}$$

where η_{boiler} is the efficiency of the boiler and η_{cycle} is the efficiency of the thermodynamic cycle and other minor associated losses. At a given air excess the surface loading Q_c is associated with a cross-sectional average gas velocity and Q_v is associated with a gas residence time.

Empirical data on loadings for suspension-fired boilers are shown in Fig. 9.11 as curves. This gives an impression of a certain precision in the data. One must remember, however, that the relationships are approximate and give a simplified picture of a complex situation. Environmental considerations and designs for fuel with different properties will affect the values. Data from various designs may vary considerably, but nevertheless the curves give a valuable indication of the conditions in large suspension-fired combustion chambers.

For comparison, the surface loading of a grate or an atmospheric stationary fluidised bed boiler is around 1 MW/m^2 and that of a circulating fluidising bed boiler is 3 to 4 MW/m^2, indicating that the latter type of boiler operates with higher gas velocity than the grate or stationary fluidised bed (more fuel is supplied to burn fuel per m^2 cross-section). If the data are multiplied by pressure in bar, the corresponding values for pressurised combustors are given. Thus, a pressurised circulating fluidised bed might (there are no commercial boilers of this type 2003) have a surface loading of 50 MW/m^2. This corresponds to a very high volumetric heat release.

The height of the combustion chamber should be sufficient to accommodate a heat transfer surface to cool the gases in order to avoid melted ash particles depositing on downstream heat transfer tube bundles, and to allow the fuel to burn out before the intensive cooling in the tube bundles. Calculations, showing these two criteria (for ash-melting and burn-out), are presented in Fig. 9.12, where a range of exit temperatures are given in

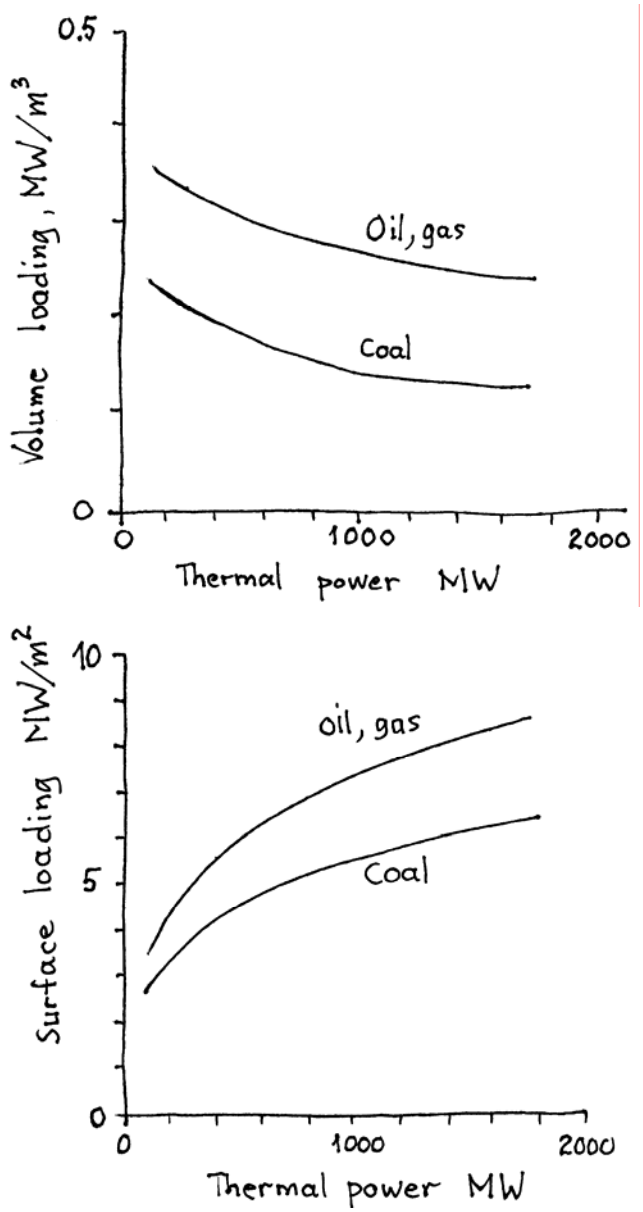

Figure 9.11.
Volume and surface loadings of suspension fired boilers. Data from Strauss.

order to cover the requirements for coals with different ash melting temperatures. It is seen that for large boilers (having a smaller wall surface to volume ratio) the height of the boiler must be larger than that necessary for the burnout of coal particles in order to cool the gas properly; the design is heat-transfer limited. For small boilers the heat transfer to the walls is not the limiting factor. Instead the burnup of particles is a decisive criterion for the determination of combustion chamber height.

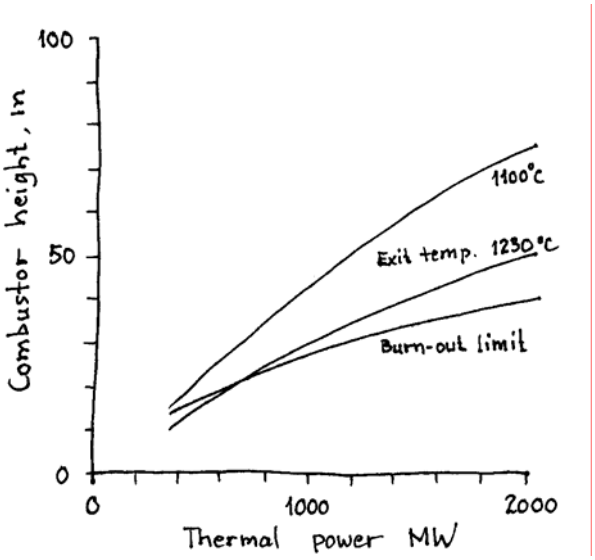

Figure 9.12.
Burn-up limit and exit temperature limit for tangentially fired pulverised coal boilers. From Strauss.

CALCULATIONS

The thermal layout of combustion chambers is based on three classes of computations: one-zone models, multi-zone models and finite difference models. The first type of model treats the combustion chamber as a well-stirred volume that exchanges heat with its surrounding walls. The multi-zone models are used in case the shape of the combustion chamber or the flames impedes the simplifying assumption of the one-zone model. The most developed models, the finite difference models, are approximations of the differential equations of mass, momentum and heat conservation, considering combustion and radiation. The latter type of models is especially useful for detailed analysis of combustion chamber processes, for instance, in connection with modifications for emission control, which can not be achieved by the simpler zone methods.

All methods have their advantages and limitations. The simple zone methods are expressed in a physically based way relying heavily on empirical input. Although more advanced, the finite difference methods also rely on empirical inputs and contain simplifications as far as radiation and chemical reactions are concerned. Furthermore, none of the methods can satisfactory handle the most important reason for the uncertainty of thermal design of combustors for solid fuels in a satisfactory way: the influence on fouling and deposition of ashes on the heat transfer surfaces.

A calculation procedure of a one-zone model taken from a textbook written by Strauss will serve as an example. The purpose of the calculation is to estimate the shape of the combustion chamber and the exit temperature of the combustion gas. The heat transfer from the luminous flames, which are assumed to fill most of the combustion chamber, depends to more than 90% of thermal radiation, and the small convective heat transfer can be estimated separately.

Radiation from the flames (temperature T_f, emissivity ε_f) to the surrounding walls (temperature T_w, emissivity ε_w) can be expressed as

$$Q_{fw} = \varepsilon_{rad,fw} A_w \ \sigma \ (T_f^4 - T_w^4) \tag{9.2}$$

Here is

$\sigma = 5.67 \cdot 10^{-8}$ W/m^{2}K^4 (Stefan-Boltzmann's constant)

A_w wall surface

$$\varepsilon_{rad,fw} = \frac{1}{1/\varepsilon_{rad,f} + 1/\varepsilon_{rad,w} - 1}$$

Examples of data:

Emissivities

$\varepsilon_{rad,w}$ = 0.6 to 0.8 (oxidised steel)

$\varepsilon_{rad,w}$ = 0.6 to 0.7 (deposits)

$\varepsilon_{rad,f} = \varepsilon_\infty(1\text{-exp}(-c_1 x))$ (flame)

and

$\varepsilon_{rad\infty}$ = 0.6 to 0.8 for oil and coals

$\varepsilon_{rad\infty}$ = 0.4 to 0.6 for gas

c_1 = 0.5 to 0.75 for blue to luminous flames

where x is a radiation path-length, in this case, roughly, the side of the combustion chamber. The heat transfer by radiation to the walls is equal to the cooling of the combustion gas from the adiabatic flame temperature T_{ad} to the temperature at the exit of the combustion chamber T_e,

$$Q_{fw} = \dot{m}_f g_v \bar{c}_{pg} (T_{ad} - T_e) \tag{9.3}$$

where $\dot{m}_f$ is fuel flow and g_v the gas yield. An average radiation temperature $T_f = \sqrt{T_{ad} T_e}$ is assumed, and then the heat balance (Eqs 9.2 and 9.3) becomes

$$(T_e/T_{ad})^2 + K_o T_e/T_{ad} = (T_w/T_{ad})^4 + K_o \tag{9.4}$$

where K_o is called the Konakow number

$$K_o = \bar{c}_{pg}\, g_v\, \dot{m}_f / (\varepsilon_{fw} \sigma A_w T_{ad}^3) \qquad (9.5)$$

If A_w is given by the size of the boiler, Eq 9.4 gives T_e. T_w is known from by the steam/water conditions chosen for the boiler (see Fig. 9.1) and a simple calculation of the temperature rise in the tube-wall. In practice, for pulverised fuel boilers, deposits may be present on the tubes, and T_w then becomes higher than that calculated. This is compensated for by some factor. In Strauss book this is done by the resulting emissivity which is expressed as

$\varepsilon_{rad,fw}$ = 0.3 to 0.45 for coal
$\varepsilon_{rad,fw}$ = 0.45 to 0.6 for oil
$\varepsilon_{rad,fw}$ = 0.55 to 0.7 for gas

Despite the uncertainties and the assumptions, the method gives an estimate of the desired exit temperature.

EXAMPLE 9.1 (from Strauss):
The shape and exit temperature shall be determined for a 740 MW coal-fired boiler.
Given:

Q_{fuel} = 1821 MW (considering efficiency)
Q_v = 0.12 MW/m^3 (Fig. 9.11)
Q_c = 5.9 MW/m^2 (Fig. 9.11)
T_w = 710 K (given by steam conditions)
T_{ad} = 2100 K (given by fuel and air ratio 1.25)
$\dot{m}_f$ = 821 kg/s, $\bar{c}_{pg}$ = 1.35 kJ kg^{-1}K^{-1} (given)
$\varepsilon_{rad,fw}$ = 0.3
T_w = 900^{o}C

Solution: $Q_c = Q_{fuel}/A_c$ and $Q_v = Q_{fuel}/V$, and the combustion chamber volume $V = x^2 \cdot l$, and cross-section $A_c = x^2$. If square, the width of the combustion chamber becomes x = 17.5 m and the height
l = 50 m.

Eqs 9.2 to 9.5 give T_e = 1220^{o}C and the exit temperature becomes T_e = 1276^{o}C.

HEAT BALANCE

The performance of a combustor is characterised by its heat balance, expressed in the form of an efficiency η_b, the ratio of the power produced Q_{out} and the power supplied Q_{in}.

$$\eta_b = Q_{out}/Q_{in} \qquad (9.6)$$

From a theoretical point of view this is a simple concept. In practice, however, especially using solid fuels, the formulation of the heat balance may become complex, as can be imagined by studying Fig. 9.13 taken from a standard formulation of a boiler heat balance in a general case, DIN 1942.

Here, following DIN 1942, we will determine the heat balance in a simple case: a hot water boiler whose energy flows are shown in Fig. 9.14. The location of the system boundary and the decisions on what should be inside or outside the boundary are important. In the present simplified case, for example, all fans and pumps are outside of the boundary. Also, a number of complications indicated on Fig. 9.13 are not included. What should be included or not within the system boundary is optional and depends on where the boundary is located and on the conditions chosen for the balance.

The system boundary is accompanied by a reference temperature, which is usually (DIN 1942) taken as $t_o = 25^oC$. All heating values, specific heats or enthalpies should be related to this base-level temperature.

The operation of a boiler is controlled to give a certain (measured) output and, for a given (measured) air supply, a given (measured) oxygen concentration in the flue gases, the fuel feed rate is determined. Especially in the case of solid fuels, expensive measurements of the fuel feed rate and of ash flows are not always carried out. This complicates the formulation of the heat balance. During a heat balance test these flows are sampled, though, to determine the heating value of the fuel and the content of unburned in the effluent streams of ashes. In the case of liquid and gaseous fuels these problems disappear: measurements of the flow rate of the input flow are simple, and sufficient data are usually available for straightforward heat balances.

Heat output

$$Q_{out} = \dot{m}_w (h_{w,out} - h_{w,in}) \qquad (9.7)$$

where

$\dot{m}_w$ is the flow of water to be heated, kg/s

h_w are the input and output enthalpies of water, kJ/kg.

In general

$$h - h_o = \int_{To}^{T} c_p \, dT$$

where $h_o(T_o)$ is the reference value. This can also be expressed by an average specific heat

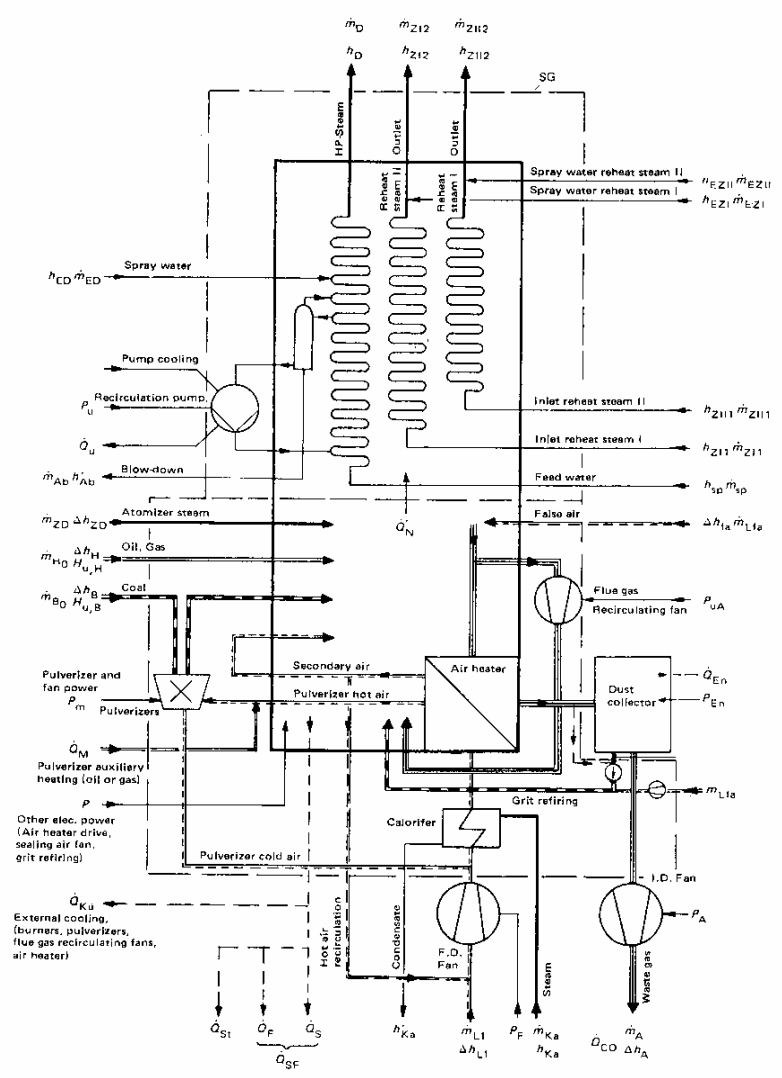

Figure 9.13.
General picture of energy and mass flows in a steam generator. (From DIN 1942).

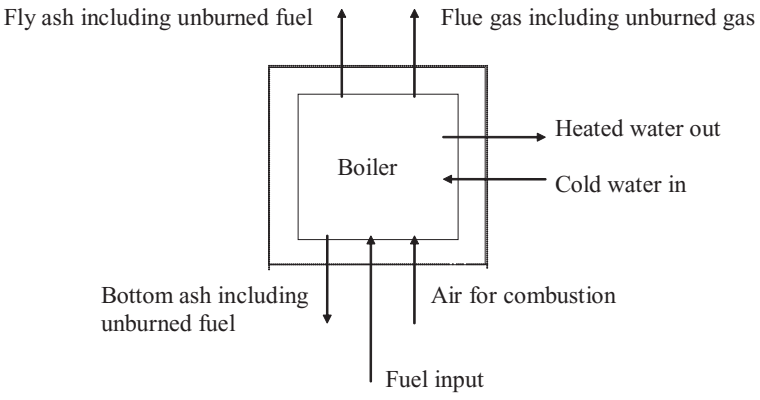

Figure 9.14.
Heat balance over a hot water boiler. The dashed line represents the system boundary for the heat balance.

$$\bar{c}_p = \frac{1}{T - T_o} \int_{T_0}^{T} c_p \, dT$$

Heat input

The input consists of chemical energy in the fuel and the thermal energy in fuel and air, kJ/s, that is kW,

$$Q_{in} = Q_{fuel} + Q_{air} \tag{9.8}$$

$$Q_{fuel} = \dot{m}_f (1 + \xi_u^*) (LHV + \Delta h_b) \tag{9.9}$$

$$Q_{air} = \dot{m}_f \ell_v \Delta h_a \tag{9.10}$$

and

$\dot{m}_f$ fuel (combustibles, water and ashes) burned, kg/s

$\dot{m}_{f,in} = \dot{m}_f (1 + \xi_u^*)$ fuel input

ξ_u^* the ratio of unburned fuel to fuel burned, -

LHV lower heating value related to one kg of fuel

$\Delta h = h - h_o = \bar{c}_p (T - T_0)$ enthalpy difference of fuel (index b) or air (index a) relative to the reference level.

ℓ_v air demand, kg/kg fuel burned

$\bar{c}_{p,fuel}$ =1.7 and $\bar{c}_{p,air}$ =1.011 kJ/kgK

The difference between the fuel burned and the fuel fed to the boiler should be noticed, ξ^* is a loss of combustibles which is found in the ashes.

Heat leaving the boiler, kW

$$Q_{loss} = Q_{flue\ gas} + Q_{fly\ ash} + Q_{bottom\ ash} + \xi_{rad} + Q_{out} \tag{9.11}$$

The heat leaving with the flue gases, including unburned gas

$$Q_{flue\ gas} = \dot{m}_f g_v h_g(T_{stack}) + \xi_{co} \tag{9.12}$$

Here :

g_v is gas yield including excess air, kg/kg fuel burned

$h_g (T_{stack}) = \bar{c}_p (T_{stack} - T_o)$ kJ/kg gas

$\bar{c}_p$ is calculated knowing the composition Y_i of the flue gas

$$\bar{c}_p = \sum_i Y_i c_{pi}$$

Simplified formulae are also available, for instance, the one below, where T = T_{stack} in ^oC

$$\bar{c}_p = 1.00366 + 1.81538 \cdot 10^{-5} T + 1.11509 \cdot 10^{-7} T^2 +$$
$$+ [0.86883 + 1.43897 \cdot 10^{-5} T + 2.87479 \cdot 10^{-7} T^2] Y_{H_2O}$$
$$- [0.09909 - 4.31904 \cdot 10^{-4} T + 3.64433 \cdot 10^{-7} T^2] Y_{CO_2}$$

(T is here in Celsius and c_p has the unit kJ/kg ^oC) valid in the range T=0 to 400^{o}C. x are the mass concentrations of H_2O and CO_2.

$\xi_{co} = \dot{m}_f \; g_{vt} \, v_{co} \, H_{u,co} R_{gas} \, / R_{co}$ kJ/kg dry gas is the heat loss due to unburned CO

v_{co} volume fraction of CO, m^3/m^3 (measured)

g_{vt} dry real flue gas yield, kg/kg fuel burned

R_{gas}=0.2870-0.07344$Y_{CO2,\,dry}$, kJ/kgK

R_{co}=0.2964 kJ/kgK, gas constant CO

$H_{u,co}$=10115 kJ/kgCO, heating value CO

Heat leaving with ashes, including unburned char

$$Q_{fly\ ash} = \dot{m}_{fa} (Y_f LHV_{,u} + \bar{c}_{pf} (T_{stack} - T_o)) \quad (9.13)$$

$$Q_{bottom\ ash} = \dot{m}_{ba} (Y_b LHV_{,u} + \bar{c}_{pb} (T_{b,a} - T_o)) \quad (9.14)$$

Here are

$\dot{m}_{fa}$ fly ash flow, kg/s

$\dot{m}_{ba}$ bottom ash flow, kg/s

Y_f, Y_b unburned fractions of fly ash and bottom ash, -

$\bar{c}_{pf}$ =0.84 and c_{pb}=1.00 kJ/kgK

$LHV_{,u}$=33000 kJ/kg (Lower heating value)

The losses of unburned can be expressed in relation to the fuel input

$$\xi_u = \frac{\dot{m}_{fa} Y_f + \dot{m}_{ba} Y_b}{(\dot{m}_b + \xi_u^* \dot{m}_b)(1 - Y_a - Y_w)} \cdot \frac{(\dot{m}_b + \xi_u^* \dot{m}_b) Y_a}{\dot{m}_{fa}(1 - Y_f) + \dot{m}_{ba}(1 - Y_b)} \quad (9.15)$$

or related to the fuel burned

$$\xi_u^* = \xi_u / (1 - \xi_u) \quad (9.16)$$

In these expressions Y_a and Y_w are fractions of ashes and water in the fuel. If $\dot{m}_{fa}$ and $\dot{m}_{ba}$ have not been measured a mass balance

$$(\dot{m}_b + \xi_u^* \dot{m}_b) Y_a = \dot{m}_{fa} (1 - Y_f) + \dot{m}_{ba} (1 - Y_b) \quad (9.17)$$

and an empirical distribution factor η_s

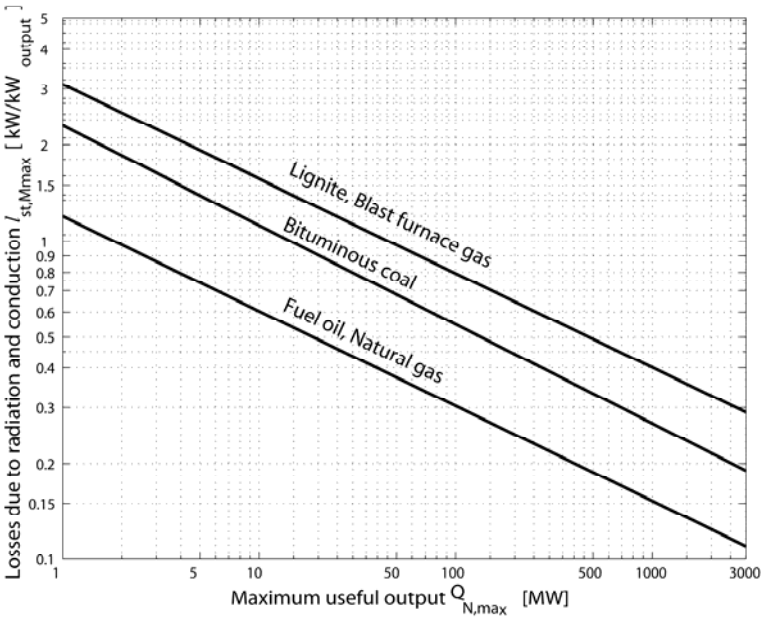

Figure 9.15.
External loss ξ_{rad} kW/kW$_{output}$ (scales in MW). (From DIN 1942).

$$\dot{m}_{ba}(1\text{-}Y_b)=\eta_s(\dot{m}_b+\xi^*_u\,\dot{m}_b)Y_a \tag{9.18}$$

$$\dot{m}_{fa}(1\text{-}Y_f)=(1\text{-}\eta_s)(\dot{m}_b+\xi^*_u\,\dot{m}_b)Y_a \tag{9.19}$$

will determine $Q_{fly\ ash}$ and $Q_{bottom\ ash}$ and ξ_u, ξ^*_u.

$$\xi_u=\left(\frac{(1-\eta_s)}{1-Y_f}Y_f+\frac{\eta_s}{1-Y_b}Y_b\right)\cdot\frac{Y_a}{1-Y_a-Y_w} \tag{9.20}$$

Finally, the loss due to radiation and convection of heat from the boiler's exterior surface to the surroundings Q_{out} has to be estimated. This can be done by calculation, but the loss is small and the calculations are extensive, so this quantity is preferably taken from a standard diagram, Fig. 9.15.

If the mass flow of fuel is not available, another calculation procedure, called **the indirect method** (in contrast to the above **direct method)** can be used. In the indirect method the efficiency is calculated by means of the losses

$$\eta_b = 1 - Q_{loss}/Q_{in} \tag{9.21}$$

The relative losses can be formulated based on the relationships given above. In this case $\dot{m}_b$ is eliminated, but the following has to be measured:

- Fuel analysis (proximate, elemental, heating value),
- Flue gas concentration (O_2 concentration for the determination of the excess-air ratio and CO for the losses),
- Temperatures of fuel, inlet air, exiting ashes, flue gas,
- Concentrations of unburned in exiting ashes.

BURNERS - SUSPENSION CONVERSION

Burners for injection of fuel and air are built in a range from small sizes up to very large unit sizes of 50 to 100 MW_{fuel}. Despite these sizes, in very large boilers multiple burners are installed. Multiple burners are also employed in cases when load turn-down is essential.

Burners are designed to inject gaseous fuel, liquid fuel in the form of drops (the burners are designed to ”atomise” the liquid fuel) and solid fuel in the form of powder, but also a major quantity of combustion air. From stoichiometry it is evident that the mass of air to be injected is in the order of ten times as great as the mass of fuel. This should be remembered when considering burner design.

BURNERS FOR LIQUID FUELS

Nozzles for atomisation of liquid fuels are described in detail for instance by A.H. Lefebvre, Gas turbine combustion, Taylor & Francis, 1983. (pp 371-375, 387-414). The droplet size distribution is essential for the performance of the burners. Definitions of size distributions of drops are presented by Lefebre (pp 375-383, 432-448). These definitions can be applied also for powders.

The spray nozzle is inserted into a burner, which provides the air for combustion of the gas, evaporated from the drops. Conditions for ignition are described by Lefebre (pp 179-188 and 126-137). The effects of a flameholder or swirl (see below) are important, not only for liquid fuels, but also for gaseous or solid pulverised fuels.

BURNERS FOR POWDERS

Solid fuel is injected in the form of a powder, heat is supplied by externally recirculated hot gases and by radiation from the flame, the particles of the powder are heated, volatiles are released and ignited. Towards the end of devolatilisation the residual char particle is ignited and burns (hopefully) to comple-

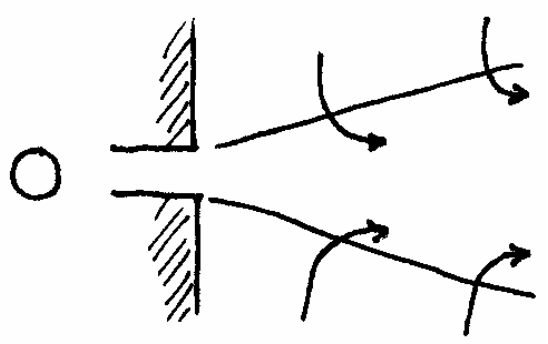

Figure 9.16.
Direct injection through a pipe. Arrows indicate entrainment of gas

tion. The remaining ashes are carried away with the gas and are finally separated from the flue gases in a filter.

A number of factors influence ignition:

- size distribution of the fuel. Sizes below 100 μm are produced by grinding in mills adjacent to the burners or in special plants (for small boilers or wood combustors),

- properties of the fuel, especially the content of volatile matter. The ignition of the volatiles promotes ignition of the char by creating high temperature, so high volatile fuels are easier to ignite than low volatile fuels,

- the burner design and the interaction with the combustion chamber (cf. stabilisation of oil flames).

There are two main groups of pulverised fuel burners: **jet burners** (strålbrännare) and **swirl burners** (virvelbrännare).

The simplest arrangement for burning a powder is by direct injection of a fuel-air mixture Fig 9.16. The hot surrounding gases, and radiation from flames, will ignite the mixture when the jet velocity has reached a sufficiently low level. In this type of jet burner, the jet velocity would be chosen so that ignition takes place at some distance (e.g. half a metre) from the nozzle, considering the rapid decay of velocity in the jet (see Lefebre pp 58-59). However, the concentration also decays at the same rate, so the limits of flammability have to be observed. When the load is decreased in such a burner, the jet velocity is reduced from its design value, and combustion takes place closer to the nozzle or even within the nozzle, which is not acceptable. Therefore, fuel and most air are supplied separately in normal commercial burners, Fig 9.17.

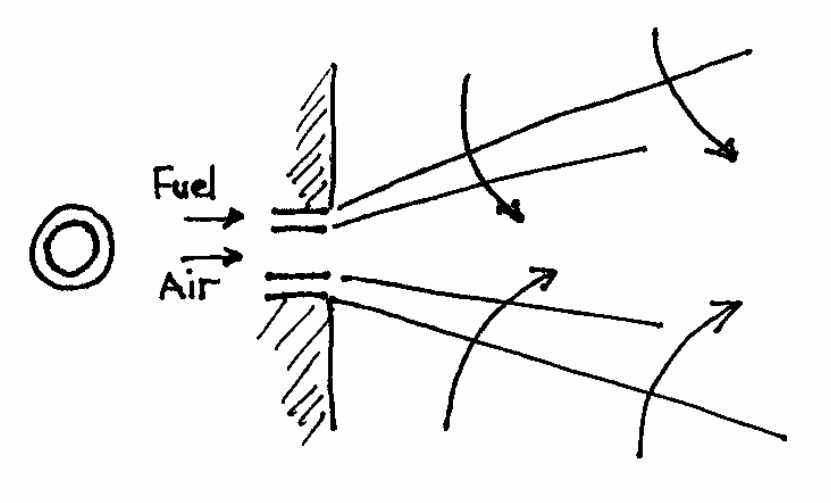

Fig. 9.17.
Jet burner arranged for pulverised fuel.

In the jet burner fuel and air are injected separately through nozzles. In one type of design the powder is injected together with some air to transport the powder in an annulus surrounding the primary air, and gas from the surrounding combustion chamber is mixed through the fuel layer.

Another common arrangement for combustion of pulverised coal is shown in Fig. 9.18 (See also Fig 9.5). Coal and air are supplied separately in vertical sets of nozzle registers located in the corners of the combustion chamber. Mixing is created in the jets themselves and by the coarse vortex set up by the tangential directions of the jets as indicated by the horizontal cross-section of the combustion chamber shown in Fig. 9.18.

Swirl burners (Lefebre pp126-135) are stabilised by rotation of the air by a set of vanes, which serve as a swirl generator, Fig. 9.19. A flame stabilised by a flame-holder without swirl is shown for comparison. Both methods create an inner recirculation vortex bringing hot gas to the injected fuel for ignition. The swirl widens the flame and creates a circulation flow in front of the burner, the **internal** gas recirculation, which is further supported by the widened opening of the wall (the quarl). The **external** gas recirculation to the flame, not shown, consists of partly burned gases from the surrounding combustion chamber, just as in the case of jet burners. (In other cases "external" recirculation could mean recirculation from the flue gases, external to the furnace.) The recirculation zone of a swirl burner is illustrated in detail in Fig. 9.20. The shape of the inner recirculation vortex, greatly determining the shape of the flame, depends on the swirl. The degree of swirl can be expressed as a swirl number

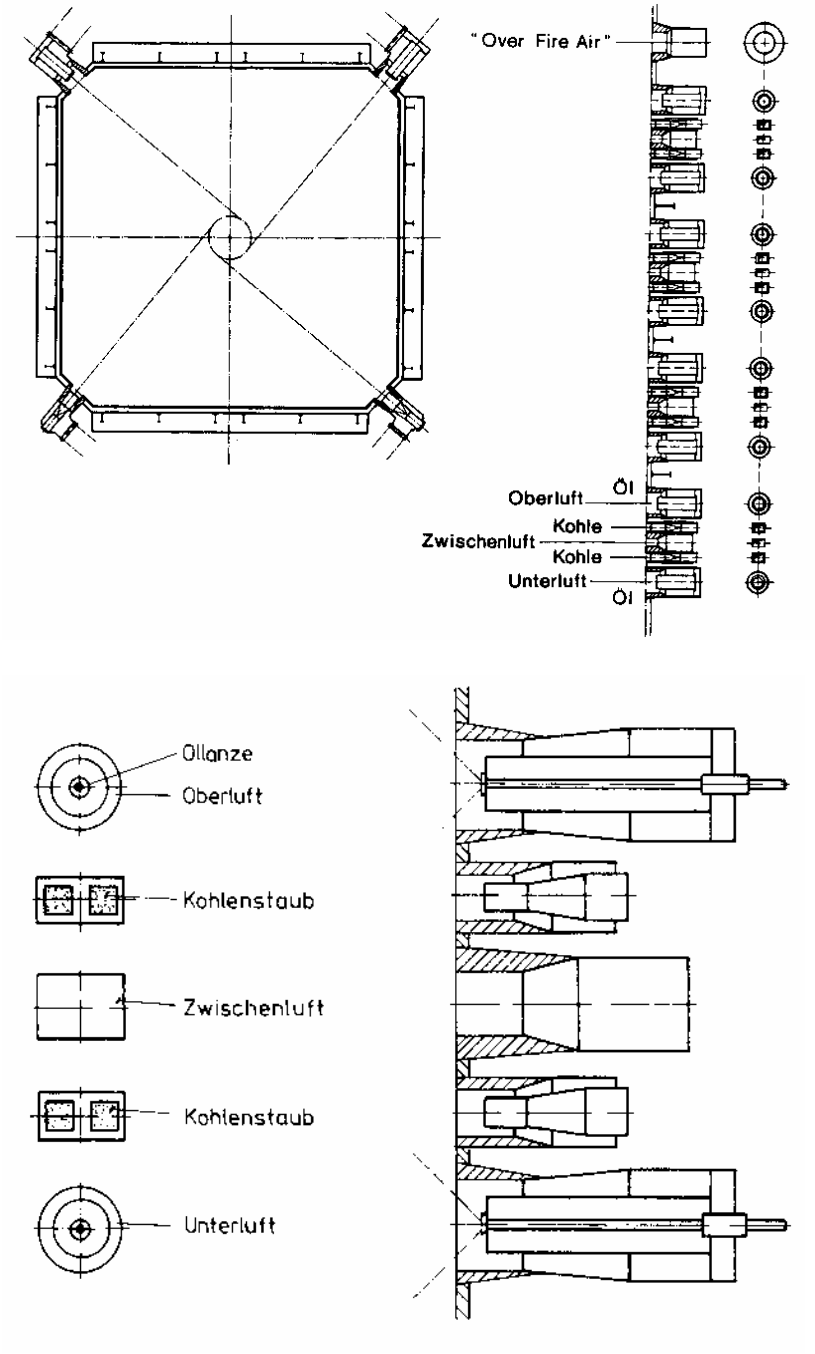

Fig. 9.18.
Tangential burners for a large coal fired boiler. The burners are composed of several sets of jet burners including also oil or gas for low load or back-up operation. In this boiler there are 16 groups of burners in each of the four corners. Each burner group has a maximum fuel power of 160 MW. The height of the 15 burners is about 25 m. The "over-fire air" is added for final burnup, allowing fuel-rich operation in the principal combustion zone (for low-NO_x emissions).

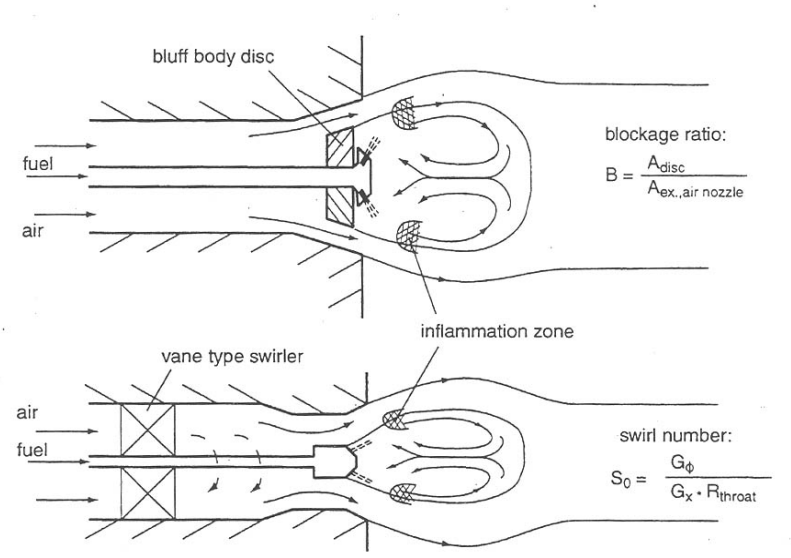

Figure 9.19.
Oil burners stabilised by flame-holder (upper figure) and by swirl (lower figure). The same principles can be applied for other fuels.

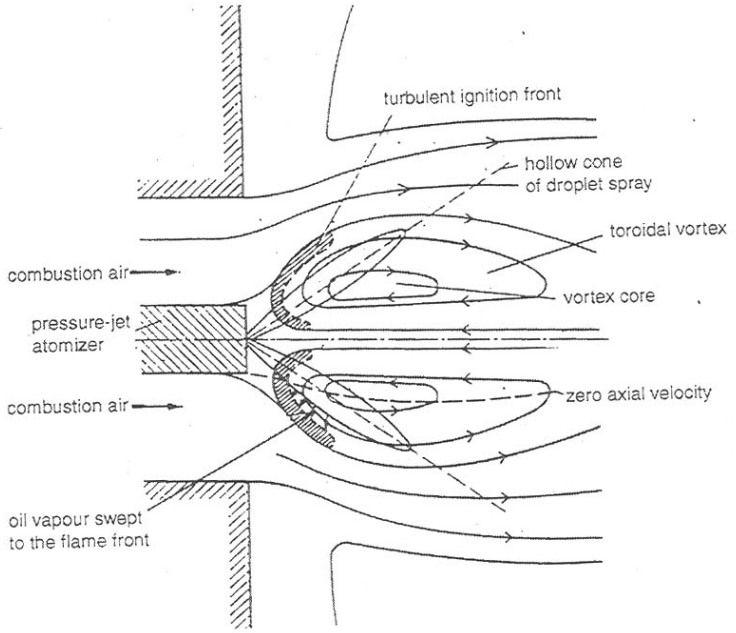

Figure 9.20.
Picture of the flow pattern formed by a swirl burner, where the fuel is added in the centre tube; oil in this case. Air may or may not be supplied through the central tube. The main combustion air is injected through the external annulus with a certain tangential velocity caused by the swirl generator.

$$S = G_\varphi / (G_x R_{throat})$$

G_φ and G_x are the axial flux of angular momentum [kgm^2/s^2] and axial thrust (momentum + pressure [kgm/s^2]), respectively. R_{throat} is the radius of the swirler or exit nozzle. A recirculation zone is formed when the swirl number is above 0.6. A further increase in swirl number gives a wider recirculation vortex. However, the shape of the flame is also influenced by the combustion. Depending on the axial momentum of the fuel jet and the properties of the fuel (volatiles, size), the fuel jet can penetrate through the internal recirculation zone, or it can remain there. According to the nomenclature of the International Flame Research Foundation (where such flames have been studied) the two cases, illustrated in Fig. 9.21, are called Flames of Type I and II, respectively.

The air supply is important for the form of the flame, as mentioned, but also for the burnout of fuel. During last decades another important requirement has been added: low NO_x emissions. The local flame stoichiometry is decisive for formation and reduction of nitrogen oxides, and designs lead to creation of locally fuel-rich conditions with staged air supply by the burner. Some examples of burner design for gradual supply of air to the flame are shown in Fig.9.22.

Combustion control, turn down and safety requirements make commercial burners complex as shown in Fig. 9.23.

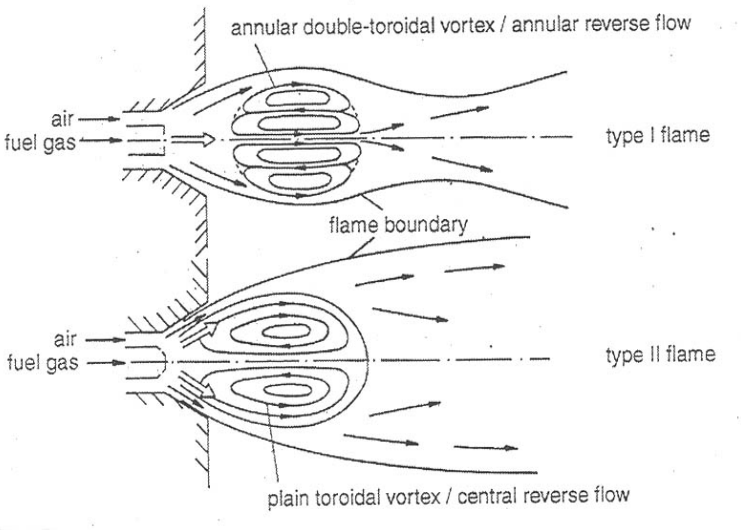

Fig. 9.21.
The flow patterns of type I and Type II flames.

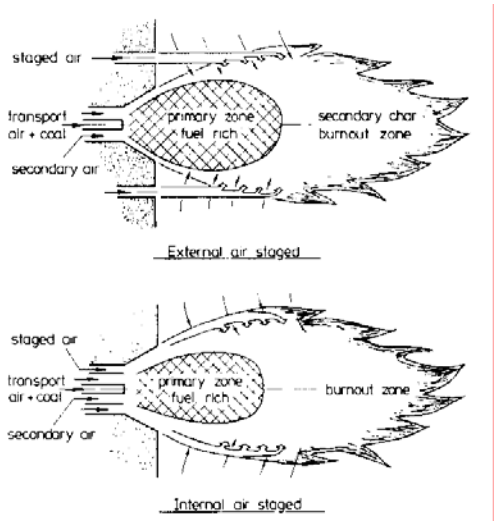

Figure 9.22.
Air staged pulverized coal burner types.

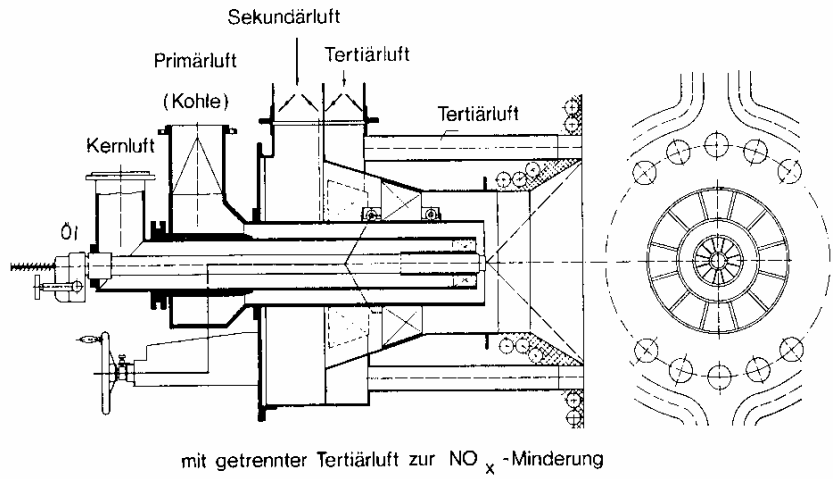

Figure 9.23.
A combined coal/oil swirl burner. Oil can be added through the central nozzle. Coal powder is carried by transport air (primary air) and injected with a velocity of 18 to 25 m/s surrounded by swirled secondary and tertiary air having velocities in the order of 30 to 50 m/s. On the right hand view the tertiary air tubes are seen as well as the swirl generators.

BURNERS FOR GAS

Burners for gas are designed according to the principles explained above, but gas is less complicated than liquid and solid fuel and other principles of burner design are feasible, such as premixed combustion and flameless oxidation (FLOX). Flameless oxidation is achieved by extreme internal or external recirculation of hot gases. In the case of external recirculation a high-temperature heat exchanger is needed. By dilution with recirculated gas, the combustion zone becomes extended in space and steep gradients of temperature are avoided.

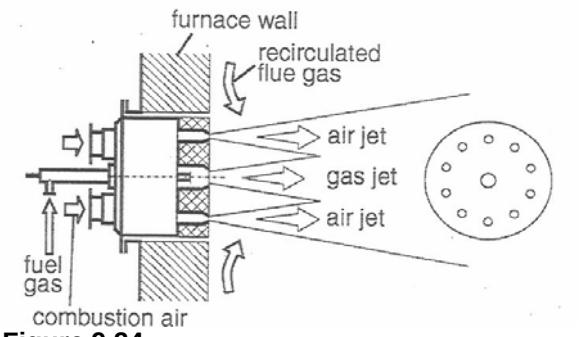

Figure 9.24.
Flow and mixing in the near-burner zone of a commercial FLOX burner.

Consequently the formation of thermal NOx is very low. An example is given in Fig. 9.24. In order to sustain combustion in the diluted gas a fairly high temperature is needed (at least 1500 K).

GASIFICATION

Also some gasifiers work in a suspension mode, in which finely ground fuel particles are injected by burners into the "combustion chamber" to be gasified, that is, to be partially burned to raise the temperature up to 1700-1900 K at a high pressure (in the order of 1 MPa) required for subsequent rapid gasification with H_2O and CO_2 in the same combustion chamber. The oxidation can be achieved by air ("air-blown" gasification), or by oxygen in order not to dilute the product gas with nitrogen ("oxygen-blown" gasification). Coal gasification to be used in ”integrated gasification combined cycles” (IGCC) has been tested in large-scale plants. The purpose is to increase the efficiency of coal conversion by combined cycle operation. At present, 2003, natural gas is available, and direct use of gas in combined cycle plants is preferred. For this reason the introduction of IGCC is slow for the moment. Figure 9.25 shows an example of a "combustion" chamber and a subsequent convection cooling section where the product gases are cooled after gasification for desulphurisation at a rather low temperature (a few hundred degrees) in a Claus process. There are some problems that remain to be solved. The necessity for sulphur cleaning at low temperature is one of the drawbacks that reduce cycle efficiency. High temperature cleaning, including filtration, aims at removing entrained particles before they are burned in the combustor of a gas turbine.

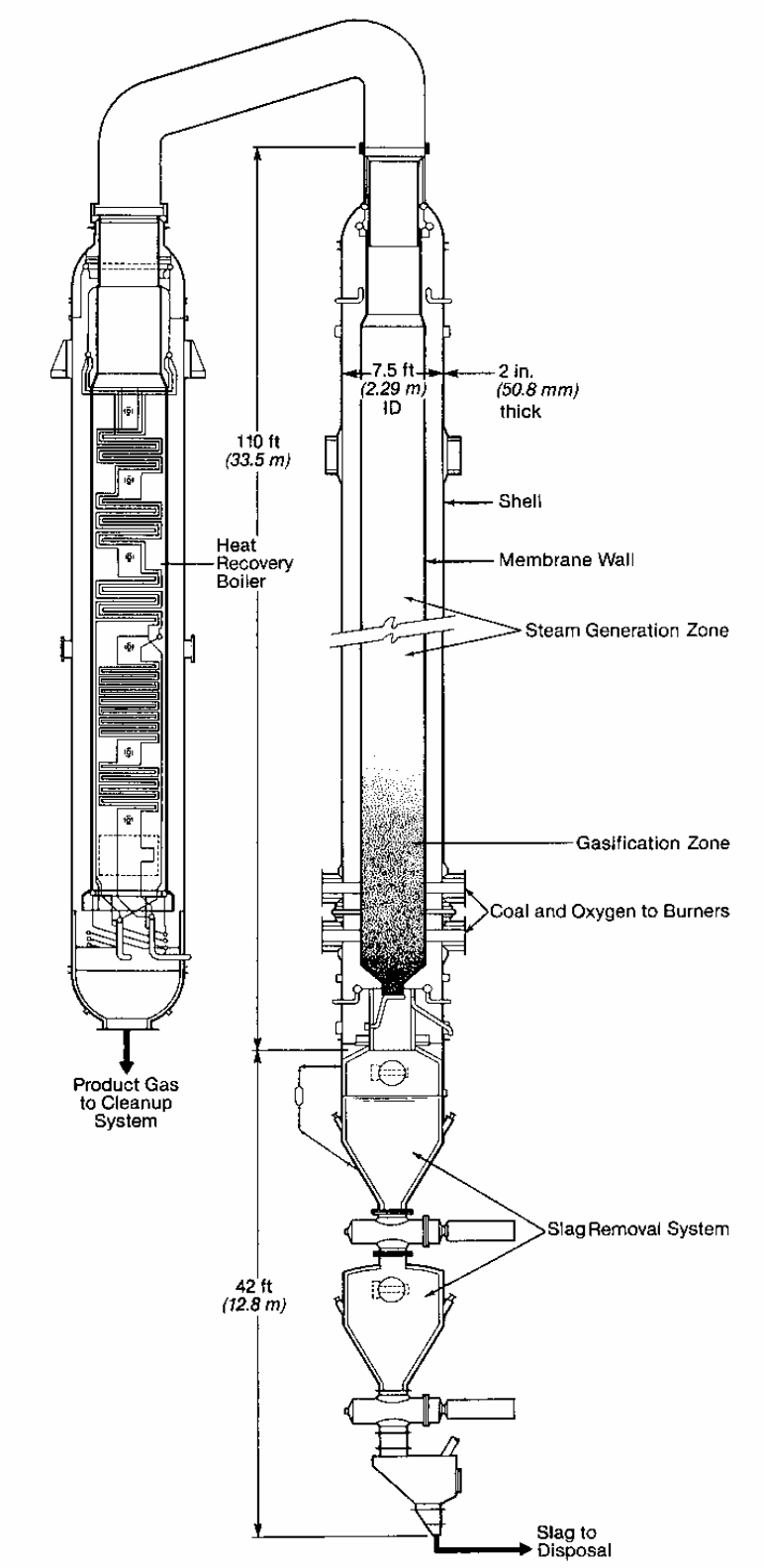

Figure 9.25.
A Texaco entrained-flow gasifier working at 1500°C and 6 bar pressure. The liquid slag removal system is also shown in the figure. (The slag formed at high temperature is removed downwards)

FIXED AND MOVING BED CONVERSION
(Omvandling i fast och rörlig bädd, förbränning på rost)

Fuel beds for conversion of solid fuels can be fed in **batches** (satsvis) or **continuously.** Batch feeding is common in small furnaces for house heating, whereas continuous feeding is usually employed in larger devices and in grate-fired plants up to sizes of 100 to 200 MW_{fuel}, but normally less than 50 MW_{fuel}.

Fuel and air can be fed in **co-current, counter-current** or **cross-current**, as shown in Fig. 9.26. The denominations co-current and counter-current are here related to the flow of air and fuel. In other applications other definitions may be used. In boilers only part of the combustion takes place on the grate. The processes in the combustion chamber of a grate-fired boiler (rosteldad panna) normally consist of several steps, as illustrated in Fig 9.27. The same steps are indicated in the sloping grate furnace shown in Fig.9.28. The fuel is fed onto the sloping grate (1) where a fuel bed is formed. In the bed the fuel is dried, devolatilised, the remaining char is burned, and ashes finally leave the grate at the lower end. The gases leaving the bed (water vapour, volatiles, and partially burned gas) are stirred by air or gas jets (recirculated flue gas) in order to mix fuel and air in the **stirred reactor volume** (2) above the bed. The walls surrounding this space are to some extent refractory surfaces from which heat will be radiated back to the first part of the bed for drying and devolatilisation and to the end of the bed for burn-up of fuel.

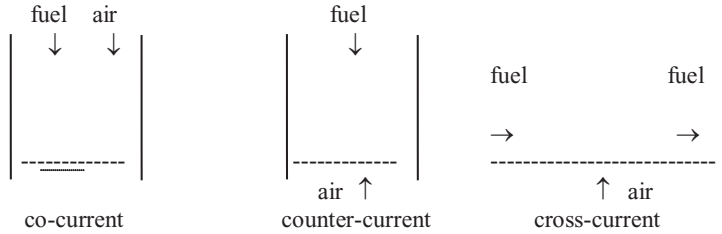

Figure 9.26.
Arrangements of fuel and air supply to a fixed bed

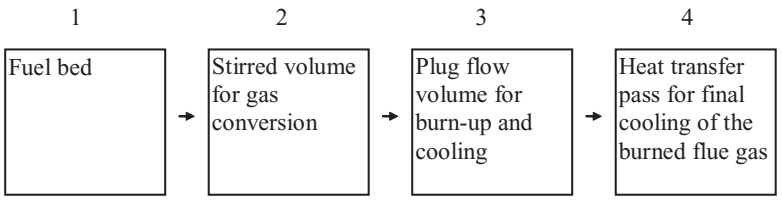

Figure 9.27.
The processes taking place in a grate-fired boiler

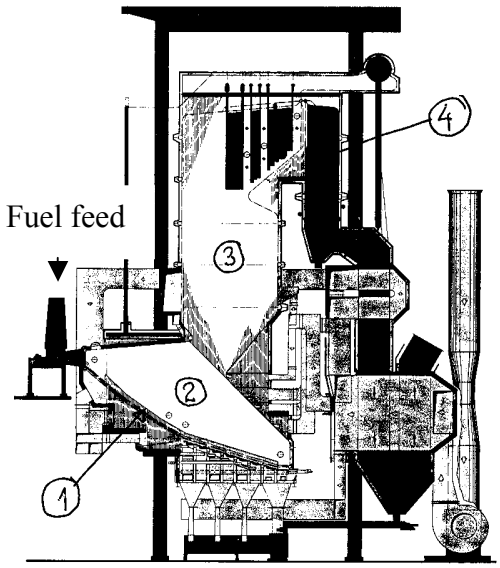

Figure9.28.
Principle figure of a grate-fired boiler. The grate is a sloping grate, for instance for bark. 1 is the fuel bed on the grate, 2 is the stirred combustion space; in this particular case surrounded by refractory walls, 3 is the combustion chamber for burnup after addition of secondary air, and 4 is the beginning of the convection gas pass.

The fractions of wall covered with refractory or cooling surface depend on type of fuel (its heating value) and aims at producing a suitable temperature in the over-bed region. If there are no cooling surfaces, the temperature approaches the adiabatic temperature of the partially burned fuel. Air for final combustion is added above the stirred region and produces initial turbulence and mixing for the burn-out in the **plug-flow** region (3), whose walls consist of heat receiving surfaces (tubes). In this region the gases should burn out and attain a predetermined temperature before they reach the **convection cooling surfaces** (4).

The classical cross-current bed design for coal combustion is the **travelling grate stoker** (Wanderrost, Grate Stoker), Fig. 9.29. The fuel is introduced into the combustion chamber resting on the moving grate (rörlig rost) at a velocity, which is suitable in order to attain a complete burn-up of the fuel at the end of the grate. The time of transport may be in the order of half an hour. The fuel rests on the surface of the grate, and this allows penetration of primary air from below. The ashes form a protective layer on the surface of the grate before they fall down into the ash bin. Another classical arrangement is the **spreader stoker (**kastmatare**),** Fig. 9.30. In this case the fuel is thrown on to the surface of the grate that moves towards the spreader side.

These grates can be used for biofuels, but the ash content of a biofuel is low and as the fuel layer burns out the grate will not

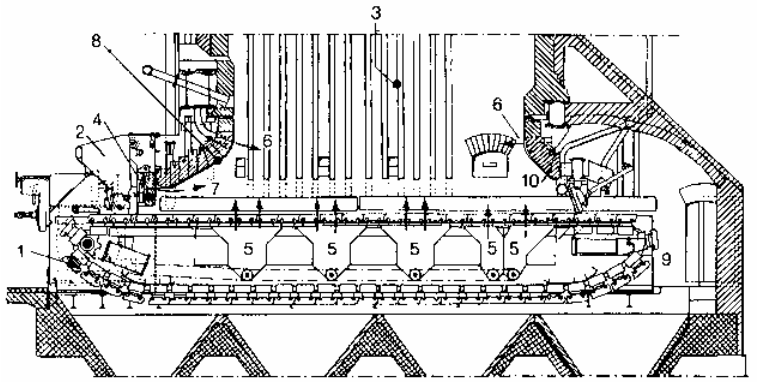

Figure 9.29.
Travelling grate stoker for combustion of coal. 1 Grate (rost), 2 Fuel feed chute (bränsleschakt), 3 Combustion chamber, 4 Bed height controller, 5 Primary air inlets, 6,7 Secondary air supply, 8, 10 Refractory wall, 9 Ash outlet

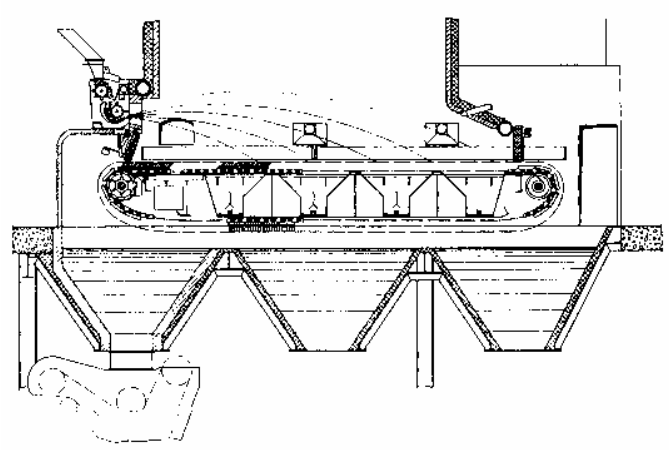

Figure 9.30.
Spreader stoker with a moving grate

be entirely protected from radiation by an ash layer. For this reason the grate will be exposed to the heat flux emitted by the flames in the stirred region and by its surrounding surfaces. Furthermore, biofuels may not have the same regularity (being actually waste fuels) as a well prepared coal, and the transport of a rigid fuel layer along the grate may produce insufficient combustion or caking of fuel in some cases (bark).

In the field of biomass and waste combustion on grates there has been a certain development during the past decades. One of the principal efforts has been to produce an even fuel layer to avoid air channelling or losses of unburned fuel.

In the 1950's plain grates with underfeed were used both for coal and dry wood. This type is characterised by a rather uncontrolled distribution of fuel and air on the grate, Fig. 9.31. Some improvements were made in the 1960's with the introduction of sloping grates where the fuel enters in the upper

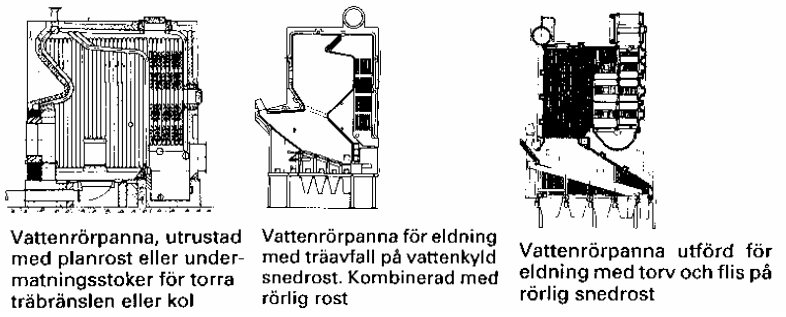

Vattenrörpanna, utrustad med planrost eller undermatningsstoker för torra träbränslen eller kol

Vattenrörpanna för eldning med träavfall på vattenkyld snedrost. Kombinerad med rörlig rost

Vattenrörpanna utförd för eldning med torv och flis på rörlig snedrost

Figure 9.31. **Figure 9.32.** **Figure 9.33.**

end and slides or is moved along the grate. However, the inclination of the grate has to be suited to a particular fuel, otherwise the movement along the grate becomes irregular. One improvement was to add a reciprocating grate (fram- och återgående rost) in the lower part of the fuel layer, Fig. 9.32. A further improvement towards control and fuel flexibility was to make the entire grate in the form of a reciprocating grate, Fig. 9.33. This is a common type of grate for combustion of wastes and biofuels in the 1990's. The combustion on this type of grate can be controlled in various ways:

a) by the height of the fuel layer
b) by the local movement of the grate
c) by a controlled supply of primary air along the grate

A reciprocating grate consists of a number of rods (roststavar), which move back and forth in relation to each other, as shown in Fig. 9.34. The black set of rods move in relation to the lighter coloured ones on the figure according to a given scheme,

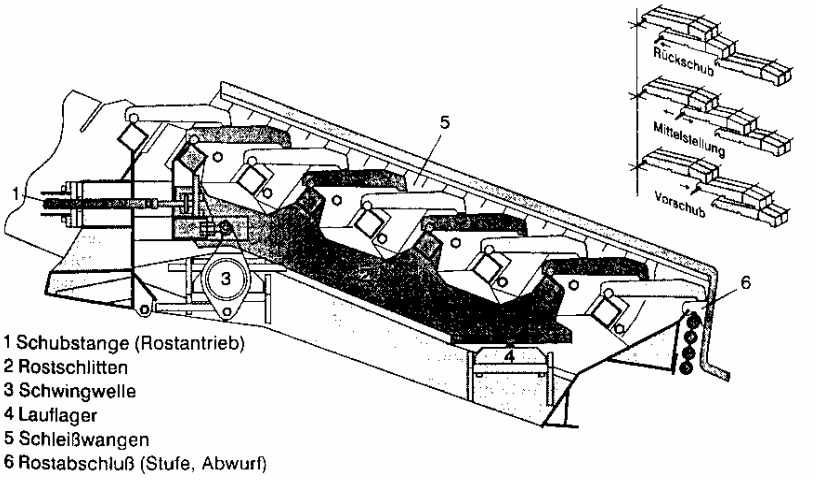

Figure 9.34.
Part of a reciprocating grate.

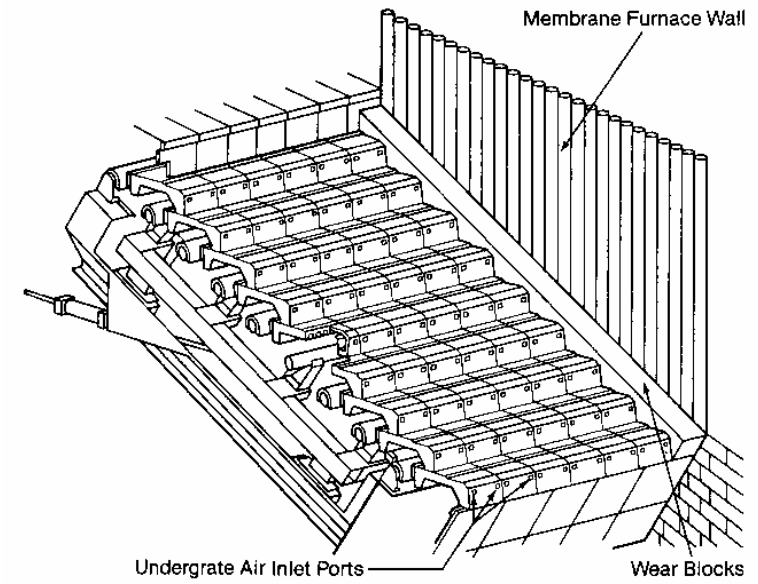

Figure 9.35.
Reciprocating grate.

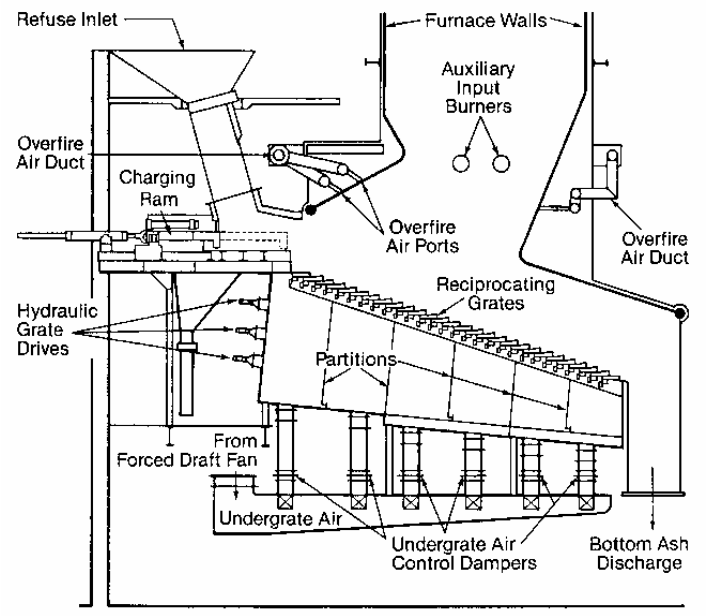

Figure 9.36.
The bottom part of a grate-fired furnace.

thus moving the fuel. The primary air is supplied in slits between the rods or in channels through the rods. A picture of a grate surrounded by cooling tube surface is shown in Fig. 9.35. (This is for combustion of a fuel with high heating value, requiring cooling surface in region 2). An example of the bottom part of the furnace is shown in Fig. 9.36. By adjustment of the movements of the reciprocating grate the transport of the fuel bed along the grate can be controlled to some extent.

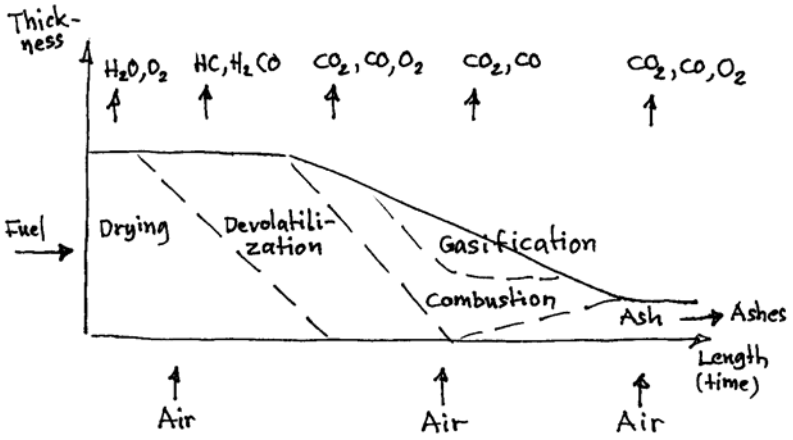

Figure 9.37.
Conversion states of a rigid fuel layer moving along a grate. The major part of the primary air is supplied to the central part of the grate. This fuel bed is ignited from above.

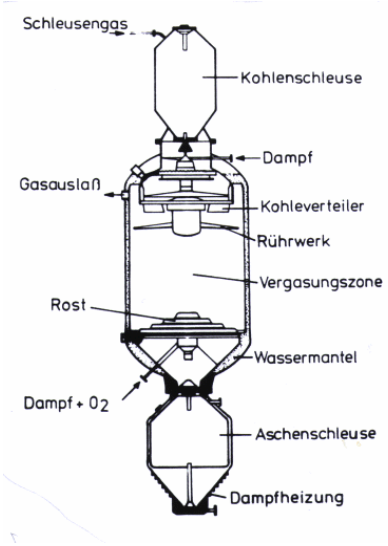

Figure 9.38.
A Lurgi gasifiers.

A selective supply of primary air (under-grate air) influences the processes taking place on the grate: drying, devolatilisation and the char burn-out. Moreover, the movements of the grate may mix the fuel bed in a vertical sense. The processes in a rigid bed (which is not stirred in the vertical sense) may be as shown in Fig. 9.37. The gases leaving the grate are first water vapour, then volatile products, combustion products, gasification products (depending on amount of oxygen supply) and gases from final burn-out of char. These gases have to be mixed in the stirred reactor volume.

An example of a counter-current bed for gasification is given by the pressurised Lurgi gasifier in Fig. 9.38. The fuel

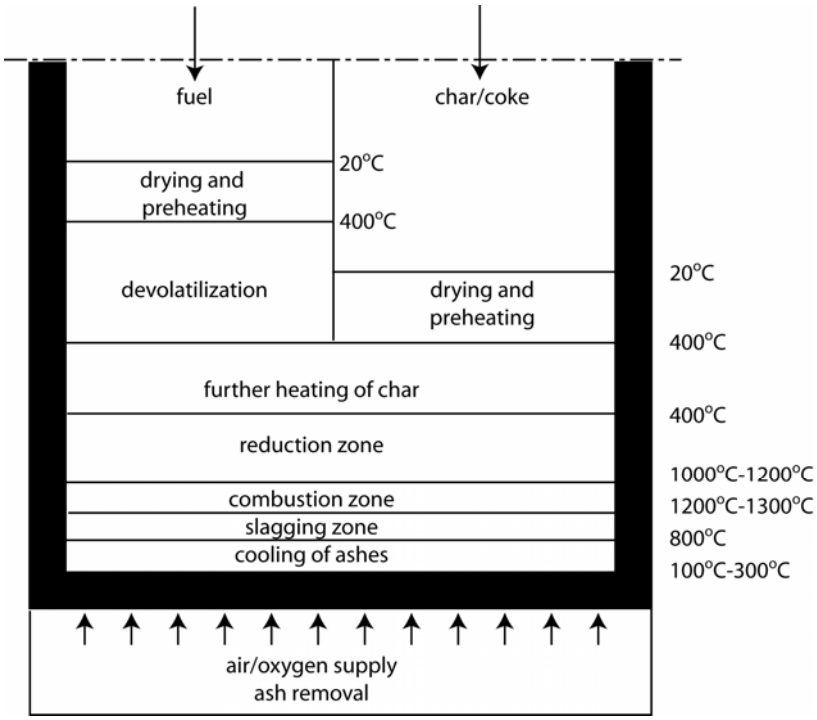

Figure 9.39.
Fuel conversion in a fixed-bed counter-current gasifier. Two cases are compared: The fuel consists either of raw fuel particles (left side) or char (right side).

is added through a lock-hopper system at the top and the ashes are withdrawn at the bottom. The different zones in the bed and the difference between gasification of devolatilised coke (right hand side of Fig. 9.39) and bituminous coal, where volatiles are released, (left side) is presented in Fig. 9.39. Air is introduced in the bottom for combustion to produce heat and CO_2 for gasification. A co-current gasifier would be organised in an analogous way, except for the obvious release of volatiles upstream of the combustion zone. In this case there is some destruction of heavy hydrocarbons (tar, tjära) in contrast to the counter-current gasifier where the tar is mixed with the product gases.

Gasmotorer. Under kriget omändrades många ottomotorer till drift med generatorgas (gengas). Gasen erhålles i en gasgenerator, och blandningen av gas och luft sker i blandningsventiler under kraftig virvelbildning.

Gasgeneratorn består av en ugn, fig. 7.4, i vars övre del bränslet, vanligen träkol med värmevärdet 7700 kcal/kg, påfylles. Ugnen är i förbränningszonen tillverkad av värmebeständigt stål eller klädd med högeldfast tegel för att motstå den höga temperaturen. I ugnens botten finns en skakrost och ett askrum. Vid kolets förbränning i förbränningszonen bildas koldioxid. När denna passerar reduktionszonen, sönderdelas den av de glödande kolen i koloxid och syre. Tillsammans med kolen bildar syret ytterligare koloxid. Vid starten tillföres förbränningsluften av en elmotordriven fläkt. Under gång räcker undertrycket i motorns sugledning till för att suga luften genom generatorn. Gasen uttages ovanför rosten, avkyles och renas. I gasrenaren, som består av en låda innehållande vertikala plåtramar, överspända med dukar, avskiljes medföljande fasta partiklar. I en blandare, som är ansluten till motorns insugningsledning, blandas gengasen med förbrännings-

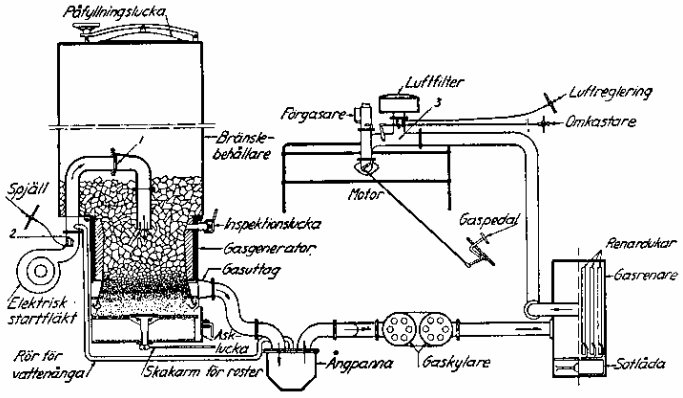

Figure 9.40.
Wood gasifier for cars (gengasaggregat) from the Second World War period

A famous example of the use of fuel bed gasifiers is seen in Fig. 9.40, a gasifier for cars (Otto engines) used in Sweden (gengas) during the Second World War.

FLUIDIZED BED COMBUSTION

GENERAL

A fixed or moving bed for combustion consists of fuel. A fluidised bed for fuel conversion consists mostly of inert material (ashes, sand or sorbents, e.g. for sulphur capture). It contains only a few percent of fuel.

COMBUSTION

A bed that rests on the air distributor grid, operating in a bubbling or exploding bubbling regime of fluidisation, is a **stationary** (or bubbling, or non-circulating) **fluidising bed** (SFB). At higher gas velocities the mode of fluidisation in the

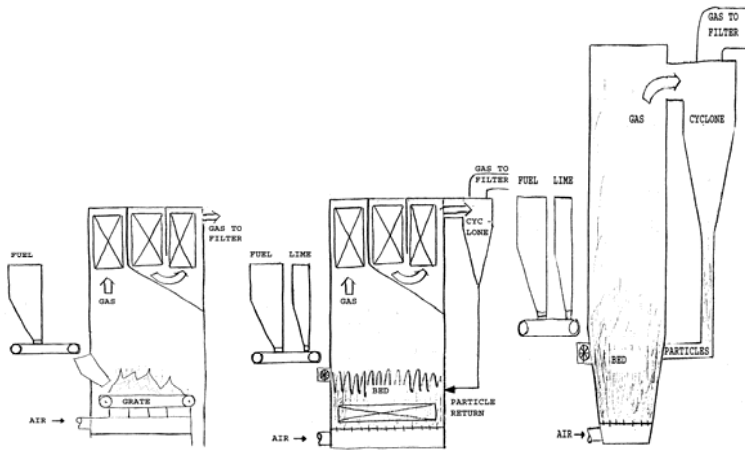

Figure 9.41.
A grate-fired boiler compared with an SFB and a CFB boiler.

bottom is similar (bubbling), but a considerable flow of particles is carried away with the gas and has to be recirculated to the combustor in order to maintain the bed; the bed is a **circulating fluidised bed** (CFB).

The fluidised bed serves as combustor in the furnace of the boiler. The boiler as such is built according to conventional boiler technologies. Figure 9.41 (left) illustrates how a boiler with a coal-fired grate looks like. The fuel is burned in a fixed, moving bed. The corresponding SFB looks similar, but here the bed is a "stirred reactor" supplied with fuel and limestone for sulphur capture from feed hoppers. A heat exchanger is submerged in the bed to maintain the desired bed temperature. In comparison, the figure shows a CFB, narrower and taller than the corresponding grate-fired furnace or the SFB furnace, and whose surrounding walls are covered with heat transfer surface.

The bed height (in a settled, non-fluidised state) of a combustion bed, operated at atmospheric pressure, is usually in the order of 1 m, corresponding to pressure drops in a range of 5 to 20 kPa. The large thermal capacity of the inert part of the bed evens out temperature variations, and the bed forms a thermally stable environment for combustion. This is one of the basic characteristics of a fluidised bed combustor: it maintains an even temperature throughout the combustion space. The bed transfers the heat produced by combustion to the heat transfer surfaces, which are in contact with the bed. The balance between the heat produced by combustion and the heat received by the heat transfer surfaces gives the bed temperature. The fuel burns in the bed consuming the oxygen in the air supplied through the bottom grid (the air distributor). The air serves two purposes: to burn the fuel at a given excess air and to fluidise the bed (together with the gases formed by combustion). This task can be expressed

$$\dot{m}_f g_v = A_c u \tag{9.22}$$

where $\dot{m}_f$ is the fuel feed rate and g_v is the corresponding gas yield at the temperature and pressure of the bed. A_c is the cross-section area of the bed and u fluidisation velocity.

The cross-sectional heat loading becomes

$$Q_c'' = \dot{m}_f LHV / A_c \quad \left[MW / m^2 \right] \tag{9.23}$$

Considering Eq 9.22 this can be expressed

$$Q_c'' = uLHV / g_v \tag{9.24}$$

Since LHV/g_v is fairly constant for most fuels at a given excess air, the surface heat loading is mostly proportional to the fluidisation velocity, and through g_v also directly proportional to pressure.

From Eq 9.24 it can be concluded that, at a given total power, the cross-section of the fluidised bed boiler can be made smaller for operation at higher gas velocities. On the other hand, erosion on heat transfer surfaces by the bed material increases with velocity and therefore the velocity becomes limited. These two factors have influenced the development of fluidised bed combustors (FBC). Heat transfer tube bundles immersed in the bed, which are necessary to cool an SFB, proves to be rapidly destroyed by erosion from the dense bed. Only at very low velocities (in the order of 1 m/s) can tubes protected by hard coatings withstand erosion. Tubes located on the walls of the combustor parallel to the main gas flow have a greater probability of survival, but this type of surface is limited in an SFB. A CFB, on the other hand, is extended over the entire combustion chamber and could transfer heat to a larger wall surface. In addition, fluidisation velocities of up to 6 m/s could be used before erosion becomes a severe problem. According to Eqn 9.24 this would give CFB (operated at 6 m/s) a six times smaller cross-section than an SFB boiler (operated at 1 m/s) for the same total fuel power. These were the reasons why CFB became the dominant fluidised bed type of combustor for large coal-fired plant. For small plant (below 100 MW) and low-calorific value fuels, such as biofuels and waste, the cooling by the wall would be sufficient, and in such cases SFBs are still used.

The surface loading is directly proportional to pressure, so at 16 bar an SFB could have a sufficiently small cross-section also at low fluidisation velocity, but tube bundles in the bed are

needed for cooling. Because of the sufficiently high surface loading even at low fluidisation velocity, the present large-scale pressurised fluidised bed combustors (PFBC) are SFBs with immersed tube bundles in the bed.

In order to find the shape of the combustion chamber, it remains to determine the height. There are two criteria: a sufficiently long residence time at a sufficiently high temperature is needed for burnup, and a certain height is needed for the heat transfer surface (CFB). We will focus attention on the last criterion. Consider a simplified heat balance over the fluidised bed combustor:

$$\dot{m}_f LHV = \overline{h_c}\ (T_b - T_w) A_w + \dot{m}_f g_v \overline{c_p}\ (T_b - T_o) \qquad (9.25)$$

Heat is supplied by combustion $Q_{fuel} = \dot{m}_f LHV$ and removed by heat transfer to the heat receiving surfaces of the wall (area $A_w = 4x\,l$, x = width, l = height, T_w surface temperature, and $\overline{h_c}$ average heat transfer coefficient). Heat is also removed by the gases, which leave the combustion chamber with temperature T_b. Eq 9.25 can be written

$$Q_{fuel}(1 - g_v \overline{c_p}(T_b - T_o)/LHV)) = \overline{h_c}(T_b - T_W) 4l\sqrt{Q_{fuel}/Q_c}$$

where $x = \sqrt{Q_{fuel}/Q_c}$. Assuming typical values: $T_b = 850$°C, T_w=300°C, Q_c=4 MW/m^2, $\overline{h_c} = 150 \cdot 10^{-6} MW/m^2 K$, the conclusion is that the height required increases with power in such a way that, with the exception of small CFB, the walls cannot be made sufficiently tall, if a height of 20 to 40 m should be considered sufficient to satisfy the burn-up criterion. Therefore additional surfaces (additional to those forming the walls of the combustion chamber) have to be located in contact with the bed. These surfaces can be placed in the upper part of the riser, where the particle concentration is lower than in the bottom, but where heat transfer is still sufficient, or in the return leg from the particle separator in the form of an external heat exchanger. Such arrangements are illustrated in Fig 9.42.

In Fig. 9.42a the inserted heat transfer surfaces are heavily exposed to particles, but they are located parallel to the main flow of particles and this reduces the risk of erosion by impact of particles. In Fig. 9.42b the additional heat exchanger surfaces are located in an external heat exchanger bed, which is fluidised at low fluidisation velocity to avoid erosion. In Fig. 9.42c extensive heat exchanger tube bundles are inserted into

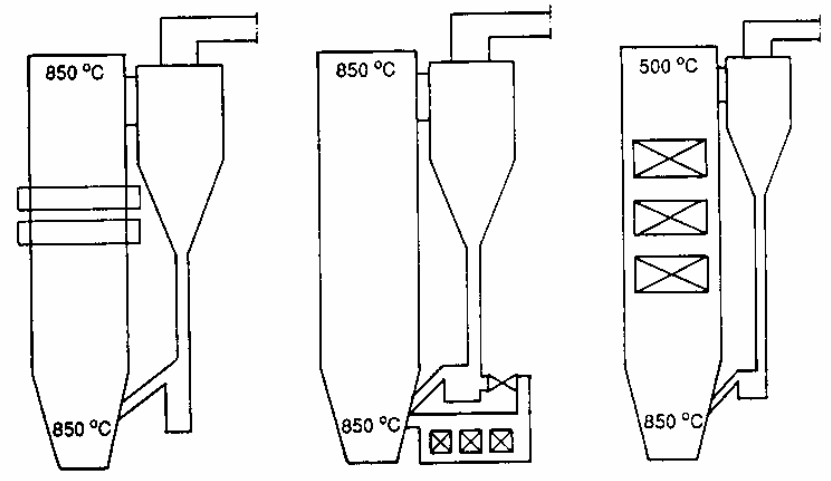

Figure 9.42.
Three types of CFB with internal a) and c) and external b) heat exchangers in addition to the surfaces of the walls of the combustion chamber.

the combustion chamber, but in this case the fluidisation velocity is lower (in between that of a CFB and an SFB) and the particle loading is less severe. Less heat is then carried with the particle suspension and the temperature falls as the gas passes the heat exchanger. Therefore, the cyclone becomes smaller in this case.

FLUIDISED BED BOILERS - SOME EXAMPLES

Figure 9.43 shows a SFB for waste combustion. The height of the combustion chamber is about 15 m. Air is introduced in an air plenum below the bed that rests on the air distributor (the bed is not shown). Fuel is fed on to the top of the bubbling bed. Since this is a boiler for combustion of waste with a low heating value, the lower part of the combustion chamber is refractory lined. Noses penetrate from the walls a few meters from the bottom. Secondary air for final combustion and mixing is injected from these noses. Downstream of the combustion chamber there is an empty gas pass to ensure final burn-up of gases. Figure 9.44 shows a small boiler for coal combustion. The height is about 25 m. The width is about 7 x 4 m. The bottom part seen is the air plenum. A bottom plate containing air-nozzles forms the bottom of the combustion chamber, whose lower part is refractory-lined. A cyclone and its return leg lead the bed material through a gas valve (siphon seal) back to the combustor.

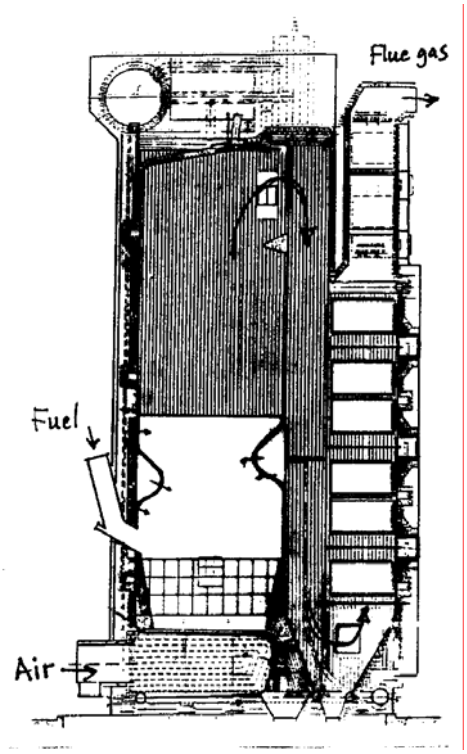

Figure 9.43.
SFB for waste combustion. 15 MW thermal power (Kvaerner Pulping)

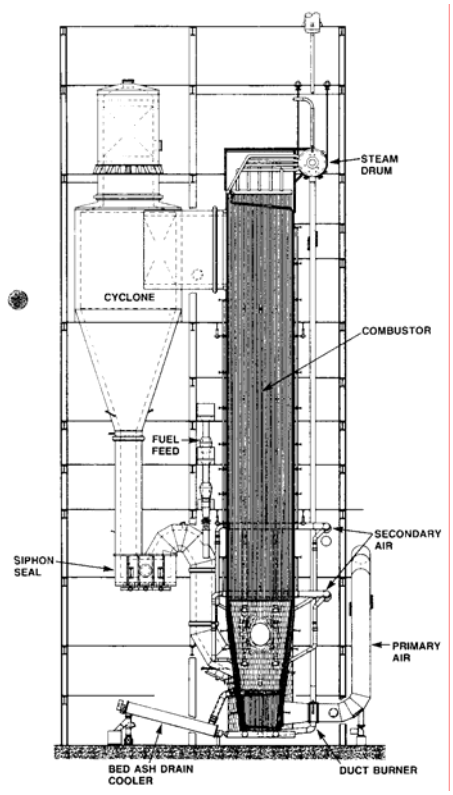

Figure 9.44.
33 MW_e (electrical) CFB boiler for coal combustion (EVT)

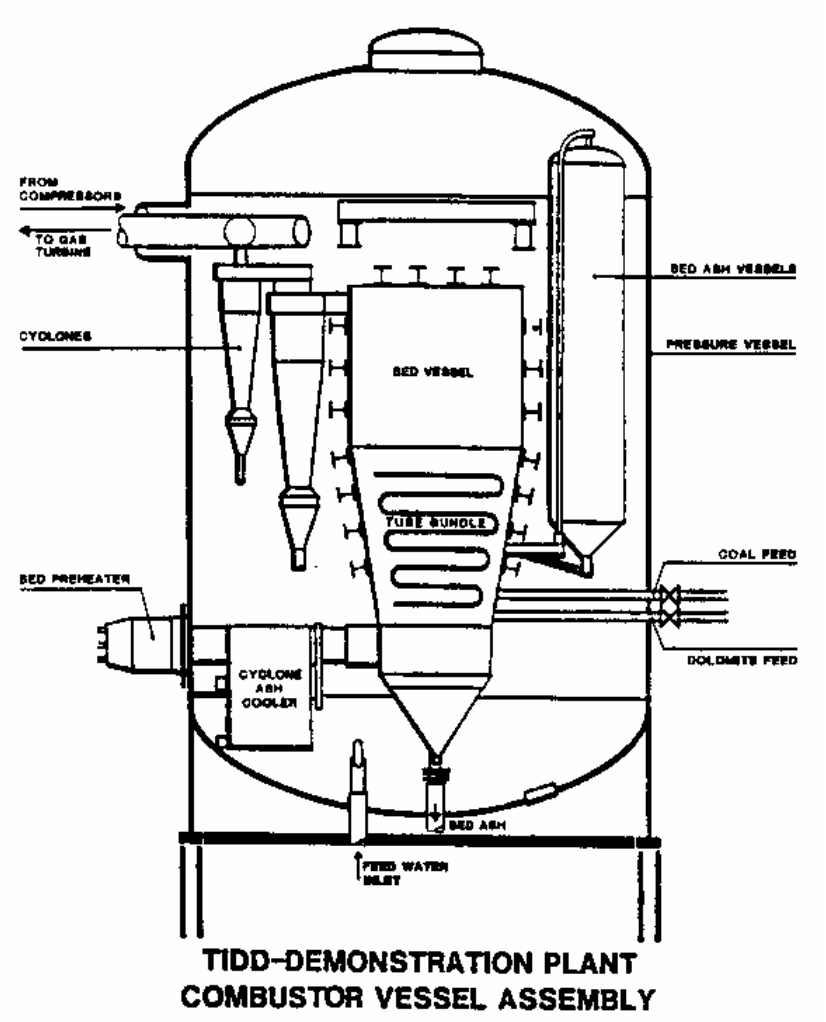

Figure 9.45.
A 70 MW_e PFBC plant (ABB, now Alstom)

Figure 9.45 shows a pressurised combustor, one of the three first plants built by ABB. The combustor with its tube bundle is seen inside the 16 bar pressure vessel. The gases leave the freeboard above the bubbling bed, cooled by immersed tubes, and pass two cyclones in series before passing to the gas turbine. The small amount of particles captured by the cyclones, whose primary task is to protect the gas turbine, is led out of the plant and not returned to the bed. The heat exchanger tubes produce steam for a steam turbine. This is the combustor of a combined cycle. The boiler load is controlled by removal or addition of bed material in order to change the heat transfer surface in the bed. This bed material uses the ”bed ash vessel” as storage.

QUESTIONS

9.1 Why is the surface loading Q_c associated with an average gas velocity and the volume loading Q_v with residence time?

9.2 How can environmental measures affect the volume loading Q_v of a boiler?

9.3 Why do larger boilers have a smaller wall surface to volume ratio than smaller boiler combustion chambers?

9.4 How can the fuel feed rate be determined from the boiler's output, air supply and flue gas oxygen concentration? (Is more information needed?).

9.5 A boiler, operated with bituminous coal has a flue gas temperature of 150^{o}C, an oxygen concentration in the flue gas of 5% on dry gases, all ashes leave as fly ash, in which a carbon concentration of 20% was obtained by analysis. The temperature of the boiler house was 40^{o}C. Establish the energy balance of the boiler and estimate the thermal efficiency of the boiler?

9.6 Compare the heat balance of a boiler employing either the higher or the lower heating value a) for a coal-fired boiler, b) for a wood-fired boiler.

REFERENCES

F. Brandt, Brenstoffe und Verbrennungsrechnung, Vulkan Verlag, Essen, 1981.
DIN 1942:

A.K. Gupta, D.G. Lilley and N. Syred, Swirl Flows, Abacus Press, Massachusetts, 1984.

J.B. Heywood, Internal combustion engine fundamentals, McGraw-Hill Book Company, New York, 1988.

R.P. van der Lans, P. Glarborg and K. Dam-Johansen, Influence of process parameters on coal combustion performance, Progress in Energy and Combustion Science (in press), 1998.

A.H. Lefebvre, Gas turbine combustion, Taylor & Francis, 1983.

H.-D. Schilling, B. Bonn and U. Krauss, Coal gasification, Graham & Trotman, London, 1981.

B. Solbräcke, Bränslen och förbränningslära, Inst. för Energiteknik, CTH, 1980.

K. Strauss, Kraftwerkstechnik, Springer-Verlag, Berlin, 1992.

J. Zelkowski, Kohleverbrennung, VGB-Kraftwerstechnik Gmbh, Essen, 1986.

Integrated Pollution Prevention and Control (IPPC), Draft document on Best Available Techniques for large combustion plants, European Commission, March 2001, http://eippcb.jrc.es

R.Zevenhoven and P. Kilpinen, Control of pollutants in flue gases and fuel gases, Helsinki University of Technology, Department of Mechanical Engineering. TKK-ENY-4, Espoo 2001. (Available on http://www.hut.fi/~rzevenho/gasbook)

DIN (Deutsche Industrie Normen) Abnahmeversuche an Dampferzeugern, DIN 1942. (Translation to English is available)

Literature in English

Two comprehensive books on boilers, their design and properties including various types of combustion devices:

Steam - its generation and use, Babcock & Wilcox, Eds. S.C. Stultz and J.B. Kitto, 40th Edition, 1992.

Combustion, Fossil Power, A reference book on fuel burning and steam generation, ABB Combustion Engineering, Ed. J.G. Singer, 1991.

A handbook containing data on fuel and other properties of matter:

Technical Data on Fuel, Eds. J.W. Rose and J.R. Cooper, The British National Committee, World Energy Conference, London, Seventh Edition 1977 (perhaps later editions are available).

A textbook focusing on coal, but useful for solid fuel combustion in general:

Coal Combustion, J. Tomeczek, Kruger Publishing Co, Malabar, Florida 1994.

Basic information on fluidization (not only combustors but also chemical reactors):

Fluidization Engineering, D. Kunii and O. Levenspiel, Butterworth-Heinemann, Boston 1991.

A comprehensive review on Fixed-bed combustion with some emphasis on modelling of fixed-bed gasifiers:

Combustion and gasification of coals in fixed-beds, M.L. Hobbs, P.T. Radulovic and L.D. Smoot, Progress in Energy and Combustion Science 19, 505-586, 1993.

A comparison of the structural properties of a variety of solid fuels including biofuels and wastes. Some information on combustion devices:

The combustion of solid fuels, D.A. Tillman, Academic Press, San Diego, 1991.

HEAT BALANCE

FOR A 12 MW_{TH} CFB BOILER

Laboratory exercise for Thermo Chemical conversion of biomass and wastes

CONTENTS

For questions and information please contact:

Robert Johansson
Energy Conversion
Chalmers University of Technology
412 96 Gothemburg

Phone: 031-772 5249

e-mail: k97joro@chalmers.se

November, 2007

INTRODUCTION

The purpose of this laboratory exercise is to give the students an insight into commercial boiler systems including magnitudes of flows, temperatures, and dimensions. The studied system is a circulating fluidized bed (CFB) boiler with a maximum capacity of 12 MW_{th} located at Chalmers University of Technology. The plant, schematically shown below, is used for research and also provides district heating to the Chalmers campus.

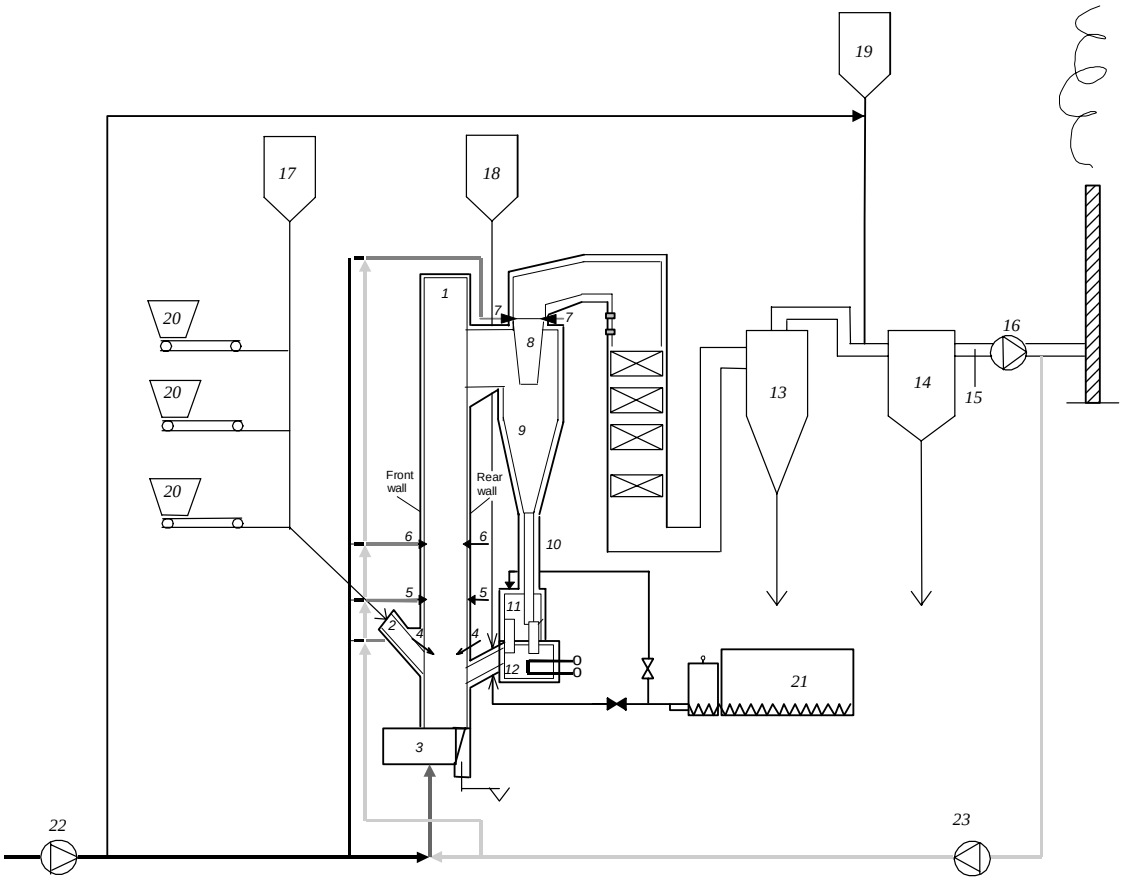

The 12-MW_{th} CFB boiler at Chalmers University of Technology

(1) combustion chamber; (2) fuel feed chute; (3) air plenum; (4) secondary air inlet at 2.1m; (5) secondary air inlet at 3.7m; (6) secondary air inlet at 5.4m; (7) secondary air inlet into cyclone exit duct; (8) cyclone exit duct (9) hot primary cyclone; (10) particle return leg; (11) particle seal; (12) particle cooler; (13) cold secondary cyclone; (14) bag house filter; (15) gas-extraction probe for emission monitoring; (16) flue gas fan; (17) sand bin; (18) lime bin; (19) hydrated lime bin;(20) fuel bunkers; (21) sludge pump; (22) air fan; (23) flue gas recirculation fan

ASSIGNMENT

The task consists of three parts:

1. **Heat Balance**

   Set up a heat balance for the boiler and calculate the boiler efficiency using

   a. the direct method (known mass flow of fuel).
   b. the indirect method (unknown mass flow of fuel).

2. **Heat Distribution in the Boiler**

   Determine the heat distribution in the boiler by calculating the amount of heat transferred to the circulating water in each of the heat-collecting parts of the boiler.

3. **Sankey Diagram**

   Draw a Sankey diagram of the system.

Information on how to solve the assignment can be found in the course literature "Boilers and Furnaces" by Bo Leckner and later in this document. The results should be summarized in a short report including:

- System limits
- Procedure
- Completed lab calculation form
- Results
- Appendix: non-obvious calculations, original readings, other data used

The reports should be handed in before the written examination of the course, preferably by e-mail. Please include the lab calculation form complete with data and results.

INSTRUCTIONS

Before arriving at Chalmers for the experiment, the students should prepare the following items:

- Read Chapter 9 "Heat Balance" in "Boilers and Furnaces" by Bo Leckner.
- Define the system limit for the heat balance. Identify which flows of matter and heat that cross the system limit, and which parameters are needed to calculate the heat of the different flows.
- Couple the needed measurable parameters with the existing measuring devices in the flow schemes given later in this document.
- Identify the parameters and the corresponding measuring devices needed to determine the heat collected in the different boiler parts.

The laboratory work will be carried out at "Chalmers Kraftcentral". The lab group, consisting of about five people, will meet the assistant at the main entrance of the building (Chalmers Tvärgata 6) at the time specified in the laboratory schedule.

An introductory presentation of the boiler (of about a half hour) will be given by Per Löveryd. The presentation will be followed by a one-hour tour of the research plant (including boiler, ducting, measuring devices, and computers used to monitor operational data). After this, the students will collect the data needed to complete a heat balance for the system. These will include:

- Flow rates and temperatures (averaged values)
- Fuel and ash analyses
- Electrical power consumption

To be able to perform an accurate heat balance, the boiler load should be kept constant during a period of time (usually about an hour) before the data are gathered. The boiler conditions at the time of the experiment will have to be accepted, but fluctuations in these conditions should be noted in order to be able to trace sources of error.

HEAT BALANCE

The heat balance for a boiler system determines its performance. A simple heat balance for a defined system is

$$Q_{in} = Q_{out} + Q_{loss}$$

It is simple in theory, but for a large boiler, the system in itself is complex with many different flows and temperatures that have to be measured with satisfactory accuracy. It is also not always straightforward where to draw the system limits in order to give a good representation of the boiler.

For the defined system, the left and right terms of the equation above should not deviate more than ~0.3 MW in the present assignment, but in a professional heat balance the deviation must be smaller.

POWER INPUT

The power input to the boiler consists of the heat added with the fuel (Q_{fuel}) and the combustion air (Q_{air}). Sometimes electrical power (Q_{el}) is also taken into account.

$$Q_{in} = Q_{fuel} + Q_{air} (+ Q_{el})$$

To estimate the power input from the fuel, the fuel heating value and the fuel feed rate are needed. Fuel and ash analysis data corresponding to the combustion conditions will be provided at the time of the experiment.

The inlet combustion air also may give a positive or negative contribution to the heat input, depending on the air temperature (as measured after the total air fan, LQ 201).

Sand, and occasionally limestone are also fed to the boiler. However, their contribution to the input heat is usually negligible. Recirculated ash and recirculated flue gas may be injected, but with a clever choice of the system boundary, these flows do not leave the system.

Depending on how the system limit is chosen, the power consumption of the electric motors for fans, pumps and fuel transport might be taken into account. The flue gas recirculation fan and the water pumps are usually included in the system, but the total air fan (LQ 201) and the flue gas fan (RQ 201) are usually not (the denominations refer to the “Total Air and Exhaust Gas Scheme” on p. 15). There are no ampere-meters installed for the different motors, but there is a meter for the whole installation. The power consumption inside the system limit can be estimated by using electric current default values for the different motors; these can be found on p. 11.

POWER OUTPUT

The useful power output from the boiler is delivered to the district heating system in form of heated water. It can be calculated from the water flow of the district heating system and the temperature difference over the corresponding heat exchanger. Note that the specific heat of the water is dependent on the water temperature.

POWER LOSSES

Power losses from the boiler correspond to heat exiting the system with the fly ash, with the bottom ash, with the flue gas (including unburned gas), and by radiation.

Energy in the form of unburned fuel and heat exits with both the fly ash and the bottom ash. Ash analysis data as well as ash collection rates will be given at the time of the experiment.

There is no measuring device for the outlet flue gas flow. Instead, the flue gas flow can be estimated using the fuel heating value, the fuel injection rate and the O_2 content in the flue gas. The specific heat of the flue gas can be estimated from the gas composition (N_2, CO_2, H_2O and O_2) and the specific heat of the gas components. The outlet flue gas also contains an amount of unburned gas (mostly CO), which results in an additional power loss.

The radiation losses from the boiler chamber can be estimated using the DIN 1942 diagram on p.12.

HEAT DISTRIBUTION IN THE BOILER

The following boiler parts are used for heat collection:

- economiser
- convection surfaces
- particle cooler
- ash classifier
- cyclone
- combustion chamber

Values of the temperature and flow of the circulating water at appropriate measuring points are used to calculate the heat collected in each boiler part according to $P = \dot{m}_w \cdot c_p \cdot \Delta T$. Please keep in mind that c_p varies with temperature. The contributions from the different parts may then be compared to each other to give the heat distribution of the boiler.

CONSTANTS

Denomination	SI unit	Explanation	Numeric Value
ρ_{air}	kg/m^3_n	Density of air at 1 bar and 0 °C	1.276
$c_{p,air}$	kJ/(kg·°C)	Specific heat of air	1.011
T_0	°C	Reference temperature	25
$c_{p,w75}$	kJ/(kg·°C)	Specific heat of water at 75 °C (liq)	4.189
$c_{p,w130}$	kJ/(kg·°C)	Specific heat of water at 130 °C (liq)	4.243
$c_{p,w170}$	kJ/(kg·°C)	Specific heat of water at 170 °C (liq)	4.339
$c_{p,fa}$	kJ/(kg·°C)	Specific heat of fly ash	0.7
$c_{p,ba}$	kJ/(kg·°C)	Specific heat of bottom ash	2.0
$H_{u,u}$	MJ/kg	Lower heating value of unburned in fly ash and bottom ash	35

Please note that it may be necessary to find additional constants for air, water, and flue gas in handbooks.

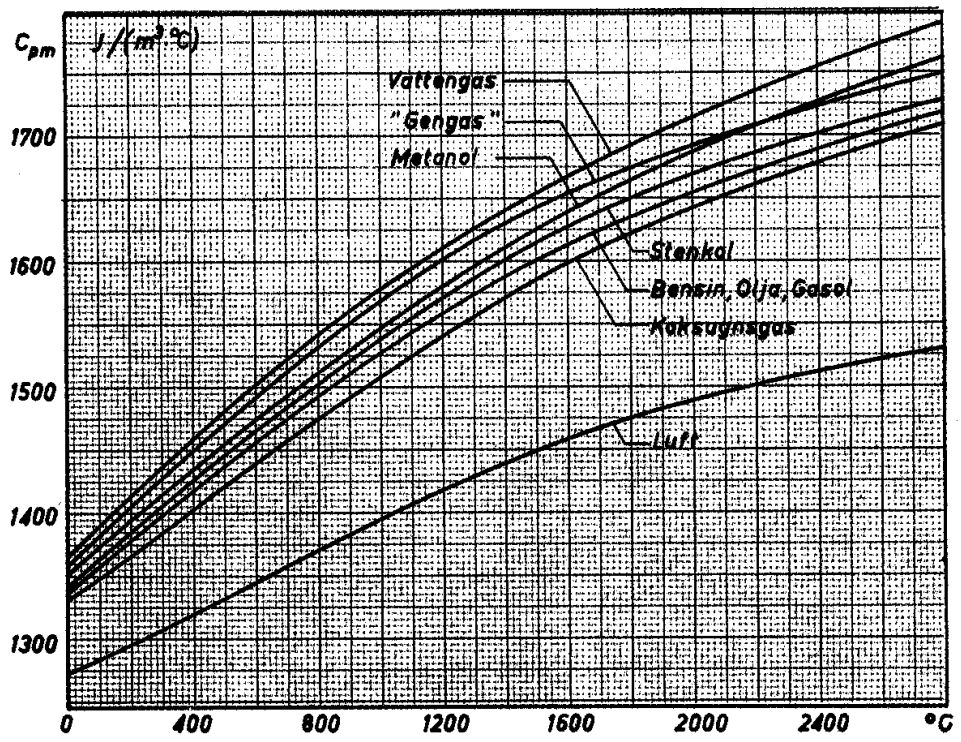

Average specific heats as a function of temperature for air and some flue gases for comparison. From *Data och diagram,* Mörstedt and Hellsten, Liber Utbildning, 1999.

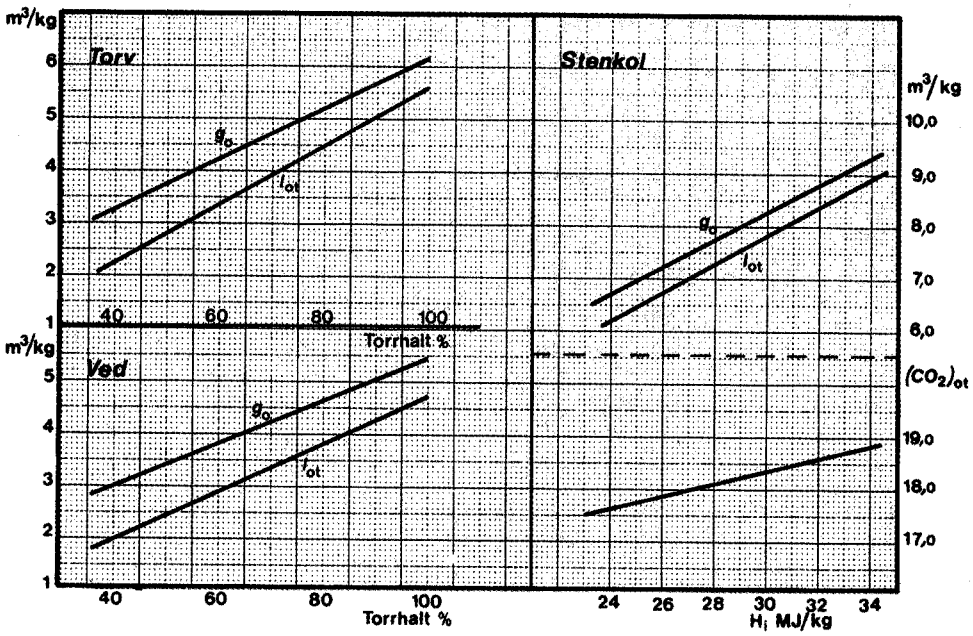

Dry air demand, flue gas yield, and CO_2 content as a function of lower heating value for some solid fuels. From *Data och diagram,* Mörstedt and Hellsten, Liber Utbildning, 1999.

LOGGED PARAMETERS

Description	Drawing code	Denomination	Reading	Unit	Measuring point
Fuel flow	FI40.1	$\dot{m}_{f1,in}$	_____	kg/s	Local
	FI40.2	$\dot{m}_{f1,in}$	_____		
	FI40.3	$\dot{m}_{f1,in}$	_____		
Lower heating value of fuel		H_{u1}	_____	kJ/kg	To be given
		H_{u2}	_____		
		H_{u3}	_____		
Air flow	LI201	$\dot{V}_{air}$	_____	m^3_n/s	Operation computer 1:1
Air temperature (after fan)	LI212	$T_{air,in}$	_____	°C	Research computer
District heating water flow	HI202	$\dot{m}_w$	_____	kg/s	Operation computer 1:3
District heating water, temperature in	HI201	$T_{w,in}$	_____	°C	Operation computer 1:3
District heating water, temperature out	HI205	$T_{w,out}$	_____	°C	Operation computer 1:3
Fly ash flow	WIA21	$\dot{m}_{fa}$	_____	kg/s	To be given
Fly ash temperature	RI211	T_{fa}	_____	°C	Operation computer 1:6
Fraction of unburned in fly ash		u_f	_____	%	To be given
Specific heat of fly ash		$c_{p,fa}$	_____	kJ/kg,°C	See Constants
Bottom ash flow		$\dot{m}_{ba}$	_____	kg/s	To be given
Bottom ash temperature	BI214	T_{ba}	_____	°C	Operation computer 1:7
Fraction of unburned in bottom ash		u_b	_____	%	To be given
Specific heat of bottom ash		$c_{p,ba}$	_____	kJ/kg,°C	See Constants
Lower heating value of unburned in fly ash and bottom ash		$H_{u,u}$	_____	kJ/kg	See Constants
Flue gas temperature	RI210	T_{stack}	_____	°C	Operation computer 1:6
Flue gas O_2 content	RI202	X_{O_2}	_____	% (wet gas)	Operation computer 2:3
Flue gas CO content	RI223	v_{CO}	_____	ppm	Operation computer

Description	Drawing code	Denomination	Reading	Unit	Measuring point
Internal electrical power consumption		P_{el}	_____	kW	Local
Economiser, water flow	PI211	$\dot{m}_{ec}$	_____	kg/s	Research computer
Economiser, temperature in	PI209	$T_{ec,in}$	_____	°C	Research computer
Economiser, temperature out	PI212	$T_{ec,out}$	_____	°C	Research computer
Convection part, water flow	PI218 PI219	$\dot{m}_{cp}$	_____ _____	kg/s	Research computer
Convection part, water temperature in	PI208	$T_{cp,in}$	_____	°C	Research computer
Convection part, water temperature out	PI214 PI215	$T_{cp,out}$	_____ _____	°C	Research computer
Particle cooler, water flow	PI218	$\dot{m}_{pc}$	_____	kg/s	Research computer
Particle cooler, water temperature in	PI214	$T_{pc,in}$	_____	°C	Research computer
Particle cooler, water temperature out	PI215	$T_{pc,out}$	_____	°C	Research computer
Ash classifier, water flow	PI219	$\dot{m}_{ac}$	_____	kg/s	Research computer
Ash classifier, water temperature in	PI216	$T_{ac,in}$	_____	°C	Research computer
Ash classifier, water temperature out	PI217(A)	$T_{ac,out}$	_____	°C	Research computer
Cyclone, water temperature out	PI220	$T_{cy,out}$	_____	°C	Research computer
Combustion chamber, water temp. out	PI213	$T_{cc,out}$	_____	°C	Research computer

INTERNAL ELECTRICAL POWER CONSUMPTION

The power consumption of each device can be estimated using the relation

$$P = U \cdot I \cdot \cos\varphi$$

assuming a voltage of 400 V and $\cos\varphi = 0.9$.

Motor code	**Description**	**Default Current Consumption (A)**
LQ 201	Total air fan	75
LQ 203	Purge air fan	11
RQ 201	Flue gas fan	50
RQ 202	Flue gas recirculation fan	25
RQ 203	Flue gas recirculation fan	25
PP 201	Boiler water circulation pump	6
PP 202	Economiser water circulation fan	4
Tryckl	Air compressor	5
FC 203	Fuel feeder (screw)	6
FC 204	Fuel feeder (scraper)	6
FC 205	Cell feeder	2
FC 206	Chute cleaner	2
BC 203	Stoker (for bottom ash)	1
HP1	Circulation pump	50

LOSSES DUE TO RADIATION AND CONDUCTION

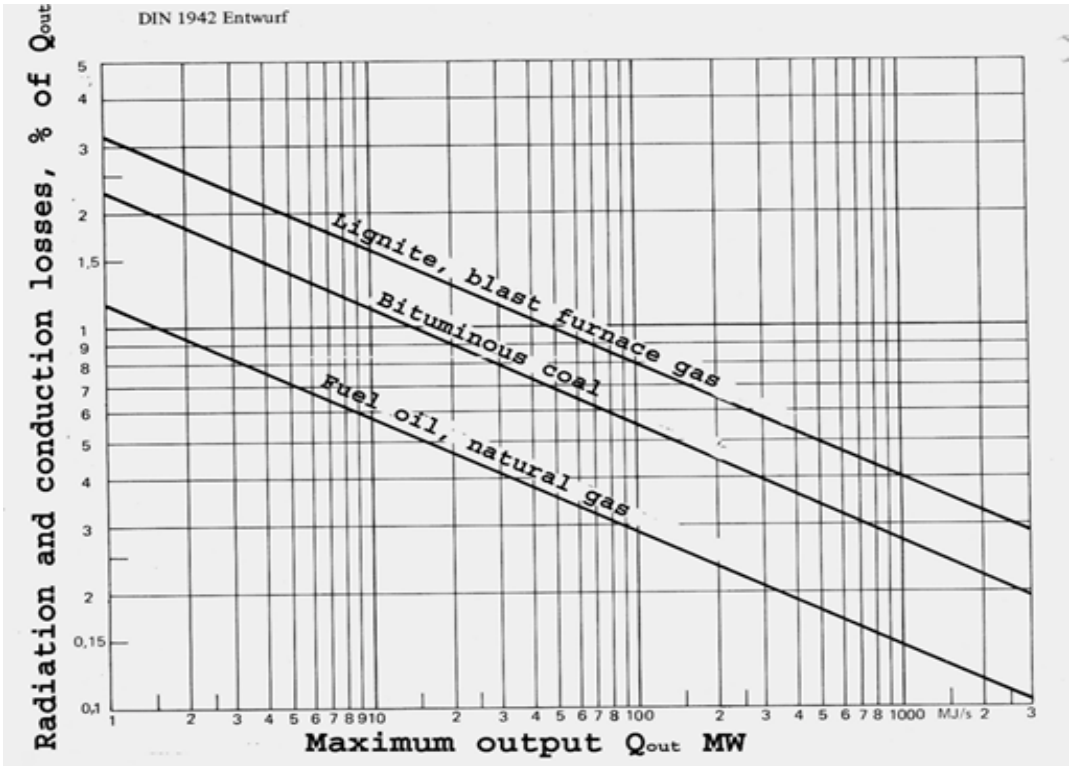

Losses due to radiation and conduction as a function of the maximum heat output. The diagram is taken from the standard norm DIN 1942.

SIMPLIFIED WATER CIRCULATION SCHEME

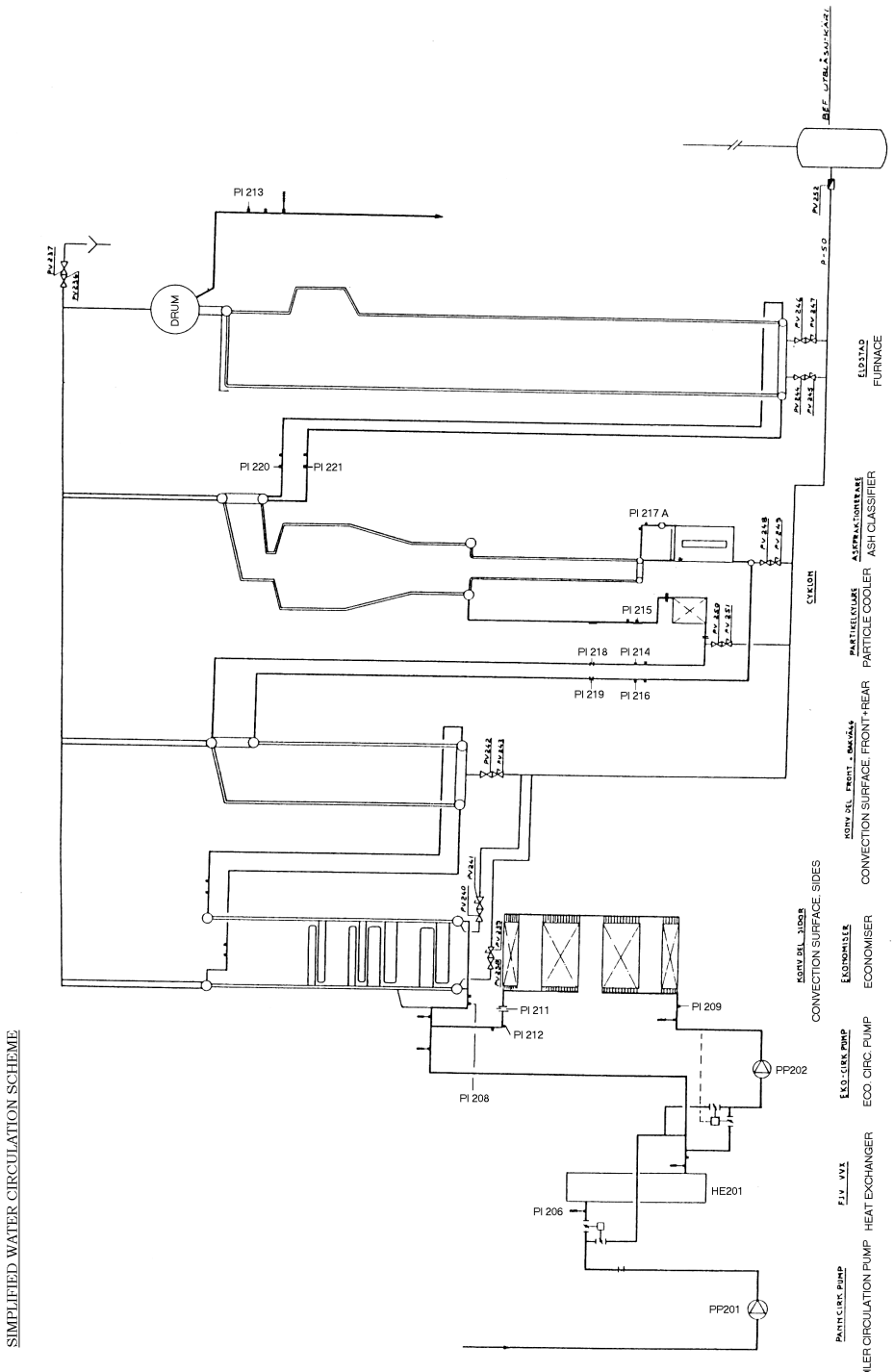

SIMPLIFIED WATER CIRCULATION SCHEME

Path of the circulating boiler water (from left to right in the scheme)

Water flows down from the drum to the circulation pump, which is denoted PP201. After the pump, part of the water flows through a heat exchanger (HE201) delivering heat to the district heating system. The remaining water bypasses the heat exchanger.

The water flow to the district heating system is omitted in the given scheme. To calculate the useful heat output from the boiler, the district water flow and the temperatures at inlet and outlet of the heat exchanger can be used. The meters for these values are HI202 (flow), HI201 (inlet temperature) and HI205 (outlet temperature).

After the heat exchanger, the two boiler water flows are mixed and then again divided into two separate flows. One of these goes into the economiser aided by an additional circulation pump (PP202). The economiser inlet water temperature is given by PI209. PI 211 and PI212 give the water flow and the temperature at the economiser outlet.

After the economiser, the water is mixed with water directly from the heat exchanger. PI 208 gives the temperature of the mixed water before it flows into the convection surfaces. At the inlet of the convection surfaces, the water flow is again parted in two. PI219 and PI 216 give the flow and temperature for one part. PI218 and PI 214 give the flow and temperature for the other part.

After the convection heat transfer surfaces, the water is still divided in two separate flows. One part flows into the particle cooler and the other part flows into the ash classifier. PI215 and PI217(A) give the water temperatures at the outlets of these two boiler parts.

After the particle cooler and the ash classifier, the water flows to the cyclone, where the water flows are mixed again. The water flow is again parted after the cyclone, and PI220 and PI221 give the water temperatures corresponding to each part. If the mixing is perfect, these meters should give same value. The water flows are not measured here.

After the cyclone, the water flows to the combustion chamber and then up to the drum. PI 213 gives the water temperature from the drum as it flows down at the right hand side of the scheme, to continue at the left side of the scheme, where this explanation started.

TOTAL AIR AND EXHAUST GAS SCHEME

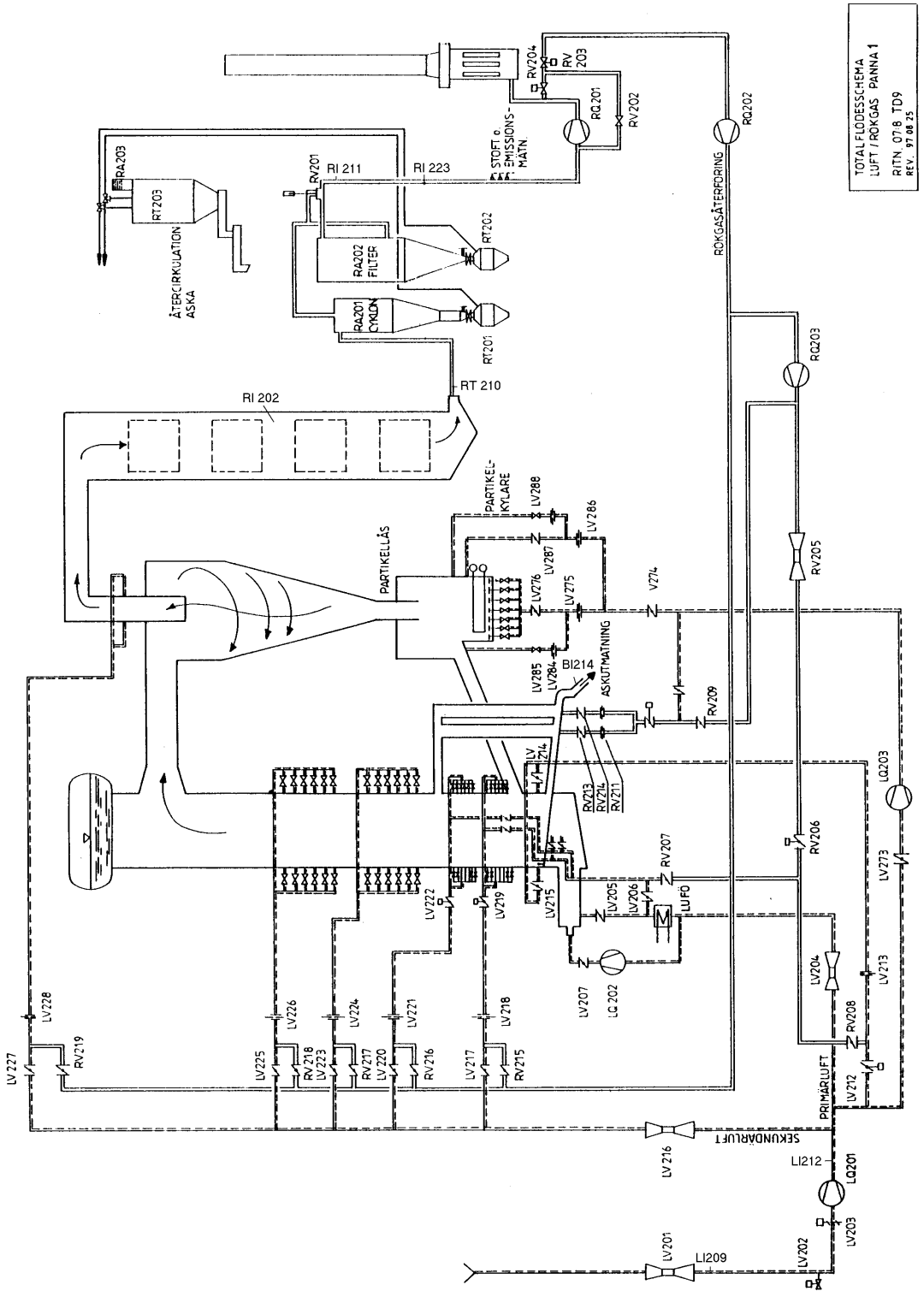

FUEL, SAND, LIMESTONE AND ASH HANDLING SCHEME

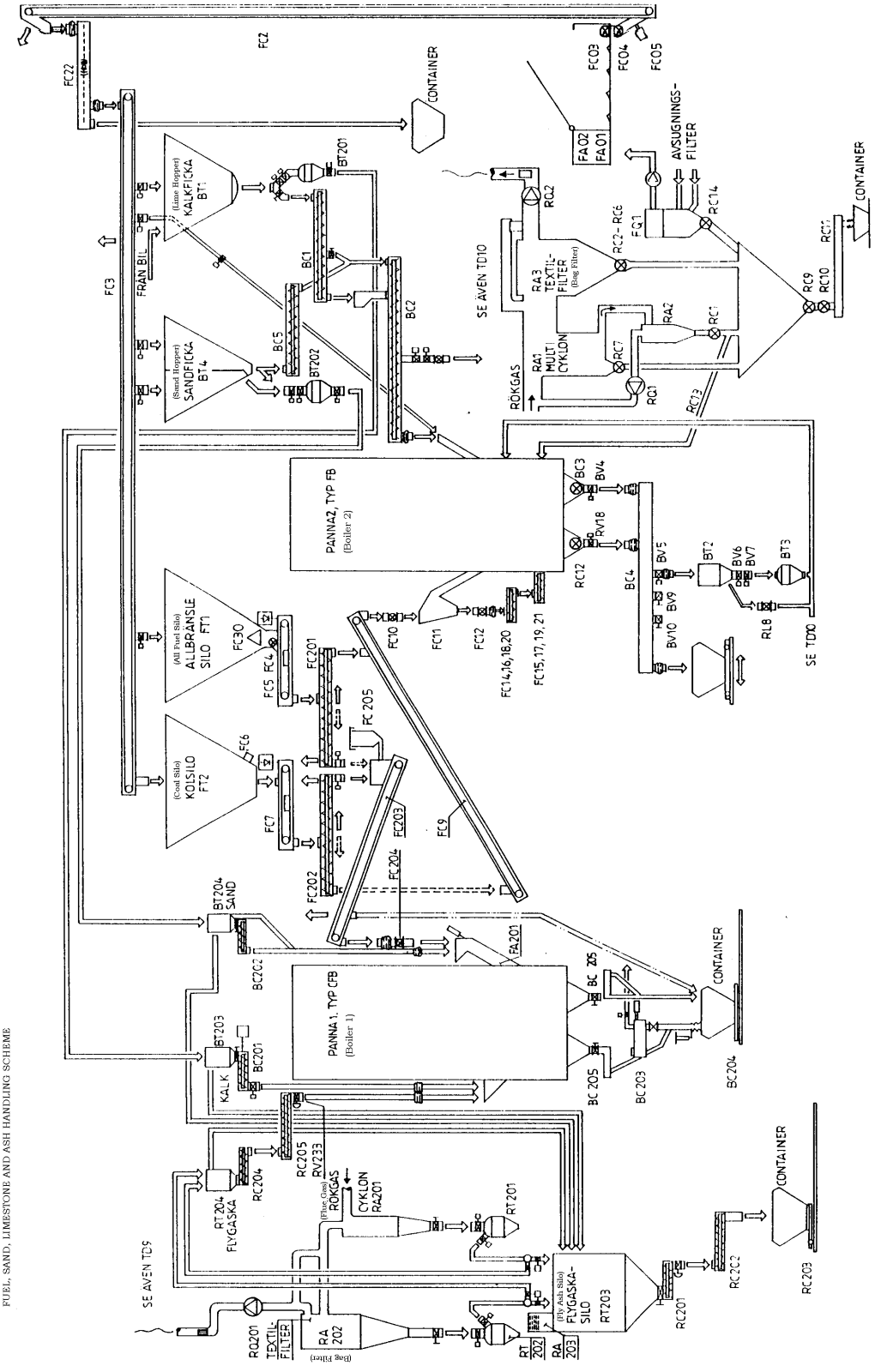

FUEL, SAND, LIMESTONE AND ASH HANDLING SCHEME

ASSIGNMENT 2

COMBUSTION OF A SOLID FUEL PARTICLE

Henrik Thunman 2002

Estimate the burnout time and the surface temperature of small spherical coal particles, with a density of 1300 kg/m^3, initial diameter of 0.1 mm and temperature of 20ºC, in a powder suspension. The coal is a bituminous coal with 10 $\%_{mass}$ moisture (as received) and 30 $\%_{mass}$ volatiles (on dry basis). The average ambient temperature is 1000ºC and the average oxygen concentration is 7% (mass fraction).

Motivate the choice of char combustion model by using the Thiele modulus.

Calculate the surface temperature for steady state combustion using the initial particle size

GUIDELINES FOR THE PROBLEM SOLUTION

Assume following

- The particles follow the gas
- The particles keep their size during drying and devolatilisation.
- The effective heat transfer coefficient and specific heat can be assumed constant during devolatilisation.
- The time for devolatilisation is given at 95% conversion.
- The combustible part of the chars consist of pure carbon
- The heating value of the chars are the same as for graphite
- Constant specific heat of the coal (1300 J / kgK) during the whole process
- The porosity of the char particles are 0.6,
- The inner active surface area of the chars are 200 m^2/g
- The particles are isothermal, and during char combustion they maintain a constant temperature.
- Effective emissivity between the particle and the surrounding: 0.9
- Assume that the molecular diffusion is the same as for the gas pair O_2 - N_2
- The primary product of the char combustion is CO

ASSIGNMENT 3

COMPARISON BETWEEN MODELS OF THE CONVERSION OF THERMALLY LARGE BIOMASS PARTICLES AND EXPERIMENTS

EXPERIMENTS

In order to illustrate the effect of different parameters on wood pyrolysis and char combustion a series of experiments has be performed. The purposes of these experiments are:

- to investigate the influence of ambient temperature and wood moisture on the pyrolysis of a single wood particle. Mass vs. time, char yield and shrinkage are studied.
- to investigate the influence of temperature, oxygen concentration and char quality on the combustion of a single char particle. Mass vs. time is studied.

The experiments will be performed in a single particle reactor shown in a photo and schematically in Fig. 1.

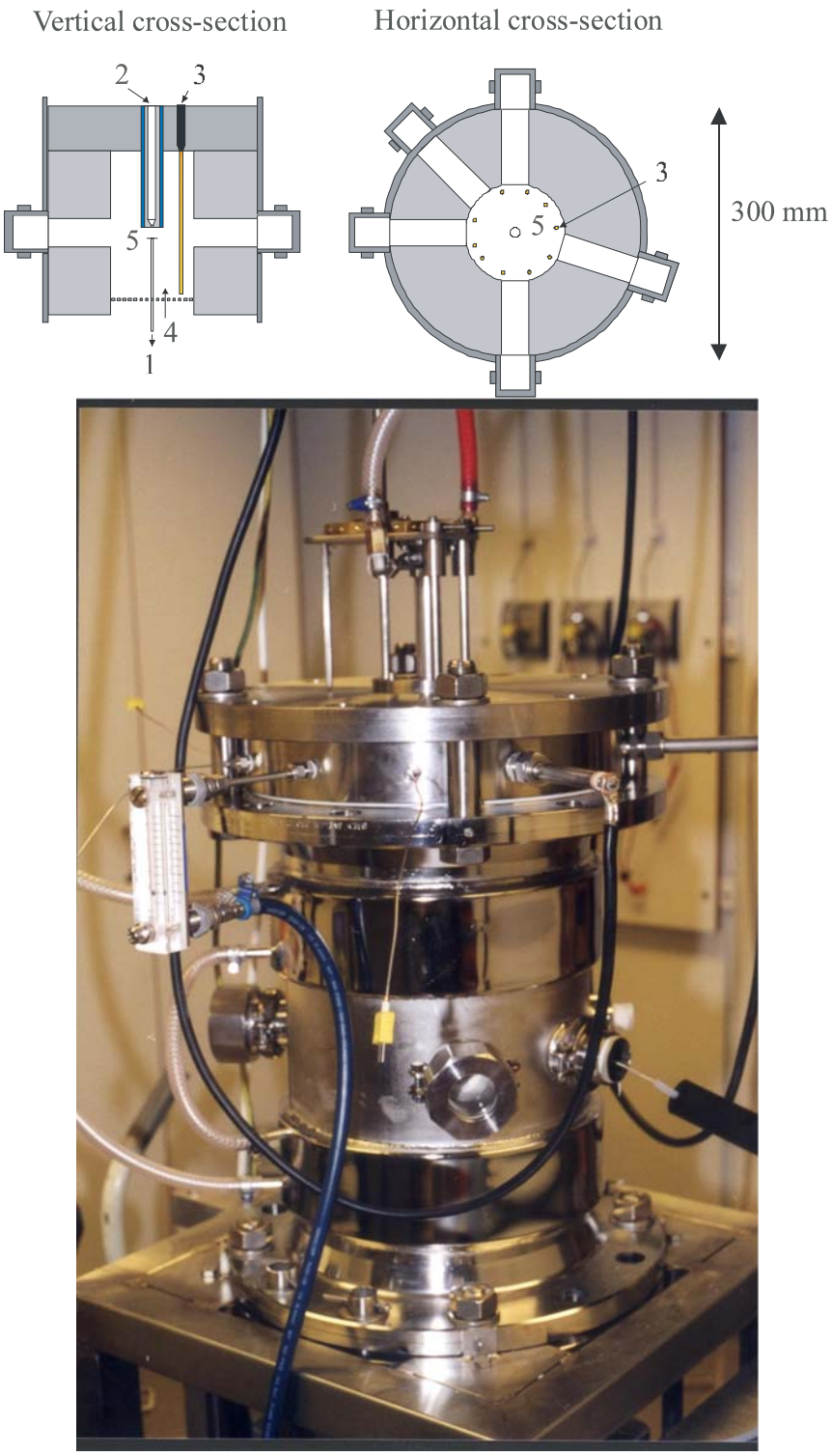

Figure 1.
Cross section of the pyrolysis furnace (1. balance, 2. air cooled insertion tube, 3. heater, 4.gas inlet, 5. sample plate.

The reactor consists of cylindrical furnace equipped with u-shaped heater elements. In the middle of the furnace is a sample plate connected to a balance. Above the sample plate is an air cooled insertion tube through which the sample falls onto the plate. Level with the sample

plate are windows for visual observation of the sample. Preheated gas enters the furnace from below through a perforated plate. During an experiment temperature and mass are recorded with a frequency of 5 Hz.

PROCEDURE OF THE EXPERIMENTS

A detailed description of the performance of one experiment is given in Table 1 and a list of experiments is given in Table 2.

Table 1.: Experimental procedure[a]

Step	Action
1	Measure length and diamter of sample.[b]
2	Dry the sample until constant mass.
3	Immerse sample in water until it has about 100 % moisture on dry basis[c]
4	Start data logging and tare the balance.
5	Insert the sample in the furnace through the fall tube.
6	Stop data logging and bring sample out of furnace when the mass is constant.
7	Measure the length and diameter of the sample, and store it. [b]

[a] The furnace is considered to be prepared as to oxygen level and temperature, and a computer file has been created for the experiment.

[b] This step is omitted for char combustion experiments.

[c] This step is omitted if sample should be dry.

PYROLYSIS OF DRY PARTICLES

Cylindrical birch wood particles (~5×5 mm) are dried in an oven at 105 °C until the mass is constant. A particle is introduced into an inert atmosphere in the preheated furnace at constant temperature. Particle mass is recorded until constant. Thereafter it is brought out and its length and diameter are measured. The above procedure is performed at furnace temperatures of 400, 500, 600, 700 and 800 °C.

Table 2.: List of experiments

Experiment #	Temperature (°C)	O_2 (%)	H_2O (% DM)	Sample
1	400	0	0	birch wood
2	400	0	100	birch wood
3	500	0	0	birch wood
4	500	0	100	birch wood
5	600	0	0	birch wood
6	600	0	100	birch wood
7	700	0	0	birch wood
8	700	0	100	birch wood
9	800	0	0	birch wood
10	800	0	100	birch wood
11	500	6	0	800 °C char
12	800	6	0	400 °C char
13	800	6	0	800 °C char
14	800	21	0	400 °C char
15	800	21	0	800 °C char

PYROLYSIS OF WET PARTICLES

This experiment is carried out in the same manner as the one described above, apart from the fact that after the drying, the particles are immersed in water until a moisture content of around 100 % on dry basis is achieved.

CHAR COMBUSTION

Char particles from the experiments from the pyrolysis experiments are combusted by sudden insertion into the preheated furnace with a certain oxygen concentration. The mass is recorded until constant. The parameters varied are furnace temperature, oxygen level and char quality.

TASK

The purpose of this task is to analyse and present raw data from experiments of the conversion of a biomass particle in various surrounding conditions. The analysis is intended to visualize the validity of the models derived in Chapters 5 to 7 and also visualize other aspects discussed during the course.

In the report from this assignment minimum requirement is that the

- compare mass loss, char yield and shrinkage experiment for different conditions
- compare char yield vs furnace temperature
- compare volume and longitudinal shrinkage vs furnace temperature
- compare combustion mass loss at different oxygen concentrations and temperatures.

EXPERIMENTAL DATA

The experimental data are provided in two Excel files distributed together with the course material

Conversion experiments 1

Experiment #	File name	Sample	dry mass (g)	wet mass (g)	h_i (mm)	h_f (mm)	d_i (mm)	d_f (mm)	Temp. (°C)	O2 (%)	Comment
1	1a	birch	-	-	5.6	5.0	5.5	3.8/3.3	400	0	
2	2b	birch	0.0733	0.1255	n. a.	n. a.	n. a.	n. a.	400	0	
3	3a	birch	-	-	5.6	4.8	5.3	3.2	500	0	
4	4b	birch	0.0793	0.1275	n. a.	n. a.	n. a.	n. a.	500	0	
5	5a	birch	-	-	5.5	4.5	5.3	3.5	600	0	
6	6a	birch	0.072	0.135	n. a.	n. a.	n. a.	n. a.	600	0	
7	7a	birch	-	-	5.3	4.4	5.3	3.5	700	0	
8	8a	birch	0.0735	0.127	n. a.	n. a.	n. a.	n. a.	700	0	
9	9a	birch	-	-	5.6	4.3	5.2	3.5	800	0	
10	10c	birch	0.0785	0.136	n. a.	n. a.	n. a.	n. a.	800	0	
11	11a	800 ° char	-	-	n. a.	n. a.	n. a.	n. a.	500	7	
12	12a	400 ° char	-	-	n. a.	n. a.	n. a.	n. a.	800	7	
13	13a	800 ° char	-	-	n. a.	n. a.	n. a.	n. a.	800	7	
14											No results
15	15a	800 ° char	-	-	n. a.	n. a.	n. a.	n. a.	800	22	

Conversion experiments 2

Experiment #	File name	Sample	dry mass (g)	wet mass (g)	h0 (mm)	hf (mm)	d0 (mm)	df (mm)	Temp. (°C)	O2 (%)
1	1a	birch	-	-	n. a.	4,95	n. a.	3.9;3.2	400	0
1	1b	birch wet	-	-	5.5	4.8	5.3	3.8;3.25	400	0
2	2a	birch	0.0536	0.0956	-	-	-	-	400	0
3	3a	birch wet	-	-	5.6	4.6	5.15	3.35	500	0
4	4a	birch	0.0787	0.1366	-	-	-	-	500	0
5	5a	birch wet	-	-	5.45	4.35	5.35	3.6	600	0
6	6a	birch	0.0768	0.1386	-	-	-	-	600	0
7	7a	birch wet	-	-	5.6	4.5	5.35	3.4	700	0
8	8a	birch	0.0801	0.1361	-	-	-	-	700	0
9	9a	birch	-	-	5.65	4.25	5.4	3.6	800	0
9	9b	birch	-	-	n. a.	n. a.	n. a.	n. a.	800	0
9	9c	birch wet	-	-	n. a.	n. a.	n. a.	n. a.	800	0
10	10a	birch	0.0803	0.1408	-	-	-	-	800	0
11	11a	char800	-	-	-	-	-	-	500	5.5
12	12a	char400	-	-	-	-	-	-	800	6
13	13a	char800	-	-	-	-	-	-	800	6
14	14a	char400	-	-	-	-	-	-	800	23
15	15a	char800	-	-	-	-	-	-	800	23

Illustration of the results of conversion experiments 2

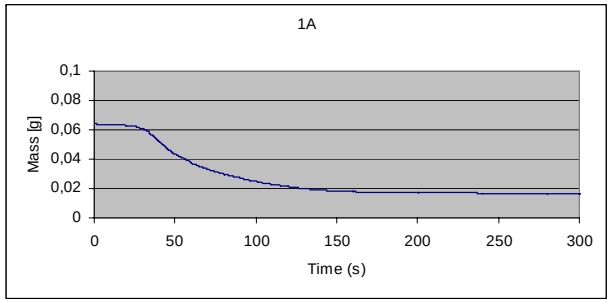

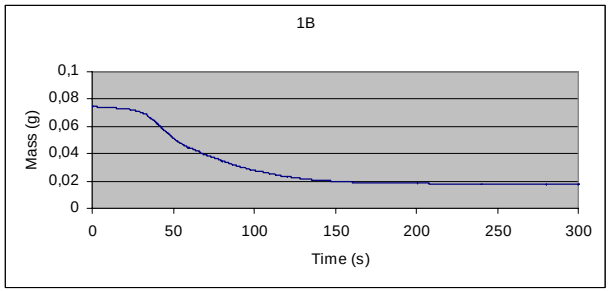

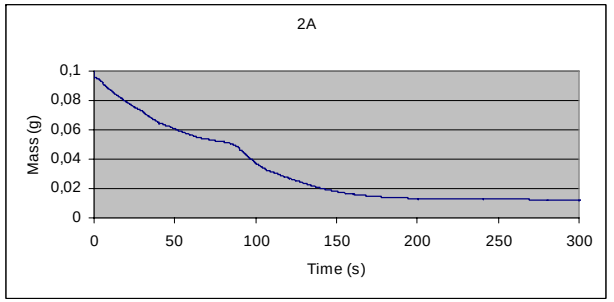

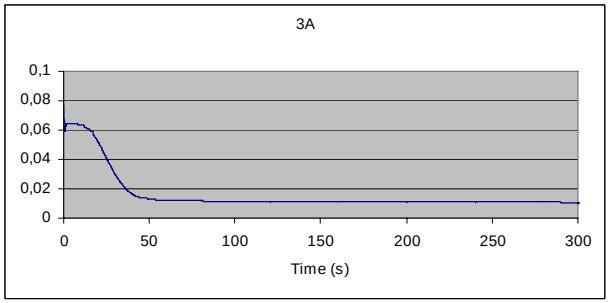

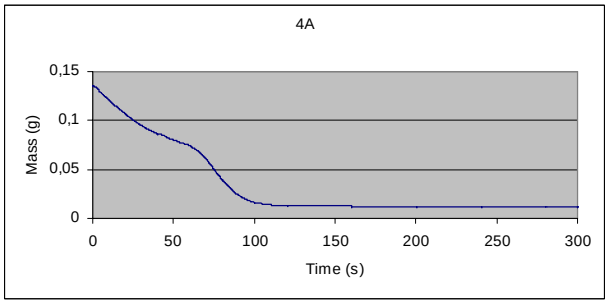

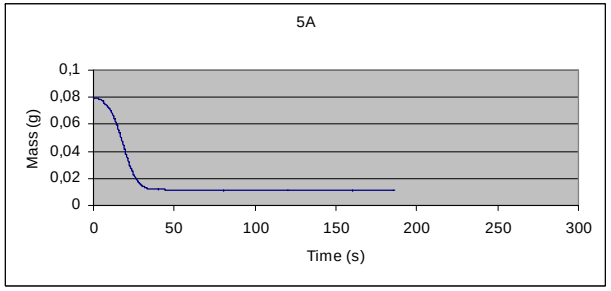

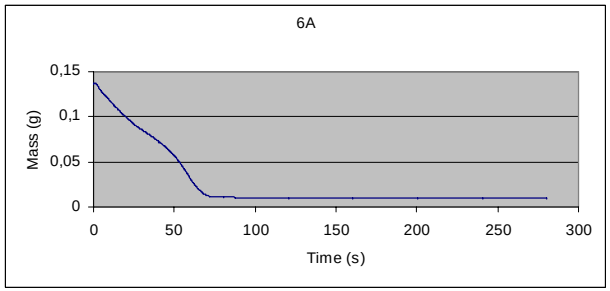

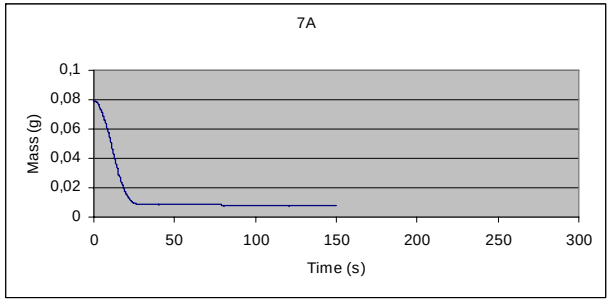

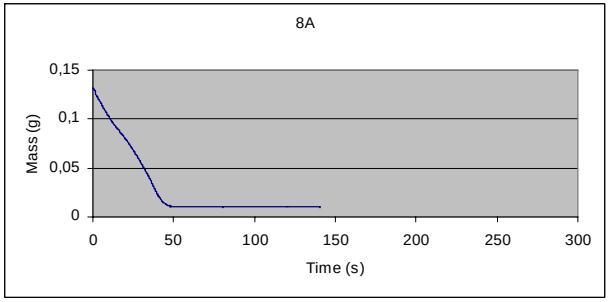

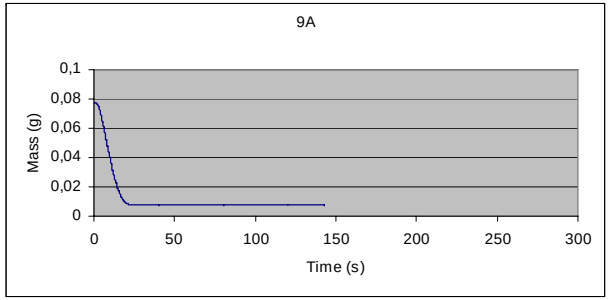
9A
Mass (g)
0,1
0,08
0,06
0,04
0,02
0
0
50
100
150
200
250
300
Time (s)

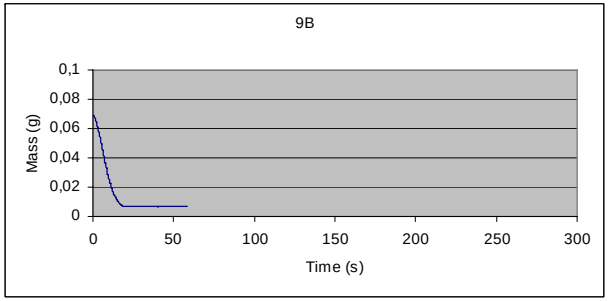
9B
Mass (g)
0,1
0,08
0,06
0,04
0,02
0
0
50
100
150
200
250
300
Time (s)

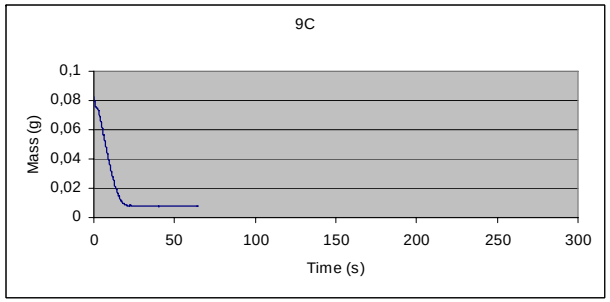
9C
Mass (g)
0,1
0,08
0,06
0,04
0,02
0
0
50
100
150
200
250
300
Time (s)

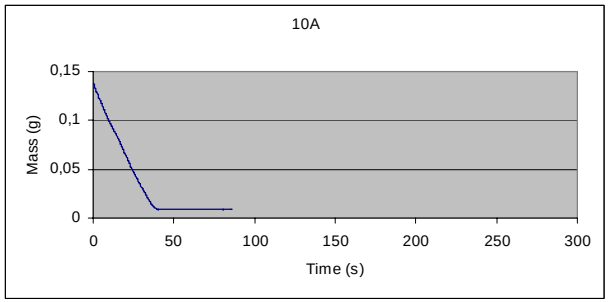
10A
Mass (g)
0,15
0,1
0,05
0
0
50
100
150
200
250
300
Time (s)

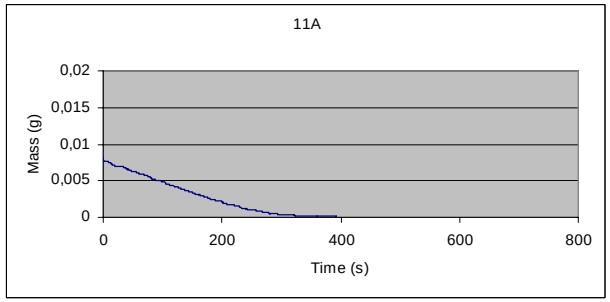
11A
Mass (g)
0,02
0,015
0,01
0,005
0
0
200
400
600
800
Time (s)

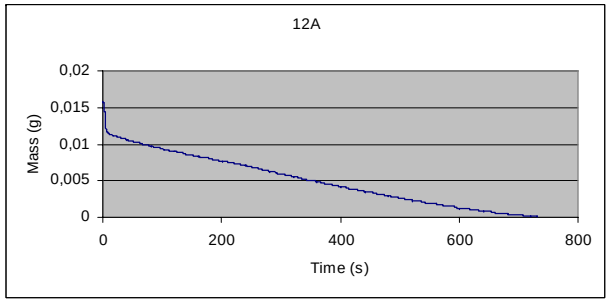
12A
Mass (g)
0,02
0,015
0,01
0,005
0
0
200
400
600
800
Time (s)

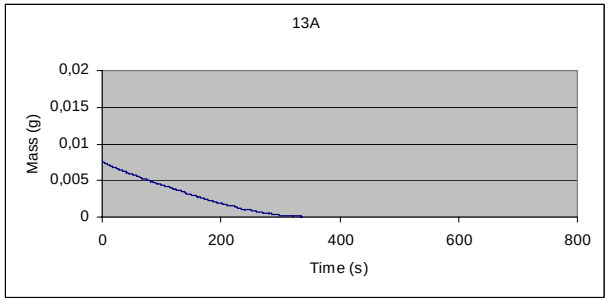
13A
Mass (g)
0,02
0,015
0,01
0,005
0
0
200
400
600
800
Time (s)

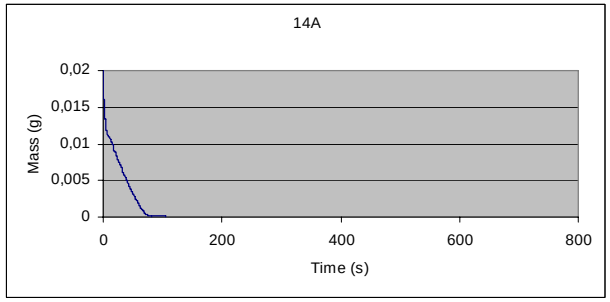
14A
Mass (g)
0,02
0,015
0,01
0,005
0
0
200
400
600
800
Time (s)

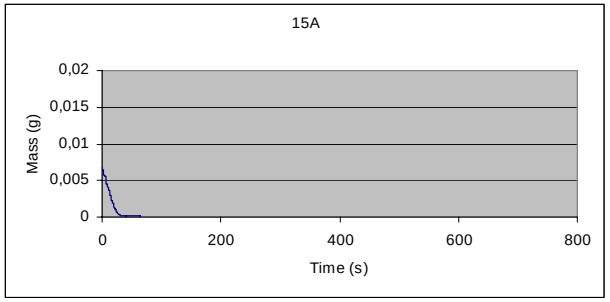
15A
Mass (g)
0,02
0,015
0,01
0,005
0
0
200
400
600
800
Time (s)

Assignment 4

Design of a stationary (bubbling) fluidised bed boiler

Henrik Thunman, Eva Johansson 2002

Design a 20MW_{th} stationary fluidised bed boiler, which would use wood chips as fuel. Legislation requires that the emissions of unburned volatiles should not exceed 100ppm. The task is to determine the dimensions of the boiler (depth, width and height), and the profiles of temperature and gas concentrations (O_2, H_2O, CO_2, CH_nO_m, N_2) along the height of the boiler.

The following data are given for a fluidised bed running under equilibrium conditions:

Superficial gas velocity through the bed is restricted to be between 1 and 2 m/s at the temperature of the fluidised bed (1123K) and at normal pressure (100kPa).
Temperature in the fluidised bed 1123K (850ºC, optimal temperature for SO_2 capture)
The excess air ratio is 1.2
All air is fed as primary air
Boiler efficiency 0.9
Combustion efficiency 1
Bed height 0.95 m

Fuel properties:
Wood chips
Lower heating value (on dry bases) 18.6 MJ/kg
Proximate analysis
40 $\%_{mass}$ moisture (as received)
80 $\%_{mass}$ volatiles, 20 $\%_{mass}$ char 0 $\%_{mass}$ ash (on dry basis)
Ultimate analysis (on dry ash free basis)
50 $\%_{mass}$ C 5 $\%_{mass}$ H, 45 $\%_{mass}$ O

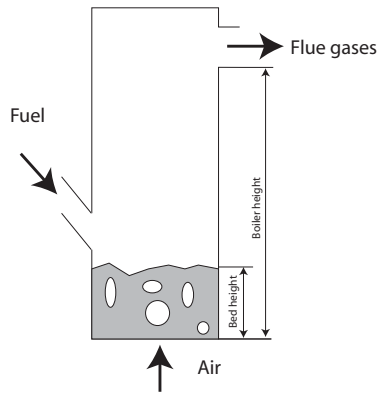

Figure 1
Schematic picture of a stationary fluidised bed boiler

NECESSARY ASSUMPTIONS:

1. The freeboard of the boiler is equipped with water cooled tube walls, assumed to have a constant surface temperature equal to the boiling temperature of water at 1 MPa.

2. Assume that the free board above the fluidised bed can be considered as a tube reactor, where the gas medium changes temperature with height.

3. Devolatilisation is assumed as thermally neutral.

4. All volatile gases are represented by a single gas CH_nO_m, with a c_p equal to that of methane.

5. The volatile gases burn as $CH_nO_m+aO_2 \rightarrow bCO_2+cH_2O$.

6. The kinetic reaction rate of the volatiles is assumed to that of cyclic hydrocarbons.

7. The mixing rate is estimated by $k_{mix} \approx D_{tur}/L^2$ [1/s], where $D_{tur} / D_{AB} \approx 10$ (estimated from experiment). D_{AB} can be taken for the diffusion coefficient of the $N_2 - nC_4H_{10}$ gas pair (condensable gas) and the characteristic length L is assumed equal to the hydraulic diameter d_h divided by 150 (arbitrary value), $d_h = 4 \times$ cross sectional area / perimeter ($4 \times$ tvärsnittsarean / omkretsen).

8. The effective reaction rate given by
$$R_{eff} = \frac{1}{R_{reak}^{-1} + R_{mix}^{-1}} \qquad \text{where } R_{mix} = k_{mix} \min[C_{reak}]$$

9. Char consists of pure carbon.

10. The char has the same heating value and c_p as graphite.

11. The char burns in the bed directly to CO_2

12. The bed is assumed to be isothermal (constant temperature) and the wall in this lower part of the boiler is covered with bricks, which have same surface temperature as the bed.

13. Drying and devolatilisation take place within the fluidised bed

14. The volume of the particle shrinks with 50 % during drying and devolatilisation, but the shape of the particle is maintained.

15. The oxygen concentration decreases linearly through the fluidised bed

16. The density of the inert bed material is 2600 kg/m^3

17. The porosity of the fluidised bed is 0.6.

18. The heat transfer coefficient to the wall above the fluidised bed is estimated by:
$h_{cw} = h_c + h_{rad}$
The convective heat transfer calculated from Nu given by:
$Nu(z) = 0.33 z^{-0.5} \mathrm{Re}^{0.5} \mathrm{Pr}^{0.33}$
where z = height x in the furnace/total height of the furnace.
The radiative heat transfer is given by:
$h_{rad} = \sigma \varepsilon_{rad} \left(T_w^4 - T_g^4\right) / \left(T_w - T_g\right) = \sigma \varepsilon_{rad} \left(T_w + T_g\right)\left(T_w^2 + T_g^2\right)$
where $\varepsilon_{rad} = (\varepsilon_{rad,g}^{-1} + \varepsilon_{rad,w}^{-1} - 1)^{-1}$. The emissivity of the gas is estimated from the dimension of the boiler and the concentration of H_2O and CO_2 to 0.25 and the emissivity of the wall is assumed to be 0.6 (oxidised steel).

19. The fuel and the air enters the combustor at ambient temperature (≈ 25°C)

EACH STUDENT SHALL COMPLETE ONE OF THE FOLLOWING ASSIGNMENTS.

1. What happens if one wants to burn bituminous coal instead of wood chips? Discuss how the boiler has to be changed in order to handle the different fuels.

2. Calculate the fuel load (mass of burning char) and mass fraction of fuel in the fluidised bed. For the calculation use an average oxygen concentration. Compare the woodchips case with a case when one burns bituminous coal (assume that the conditions in the bed is similar to the wood chips case, except oxygen concentration, and that the initial particle size is 10 mm). Discuss how this will affect the ability to control the boiler.

3. In a real boiler the combustion air is often staged, which means that the air is introduced as primary air in the bottom and secondary air just above the fluidised bed (in some cases even tertiary air is introduced further up in the boiler). Calculate, the profiles of temperature and gas concentration in a case when the primary air correspond to 50% excess of the air needed for the char combustion and the rest of the air is introduced as secondary air? Compare this case with the case with only primary air and discuss why air staging is used.

GUIDELINES FOR THE PROBLEM SOLUTION

Simplify the problem as much as possible, but motivate the assumption needed for the simplifications.

1. Estimate the fuel demand.
2. Estimate the cross-sectional area of the bed
3. Determine the heating value of the char and volatiles
4. Determine the composition of the equivalent volatile gas
5. Make a heat balance over the fluidised bed and estimate the amount of volatiles that is converted inside the bed
6. Determine the gas composition of the gas leaving the bed
7. Calculate the profiles of temperature and gas concentration up through the free-board
8. Estimate the height of the free-board
9. Submit a written report and get it approved.
10. Perform one of the special tasks chosen by the student.
11. Submit the report on the special task at before the 4th of December.

In the written reports the assumptions given in the exercise shall be critically discussed. The report shall be kept as short as possible and is to be organised in a lucid manner. The report shall be submitted by email and the reports on the special tasks will be distributed among the course participants on the 4th of December.

APPENDIX A

COMBUSTION CALCULATIONS FOR CHEMICAL REACTORS

HENRIK THUNMAN

The conservations equations given in the previous chapter are rather complicated to solve and in most practical cases they are simplified significantly. Often one talks about models of different orders, where the simplest models are the zero-order models, which include simple heat and mass balances. The order of the model is given by the resolution of the calculation in time and number of dimensions in space. A zero order model gives no information of the evolution of temperature, fuel conversion etc. in a volume as it treats the whole volume as a black box. A zero order model, however, can be powerful despite its simplicity; an example of such a model is the continuously stirred reactor, which is widely used for various applications and is described in detail below. Another example is the use of heat and mass balances to estimate the composition of the volatile gases, which leave a solid fuel particle during devolatilisation, as given in Appendix A.

If one is interested in the evolution of temperature, fuel conversion etc. in a volume, the flow in such a volume can often be simplified to one dimension. In this case a first order-model can be used. The most common first order model of this kind is the plug flow reactor, which also is described below.

CONTINUOUSLY STIRRED REACTOR

The continuously-stirred (also called perfectly stirred, well stirred or partially stirred (if not perfectly mixed on molecular level) reactor in the literature) is an ideal reactor in which perfect mixing is achieved inside the control volume, as shown

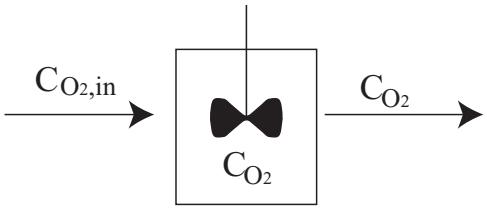

Figure A.1.
Continuously Stirred Reactor

in Fig. A.1. Experimental reactors employing high-velocity inlet jets approach this ideal situation and have been used to study many aspects of combustion, such as flame stabilization and NO_x formation. Continuously stirred reactors (CSR) also have been used to obtain values for global reaction parameters. The continuously-stirred reactor is sometimes called a Longwell reactor.

In the simplest form of the CSR it is assumed that the temperature is constant through the reactor and that the flow is isothermal. This makes the solution of the energy equation trivial (nothing changes). Furthermore, the reactions are assumed to be equimolar, which means that the same number of molecules produced by the reaction is consumed by the same reaction. This makes the solution of the momentum and conservation equations trivial. The only equations that have to be considered in this case are the conservation equations for the species. However, very few reactions fulfil the requirement of being equimolar, but example of such reactions are the water-gas shift reaction $CO + H_2O \leftrightarrow CO_2 + H_2$ and the methane-oxygen reaction, if the methane is completely converted to CO_2 and H_2O, $CH_4 + 2O_2 \rightarrow CO_2 + 2H_2O$. It is more difficult to find reactions that are thermally neutral, even if this can be fulfilled at some specific temperatures. The question that can be raised here is whether the simplest form of the continuously stirred reactor model is useful for modelling of a combustion system? The answer is yes, this simple reactor is widely applied, but as seen from the assumptions, the simplest form of the CSR cannot be used for the main chemistry in the cases where the temperature of the system is not known, or where there are great changes in the number of moles caused by the reactions that take place in the system. The term " main chemistry" means the reactions that give the major part of the heat release in the combustion system. In general the equimolar assumption is not a restriction in a combustion system where a fuel is oxidized by air, since the major part of the gas consists of nitrogen.

The continuously stirred reactor can be derived from the conservation equation of species applied across the reactor,

$$\rho \frac{\partial Y_i}{\partial t} + A\rho u \frac{\partial Y_i}{\partial Ax} = \frac{\partial}{\partial Ax}\left(A\rho D_{AB} \frac{\partial Y_i}{\partial x} \right) + \dot{m}_i''' \qquad \text{(A.1)}$$

with the assumptions made above, and given that the diffusion term is negligible. Solving the equation with a backward discretisation scheme in space and using that $\partial Ax \equiv \partial V$, the equation becomes,

$$\rho \frac{\partial Y_i}{\partial t} + A\rho u \frac{Y_{i-1} - Y_i}{\Delta V} = \dot{m}_i''' \qquad \text{(A.2)}$$

where Y_{i-1} is the mass fraction of the species entering the reactor. Since, the reactor is isothermal and equimolar, the equation can be written in molar concentration instead of mass fraction. If the reaction rate also is described by a reaction rate, it can be written

$$\frac{\partial C_i}{\partial t} + Au \frac{C_{i-1} - C_i}{\Delta V} = C_i k_r \qquad \text{(A.3)}$$

Assuming steady state and defining the residence time in the reactor as $\tau = \Delta V/(Au)$, the familiar form of the well stirred reactor is obtained.

$$\frac{C_{i-1} - C_i}{\tau} = C_i k_r \qquad \text{(A.4)}$$

in this equation k_r is the reaction rate constant, which in its simplest form is given by an Arrhenius rate expression for a first order reaction,

$$\frac{dC}{dt} = Ck_r \quad \text{where} \quad k_r = k_{r0} \exp\left(-E/\Re T\right) \qquad \text{(A.5)}$$

where k_{r0} is the pre-exponential factor and E is the activation energy.

EXAMPLE A.1 A gas mixture that contain 1000 ppm cyclopentane $C_5H_{10}O$,a cyclic hydrocarbon, and 6% oxygen is injected into a well insulated, continually stirred reactor with a mass flow of 10^{-4}kg/s. The volume of the reactor is 10^{-5} m^3, the temperature inside the reactor is 900 K and the density of the gas is 0.35 kg/m^3. Calculate the concentration of the cyclopentane that leaves the reactors. Reaction rate is given by:

$R_c = 930 \times 10^3 T C_{CnHmOk} C_{O_2} \exp(-9650/T)$ [mole/s]

Solution. The change of the oxygen concentration can be neglected and the concentration can be calculated directly from Eq A.4 where the reaction rate is

$$k_r = 930\times10^3 TC_{O_2}\exp(-9650/T) =$$
$$= 930\times10^3\times900\times\left(0.06\times10^5/8.314/900\right)\times$$
$$\times\exp(-9650/900) = 14800\left[1/s\right]$$

Total concentration in the reactor is

$$C = 10^5/(8.314\times900) = 13.6$$

The residence time in the reactor is

$\tau = 10^{-5}/(10^{-4}/0.35)=35\times10^{-3}$s

The concentration of the cyclopentane can now be calculated from Eq A.4.

$$\frac{C\left(X_{i-1}-X_i\right)}{\tau} = CX_i k_r \Rightarrow \frac{13.6\left(1\times10^{-3}-X_i\right)}{35\times10^{-3}} = 13.6\times X_i\times14800\Rightarrow$$
$$X_i = 2\,ppm$$

The continuously stirred reactor model can be derived for a more general case from a control volume as shown in Fig. A.2. We start by writing the mass conservation of an arbitrary species *i*, for a control volume V as

$$\frac{dm_{i,cv}}{dt} = \dot{m}_i'''V + \dot{m}_{i,in} - \dot{m}_{i,out} \qquad \text{(A.6)}$$

Rate at which mass of i accumulates within CV	Rate at which mass of i is generated within CV	Mass flow of i into CV	Mass flow of i out of CV

The presence of the generation term $\dot{m}'''V$ distinguishes Eq A.6 from the overall continuity equation Eq. 4.1. This term arises because chemical reactions transform one species into another; hence, a positive generation rate indicates the formation of species, while a negative generation rate implies that species are consumed during the reaction. In the combustion literature, this generation term is frequently referred to as a source or sink. When the appropriate form of Eq A.6 is written for each of the species in the reactor (i = 1,2,...,N), the sum of these equations yields the continuity equation,

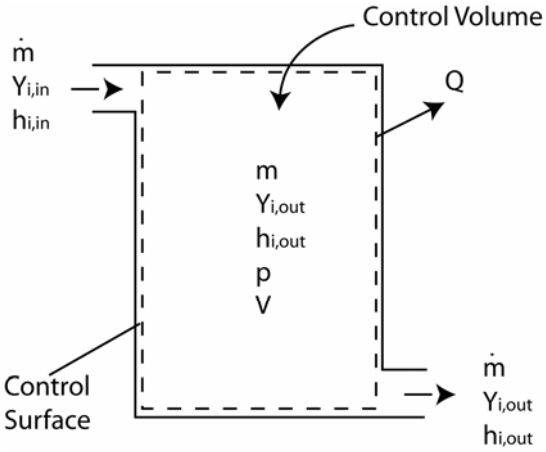

Figure A.2.
Schematic of a continuously stirred reactor

$$\frac{dm_{cv}}{dt} = \dot{m}_{in} - \dot{m}_{out} \tag{A.7}$$

Ignoring any diffusional flux, the mass flow rate of individual species is simply the product of the total mass flow rate and that species mass fraction, i.e.,

$$\dot{m}_i = \dot{m} Y_i \tag{A.8}$$

When Eq A.6 is applied to the continuously stirred reactor, under the assumption of steady-state operation, the time derivative of the left-hand-side disappears. With this assumption Eq A.6 becomes

$$\dot{m}_i''' V + \dot{m}\left(Y_{i,in} - Y_{i,out}\right) = 0 \text{ for i =1,2,…N species.} \tag{A.9}$$

Furthermore, we can identify the outlet mass fractions, $Y_{i,out}$ as being equal to the mass fractions within the reactor. Since the composition within the reactor is everywhere the same, the composition at the outlet of the control volume must be the same as in the interior. Using this knowledge, the species product rates have the form

$$\dot{m}_i''' = f\left(Y_{i,cv}, T\right) = f\left(Y_{i,out}, T\right) \tag{A.10}$$

The mass fractions and molar concentrations are related by

$$Y_i = \frac{X_i M_i}{\sum_{j=1}^{N} X_i M_i} \tag{A.11}$$

Equation A.9, when written for each species, results in N equations with $N + 1$ unknowns, with the assumed known parameters $\dot{m}$ and V. An energy balance provides the additional equation needed for closure.

The steady-state conservation of energy equation applied to the continuously -stirred reactor is

$$Q = \dot{m}\left(h_{in} - h_{out}\right) \tag{A.12}$$

where we neglect changes in kinetic and potential energies. Re-writing Eq A.12 in terms of the individual species,

$$Q = \dot{m}\left(\sum_{i=1}^{N} Y_{i,in} h_i\left(T_{in}\right) - \sum_{i=1}^{N} Y_{i,out} h_i\left(T_{out}\right)\right) \tag{A.13}$$

where

$$h_i = h_{f,i}^0 + \int_{T_{ref}}^{T} c_{p,i} dT \tag{A.14}$$

Solving for the temperature, T, and species mass fractions, $Y_{i,out}$, is actually quite similar to our computation of adiabatic flame temperatures in Chapter 3; however, now the product composition is constrained by chemical kinetics, rather than by chemical equilibrium. The heat leaving the system Q is transported by a combination of convection and radiation

$$\begin{aligned} Q &= A\left(h_c\left(T_{out} - T_w\right) + \varepsilon_{eff}\sigma\left(T_{out}^4 - T_w^4\right)\right) = \\ &= \dot{m}\left(\sum_{i=1}^{N} Y_{i,in} h_i\left(T_{in}\right) - \sum_{i=1}^{N} Y_{i,out} h_i\left(T_{out}\right)\right) \end{aligned} \tag{A.15}$$

It is common in the discussion of continuously-stirred reactors to define a mean residence time for the gases in the reactor:

$$\tau = \rho V / \dot{m} \tag{A.16}$$

where the density of the mixture is calculated from the ideal-gas law

$$\rho = \frac{p\sum_i X_i M_i}{\Re T} \tag{A.17}$$

CSR-REACTOR MODEL SUMMARY

Because the continuously-stirred reactor is assumed to be operating at steady state, there is no time-dependence in the mathematical model. The equations describing the reactor are a set of coupled nonlinear algebraic equations, rather than a system of ordinary differential equations, which was the result for the previous two examples. Thus the reaction term, $\dot{m}'''$, depends only on the mass fraction Y_i (or X_i) and temperature, not time. To solve this system of N + 1 equations, Eqs A.10 and A.15, the generalized Newton's method can be employed. Depending on the chemical system under study, it may be difficult to achieve convergence with Newton's method and more sophisticated numerical techniques may be necessary, for example, one can introduce fictitious time dependence and setup a set of first order differential equations (ODE), which can be solved by an ODE-solver.

EXAMPLE A.2 A cyclic hydrocarbon, cyclopentane, $C_5H_{10}O$ burns with air at stoichiometric conditions in a reactor, which can be represented as a continually stirred reactor. The mass flow through the reactor is 0.2 kg/s, the volume of the reactor is 20×10^{-6} m^3 and it has a surface area of 2.7×10^{-3} m^2, with a temperature of 600°C. The heat transfer coefficient to the walls is 20 W/m^{2}K and the effective emissivity between the gas and the reactor wall is 0.2. Calculate the temperature and composition of the gas leaving the reactor.

Guidelines to the problem

Assume that the hydrocarbons is directly converted to CO_2 and H_2O

Solution. The reaction rate of the cyclic hydrocarbons can be taken from Appendix B page B.6

$$\dot{m}''' - k_r C_{C_5H_{10}O}^{0.5} C_{O_2} M_{C_5H_{10}O}$$
$$k_r = 2.07\times10^3 T \exp(-9650/T)$$

The molar mass of the hydrocarbon is 0.086 kg/mole

The reaction can be written

$$C_5H_{10}O + 7.5O_2 \rightarrow 5CO_2 + 5H_2O$$

Calculate reference enthalpy from the lower heating value of $C_5H_{10}O$, 43798 kJ/kg Appendix B, page B27.

$$43798 \times 10^3 \times 0.086 = h^0_{C_5H_{10}O} - 5(-394088 + -242174) \Rightarrow$$

$$h^0_{C_5H_{10}O} = 585318 J / mole$$

The specific heat of $C_5H_{10}O$ is here only available at reference temperature, 1600 J/kg or 138 J/mole. As the amount of $C_5H_{10}O$ in the gas composition is small, the influence on the temperature of the gas mixture is negligible. For this reason and due to lack of information the temperature dependence of the specific heat of $C_5H_{10}O$ is not taken into account.

The problem can now be solved by e.g. Matlab. A Matlab program with a general structure is presented below for the solution of the problem. The program can be used preferable to solve any continually stirred reactor, where the correlations of the reactions are of the Arrhenius type.

The solution given by the program is shown in the figure below, where it can be seen that steady state is gained after less than 1 ms and the temperature within the reactor is 2272 K and the composition on mass fractions of the outgoing species are 0.057 O_2, 0.708 N_2, 0.059 H_2O, 0.145 CO_2, 0.020 $C_5H_{10}O$.

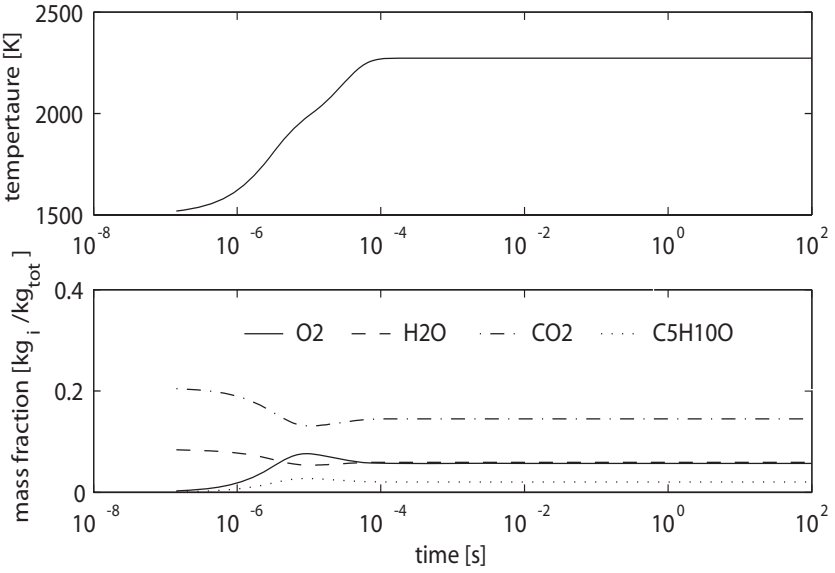

First we write a general function for a continually stirred reactor "CSR.m", which gives the derivative of temperature and mass fractions. Into the function we put time evolved from initial condition t, temperature *T* and mass fractions Y_i lumped together into the variable *y*, the variable *flag* used by the solver (not active here - see help in Matlab for more information of its use), and a structured variable *R*, which contains constants that are used for the determination of the derivatives. The % in the program code mark comments.

```
*********************************************************
function dy=CSR(t,y,flag,R)

%extract information of number of species and number of reactions from
%input data

n_species=size(R.stoic,1);          %number of species in the system
n_reactions=size(R.expo,2);         %number of reactions

%Extract input data, mass fractions in all except in the last position of the
%vector indexed 1:end-1.

Yi=y(1:end-1,1);
T=y(end);

%variables need to be initiated before they are called

dYi=zeros(size(Yi));                %initiate derivative of mass fraction
dT=0;                               %initiate temperature derivative
cp=0;                               %initiate specific heat
h=zeros(size(Yi));                  %initiate enthalpy of spcies i at T


%calculate properties used to determine the derivatives

C=R.P./8.314./T;                                %Total concentration at x
Ci=C*(Yi./R.Mi/sum(Yi./R.Mi));                  %Concentration of species i

%calculate enthalpy for each specie and specific heat for the mixture
for i=1:size(Yi,1)
   cp=cp+Yi(i)*polyval(R.cp(i,:),T);
   %calculate dhi by integrating cp from Tref  to T
   cp_int=[R.cp(i,:).*(1./(size(R.cp,2):-1:1)),0];
   dhi= polyval(cp_int,T)-polyval(cp_int,298);
   h(i)=R.href(i)+dhi;
end

%density of the gas

rho=sum(Ci.*R.Mi,1);

%calculate enthalpy of inflowing gas
hi0=zeros(size(Yi));            %initiate enthalpy of spcies i at T
for i=1:size(Yi,1)
   %calculate dhi by integrating cp from Tref  to T
   cp_int=[R.cp(i,:).*(1./(size(R.cp,2):-1:1)),0];
   dhi0= polyval(cp_int,R.T0)-polyval(cp_int,298);
   hi0(i)=R.href(i)+dhi0;
end

%Reaction, calculate the reaction rate, RR [mol/m^3], without the
%stoichiometric constant for each reaction see Eq. A.21

nn= ones(1,n_reactions);

%nn is used to expand the concentration vector to a matrix with a width equal
%to the number of reactions , where all columns  are the same.
```

```
%prod(x,1) is the product and ,1 mark the direction in which the operation
%shall by performed

RR=R.kr0.*T.^R.krTex.*prod(Ci(:,nn).^R.expo,1).*exp(-R.Ea./T);

%Calculate derivative of the mass fraction according to Eq A.6 where mass-
%flow of each specie is calculated according to Eq A.8. The stoichiometric
%coefficient is multiplied to the reaction rate for each reaction and all
%reaction is summarized together according to Eq A.21. To get the
%conversion rate of each specie in kg/m^3s the reaction rate is multiplied
%with the molar mass. The notation ,2 in the sum mark the direction of
%the summation

dYi= (sum(RR(ones(n_species,1),:).*R.stoic,2).*R.Mi*R.V…
      +R.mprick*(R.Yi-Yi))/(R.V.*rho);

%Heat balance over the reactor Eq A.6 rewritten for energy complemented
%with a heat loss according to Eq A.15.

dT=(R.mprick*sum(R.Yi.*hi0-Yi.*h,1)-...
R.A*(R.hm*(T-R.Tw)+R.eps*R.sigma*(T.^4-R.Tw.^4)))/(cp*R.V*rho);

%Lump the derivatives together into a vector according to the instruction of
%the ode solver

dy=[dYi;dT];
************************************************************
```

The function, which calculates the derivatives, needs a large number of input data and a program that initiates the calculation, performs the calculation and present the result. The program that does this is here called “Calc_CSR.m”

```
************************************************************
%Calc_CSR
%Species { 1=O2; 2=N2; 3=H2O; 4=CO2; 5=C5H10O}
%initiate variable for: mass fraction; Molar mass;
n_species=5;
R.Yi=zeros(n_species,1);R.Mi=zeros(n_species,1);


R.Yi(1)=0.21*0.032/(0.21*0.032+0.79*0.028);   R.Mi(1)=0.032;
R.Yi(2)=0.79*0.028/(0.21*0.032+0.79*0.028);   R.Mi(2)=0.028;
R.Yi(3)=0;                                    R.Mi(3)=0.018;
R.Yi(4)=0;                                    R.Mi(4)=0.044;
R.Yi(5)=R.Yi(1)*0.086/(7.5*0.032);            R.Mi(5)=0.086;

%normalize mass fractions to ingoing flow instead of to flow of air
R.Yi=R.Yi/sum(R.Yi);

%Initial condition inside reactor (assume that all fuel is conversted to CO2
and H2O)
R.Yi0=R.Yi;
R.Yi0(3)=R.Mi(3)/(R.Mi(3)+R.Mi(4))*(R.Yi(1)+R.Yi(5));
R.Yi0(4)=R.Mi(4)/(R.Mi(3)+R.Mi(4))*(R.Yi(1)+R.Yi(5));
R.Yi0(1)=0;
R.Yi0(5)=0;
```

```
%Initial Temperature within reactor

R.Ti0=1500;

%Reference enthalpy and specific heat polynomial fit of 2nd degree
% according to Appendix B12
R.href=zeros(n_species,1);R.cp=zeros(n_species,2);

%Species specific properties (here the reference enthalpy and
%specific heat is given per mole table page B.12 in Appendix B)

R.href(1)=0;                R.cp(1,:)=[0.00349 30.5041];
R.href(2)=0;                R.cp(2,:)=[0.00307 29.2313];
R.href(3)=-242174;          R.cp(3,:)=[0.00862 32.4766];
R.href(4)=-394088;          R.cp(4,:)=[0.00730 44.3191];
R.href(5)=585318;           R.cp(5,:)=[0          138.000];

%recalculate ethalpy and specific heat given per unit mass
R.href=R.href./R.Mi;
R.cp=R.cp./R.Mi(:,ones(1,size(R.cp,2)));

%input data
R.mprick=0.2;       %mass flow
R.T0=298;           %Input temperature
R.Tw=600+273;       %Wall temperature

R.P=100e3;          %pressure
R.hm=20;            %heat transfer coefficient
R.sigma=5.67e-8;    %Stefan Boltzmann's constant
R.eps=0.2;          %emissivity

%Geometrical data
R.V=10e-6;          %Volume of reactor
R.A=2.7e-3;         %Surface area inside reactor

%Initiate data for calculation
%Assume that the reactor has the same composition as the ingoing gas
%mixture. To ignite the gas mixture a rather high initial temperature
%within the reactor is needed here assumed to 1500K
y=[R.Yi0;R.Ti0];

%start and end time of reactor (steady state is assumed to be achieved
%before 100s)
x=[0;100];

%Data for reactions,
%reaction of the form dCi/dt =vi*kr0*T^n*Ca^a*Cb^b*…*exp(-E/RT)
%stoiciometric factor, vi

R.stoic =[  -7.5
            0
            5
            5
            -1              ];

%pre-exponential factor, kr0
R.kr0  =[   20.7e3];
```

```
%temperature exponent n
R.krTex=[   1   ];

%exponent on concentration
R.expo =[   1
            0
            0
            0
            0];

%activation energy divided by gas constant
R.Ea   =[    9650      ];

%calculation with the built in function ode15s

[x,y]=ode15s('CSR',x,y,[],R);

%Extract result from the calculation
Yi=y(:,1:end-1)';
T=y(:,end)';

%plot result
subplot(2,1,1);semilogx(x,T);ylabel('tempertaure [K]')
subplot(2,1,2);semilogx(x,Yi(1,:),x,Yi(3,:),'--',x,Yi(4,:),'-.',x,Yi(5,:),':');
legend('O2','H2O','CO2','C5H10O')
ylabel('mass fraction [kg_{i}/kg_{tot}]')
xlabel('time[s] ')
************************************************************
```

PLUG FLOW REACTOR

If one wishes to follow the progress of combustion in a system, which is not complex, a one-dimensional description may be sufficient. In these combustion situations a first order model is appropriate. The most common first order model is what in the chemical literature is called, a plug flow reactor, illustrated in Fig A.3. A general plug-flow reactor represents an ideal reactor that has the following attributes:

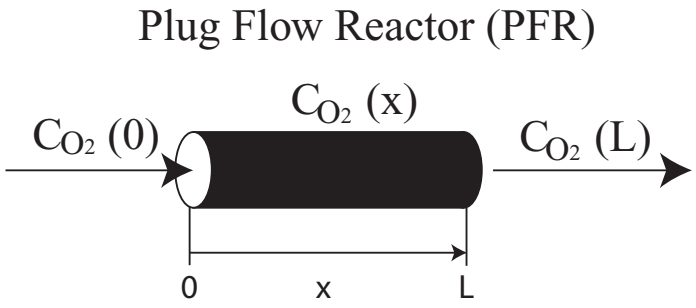

Figure A.3.
Plug flow reactor

1. Steady-state.
2. No mixing in the axial direction. This implies that molecular and/or turbulent mass diffusion is negligible in the flow direction.
3. Uniform properties in the direction perpendicular to the flow, i.e., an assumption of one-dimensional flow. This means that at any cross-section, a single velocity, temperature, composition, etc., completely characterizes the flow.
4. Ideal frictionless flow. This assumption allows the use of the simple Euler equation to relate pressure and velocity.
5. Ideal-gas behaviour. This assumption allows simple state relations to be employed to relate T, p, ρ, Y_i, and h.

In its simplest form it is also assumed that the reactor is isothermal and equimolar, which makes it possible to derive the plug flow reactor from the conservation equation for the species of interest.

$$\rho\frac{\partial Y_i}{\partial t}+\rho u\frac{\partial Y_i}{\partial x}=\frac{\partial}{\partial x}\left(\rho D_{AB}\frac{\partial Y_i}{\partial x}\right)+\dot{m}_i''' \tag{A.18}$$

The plug flow reactor assumes steady state and that the diffusive term is negligible in relation to the convective term. This reduces the conservation equation of the species to the simplest form of the plug flow reactor model,

$$\rho u\frac{\partial Y_i}{\partial x}=\dot{m}_i''' \tag{A.19}$$

In the chemical literature this equation is usually written as a function of residence time in the reactor ($u=x/\tau$) and by the molar concentration (C) instead of the mass fraction (Y), which is possible since the system is isothermal and the reactions are equimolar,

$$\frac{dC_i}{d\tau}=C_i k_r \tag{A.20}$$

EXAMPLE A.3 A gas mixture that contain 1000 ppm cyclopentane, $C_5H_{10}O$,a cyclic hydrocarbon, and 6% oxygen is injected into a well insulated plugflow reactor with a mass flow of 10^{-4}kg/s. The volume of the reactor is 10^{-5} m^3, the temperature inside the reactor is 900 K and the density of the gas is 0.35 kg/m^3. Calculate the concentration of the cyclopentane that leaves the reactors. Reaction rate is given by:

$R_c = 930\times10^3 T C_{CnHmOk} C_{O_2} \exp(-9650/T)$ [mole/s]

Solution. The change of the oxygen concentration can be neglected and the concentration can be calculated directly from Eq A.4 where the reaction rate is taken from Appendix B page B.12

$$k_r = 930\times10^3 TC_{O_2}\exp(-9650/T) =$$
$$= 930\times10^3\times900\times\left(0.06\times10^5/8.314/900\right)\times$$
$$\times\exp(-9650/900) = 14800\left[1/s\right]$$

Total concentration in the reactor is

$$C = 10^5/(8.314\times1000) = 13.6$$

The residence time in the reactor is

$\tau = 1\times10^{-5}/(10^{-4}/0.35)=35\times10^{-3}$s

The concentration of the cyclopentane can now be calculated from Eq A.20.

$$\frac{dC_i}{d\tau} = C_i k_r \Rightarrow \frac{dX_i}{d\tau} = X_i k_r$$

Integrate the resulting equation with the initial condition that $X_{i0}=10^{-3}$

$$X_i = X_{i0}\exp(-k_r\tau) = 10^{-3}\exp(-14800\times35\times10^{-3}) = 1\times10^{-228}\ ppm$$

This result can be compare with the continually stirred reactor Example A.1, which give 2 ppm during the same conditions.

If several reactions, not necessarily only of first order, are involved, and if these reactions depend on more than a single species, a system of first order differential equations can be derived and solved by an ordinary differential equation (ODE) solver. The system of equations can be written as,

$$\begin{aligned}
\frac{dC_1}{d\tau} &= \sum_{i=1}^{N_{rek}}\Omega_{1i}k_{r0i}\exp\left(-E_i/\Re T\right)\prod_{j=1}^{n}C_j^{\gamma_{ij}}\\
\frac{dC_2}{d\tau} &= \sum_{i=1}^{N_{rek}}\Omega_{2i}k_{r0i}\exp\left(-E_i/\Re T\right)\prod_{j=1}^{n}C_j^{\gamma_{ij}}\\
&\vdots\\
\frac{dC_n}{d\tau} &= \sum_{i=1}^{N_{rek}}\Omega_{ni}k_{r0i}\exp\left(-E_i/\Re T\right)\prod_{j=1}^{n}C_j^{\gamma_{ij}}
\end{aligned} \qquad \text{(A.21)}$$

where the initial condition is given by the concentrations of respective species at the inlet.

For the more general case, when the reactor is not isothermal, the energy equation must be included and if it can be assumed that the pressure drop over the reactor is small, the momentum equation becomes trivial and the velocity of the flow can be calculated from the ideal gas law. When treating a system which changes in temperature and is not equimolar it is convenient to express the species concentrations by the mass fraction or molar fraction instead of the molar concentration. The conservation equations which have to be solved are

mass conservation

$$\frac{d(\rho u A)}{dx} = 0 \tag{A.22}$$

energy conservation

$$\frac{dh}{dx} + \frac{Q'' S}{\dot{m}} = 0 \tag{A.23}$$

species conservation

$$\frac{dY_i}{dx} - \frac{\dot{m}_i'''}{\rho u} = 0 \tag{A.24}$$

The symbols u represents the axial velocity, A cross-sectional area and S local perimeter of the reactor, respectively. The other quantities have been defined previously. The temperature of the mixture is given by h

$$h = \sum_i \left[h_{f,i}^0 + \int_{T_{ref}}^{T} c_{p,i} dT \right] \tag{A.25}$$

The density is given by Eq A.17, the heat exchange with the reactor walls is given by Eq A.15 and the velocity by:

$$u = \frac{\dot{m}}{A\rho} \tag{A.26}$$

If the cross-sectional area is constant along the reactor the mass conservation gives that $u\rho$ is constant and equal to $\dot{m}$. The residence time of the system is:

$$\tau = \int_0^x 1/u \, dx \tag{A.27}$$

Initial conditions necessary to solve Eqs. A.22-A.24 are:

$$T(0) = T_0 \tag{A.28}$$

$$Y_i(0) = Y_{i,0} \quad i = 1,2,...,N, \tag{A.29}$$

PFR-REACTOR MODEL SUMMARY

In summary, the mathematical description of the plug-flow reactor results in a coupled set of ordinary differential equations as a function of spatial coordinates, which can be solved by an ODE-solver, for example ode15s in MATLAB. (This solver or any solver for stiff problems is to be recommended as a first choice. Highly nonlinear reactions are involved in most combustion problems, which show great variations in the derivatives with the distance. The resulting system of equations that has to be solved is a stiff system.)

EXAMPLE A.4 Use a plug flow reactor to calculate the adiabatic temperature of H_2 burning in air at stoichiometric conditions, where the initial temperature of H_2 and air 298 K and pressure inside the reactor is 100 kPa.

Guidelines to the problem

$$H_2 + \tfrac{1}{2} O_2 \leftrightarrow H_2O$$

As only the final temperature is of interest the forward reaction rate can be set as $dC_{H_2} = 1 \times C_{H_2} C_{O_2}^{1/2}$, which assures conversion of the hydrogen for all temperatures.

Solution. The adiabatic temperature is obtained by letting the residence time in the reactor go towards infinity and the heat transport to the surrounding should by definition be sat equal to 0, which mean that $Q'' = 0$ in Eq.A.23. This is obtained if the heat transfer coefficient and emissivity are set to 0. At high temperatures water vapour will dissociate to H_2 and O_2, which means that we need to formulate the backward reaction. From Eq 3.4b

$$k_p = \frac{k_r}{K_C} = \frac{k_r}{K_p \left((P_{Pa} / P_{bar}) / RT \right)^{1-1/2-1}}$$

Correlation for equilibrium constant *Kp* can be taken from Appendix B page B.A.

$$K_p = 1/\left(855\exp\left(-29840/T\right)\right)$$

which gives the backward reaction rate as

$$k_p = 855\exp(-29840/T)\left(1\times10^5/(1\times8.314T)\right)^{1/2} =$$
$$= 93770T^{-1/2}\exp\left(-29840/T\right)$$

The problem can now be solved by e.g. Matlab. Below a Matlab program with a general structure is presented for the solution of the problem. The program can be preferable used to solve any plug flow reactor, where the correlations of the reactions is of the Arrhenius type. This program is nearly identical with the program for the CSR, basically is it only the geometrical data, initial data, and the derivative of temperature and species that differ. (For the calculation made here the cross sectional area is sat to 1 m^2 and the mass flow is sat to 1 kg/s).

The solution given by the program is shown in the figure below, where it can be seen that the adiabatic temperature is reached after approximately 100m. The adiabatic temperature obtained is 2447 K, which can be compared with 2323 K that is given in table in Appendix B page B. 30. The difference is caused, by the behaviour of the specific heat. The concentrations of the different species agree better; the calculation gives 0.8 $\%_{vol}$ O_2, 64.8 $\%_{vol}$ N_2, 32.8 $\%_{vol}$ H_2O and 1.6 % H_2, which are the same as the ones given in the table.

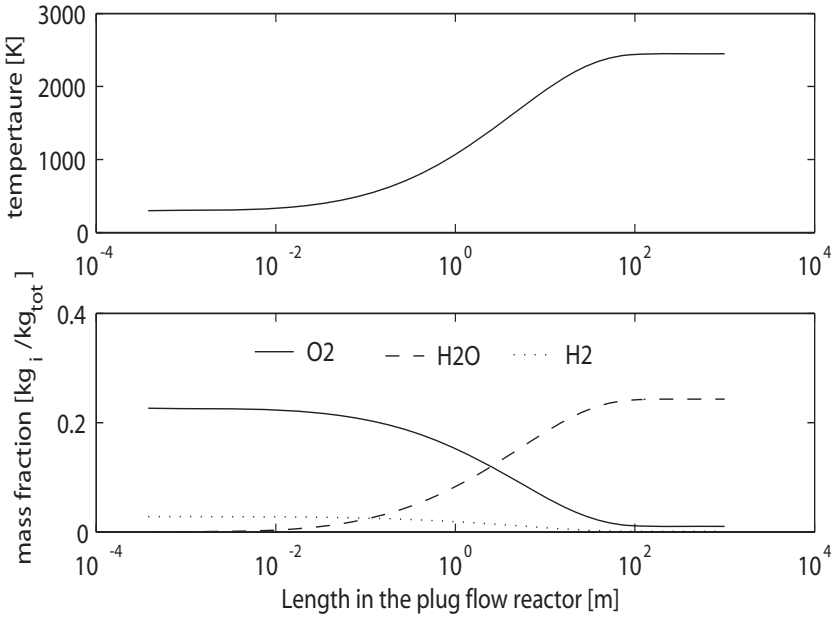

First we write a general function for a plug flow reactor “plug-flow_reactor.m”, which gives the derivative of temperature and mass fractions. Into the function we put the position inside the reactor *x*, the variable *y* that contains temperature *T* and mass fractions Y_i, the variable *flag* used by the solver, (not active here see help in Matlab for more information of its use), and a structured variable *R*, which contains constants that are used for the determination of the derivatives. The % in the program code mark comments.

```
*********************************************************
function dy=plugflow_reactor(x,y,flag,R)

%extract information of number of species and number of reactions from
%input data

n_species=size(R.stoic,1);        %number of species in the system
n_reactions=size(R.expo,2);       %number of reactions

%Extract input data, mass fractions in all except in the last position of the
%vector indexed 1:end-1.

Yi=y(1:end-1,1);
T=y(end);

%variables need to be initiated before they are called

dYi=zeros(size(Yi));              %initiate derivative of mass fraction
dT=0;                             %initiate temperature derivative
cp=0;                             %initiate specific heat
h=zeros(size(Yi));                %initiate enthalpy of spcies i at T


%calculate properties used to determine the derivatives

C=R.P./8.314./T;                          %Total concentration at x
Ci=C*(Yi./R.Mi/sum(Yi./R.Mi));            %Concentration of species i

%calculate enthalpy for each specie and specific heat for the mixture
for i=1:size(Yi,1)
   cp=cp+Yi(i)*polyval(R.cp(i,:),T);
   %calculate dhi by integrating cp from Tref  to T
   cp_int=[R.cp(i,:).*(1./(size(R.cp,2):-1:1)),0];
   dhi= polyval(cp_int,T)-polyval(cp_int,298);
   h(i)=R.href(i)+dhi;
end

%Reaction, calculate the reaction rate, RR [mol/m^3], without the
%stoichiometric constant for each reaction see Eq. A.21

nn= ones(1,n_reactions);

%nn is used to expand the concentration vector to a matrix with a width equal
%to the number of reactions , where all columns  are the same.
%prod(x,1) is the product and ,1 mark the direction in which the operation
%shall by performed
```

```
RR=R.kr0.*T.^R.krTex.*prod(Ci(:,nn).^R.expo,1).*exp(-R.Ea./T);

%Calculate derivative of the mass fraction according to Eq A.24 where u is
%given by Eq A.26. The stoichiometric coefficient is multiplied to the
%reaction rate for each reaction and all reaction is summarized together
%according to Eq A.21. To get the conversion rate of each specie in kg/m^3s
% the reaction rate is multiplied with the molar mass. The notation ,2 in the
%sum mark the direction of the summation

dYi= sum(RR(ones(n_species,1),:).*R.stoic,2).*R.Mi*R.Ac/R.mprick;

%Heat balance is calculated according to Eq A.23 and A.15 rewritten for
%change in temperature per unit length in the reactor instead of change
%in enthalpy

dT=(R.mprick*sum(dYi.*(-h),1)+…
R.S*(R.hm*(R.Tw-T)+R.eps*R.sigma*(R.Tw.^4-T.^4)))/cp/R.mprick;

%Lump the derivatives together into a vector according to the instruction of
%the ode solver

dy=[dYi;dT];
************************************************************
```

The function, which calculate the derivatives need a large number of input data and also a program that initiates the calculation, performs the calculation and present the result. The program that does this is here called “Calc_plugflow.m”

```
************************************************************
%Calc_plugflow
%Species { 1=O2; 2=N2; 3=H2O; 4=H2;}
%initiate variable for: mass fraction; Molar mass;
n_species=4;
R.Yi=zeros(n_species,1);R.Mi=zeros(n_species,1);


R.Yi(1)=0.21*0.032/(0.21*0.032+0.79*0.028);   R.Mi(1)=0.032;
R.Yi(2)=0.79*0.028/(0.21*0.032+0.79*0.028);   R.Mi(2)=0.028;
R.Yi(3)=0;                                    R.Mi(3)=0.018;
R.Yi(4)=R.Yi(1)*0.002/0.016;                  R.Mi(4)=0.002;

%normalize mass fractions to ingoing flow instead of to flow of air
R.Yi=R.Yi/sum(R.Yi);

%Reference enthalpy and specific heat polynomial fit of 2nd degree
% according to Appendix B12
R.href=zeros(n_species,1);R.cp=zeros(n_species,2);

%Species specific properties (here the reference enthalpy and
%specific heat is given per mole according to table in Appendix B)

R.href(1)=0;          R.cp(1,:)=[0.00349 30.5041];
R.href(2)=0;          R.cp(2,:)=[0.00307 29.2313];
R.href(3)=-242174;    R.cp(3,:)=[0.00862 32.4766];
R.href(4)=0;          R.cp(4,:)=[0.00335 27.3198];

%recalculate ethalpy and specific heat given per unit mass
```

```
R.href=R.href./R.Mi;
R.cp=R.cp./R.Mi(:,ones(1,size(R.cp,2)));

%input data
R.mprick=1;             %mass flow
R.T0=298;               %Input temperature
R.Tw=400;               %Wall temperature

R.P=100e3;              %pressure
R.hm=0;                 %heat transfer coefficient
R.sigma=5.67e-8;        %Stefan Boltzmann's constant
R.eps=0;                %emissivity

%Geometrical data (for the specific case put as arbitrary values)
R.Length=1000;          %length of tube
R.d=1;                  %diameter of tube
R.S=R.d*pi;             %perimeter of tube
R.Ac=pi*R.d^2/4;        %cross-sectional area

%Initiate data for calculation
%variable vector
y=[R.Yi;R.T0];
%start and end position of reactor
x=[0;R.Length];

%Data for reactions,
%reaction of the form dCi/dt =vi*kr0*T^n*Ca^a*Cb^b*…*exp(-E/RT)
%stoiciometric factor, vi

R.stoic =[   -1/2              1/2
             0                 0
             1                 -1
             -1                 1];

%pre-exponential factor, kr0
R.kr0  =[    1                 93770];

%temperature exponent n
R.krTex=[    0                 -1/2];

%exponent on concentration
R.expo =[    1/2               0
             0                 0
             0                 1
             1                 0];

%activation energy divided by gas constant
R.Ea   =[    0                 29840];

%calculation with the built in function ode15s

[x,y]=ode15s('plugflow_reactor',x,y,[],R);

%Extract result from the calculation
Yi=y(:,1:end-1)';
T=y(:,end)';

%plot result
```

```
subplot(2,1,1);semilogx(x,T);ylabel('tempertaure [K]')
subplot(2,1,2);semilogx(x,Yi(1,:),x,Yi(3,:),'--',x,Yi(4,:),':');
legend('O2','H2O','H2')
ylabel('mass fraction [kg_{i}/kg_{tot}]')
xlabel('Length in the plug flow reactor [m]')
**********************************************************
```

APPLICATIONS TO COMBUSTION SYSTEM MODELLING

Various combinations of continuously stirred reactors and plug-flow reactors are used to approximate more complex combustion systems. A simple illustration of this approach is shown in Fig. A.4. Here a gas-turbine combustor is modelled as two continuously-stirred reactors and a plug-flow reactor, all in series, with provisions for some recycling (recirculation) of combustion products in the first reactor, which represents the primary zone. The secondary zone and dilution zones are modelled by the second continuously-stirred reactor and the plug-flow reactor, respectively. To accurately model a real combustion device, many reactors may be required, with a judicious selection of the proportioning of the various flows into each reactor. This approach relies much on the art and craft of an experienced designer to achieve useful results. Reactor modelling approaches are often used to complement more sophisticated (finite- volume, finite-difference or finite-element) numerical models of turbine combustors, furnaces, and boilers, etc.

SUMMARY

In this chapter, two model reactors were explored: a continuously-stirred reactor, and a plug-flow reactor. A description of each of these systems was developed from fundamental con-

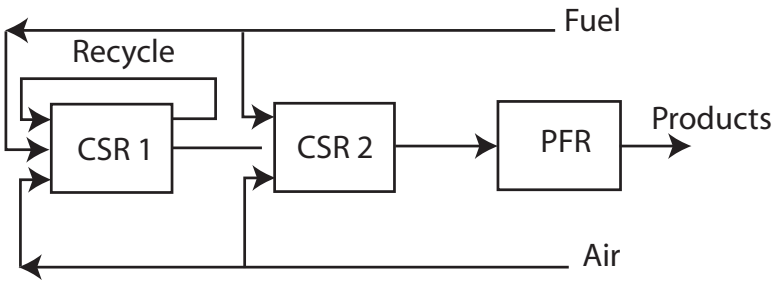

Figure A.4.
Conceptual model of gas-turbine combustor using combinations of continuously stirred (CSR) and plug-flow reactors (PFR)

servation principles and linked to chemical kinetics. One should be familiar with these principles and be able to apply them to the model reactors. With a firm grasp of these simple models, one should be in a good position to understand more complex and more rigorous analyses of combustion systems. Nevertheless, these simple models are frequently used as a first step in analyzing many real devices.

QUESTIONS

A.1 In a combustion facility there is an insulated channel between the furnace and the convection part of the combustor, which is 4 m long and has a cross-area of 2 m^2. For a given operation the flue gas flow is 20 kg/s, the temperature is 850°C and the concentration of CO is 5000 ppm at the inlet of the channel and 100 ppm at the outlet. If one assumes that the oxidation of CO follows a first order reaction, what is then the reaction rate coefficient a) if this part is considered as a plug flow and b) if it is considered as a continuously stirred? Approximate the properties of the flue gases with air.

A.2 To decrease the emissions of CO one can delay the fall of temperature by insulating the beginning of the convection passage, which has a cross-sectional area of 2 m^2. The temperature of the flue gases in this part of the combustor is 850ºC, the flow is 20 kg/s and the concentration of CO is 1% by volume. How far must the insulation be extended if the concentration of CO has to be reduced to 100 ppm? Assume that the oxidation of CO follows a first order reaction with the pre-exponential factor 10.1×10^6 1/s and the activation energy is 122500 J/mole. The properties of the flue gases can be approximated with air.

ANSWERS

A.1 a) 31.5 1/s b) 394 1/s
A.2 7.3 m

APPENDIX B

FORMULAS, PHYSICAL AND CHEMICAL PROPERTIES

Referenses

Bartok W och Sarofim A.F., Fossile Fuel Combustion, John Wiley & Sons, New York, 1991.

Flagan R.C. och Seinfeld J.H., Fundamentals of Air and Pollution Engineering, Prentice-Hall, Englewood Cliffs, 1988.

Handbook of Chemistry and Physics 58th ed., CRC Press, Florida, 1978.

Incropera F.P. och DeWitt D.P., Fundamentals of heat and mass transfer, John Wiley & Sons, New York, 1990.

Kanury A.M., Introduction to Combustion Phenomena, Gordon and Breach Science Publishers, New York, 1977.

Mörtstedt S.-E. och Hellsten G., Data och Diagram, Nordstedts Tryckeri, Stockholm, 1985.

Rose J.W. och Cooper J.R., Technical data on fuel 7th ed., The British National Committee, World Energy Conference, 1977.

NOMENCLATURE

ROMAN LETTER

A	[m^2]	area
A_{int}	[m^2/m^3]	internal surface area
a	[m^2/s]	thermal diffusivity,
b	[-]	mass transfer number
B	[-]	mass transfer number
Bi	[-]	Biot number $h_c R/k_{cs}$
c_p	[J/kg·K]	specific heat at constant pressure
c_v	[J/kg K]	specific heat at constant volume
D	[m^2/s]	diffusivity
D_{AB}	[m^2/s]	diffusivity of species *of gas par A and B*
D_i	[m^2/s]	diffusivity of species *i*,
D_{i0}	[m^2/s]	diffusivity of species *i* at STP,
d	[m]	diameter, or characteristic length
E	[J/mole]	activation energy
E'_{min}	[J]	minimum ignition energy
Fr	[-]	Froude number, u^2/gd
f	[-]	kg fuel /kg oxygen
Gr	[-]	Grashof number, $d^3\rho^2(T_w-T_\infty)g / (T_w \mu^2)$
G	[- or J/kg]	group combustion number or Gigg's free energy
G_X	[kg m / s^2]	axial trust
G_φ	[kg m^2 / s^2]	axial flux of angular momentum
g	[m/s^2]	gravity (vertical)
g_v	[-]	gas yield including excess air kg / kg fuel burned
HHV	[J/kg]	higher heating value
$\Delta H,H$	[J/kg]	heat of reaction, or (enthalpy [J/kg] in chapter 3)
HR	[-]	heat rate
h	[J/kg]	enthalpy
h_{rad}	[W/(K m^2)]	radiative heat transfer coefficient
h_c	[W/(K m^2)]	convective heat transfer coefficient
h_D	[m/s]	mass transfer coefficient
k_c	[W/(K·m)]	heat conductivity
k_r	[[]/([]s)]	reaction rate constant
$k_{r,0}$	[[]/([]s)]	pre-exponential factor
k_{rC}	[m/s]	surface reaction rate
k_{turb}	[m^2/s^2]	turbulent energy

Le	[-]	Lewis number, Sc / Pr
LHV	[J/kg]	lower heating value
ℓ_v	[-]	air demand , kg / kg fuel burned
Nu	[-]	Nusselt number, $h_c d / k_c$
n	[-]	number of mole, or order of reaction
M_i	[kg/mole]	molecular weight of species *i*
m	[kg]	mass
P	[-]	dimensionless pressure, -
p	[Pa, atm]	pressure
Pe	[-]	Peclet number, ud/a
Pr	[-]	Prandtl number, $c_p\mu / k_c$
Q	[W]	power
q	[J/s]	heat exchange,
Re	[-]	Reynolds number, ud/ν
R_c	[[]/[]s]	reaction rate
R	[m]	radius
r	[m]	radius
$\mathcal{R}$	[J/mole K]	gas constant 8.314
S	[m, J /kg K, -]	perimeter, entropy, or swirl number
Sc	[-]	Schmidt number, ν/D
Sh	[-]	Sherwood number, $h_m d/D$
T	[°C, K]	temperature,
T_{char}	[°C, K]	characteristic temperature
Th	[-]	$R(k_r/D_{eff})^{1/2}$
t	[s]	time
t_s	[s]	time for averaging
U	[- or J / kg]	dimensionless velocity, - (or internal energy in chapter 2)
u	[m/s]	gas velocity
u_{char}	[m/s]	characteristic gas velocity
u'	[m/s]	gas velocity fluctuation
V	[m^3]	volume
x	[m]	length coordinate
x_{char}	[m]	characteristic length
Y_i	[kg/kg]	mass fraction of species *i*
Y_{ichar}	[kg/kg]	characteristic mass fraction of species *i*

GREEK LETTER

Ω	[-]	stoichiometric coefficient
α	[-]	chain branching factor
β	[1/K]	volumetric expansion coefficient.
γ	[-]	expansion coefficient for the gas
η	[-]	efficiency
δ,δ_m,δ_t	[m]	boundary layer or reaction zone thickness
ε	[-]	dissipation of turbulent energy
ε_{rad}	[-]	emissivity
ε_{por}	[-]	porosity
ε_{por}	[m^2/s^3]	dissipation
λ	[m^2/s]	evaporation constant
μ	[Pa·s]	dynamic viscosity
ν_{lam}	[m^2/s]	laminar kinematic viscosity
ν_{turb}	[m^2/s]	turbulent viscosity
θ	[-]	dimensionsless temperature

ρ	[kg/m^3]	density
σ	[W/m^{2}K^4]	Stafan Boltzmann constant, 5.67×10^{-8}
τ	[s, - , -]	residence time, dimensionless time *or* tortuosity
ω_i	[-]	dimensionless mass fraction
ξ	[-]	dimensionless length coordinate, or efficiency losses
ψ	[-]	dimensionless concentration

SUPERSCRIPT

0 reference state
- average value
· per unit time
″ per unit area
‴ per unit volume

SUBSCRIPT

0 initial state (for reaction rate it is the pre-exponential factor)
s solid phase
g gas phase
f fuel
pr product

DIMENSIONLESS NUMBERS

$Ar = \frac{gd^3}{\nu^2}\frac{\rho_p - \rho_g}{\rho_g}$	Archimedes number for a sphere
B	Mass transport number
$Bi_t = \frac{h_c R}{k_c}$	Biot number (thermal)
$Bi_m = \frac{h_m R}{D_{AB,eff}}$	Biot number (mass) $D_{AB,eff} = \varepsilon_{por}^2 D_{AB}$
$Gr = \frac{x_{char}^3 h_m (T_w - T_\infty) g}{\nu^2}$	Grashof number
$Le = \frac{Sc}{\mathrm{Pr}} = \frac{k_{cg}}{\rho_g c_{p,g} D}$	Lewis number
$Nu = \frac{h_c x_{char}}{k_{cg}}$	Nusselt number
$\mathrm{Pr} = \frac{c_p \mu}{k_c}$	Prandtl number
$Pe = \frac{du}{a}$	Peclet number
$\mathrm{Re} = \frac{u x_{char}}{\nu}$	Reynolds number
$Sc = \frac{\nu}{D}$	Schmidt number
$Sh = \frac{h_m x_{char}}{D}$	Sherwood number
$Th = R\sqrt{\frac{k_r}{D_{AB,eff}}}$	Thiele-modulus

If nothing else is given, the characteristic length for flow in tubes is equal to the hydraulic diameter d_h.

$$d_h = \frac{4 \times \text{Area of cross section (tvärsnittsarea)}}{\text{Perimeter (omkrets)}}$$

HEAT AND MASS TRANSFER

Sphere:
Gas properties are taken at average temperature
- a single sphere

$$\mathrm{Nu} = 2 + 0.6\,\mathrm{Re}^{1/2}\,\mathrm{Pr}^{1/3}$$

$$\mathrm{Sh} = 2 + 0.6\,\mathrm{Re}^{1/2}\mathrm{Sc}^{1/3}$$

- in a fixed bed

$$\mathrm{Nu} = 2\varepsilon_b + 0.925\,\mathrm{Re}^{0.625}\,\mathrm{Pr}^{0.33}$$

$$\mathrm{Sh} = 2\varepsilon_b + 0.925\,\mathrm{Re}^{0.625}\mathrm{Sc}^{0.33}$$

Re is based on the velocity in a empty cross-section and ε_b is the porosity of the bed.

- in a stationary fluidised bed

$$\mathrm{Nu} = 6 + 0.117\,\mathrm{Ar}^{0.39}\,\mathrm{Pr}^{0.33}$$

$$\mathrm{Sh} = 2\varepsilon_b + 0.117\,\mathrm{Ar}^{0.39}\mathrm{Sc}^{0.33}$$

ε_b is the bed porosity.

- suspension burner

$$\mathrm{Nu} = \mathrm{Sh} = 2$$

- natural convection

$$\mathrm{Nu} = 2 + 0.6\,\mathrm{Gr}^{1/4}\,\mathrm{Pr}^{1/3}$$

$$\mathrm{Sh} = 2 + 0.6\,\mathrm{Gr}^{1/4}\mathrm{Sc}^{1/3}$$

Thermal radiation

Two (infinite) parallel plates:

$$Q = \left[\varepsilon_1^{-1} + \varepsilon_2^{-1} - 1\right]^{-1} A\sigma\left(T_1^{\,4} - T_2^{\,4}\right) = Ah_{rad}\left(T_1 - T_2\right)$$

$$h_{rad} = \left[\varepsilon_1^{-1} + \varepsilon_2^{-1} - 1\right]^{-1} \sigma\left(T_1^{\,2} + T_2^{\,2}\right)\left(T_1 + T_2\right)$$

Two concentric spheres: (the inner sphere has the index 1)

$$Q = \left[1/\varepsilon_1 + \left(1 - \varepsilon_2\right)/\varepsilon_2\left(r_1/r_2\right)^2\right]^{-1} A_1\sigma\left(T_1^{\,4} - T_2^{\,4}\right)$$

A small convex object (1) in a large room (2):

$$Q = \varepsilon_1 A_1\sigma\left(T_1^{\,4} - T_2^{\,4}\right)$$

The emissivity of the surface of a char particle is approximately 0.85.

IGNITION

Thermal ignition (spontaneous)

$$\Delta HVM_A k_{rn} C_{Acr}^n \exp\left[-E/\Re T_{cr}\right]\left(\frac{E}{\Re T_{cr}^2}\right) = h_c A$$

Forced ignition

$$E_{\min} = \frac{c_p \rho \Delta T \pi d^3}{6};$$ ΔT is the temperature rise due to combustion

$$d \propto P^{-n/2}$$

$$E_{\min} \propto P^{(2-3n)/2}$$

PREMIXED FLAMES

Laminar flame velocity

$$u_L = \left[\frac{\left(a\,\overline{\dot{m}_f'''}\right)\left(T_p - T_{ig}\right)}{\rho Y_{f,i}\left(T_{ig} - T_r\right)}\right]^{1/2}$$

$T_p \approx T_{ad}$ To evaluate the average density and average reaction rate the average temperature, $T_m = (T_p + T_{ig})/2$, and the average concentration, $C_{x,m} = (C_{x,in} + C_{x,out})/2$ are used. For a average temperature $T_m = (T_r + T_{ig})/2$ is used. $Y_{f,i}$ is the initial mass fraction.

Combustion of liquid fuels

Group combustion number,

$$G = 3\left(1 + 0.276\,\mathrm{Re}^{1/2}\,Sc^{1/2}\right) LeN^{2/3}\left(R/s\right)$$

Evaporation of a liquid droplet:

$$d^2 = {d_0}^2 - \lambda_{vap} t$$

The evaporation constant is given by:

$$\lambda_{vap} = \frac{8k_g}{\rho_F c_{p,g}} \ln\left(B+1\right); \quad B \equiv B_T \equiv B_D$$

Without combustion the mass transfer number is equal to:

$$B_T = \frac{c_{p,g}\left(T_\infty - T_s\right)}{H_{evap,eff}};\ B_D = \frac{Y_{F\infty} - Y_{Fw}}{Y_{Fw} - Y_{FR}}$$

With combustion :

$$B_T = \frac{c_{p,g}\left(T_\infty - T_s\right) + f\Delta h_i Y_{O_2,\infty}}{H_{evap,eff}}$$

The properties of the gas are taken at average temperature:

$$T_m = \left(T_\infty + T_{Fw}\right)/2$$

$$k_{c,g} = \left(k_{cF(g)}\left(T_m\right) + k_{c\infty}\left(T_m\right)\right)/2$$

$$c_{p,g} = \left(c_{pF(g)}\left(T_m\right) + c_{p,\infty}\left(T_m\right)\right)/2$$

CHEMICAL REACTORS

Continuously stirred reactor

$$\dot{m}_i''' V + \dot{m}\left(Y_{i,in} - Y_{i,out}\right) = 0 \text{ for i =1,2,…N species}$$

$$Q = A\left(h_c\left(T_{out} - T_w\right) + \varepsilon_{eff}\sigma\left(T_{out}^4 - T_w^4\right)\right) =$$
$$= \dot{m}\left(\sum_{i=1}^{N} Y_{i,out} h_i\left(T_{out}\right) - \sum_{i=1}^{N} Y_{i,in} h_i\left(T_{in}\right)\right)$$

$$\tau = \rho V / \dot{m}$$

Equimolar, isothermal and first order reaction,

$$\frac{C_{i-1} - C_i}{\tau} = C_i k_r$$

Plug flow reactor

$$\frac{dh}{dx} + \frac{\dot{Q}'' S}{\dot{m}} = 0$$

$$\frac{d\left(\rho u A\right)}{dx} = 0$$

$$\frac{dY_i}{dx} - \frac{\dot{m}_i'''}{\rho u} = 0$$

$$u = \frac{\dot{m}}{A\rho}$$

$$\tau = \int_0^x 1/u \, dx$$

Initial conditions necessary:

$$T\left(0\right) = T_0\,)$$

$$Y_i\left(0\right) = Y_{i,0} \quad i = 1,2,..., N,$$

Equimolar, isotermal and first order reaction,

$$\frac{dC_i}{d\tau} = C_i k_r$$

EQUILIBRIUM CONSTANTS

Observe! Pressure in bar (1×10^5 Pa)

Equilibrium reactions:

1 $SO_2 + ½O_2 \rightleftharpoons SO_3$
2 $½O_2 + ½N_2 \rightleftharpoons NO$
3 $½O_2 \rightleftharpoons O$
4 $½H_2 \rightleftharpoons H$
5 $½N_2 + {}^3/_2H_2 \rightleftharpoons NH_3$
6 $½N_2 \rightleftharpoons N$
7 $NO \rightleftharpoons N + O$
8 $H_2O \rightleftharpoons H_2 + ½O_2$
9 $H_2O \rightleftharpoons ½H_2 + OH$
10 $CO_2 + H_2 \rightleftharpoons CO + H_2O$
11 $CO_2 + C \rightleftharpoons 2CO$
12 $CO_2 \rightleftharpoons CO + ½O_2$
13 $2C + H_2 \rightleftharpoons C_2H_2$
14 $H_2 + CO \rightleftharpoons C + H_2O$
15 $C + 2H_2 \rightleftharpoons CH_4$
16 $CO + 2H_2 \rightleftharpoons CH_3OH$
17 $CO + 3H_2 \rightleftharpoons CH_4 + H_2O$

Coefficients for equilibrium constants of the form $K_p=c_1\ \exp(c_2/T)$

	1	2	3	4	5	6	7	8	9
c_1	1.81×10^{-5}	4.62	3083	1513	4.86×10^{-7}	4350	2.81×10^{6}	855	4613
c_2	11446	-10812	-30292	-27195	6815	-44267	-63577	-29840	-32637

	10	11	12	13	14	15	16	17
c_1	33.7	1.29×10^{9}	26900	968	2.59×10^{-8}	6.30×10^{-7}	5.70×10^{-13}	1.63×10^{-14}
c_2	-4094	-20394	-33806	-26929	16300	11819	11609	28116

Table values for $Log_{10}[K_P]$

T [K]	1	2	3	4	5	6	7	8	9	10	11	12	13	14	15	16	17
298.2	11.91	-15.04			3.70					-4.50	-20.52			16.02	11.00	4.62	27.02
400	7.68	-11.07			1.07					-2.90	-13.02			10.12	6.65	0.35	16.77
500	5.21	-8.74			-0.45					-2.02	-8.64			6.62	4.08	-2.15	10.70
600	3.57	-7.20			-1.41					-1.43	-5.69	-20.11		4.26	2.36	-3.81	6.60
700	2.37	-6.07			-2.11			-15.75	-16.60	-1.00	-3.59	-16.59	-13.73	2.59	1.12	-5.02	3.71
800	1.47	-5.11			-2.63	-20.40		-13.26	-14.06	-0.67	-1.98	-13.93	-11.63	1.31	0.20	-5.92	1.51
900	0.78	-4.58	-11.06	-9.95	-3.05	-17.70		-11.45	-12.07	-0.41	-0.74	-11.86	-10.02	0.33	-0.53	-6.63	-0.20
1000	0.22	-4.06	-9.67	-8.65	-3.34	-15.59	-21.15	-10.01	-10.50	-0.22	0.26	-10.23	-8.72	-0.48	-1.05	-7.20	-1.53
1100	-0.23	-3.62	-8.45	-7.55	-3.61	-13.80	-18.60	-8.82	-9.22	-0.07	1.08	-8.89	-7.67	-1.15	-1.49	-7.63	-2.64
1200	-0.59	-3.29	-7.46	-6.66	-3.86	-12.49	-16.52	-7.85	-8.14	0.06	1.74	-7.79	-6.78	-1.68	-1.91	-8.02	-3.59
1300	-0.92	-2.99	-6.60	-5.90	-4.05	-11.10	-14.75	-6.98	-7.22	0.17	2.30	-6.81	-6.02	-2.13	-2.24	-8.37	-4.37
1400	-1.19	-2.71	-5.91	-5.25	-4.21	-10.06	-13.29	-6.27	-6.45	0.27	2.77	-6.01	-5.40	-2.50	-2.54	-8.64	-5.06
1500	-1.42	-2.47	-5.29	-4.69	-4.35	-9.18	-11.98	-5.68	-5.78	0.35	3.18	-5.33	-4.84	-2.83	-2.79	-8.87	-5.64
1600	-1.61	-2.27	-4.75	-4.19	-4.47	-8.37	-10.81	-5.14	-5.20	0.42	3.56	-4.73	-4.35	-3.14	-3.01	-9.08	-6.15
1700	-1.81	-2.09	-4.25	-3.75	-4.59	-7.67	-9.79	-4.67	-4.66	0.48	3.89	-4.19	-3.94	-3.41	-3.20	-9.27	-6.61
1800	-1.98	-1.94	-3.83	-3.37	-4.68	-7.06	-8.93	-4.25	-4.21	0.54	4.18	-3.71	-3.56	-3.64	-3.36	-9.44	-7.00
1900	-2.11	-1.82	-3.44	-3.02	-4.76	-6.49	-8.11	-3.87	-3.79	0.59	4.45	-3.27	-3.20	-3.86	-3.51	-9.59	-7.37
2000	-2.25	-1.70	-3.10	-2.74	-4.83	-5.98	-7.40	-3.52	-3.49	0.64	4.69	-2.88	-2.88	-4.05	-3.64	-9.72	-7.69
2100	-2.37	-1.58	-2.78	-2.44	-4.89	-5.52	-6.73	-3.20	-3.07	0.69	4.91	-2.54	-2.61	-4.22	-3.75	-9.84	-7.97
2200	-2.48	-1.47	-2.53	-2.20	-4.95	-5.10	-6.12	-2.92	-2.79	0.73	5.10	-2.24	-2.37	-4.37	-3.86	-9.95	-8.23
2300	-2.57	-1.38	-2.29	-1.97	-5.01	-4.72	-5.57	-2.67	-2.52	0.76	5.27	-1.96	-2.14	-4.51	-3.96	-10.05	-8.47
2400	-2.66	-1.29	-2.06	-1.75	-5.07	-4.38	-5.07	-2.45	-2.27	0.79	5.43	-1.69	-1.92	-4.64	-4.06	-10.14	-8.70
2500	-2.75	-1.21	-1.84	-1.55	-5.12	-4.06	-4.62	-2.25	-2.03	0.82	5.58	-1.43	-1.72	-4.76	-4.15	-10.22	-8.90
2600	-2.83	-1.14	-1.63	-1.36	-5.17	-3.77	-4.19	-2.06	-1.81	0.85	5.72	-1.21	-1.53	-4.87	-4.23	-10.30	-9.10
2700	-2.90	-1.07	-1.44	-1.19	-5.21	-3.49	-3.79	-1.87	-1.60	0.87	5.84	-1.00	-1.35	-4.97	-4.30	-10.41	-9.27
2800	-2.97	-1.01	-1.26	-1.03	-5.25	-3.23	-3.42	-1.70	-1.41	0.89	5.95	-0.81	-1.18	-5.06	-4.37	-10.44	-9.43
2900	-3.03	-0.95	-1.09	-0.89	-5.29	-3.00	-3.08	-1.54	-1.24	0.91	6.05	-0.63	-1.04	-5.14	-4.43	-10.50	-9.57
3000	-3.09	-0.90	-0.93	-0.76	-5.32	-2.79	-2.77	-1.39	-1.07	0.93	6.16	-0.46	-0.91	-5.23	-4.49	-10.56	-9.72
3100	-3.14	-0.85	-0.78	-0.63	-5.36	-2.60	-2.47	-1.25	-0.92	0.95	6.25	-0.30	-0.79	-5.30	-4.55	-10.61	-9.85
3200	-3.19	-0.80	-0.63	-0.51	-5.39	-2.41	-2.19	-1.12	-0.78	0.97	6.33	-0.15	-0.68	-5.37	-4.61	-10.66	-9.98
3300	-3.24	-0.76	-0.50	-0.40	-5.42	-2.22	-1.93	-1.00	-0.64	0.99	6.41	-0.01	-0.57	-5.44	-4.66	-10.71	-10.10
3400	-3.28	-0.71	-0.38	-0.30	-5.45	-2.04	-1.69	-0.89	-0.51	1.01	6.49	0.12	-0.47	-5.50	-4.71	-10.76	-10.21
3500	-3.32	-0.67	-0.26	-0.21	-5.47	-1.86	-1.46	-0.78	-0.28	1.02	6.56	0.24	-0.37	-5.56	-4.75	-10.81	-10.31
3600	-3.36	-0.63	-0.15	-0.11	-5.49	-1.69	-1.24	-0.68	-0.26	1.03	6.63	0.35	-0.28	-5.62	-4.78	-10.85	-10.40
3700	-3.40	-0.59	-0.05	-0.02	-5.51	-1.53	-1.03	-0.58	-0.13	1.04	6.71	0.36	-0.19	-5.67	-4.81	-10.89	-10.48
3800	-3.44	-0.56	0.05	0.07	-5.53	-1.39	-0.83	-0.49	-0.04	1.05	6.78	0.56	-0.11	-5.72	-4.84	-10.93	-10.56
3900	-3.47	-0.53	0.14	0.15	-5.55	-1.26	-0.63	-0.41	0.05	1.06	6.85	0.65	-0.03	-5.78	-4.87	-10.96	-10.65
4000	-3.50	-0.50	0.23	0.23	-5.57	-1.11	-0.44	-0.33	0.13	1.07	6.91	0.74	0.05	-5.83	-4.90	-10.99	-10.73
4500	-3.65	-0.37	0.61	0.56	-5.64	-0.63	0.36	0.03	0.51	1.12	7.17	1.15	0.37	-6.05	-5.05	-11.14	-11.10
5000	-3.75	-0.28	0.86	0.81	-5.71	-0.22	0.91	0.33	0.82	1.17	7.34	1.50	0.63	-6.17	-5.19	-11.24	-11.36

REACTION CONSTANTS FOR VARIOUS REACTIONS

Reaction rate constants for one and two-step global reaction, which give best agreement between experimental and calculated explosion limits								
	One step mechanism $C_nH_m + (n+m/4)O_2 \rightarrow nCO_2 + (m/2)H_2O$				Two-step mechanism $C_nH_m + (n/2+m/4)O_2 \rightarrow nCO + (m/2)H_2O$			
FUEL	$K_{r0}\cdot10^{-6}$	$(E/\Re)\cdot10^{-3}$	**a**	**b**	$K_{r0}\cdot10^{-6}$	$(E/\Re)\cdot10^{-3}$	**a**	**b**
Methane (CH_4)	130	24.4	-0.3	1.3	2800	24.4	-0.3	1.3
Ethene (C_2H_6)	34	15.0	0.1	1.65	41	15.0	0.1	1.65
Propane (C_3H_8)	27	15.0	0.1	1.65	31	15.0	0.1	1.65
Butene (C_4H_{10})	23	15.0	0.15	1.6	27	15.0	0.15	1.6
Pentene C_5H_{12}	20	15.0	0.25	1.5	24	15.0	0.25	1.5
Hexane C_6H_{14}	18	15.0	0.25	1.5	22	15.0	0.25	1.5
Heptene C_7H_{16}	16	15.0	0.25	1.5	19	15.0	0.25	1.5
Octene C_8H_{18}	14	15.0	0.25	1.5	18	15.0	0.25	1.5
Nonane C_9H_{20}	13	15.0	0.25	1.5	16	15.0	0.25	1.5
Decane $C_{10}H_{22}$	12	15.0	0.25	1.5	14	15.0	0.25	1.5
Methanol (CH_2OH)	101	15.0	0.25	1.5	117	15.0	0.25	1.5
Ethanol (C_2H_5OH)	47	15.0	0.15	1.6	56	15.0	0.15	1.6
Benzene (C_6H_6)	6	15.0	-0.1	1.85	7	15.0	-0.1	1.85
Tolune (C_7H_8)	5	15.0	-0.1	1.85	6	15.0	-0.1	1.85
Ethylene (C_2H_4)	63	15.0	0.1	1.65	75	15.0	0.1	1.65
Propene (C_3H_6)	13	15.0	-0.1	1.85	15	15.0	-0.1	1.85
Acetylen (C_2H_2)	205	15.0	0.5	1.25	246	15.0	0.5	1.25
units: m, s, mol och K $\dot{m}''' = -k_{r0}C_f{}^a C_{O_2}{}^b \exp(-E/RT)M_f$								
Based on Flagan and Seinfeld, table 2.7 and Westbrook and Dryer 1981								

Other gases

Carbon monoxide (Howard *et al.* 1972):

$$\dot{m}''' = -k_r C_{CO} C_{O_2}{}^{½} C_{H_2O}{}^{½} M_{CO}; \qquad k_r = 1.3\cdot10^8 \exp[-15114/T]$$

Methane (continuous combustion) (Dryer et al 1972)

$$\dot{m}''' = -k_r C_{O_2}{}^{0.7} C_{CH_4}{}^{0.8} M_{CH_4}; \qquad k_r = 1.585\times10^{10} \exp[-24392/T]$$

Cyclic hydrocarbons (continuous combustion) (Siminski 1972)

$$\dot{m}''' = -k_r C_{C_nH_mO_k}^{0.5} C_{O_2} M_{C_nH_mO_k}; \qquad k_r = 20.7\times10^3 T \exp[-9650/T]$$

Nitrogen oxide (Flagan & Seinfeld):

$O + N_2 \leftrightarrow NO + N$ (1)

$O_2 + N \leftrightarrow NO + O$ (2)

$N + OH \leftrightarrow NO + H$ (3)

$k_{r+1} = 1.8\cdot10^8 \exp[-320\cdot10^3/\Re T]$ $\quad k_{r-1} = 3.8\cdot10^7 \exp[-3.5\cdot10^3/\Re T]$ [m^3/mol,s]

$k_{r+2} = 1.8\cdot10^4 \exp[-38.9\cdot10^3/\Re T]$ $\quad k_{r-2} = 3.8\cdot10^3 \exp[-173\cdot10^3/\Re T]$ [m^3/mol,s]

$k_{r+3} = 7.1\cdot10^7 \exp[-3.7\cdot10^3/\Re T]$ $\quad k_{r-3} = 1.7\cdot10^8 \exp[-204\cdot10^3/\Re T]$ [m^3/mol,s]

For low concentrations of NO, lower than the equilibrium concentration, the system of reactions can be reduced to a single reaction rate ($K_{C,O2}$ is the equilibrium constant (based on conc.) for $O_2 \leftrightarrow 2\,O$)

$$\frac{dC_{NO}}{dt} = 2k_{r+1}K_{O_2}^{1/2} C_{N_2} C_{O_2}^{1/2}$$

Solid fuels

Drying

$$t_{dry} \approx \frac{\left(m_w c_{pw} + m_{df} c_{pdf}\right)\left(373 - T_i\right) + m_w H_{evap}}{\varepsilon_{rad}\sigma A_p\left(T_b^4 - T_p^4\right) + h_c A_p\left(T_g - T_p\right)}$$

where index w is water and df is dry fuel

Kinetically controlled pyrolysis (Borman & Ragland):

$\dot{m}_v = -k_{pyr} m_v$

där $m_v = m_p - m_k - m_a$

och $k_{pyr} = k_{pyr,0} \exp\left[-E_{pyr}/\Re T\right].$

Representative pyrolysis parameters for three solid fuels.

Fuel	$k_{,pyr,0}$ (1/s)	$E_{pyr}/\Re$ (K)
Bituminous coal	280	5940
Lignite	700	5690
Wood	1.9×10^{12}	21500

Char combustion

Cases when char oxidation takes place close to particle surface

$$\frac{dm_C}{dt} = -i\left(\frac{M_C}{M_{O_2}}\right) A_p k_{rC,eff}\, \rho_{O_2,\infty}$$

where i is mole C that is consumed by one mole of O_2, and $\rho_{O2,\infty}$ is the oxygen concentration in the surrounding. The effective reaction rate is given by:

$$k_{rC,eff} = 1/\left(\left(k_{rC,0} \exp\left[-E/\Re T\right]\right)^{-1} + h_m^{-1}\right)$$

Representative global char coal oxidation rate constants. (Pomerantsev 1986)
$k_{rC,0}$ = 10^(0.2×10 $^{-4}$ E + 2) (m/s)

Fuel	**E_1 (J/mol) $C+O_2\rightarrow CO_2$**	**E_2 (J/mol) $C+½O_2\rightarrow CO$**	**E_3 (J/mol) $C+CO_2\rightarrow 2CO$**	**E_4 (J/mol) $C+H_2O\rightarrow CO+H_2$**
Char coal (char from wood)	**75000 - 84000**	**$1.1\times E_1$**	**$2.2\times E_1$**	**$1.6\times E_1$**
Peat	**84000**	**$1.1\times E_1$**	**$2.2\times E_1$**	**$1.6\times E_1$**
Lignite	**92000 - 105000**	**$1.1\times E_1$**	**$2.2\times E_1$**	**$1.6\times E_1$**
Bituminous coal	**117000 - 134000**	**$1.1\times E_1$**	**$2.2\times E_1$**	**$1.6\times E_1$**

Cases when oxidation takes place in the entire particle

$$\frac{dm_C}{dt} = -i\left(\frac{M_C}{M_{O_2}}\right) V_p A_{\text{int}} k_{rC} \rho_{O_2}$$

The internal area A_{int} is given as area per unit volume

APPROXIMATIONS FOR MIXTURES PHYSICAL PROPERTIES

Enthalpy:

$$h = \begin{cases} \sum Y_i h_i, \ h_i = [J/kg] \\ \sum X_i h_i, \ h_i = [J/mol] \end{cases}.$$

Specific heat:

$$c_p = \begin{cases} \sum Y_i c_{p,i}, \ c_{p,i} = [J/kgK] \\ \sum X_i c_{p,i}, \ c_{p,i} = [J/molK] \end{cases}.$$

Dynamic viscosity:

$$\mu_m = \sum_i \left[\frac{X_i \mu_i}{\sum_j X_j \phi_{ij}} \right]$$

where

$$\phi_{i,j} = \left[1 + \left(\mu_i/\mu_j\right)^{1/2} \left(M_j/M_i\right)^{1/4}\right]^2 \Big/ 2\sqrt{2}\left(1 + M_i/M_j\right)^{1/2} .$$

Thermal conductivity:

$$k_{c,m} = \sum_i \sum_j X_i X_j k_{ij}$$

where

$$k_{c,ij} = 2\left(k_{c,i}^{-1} + k_{c,j}^{-1}\right)^{-1}.$$

TRANSPORT PROPERTIES FOR GASES

Thermal conductivity for gases and vapours			
Gas	**$k_{c0}(T_0 = 273$ K), W/m·K**	**Gas**	**$k_{c0}(T_0 = 273$ K), W/m·K**
*Air (O_2+N_2)	$2.44 \cdot 10^{-2}$	*Helium (He)	$1.36 \cdot 10^{-1}$
*Argon (Ar)	$1.63 \cdot 10^{-2}$	Heptane (C_7H_{16})	$1.07 \cdot 10^{-2}$
Acetone (C_3H_6O)	$9.72 \cdot 10^{-3}$	Hexane (C_6H_{14})	$1.12 \cdot 10^{-2}$
Ammonia (NH_3)	$2.10 \cdot 10^{-2}$	Methane (CH_4)	$3.07 \cdot 10^{-2}$
Benzene (C_6H_6)	$9.22 \cdot 10^{-3}$	Methanol (CH_3OH)	$1.28 \cdot 10^{-2}$
Butane (C_4H_7)	$1.33 \cdot 10^{-2}$	*Nitrogen (N_2)	$2.30 \cdot 10^{-2}$
Butyl alcohol ()	$1.11 \cdot 10^{-2}$	Octan (C_8H_{18})	$9.76 \cdot 10^{-3}$
*Carbon dioxid (CO_2)	$1.51 \cdot 10^{-2}$	*Oxygene (O_2)	$2.62 \cdot 10^{-2}$
*Carbon monoxid (CO)	$2.22 \cdot 10^{-2}$	Pentane (C_5H_{12})	$1.23 \cdot 10^{-2}$
Chloroform (CH_4Cl_4)	$6.37 \cdot 10^{-3}$	Propane (C_3H_8)	$1.53 \cdot 10^{-2}$
Cyclo hexan (C_6H_{10})	$9.72 \cdot 10^{-3}$	Toluene (C_7H_8)	$1.29 \cdot 10^{-2}$
Ether ($C_4H_{10}O$)	$1.30 \cdot 10^{-2}$	Steam (H_2O)	$1.51 \cdot 10^{-2}$
Ethane (C_2H_6)	$1.89 \cdot 10^{-2}$	*Sulfur dioxid (SO_2)	$8.38 \cdot 10^{-3}$
Ethanol (C_2H_6O)	$1.29 \cdot 10^{-2}$	*Hydrogen (H_2)	$1.69 \cdot 10^{-1}$

$k_c = k_{c0}(T/T_0)^n$
n ≈ 0.94 for permanent gases (asterisked), T_{max} < 1000 °C
n ≈1.83 for condensable gases, T_{max} < 600 °C
Based on Kanury, table D.2

Dynamic viscosity and thermal conductivity for gas mixtures (T=273K)					
X_1	μ, (10^{-6}Pa·s)	k_c, (10^{-2} W/m·K)	X_1	μ, (10^{-6} Pa·s)	k_c, (10^{-2} W/m·K)
H_2 + CO_2			**H_2 + O_2 (T = 295K)**		
0.000	13.7	1.51	0.000	20.5	2.62
0.100	13.9	2.14	0.034	20.4	2.73
0.142	13.9	2.39	0.250	19.9	4.66
0.250	14.1	3.23	0.500	18.6	7.66
0.355	14.2	4.19	0.750	15.9	1.15
0.500	14.2	5.66	0.947	10.9	15.7
0.750	13.4	9.51	1.000	8.87	17.5
0.901	11.6	13.2			
1.000	8.54	16.9			
H_2 + CO			**H_2 + Ar**		
0.000	17.1	2.22	0.000	21.4	1.63
0.163	17.2	3.35	0.090	21.3	2.30
0.272	16.5	4.32	0.180	21.1	3.06
0.566	15.4	7.54	0.400	20.2	5.28
0.634	14.9	8.76	0.600	18.6	7.84
0.794	13.0	11.3	0.802	14.8	11.3
1.000	8.53	16.9	1.000	8.54	16.9
H_2 + N_2			**N_2 + Ar**		
0.000	16.9	2.30	0.000	20.9	1.61
0.159	16.7	3.35	0.204	29.4	1.75
0.390	16.0	5.32	0.359	30.6	1.86
0.652	14.5	8.13	0.611	30.4	2.05
0.795	12.9	10.6	0.780	28.6	2.20
1.000	8.53	16.9			

X_1 is molar fraction of the lighter species.
Based on Kanury, table D.3

Dynamic viscosity for some fuels		
	T	μ
	°C	**10^{-6}Pa·s**
Acetylene (C_2H_2)	0	9.35
Benzene (C_6H_6)	14.2	7.38
Ethane (C_2H_6)	0	84.8
	17.2	9.01
Hydrogen (H_2)	0	8.35
	20.7	8.76
Methane (CH_4)	0	10.26
	20	10.87
Propane (C_3H_8)	17.9	7.95

Thermal conductivity of gas mixtures					
X_1	k_c,(10^{-2} W/m,K)	X_1	k_c, (10^{-2}W/m,K)	X_1	k_c,(10^{-2}W/m,K)
He + Ar (273 K)		**H_2 + CO_2 (273 K)**		**H_2O + Air (353 K)**	
0.000	1.63	0.000	1.42	0.000	2.87
0.270	3.10	0.170	2.55	0.197	3.00
0.454	4.51	0.370	4.34	0.306	2.97
0.847	9.71	0.607	7.22	0.444	2.89
0.946	12.3	0.834	11.7	0.519	2.82
1.000	14.2	1.000	17.5	1.000	2.19
NH_3 + Air (293 K)		**H_2 + CO (273 K)**		**C_2H_2 + Air (293 K)**	
0.000	2.51	0.000	2.22	0.000	2.51
0.246	2.64	0.163	3.35	0.141	2.50
0.366	2.63	0.272	4.32	0.320	2.45
0.608	2.55	0.566	7.55	0.536	2.37
0.805	2.41	0.634	8.76	0.630	2.33
1.000	2.30	0.794	11.3	0.900	2.22
		1.000	16.9	1.000	2.19
NH_3 + CO (295 K)		**H_2 + C_2H_4 (278 K)**		**CO + Air (291 K)**	
0.000	2.41	0.000	2.21	0.000	2.50
0.220	2.50	0.170	3.61	0.108	2.49
0.338	2.53	0.314	4.81	0.321	2.47
0.620	2.49	0.514	7.09	0.562	2.44
0.790	2.44	0.611	8.64	0.978	2.38
1.000	2.33	0.865	13.8	1.000	2.38
		1.000	18.3		
CH_4 + Air (295 K)					
0.000	2.53				
0.076	2.57				
0.390	2.72				
0.700	2.88				
0.880	2.97				
1.000	2.51				

X_1 is mole fraction of the first gas. k_c is given in W/m·K
Based on Kanury, table D.4

Binary diffusion coefficients (At T_0 = 298 K and p_0 = 1 atm)			
Gas pair	**D_0, (10^{-6} m^2/sec)**	**Gas pair**	**D_0, (10^{-6} m^2/sec)**
N_2-He	71	H_2-C_4H_{10}	38
N_2-Ar	20	H_2-O_2	81
N_2-H_2	78	H_2-CO	75
N_2-O_2	22	H_2-CO_2	65
N_2-CO	22	H_2-CH_4	73
N_2-CO_2	16	H_2-C_2H_4	60
N_2-H_2O	24	H_2-C_2H_6	54
N_2-C_2H_4	16	H_2-H_2O	99
N_2-C_2H_6	15	H_2-Br_2	58
N_2-nC_4H_{10}	10	H_2-C_6H_6	34
CO_2-O_2	18	Air-H_2	63
CO_2-CO	14	Air-O_2	18
CO_2-C_2H_4	15	Air-CO_2	14
CO_2-CH_4	15	Air-H_2O	23
CO_2-H_2O	19	Air-CS_2	10
CO_2-C_3H_8	9	Air Ether	8
CO_2-CH_3OH	9	Air-CH_3OH	11
CO_2-C_6H_6	6	Air-C_6H_6	8
O_2-C_6H_6	7	H_2O-CH_4	28
O_2-CO	21	H_2O-C_2H_4	20
CO-C_2H_4	13	H_2O-O_2	27

$D = D_0(T/T_0)^m(p_0/p)$
$m \approx 1.75$ for permanent gases
$m \approx 2.00$ for condensable gases
Based on Kanury, table D.5 and A. A. Westenberg, Combustion and Flame, **1,** p. 346 (1957).

SPECIFIC HEAT

Approximate thermochemical data for combustion related species					
Specie	**Name**	**$\Delta h_f°$ (298 K) (J/mol)**	**s^o(298 K) (J/mol,K)**	**c_p = a + bT (J/mol,K)**	
				a	**b**
C	Coal, monatomic	716033	158.215	20.5994	0.00026
C (*s*)	Graphite (ref.)	0	5.694	14.926	0.00437
CH	Methylidine	594983	183.187	27.6451	0.00521
CH_2	Methylene	385775	181.302	35.5238	0.01000
CH_3	Methyl	145896	194.337	42.8955	0.01388
CH_4	Methane	-74980	186.413	44.2539	0.02273
CN	Cyano	435762	202.838	28.2979	0.00469
CO	Carbon monoxide	-110700	197.810	29.6127	0.00301
COS	Carbonyl sulphide	-138605	231.804	47.6042	0.00659
CO_2	Carbon dioxide	-394088	213.984	44.3191	0.00730
C_2H	CCH radical	447662	207.615	40.4732	0.00880
C_2H_2	Acetylene	227057	201.137	51.7853	0.01383
C_2H_4	Ethylen	52543	219.540	60.2440	0.02637
C_2H_4O	Ethyleneoxide	-52710	243.272	70.1093	0.03319
C_2N_2	Cyanogen	309517	241.810	63.7996	0.00913
H	Hydrogen, monatomic	218300	114.773	20.7859	0
HCHO	Formaldehyde	-116063	218.970	43.3037	0.01465
HCN	Hydrogen cyanide	135338	202.000	38.9985	0.00885
HCO	Formyl	-12151	245.882	37.3667	0.00766
HNO	Nitroxyl hydride	99722	220.935	38.2143	0.00750
HNO_2	Nitrous acid, *cis*-	-76845	249.666	54.0762	0.01100
HNO_2	Nitrious acid, *trans*-	-78940	249.498	54.5058	0.01075
HNO_3	Nitric acis vapour	-134499	266.749	68.1195	0.01549
HO_2	Hydroperoxyl	20950	227.865	38.3843	0.00719
H_2	Hydrogen (ref.)	0	130.770	27.3198	0.00335
$H_2O_{(l)}$	Water	-285830	69.950	75.288	0.00658
H_2O	Water vapour	-242174	188.995	32.4766	0.00862
H_2O_2	Hydrogen peroxid	-136301	232.965	41.6720	0.01952
H_2S	Hydrogen sulfide	-20447	205.939	35.5142	0.00883
H_2SO_4	Sulfuric acid vapour	-741633	289.530	101.7400	0.02143
H_2SO_4	Sulfuric acid liquid	-815160	157.129	144.0230	0.02749
N	Nitrogen, monatomic	473326	153.413	20.7440	0.00004
NH	Imidogen	339392	181.427	28.0171	0.00349
NH_2	Amidogen	167894	194.785	33.5349	0.00837
NH_3	Ammoniak	-45965	192.866	38.0331	0.01593
NO	Nitrogen oxide	90421	210.954	30.5843	0.00278
NO_2	Nitrogen dioxide	33143	240.255	43.7014	0.00575
NO_3	Nitrogen trioxide	71230	253.077	61.1847	0.00932
N_2	Nitrogen (ref.)	0	191.777	29.2313	0.00307
N_2H	Dimide	213272	218.719	43.2755	0.01466
N_2O	Nitrius oxide, (lustgas)	82166	220.185	44.9249	0.00693
N_2O_5	Dinitrogen pentoxide	11313	346.933	122.4940	0.01018
O	Oxygen, monatomict	249553	161.181	21.2424	-0.0002
OH	Hydroxyl	39520	183.858	28.0743	0.00309
O_2	Oxygen (ref.)	0	205.310	30.5041	0.00349
T in Kelvin Based on Flagan and Seinfeld, table 2.5					

Thermochemical data for Nitrogen (N_2)

Ideal gas, mole mass 28.0134×10^{-3} kg/mole

T_r = 298.15 K, Standard state pressure = p =0.1 MPa

T	C_p^0	S^0	$-[G_0-H_0(T_r)]/T$	$H^0-H^0(T_r)$	$\Delta_f H^0$	$\Delta_f G^0$	Log K_f
K	*J/mole•K*	*J/mole•K*	*J/mole•K*	*kJ/mole*	*kJ/mole*		
0	0	0	INFINITE	-8.670	0	0	0
100	29.104	159.811	217.490	-5.768	0	0	0
200	29.107	179.985	194.272	-2.857	0	0	0
298.15	29.111	191.609	191.609	0	0	0	0
300	29.124	191.789	191.610	0.054	0	0	0
400	29.125	200.181	192.753	2.971	0	0	0
500	29.165	206.739	194.917	5.911	0	0	0
600	29.249	212.176	197.353	8.894	0	0	0
700	29.387	216.866	199.813	11.937	0	0	0
800	29.580	221.017	202.209	15.046	0	0	0
900	30.110	224.757	204.510	18.223	0	0	0
1000	30.754	228.170	206.708	21.463	0	0	0
1100	31.433	231.313	208.804	24.760	0	0	0
1200	32.090	234.226	210.802	28.109	0	0	0
1300	32.697	236.943	212.710	31.503	0	0	0
1400	33.241	239.487	214.533	34.936	0	0	0
1500	33.723	241.880	216.277	38.405	0	0	0
1600	34.147	244.138	217.948	41.904	0	0	0
1700	35.378	246.275	219.552	45.429	0	0	0
1800	35.600	248.304	221.094	48.978	0	0	0
1900	35.796	250.234	222.577	52.548	0	0	0
2000	35.971	252.074	224.006	56.137	0	0	0
2100	36.126	253.833	225.385	59.742	0	0	0
2200	36.268	255.517	226.717	63.361	0	0	0
2300	36.395	257.132	228.004	66.995	0	0	0
2400	36.511	258.684	229.250	70.640	0	0	0
2500	36.616	260.176	230.458	74.296	0	0	0
2600	36.713	261.614	231.629	77.963	0	0	0
2700	36.801	263.001	232.765	81.639	0	0	0
2800	36.883	264.341	233.869	85.323	0	0	0
2900	36.959	265.637	234.942	89.015	0	0	0
3000	37.030	266.891	235.986	92.715	0	0	0
3100	37.096	268.106	237.003	96.421	0	0	0
3200	37.158	269.285	237.993	100.134	0	0	0
3300	37.216	270.429	238.959	103.852	0	0	0
3400	37.271	271.541	239.901	107.577	0	0	0
3500	37.323	272.622	240.821	111.306	0	0	0
3600	37.373	273.675	241.719	115.041	0	0	0
3700	37.420	274.699	242.596	118.781	0	0	0
3800	37.465	275.698	243.454	122.525	0	0	0
3900	37.508	276.671	244.294	126.274	0	0	0
4000	37.550	276.620	245.115	130.027	0	0	0

Taken from Per-Erik Bengtsson, 2002

Thermochemical data for Oxygen (O_2)

Ideal gas, molar mass 31.9988×10^{-3} kg/mole,

T_r= 298.15 K, Standard state pressure = p=0.1 MPa

T	C_p^0	S^0	$-[G_0-H_0(T_r)]/T$	$H^0-H^0(T_r)$	$\Delta_f H^0$	$\Delta_f G^0$	Log K_f
K	*J/mole•K*	*J/mole•K*	*J/mole•K*	*kJ/mole*	*kJ/mole*	*kJ/mole*	
0	0	0	INFINITE	-8.683	0	0	0
100	29.106	173,307	231,094	-5,779	0	0	0
200	29.126	193,485	207,823	-2.868	0	0	0
298.15	29.376	205,147	205,147	0	0	0	0
300	29.385	205,329	205,148	0.054	0	0	0
400	30.106	213,871	206,638	3,025	0	0	0
500	31.091	220,693	208,524	6,084	0	0	0
600	32.090	226,451	211,044	9,244	0	0	0
700	32.981	231,466	213,611	12,499	0	0	0
800	33.733	235,921	216,126	15,835	0	0	0
900	34.355	239,931	218,552	19,241	0	0	0
1000	34.870	243,578	220,875	22,703	0	0	0
1100	35.300	246,922	223,093	26,212	0	0	0
1200	35.667	250,010	225,209	29,761	0	0	0
1300	35.988	252,878	227,229	33,344	0	0	0
1400	36.277	255,556	229,158	36.597	0	0	0
1500	36.544	258,068	231,002	40,599	0	0	0
1600	36.796	260,434	232,768	44,266	0	0	0
1700	37.040	262,672	234,462	47,958	0	0	0
1800	37.277	264,796	236,089	51,673	0	0	0
1900	37.510	266,818	237,653	55,413	0	0	0
2000	37.741	268,748	239,160	59,175	0	0	0
2100	37.969	270,595	240,613	62,961	0	0	0
2200	38.195	272,366	242,017	66,769	0	0	0
2300	38.419	274,069	243,374	70,600	0	0	0
2400	38.639	275,709	244,687	74,453	0	0	0
2500	38.856	277,290	245,959	78,328	0	0	0
2600	39.068	278,819	247,194	82,224	0	0	0
2700	39.276	280,297	248,393	86,141	0	0	0
2800	39.478	281,729	249,558	90,079	0	0	0
2900	39.674	283,118	250,691	94,036	0	0	0
3000	39.864	284,466	251,795	98,013	0	0	0
3100	40.048	285,776	252,870	102,009	0	0	0
3200	40.225	287,050	253,918	106,023	0	0	0
3300	40.395	288,291	254,941	110,054	0	0	0
3400	40.559	2898,499	255,940	114,102	0	0	0
3500	40.716	290,677	256,916	118,165	0	0	0
3600	40.868	291,826	257,870	122,245	0	0	0
3700	41.013	292,948	258,802	126,339	0	0	0
3800	41.154	294,044	259,716	130,447	0	0	0
3900	41.289	295,115	260,610	134,569	0	0	0
4000	41.421	296.162	261,485	138,705	0	0	0

Taken from Per-Erik Bengtsson, 2002

Thermochemical data for Hydrogen (H_2)

Ideal gas, mole mass 2.01588×10^{-3} kg/mole

T_r= 298.15 K, Standard state pressure = p=0.1 MPa

T	C_p^0	S^0	$-[G_0-H_0(T_r)]/T$	$H^0-H^0(T_r)$	$\Delta_f H^0$	$\Delta_f G^0$	Log K_f
K	*J/mole•K*	*J/mole•K*	*J/mole•K*	*kJ/mole*	*kJ/mole*	*kJ/mole*	
0	0	0	INFINITE	-8.467	0	0	0
100	28.154	100.727	155.408	-5.468	0	0	0
200	27.447	119.412	133.284	-2.774	0	0	0
298.15	28.836	130.680	130.680	0	0	0	0
300	28.849	130.858	130.680	0.053	0	0	0
400	29.181	139.216	131.817	2.959	0	0	0
500	29.260	145.737	133.973	5.882	0	0	0
600	29.327	151.077	136.392	8.811	0	0	0
700	29.441	155.606	138.822	11.749	0	0	0
800	29.624	159.548	141.171	14.702	0	0	0
900	29.881	163.051	143.411	17.676	0	0	0
1000	30.205	166.216	145.536	20.680	0	0	0
1100	30.581	169.112	147.549	23.719	0	0	0
1200	30.992	171.790	149.459	26.797	0	0	0
1300	31.423	174.288	151.274	29.918	0	0	0
1400	31.861	176.633	153.003	33.082	0	0	0
1500	32.298	178.846	154.652	36.290	0	0	0
1600	32.725	180.944	156.231	39.541	0	0	0
1700	33.139	182.940	157.743	42.835	0	0	0
1800	33.537	184.846	159.197	46.169	0	0	0
1900	33.917	186.669	160.595	49.541	0	0	0
2000	34.280	188.418	161.943	52.951	0	0	0
2100	34.624	190.099	163.244	56.397	0	0	0
2200	34.952	191.718	164.501	59.876	0	0	0
2300	35.263	193.278	165.719	63.387	0	0	0
2400	35.559	194.785	166.899	66.928	0	0	0
2500	35.842	196.243	168.044	70.498	0	0	0
2600	36.111	197.654	169.155	74.096	0	0	0
2700	36.370	199.021	170.236	77.720	0	0	0
2800	36.618	200.349	171.288	81.369	0	0	0
2900	36.856	201.638	172.313	85.043	0	0	0
3000	37.087	202.891	173.311	88.740	0	0	0
3100	37.311	204.111	174.285	92.460	0	0	0
3200	37.528	205.299	175.236	96.202	0	0	0
3300	37.740	206.457	176.164	99.966	0	0	0
3400	37.946	207.587	177.072	103.750	0	0	0
3500	38.149	208.690	177.960	107.555	0	0	0
3600	38.348	209.767	178.828	111.380	0	0	0
3700	38.544	210.821	179.679	115.224	0	0	0
3800	38.738	211.851	180.512	119.089	0	0	0
3900	38.928	212.860	181.328	122.972	0	0	0
4000	39.116	213.848	182.129	126.874	0	0	0

Taken from Per-Erik Bengtsson, 2002

Thermochemical data for Carbon monoxide (CO)

Ideal gas, mole mass 28.0104×10^{-3} kg/mole

T_r = 298.15 K, Standard state pressure = p=0.1 MPa

T	C_p^0	S^0	$-[G_0-H_0(T_r)]/T$	$H^0-H^0(T_r)$	$\Delta_f H^0$	$\Delta_f G^0$	Log K_f
K	*J/mole•K*	*J/mole•K*	*J/mole•K*	*kJ/mole*	*kJ/mole*	*kJ/mole*	
0	0	0	INFINITE	-8.671	-113.805	-113.805	INFINITE
100	29.104	165.850	223.539	-5.769	-112.415	-120.239	62.807
200	29.108	186.025	200.317	-2.858	-111.286	-128.526	33.568
298.15	29.142	197.653	197.653	0	-110.527	-137.163	24.030
300	29.142	197.833	197.653	0.054	-110.516	-137.328	23.911
400	29.342	206.238	198.798	2.976	-110.102	-146.338	19.110
500	29.794	212.831	200.968	5.931	-110.003	-155.414	16.236
600	30.443	218.319	203.415	8.942	-110.150	-164.486	14.320
700	31.171	223.066	205.890	12.023	-110.469	-173.518	12.948
800	31.899	227.277	208.305	15.177	-110.905	-182.497	11.916
900	32.577	231.074	210.628	18.401	-111.418	191.416	11.109
1000	33.183	234.538	212.848	21.690	-111.983	-200.275	10.461
1100	33.710	237.726	214.967	25.035	-112.586	-209.075	9.928
1200	34.175	240.679	216.988	28.430	-113.217	-217.819	9.481
1300	34.572	243.431	218.917	31.868	-113.870	-226.509	9.101
1400	34.920	246.06	220.761	35.343	-114.541	-235.149	8.774
1500	35.217	248.426	222.526	38.850	-115.229	-243.740	8.488
1600	35.480	250.707	224.216	42.385	-115.933	-252.284	8.236
1700	35.710	252.865	225.839	45.945	-116.651	-260.784	8.013
1800	35.911	254.912	227.398	49.526	-117.384	-269.242	7.813
1900	36.091	256.859	228.897	53.126	-118.133	-277.658	7.633
2000	36.250	258.714	230.342	56.744	-118.896	-286.034	7.470
2100	36.392	260.486	231.736	60.376	-119.675	-294.372	7.322
2200	36.518	262.182	233.081	64.021	-120.470	-302.672	7.186
2300	36.635	263.809	234.382	67.683	-121.278	-310.936	7.062
2400	36.740	265.359	235.641	71.324	-122.133	-319.164	6.946
2500	36.836	266.854	236.860	74.985	-122.994	-327.356	6.840
2600	36.924	268.300	238.041	78.673	-123.854	-335.514	6.741
2700	37.003	269.695	239.188	82.369	-124.731	-343.638	6.648
2800	37.083	271.042	240.302	86.074	-125.623	-351.729	6.562
2900	37.150	272.345	241.384	89.786	-126.532	-359.789	6.480
3000	37.217	273.605	242.437	93.504	-127.457	-367.816	6.404
3100	37.279	274.827	243.463	97.229	-128.397	-375.812	6.332
3200	37.338	276.011	244.461	100.960	-129.353	-383.778	6.265
3300	37.392	277.161	245.435	104.696	-130.325	-391.714	6.200
3400	37.443	278.278	246.385	108.438	-131.312	-399.620	6.139
3500	37.493	279.364	247.311	112.185	-132.313	-407.497	6.082
3600	37.543	280.421	248.216	115.937	-133.329	-415.345	6.027
3700	37.589	281.450	249.101	119.693	-134.360	-423.165	5.974
3800	37.631	282.453	249.965	123.454	-135.405	-430.956	5.924
3900	37.673	283.431	250.811	127.219	-136.464	-438.720	5.876
4000	37.715	284.386	251.638	130.989	-137.537	-446.457	5.830

Taken from Per-Erik Bengtsson, 2002

Thermochemical data for Nitrogen monoxide (NO)

Ideal gas, mole mass 28.0104×10^{-3} kg/mole

T_r = 298.15 K, Standard state pressure = p =0.1 MPa

T	C_p^0	S^0	$-[G_0-H_0(T_r)]/T$	$H^0-H^0(T_r)$	$\Delta_f H^0$	$\Delta_f G^0$	Log K_f
K	*J/mole•K*	*J/mole•K*	*J/mole•K*	*kJ/mole*	*kJ/mole*	*kJ/mole*	
0	0	0	INFINITE	-9.192	89.775	89.775	INFINITE
100	32.302	177.031	237.757	-6.073	89.991	88.994	-46.460
200	30.420	198.747	213.501	-2.951	90.202	87.800	-22.931
298.15	29.845	210.758	210.758	0	90.291	86.600	-15.172
300	29.841	210.943	210.759	0.055	90.292	86.577	-15.074
400	29.944	219.529	211.929	3.040	90.332	85.331	-11.143
500	30.486	226.263	214.145	6.059	90.352	84.079	-8.784
600	31.238	231.886	216.646	9.144	90.366	82.822	-7.210
700	32.028	236.761	219.179	12.307	90.381	81.564	-6.086
800	32.767	241.087	221.652	15.548	90.398	80.303	-5.243
900	33.422	244.985	224.031	18.858	90.417	79.041	-4.587
1000	33.987	248.536	226.307	22.229	90.437	77.775	-4.063
1100	34.468	251.799	228.478	25.653	90.457	76.508	-3.633
1200	34.877	254.816	230.549	29.120	90.476	75.239	-3.275
1300	35.226	257.621	232.525	32.626	90.493	73.969	-2.972
1400	35.524	260.243	234.412	36.164	90.508	72.697	-2.712
1500	35.780	262.703	236.217	39.729	90.518	71.425	-2.487
1600	36.002	265.019	237.945	43.319	90.525	70.151	-2.290
1700	36.195	267.208	239.603	46.929	90.526	68.878	-2.116
1800	36.364	269.282	241.195	50.557	90.522	67.605	-1.962
1900	36.514	271.252	242.725	54.201	90.511	66.332	-1.824
2000	36.647	273.128	244.199	57.859	90.494	65.060	-1.699
2100	36.767	274.919	245.619	61.530	90.469	63.788	-1.587
2200	36.874	276.632	246.990	65.212	90.438	62.519	-1.484
2300	36.971	278.273	248.315	68.904	90.398	61.251	-1.391
2400	37.060	279.849	249.596	72.606	90.350	59.984	-1.306
2500	37.141	281.363	250.837	76.316	90.295	58.720	-1.227
2600	37.216	282.822	252.039	80.0334	90.231	57.458	-1.154
2700	37.285	284.227	253.205	83.759	90.160	56.199	-1.087
2800	37.350	285.585	254.338	87.491	90.081	54.943	-1.025
2900	37.410	286.896	255.438	91.229	89.994	53.689	-0.967
3000	37.466	288.165	256.508	94.973	89.899	52.439	-0.913
3100	37.519	289.395	257.549	98.722	89.798	51.192	-0.863
3200	37.570	290.587	258.563	102.477	89.689	49.948	-0.815
3300	37.617	291.744	259.551	106.236	89.574	48.708	-0.771
3400	37.663	292.867	260.514	110.000	89.451	47.472	-0.729
3500	37.706	293.960	261.454	113.768	89.323	46.239	-0.690
3600	37.747	295.022	262.372	117.541	89.189	45.010	-0.653
3700	37.787	296.057	263.269	121.318	89.049	43.784	-0.618
3800	37.825	297.065	264.145	125.098	88.903	42.563	-0.585
3900	37.862	298.048	265.902	128.883	88.752	41.346	-0.554
4000	37.898	299.008	265.840	132.671	88.596	40.132	-0.524

Taken from Per-Erik Bengtsson, 2002

Thermochemical data for carbon dioxide (CO_2)
Ideal gas, mole mass 44.0098×10^{-3} kg/mole
T_r = 298.15 K, Standard state pressure = p =0.1 MPa

T	C_p^0	S^0	$-[G_0-H_0(T_r)]/T$	$H^0-H^0(T_r)$	$\Delta_f H^0$	$\Delta_f G^0$	Log K_f
K	*J/mole•K*	*J/mole•K*	*J/mole•K*	*kJ/mole*	*kJ/mole*	*kJ/mole*	
0	0	0	INFINITE	-9.364	-393.151	-393.151	INFINITE
100	29.208	179.009	243.568	-6.456	-393.208	-393.683	205.639
200	32.359	199.975	217.046	-3.414	-393.404	-394.085	102.924
298.15	37.129	213.795	213.795	0	-393.522	-394.389	69.095
300	37.221	214.025	213.795	0.069	-393.523	-394.394	68.670
400	41.325	225.314	215.307	4.003	-393.583	-394.675	51.539
500	44.627	234.901	218.290	8.305	-393.666	-394.939	41.259
600	47.321	243.283	221.772	12.907	-393.803	-395.182	34.404
700	49.564	250.750	225.388	17.754	-393.983	-395.398	29.505
800	51.434	257.494	228.986	22.806	-394.168	-395.586	25.829
900	52.999	263.645	232.500	28.030	-394.405	-395.748	22.969
1000	54.308	269.299	235.901	33.397	-394.623	-395.886	20.679
1100	55.409	274.528	239.178	38.884	-394.838	-396.001	18.805
1200	56.342	279.390	242.329	44.473	-395.050	-396.098	17.242
1300	57.137	283.932	245.356	50.148	-395.257	-396.177	15.919
1400	57.802	288.191	248.265	55.896	-395.462	-396.240	14.784
1500	58.379	292.199	251.062	61.705	-395.668	-396.288	13.800
1600	58.886	295.983	253.753	67.569	-395.876	-396.323	12.939
1700	59.317	299.566	256.343	73.480	-396.090	-396.344	12.178
1800	59.701	302.968	258.840	79.431	-396.311	-396.353	11.502
1900	60.049	306.205	261.248	85.419	-396.542	-396.349	10.896
2000	60.350	309.293	263.574	91.439	-396.784	-396.333	10.351
2100	60.622	312.244	265.822	97.488	-397.039	-396.304	9.858
2200	60.865	315.070	267.996	103.562	-397.309	-396.262	9.408
2300	61.086	317.781	270.102	109.660	-397.596	-396.209	8.998
2400	61.287	320.385	272.144	115.779	-397.900	-396.142	8.622
2500	61.471	322.890	274.124	121.917	-398.222	-396.062	8.275
2600	61.647	325.305	276.046	128.073	-398.562	-395.969	7.955
2700	61.802	327.634	277.914	134.246	-398.921	-395.862	7.658
2800	61.952	329.885	279.730	140.433	-399.299	-395.742	7.383
2900	62.095	332.061	281.497	146.636	-399.695	-395.609	7.126
3000	62.229	334.169	283.218	152.852	-400.111	-395.461	6.886
3100	62.347	336.211	284.895	159.081	-400.545	-395.298	6.661
3200	62.462	338.192	286.529	165.321	-400.998	-395.122	6.450
3300	62.573	340.116	288.124	171.573	-401.470	-394.932	6.251
3400	62.681	341.986	289.681	177.836	-401.960	-394.726	6.064
3500	62.785	343.804	291.202	184.109	-402.467	-394.506	5.888
3600	62.884	345.574	292.687	190.393	-402.991	-394.271	5.721
3700	62.980	347.299	294.140	196.686	-403.532	-394.022	5.563
3800	63.074	348.979	295.561	202.989	-404.089	-393.756	5.413
3900	63.166	350.619	296.952	209.301	-404.662	-393.477	5.270
4000	63.254	352.219	298.314	215.622	-405.521	-393.183	5.134

Taken from Per-Erik Bengtsson, 2002

Thermochemical data for water (H_2O)

Ideal gas, mole mass 18.01528×10^{-3} kg/mole

T_r = 298.15 K, Standard state pressure = p =0.1 MPa

T	C_p^0	S^0	$-[G_0-H_0(T_r)]/T$	$H^0-H^0(T_r)$	$\Delta_f H^0$	$\Delta_f G^0$	Log K_f
K	*J/mole•K*	*J/mole•K*	*J/mole•K*	*kJ/mole*	*kJ/mole*	*kJ/mole*	
0	0	0	INFINITE	-9.904	-238.921	-238.921	INFINITE
100	33.299	152.388	218.534	-6.615	-240.083	-236.584	123.579
200	33.349	175.485	191.896	-3.282	-240.900	-232.766	60.792
298.15	33.590	188.834	188.834	0	-241.826	-228.582	40.047
300	33.596	189.042	188.835	0.062	-241.844	-228.500	39.785
400	34.262	198.788	190.159	3.452	-242.846	-223.901	29.238
500	35.226	206.534	192.685	6.925	-243.826	-219.051	22.884
600	36.325	213.052	195.550	10.501	-244.758	-214.007	18.631
700	37.495	218.739	198.465	14.192	-245.632	-208.612	15.582
800	38.721	223.825	201.322	18.002	-246.443	-203.496	13.287
900	39.987	228.459	204.084	21.938	-247.185	-198.083	11.496
1000	41.268	232.738	206.738	26.000	-247.857	-192.590	10.060
1100	42.536	236.731	209.285	30.191	-248.460	-187.033	8.881
1200	43.768	240.485	211.730	34.506	-248.997	-181.425	7.897
1300	44.945	244.035	214.080	38.942	-249.473	-175.774	7.063
1400	46.054	247.407	216.341	43.493	-249.894	-170.089	6.346
1500	47.090	250.620	218.520	48.151	-250.265	-164.376	5.724
1600	48.050	253.690	220.623	52.908	-250.592	-158.639	5.179
1700	48.935	256.630	222.655	57.758	-250.881	-152.883	4.698
1800	49.749	259.451	224.621	62.693	-251.138	-147.111	4.269
1900	50.496	262.161	226.526	67.706	-251.368	-141.325	3.885
2000	51.180	264.769	228.374	72.790	-251.575	-135.528	3.540
2100	51.823	267.282	230.167	77.941	-251.762	-129.721	3.227
2200	52.408	269.706	231.909	83.153	-251.934	-123.905	2.942
2300	52.947	272.048	233.604	88.421	-252.092	-118.082	2.682
2400	53.444	274.312	235.253	93.741	-252.239	-112.252	2.443
2500	53.904	276.503	236.860	99.108	-252.379	-106.416	2.223
2600	54.329	278.625	238.425	104.520	-252.513	-100.575	2.021
2700	54.723	280.683	239.952	109.973	-252.643	-94.729	1.833
2800	55.089	282.680	241.443	115.464	-252.771	-88.878	1.658
2900	55.430	284.619	242.899	120.990	-252.897	-83.023	1.495
3000	55.748	286.504	244.321	126.549	-253.024	-77.163	1.344
3100	56.044	288.337	245.711	132.139	-253.152	-71.298	1.201
3200	56.323	290.120	247.071	137.757	-253.282	-65.430	1.068
3300	56.583	291.858	248.402	143.403	-253.416	-59.558	0.943
3400	56.828	293.550	249.705	149.073	-253.553	-53.681	0.825
3500	57.058	295.201	250.982	154.768	-253.696	-47.801	0.713
3600	57.276	296.812	252.233	160.485	-253.844	-41.916	0.608
3700	57.480	298.384	253.459	166.222	-253.997	-36.027	0.509
3800	57.675	299.919	254.661	171.980	-254.158	-30.133	0.414
3900	57.859	301.420	255.841	177.757	-254.326	-24.236	0.325
4000	58.033	302.887	256.999	183.552	-254.501	-18.334	0.239

Taken from Per-Erik Bengtsson, 2002

Thermochemical data for methane (CH_4)

Ideal gas, mole mass16.04276×10^{-3} kg/mole

T_r = 298.15 K, Standard state pressure = p =0.1 MPa

T	C_p^0	S^0	$-[G_0-H_0(T_r)]/T$	$H^0-H^0(T_r)$	$\Delta_f H^0$	$\Delta_f G^0$	Log K_f
K	*J/mole•K*	*J/mole•K*	*J/mole•K*	*kJ/mole*	*kJ/mole*	*kJ/mole*	
0	0	0	INFINITE	-10.024	-66.911	-66.911	INFINITE
100	33.258	149.500	216.485	-6.698	-69.644	-64.353	33.615
200	33.473	172.577	189.418	-3.368	-72.027	-58.161	15.190
298.15	35.639	186.251	186.251	0	-74.873	-50.768	8.894
300	35.708	186.472	186.252	0.066	-74.929	-50.618	8.813
400	40.500	197.356	187.704	3.861	-77.969	-42.054	5.492
500	46.342	207.014	190.614	8.200	-80.802	-32.741	3.420
600	52.227	215.987	194.103	13.130	-83.308	-22.887	1.993
700	57.794	224.461	197.840	18.635	-85.452	-12.643	0.943
800	62.932	232.518	201.675	24.675	-87.238	-2.115	0.138
900	67.601	240.205	205.532	31.205	-88.692	8.616	-0.500
1000	71.795	247.549	209.370	38.179	-89.849	19.492	-1.018
1100	75.529	254.570	213.162	45.549	-90.750	30.472	-1.447
1200	78.833	261.287	216.895	53.270	-91.437	41.524	-1.807
1300	81.744	267.714	220.558	61.302	-91.945	52.626	-2.115
1400	84.305	273.868	224.148	69.608	-92.308	63.761	-2.379
1500	86.556	279.763	227.660	78.153	-92.553	74.918	-2.609
1600	88.537	285.413	231.095	86.910	-92.703	86.088	-2.810
1700	90.283	290.834	234.450	95.853	-92.780	97.265	-2.989
1800	91.824	296.039	237.728	104.960	-92.797	108.445	-3.147
1900	93.188	301.041	240.930	114.212	-92.770	119.624	-3.289
2000	94.399	305.853	244.057	123.592	-92.709	130.802	-3.416
2100	95.477	310.485	247.110	133.087	-92.624	141.975	-3.531
2200	96.439	314.949	250.093	142.684	-92.521	153.144	-3.636
2300	97.301	319.255	253.007	152.371	-92.409	164.308	-3.732
2400	98.075	323.413	255.854	162.141	-92.291	175.467	-3.819
2500	98.772	327.431	258.638	171.984	-92.174	186.622	-3.899
2600	99.401	331.317	261.359	181.893	-92.060	197.771	-3.973
2700	99.971	335.080	264.020	191.862	-91.954	208.916	-4.042
2800	100.489	338.725	266.623	201.885	-91.857	220.058	-4.105
2900	100.960	342.260	269.171	211.958	-91.773	231.196	-4.164
3000	101.389	345.690	271.664	222.076	-91.705	242.332	-4.219
3100	101.782	349.021	274.106	232.235	-91.653	253.465	-4.271
3200	102.143	352.258	276.498	242.431	-91.621	264.598	-4.319
3300	102.474	355.406	278.842	252.662	-91.609	275.730	-4.364
3400	102.778	358.470	281.139	262.925	-91.619	286.861	-4.407
3500	103.060	361.453	283.391	273.217	-91.654	297.993	-4.447
3600	103.319	364.360	285.600	283.536	-91.713	309.127	-4.485
3700	103.560	367.194	287.767	293.881	-91.798	320.262	-4.521
3800	103.783	369.959	289.894	304.248	-91.911	331.401	-4.555
3900	103.990	372.658	291.982	314.637	-92.051	342.542	-4.588
4000	104.183	375.293	294.032	325.045	-92.222	353.687	-4.619

Taken from Per-Erik Bengtsson, 2002

Thermochemical data for C_2H_4

Ideal gas, mole mass 28.05376×10^{-3} kg/mole

T_r = 298.15 K, Standard state pressure = p=0.1 MPa

T	C_p^0	S^0	$-[G_0-H_0(T_r)]/T$	$H^0-H^0(T_r)$	$\Delta_f H^0$	$\Delta_f G^0$	Log K_f
K	*J/mole•K*	*J/mole•K*	*J/mole•K*	*kJ/mole*	*kJ/mole*	*kJ/mole*	
0	0	0	INFINITE	-10.518	-60.986	-60.986	INFINITE
100	33.270	180.542	252.466	-7.192	58.194	60.476	-31.589
200	35.359	203.955	222.975	-3.804	55.542	63.749	-16.649
298.15	42.886	219.330	219.330	0	52.467	68.421	-11.987
300	43.063	219.596	219.331	0.079	52.408	68.521	-11.930
400	53.048	233.343	221.138	4.882	49.354	74.360	-9.710
500	62.477	246.215	224.879	10.668	46.641	80.933	-8.455
600	70.663	258.348	229.456	17.335	44.294	88.017	-7.663
700	77.714	269.783	234.408	24.763	42.300	95.467	-7.124
800	83.840	280.570	239.511	32.847	40.637	103.180	-6.737
900	89.200	290.761	244.644	41.505	39.277	111.082	-6.447
1000	93.899	300.408	249.742	50.665	38.183	119.122	-6.222
1100	98.018	309.555	254.768	60.266	37.318	127.259	-6.043
1200	101.626	318.242	259.698	70.252	36.645	135.467	-5.897
1300	104.784	326.504	264.522	80.576	36.129	143.724	-5.775
1400	107.550	334.372	269.233	91.196	35.742	152.016	-5.672
1500	109.974	341.877	273.827	102.074	35.456	160.331	-5.583
1600	112.103	349.044	278.306	113.181	35.249	168.663	-5.506
1700	113.976	355.898	282.670	124.486	35.104	177.007	-5.439
1800	115.628	362.460	286.922	135.968	35.005	185.357	-5.379
1900	117.089	368.752	291.064	147.606	34.938	193.712	-5.326
2000	118.386	374.791	295.101	159.381	34.894	202.070	-5.278
2100	119.540	380.596	299.035	171.278	34.864	210.429	-5.234
2200	120.569	386.181	302.870	183.284	34.839	218.790	-5.195
2300	121.491	391.561	306.610	195.388	34.814	227.152	-5.159
2400	122.319	396.750	310.258	207.580	34.783	235.515	-5.126
2500	123.064	401.758	313.818	219.849	34.743	243.880	-5.096
2600	123.738	406.596	317.294	232.190	34.688	252.246	-5.068
2700	124.347	411.280	320.689	244.595	34.616	260.615	-5.042
2800	124.901	415.812	324.006	257.058	34.524	268.987	-5.018
2900	125.404	420.204	327.248	269.573	34.409	277.363	-4.996
3000	125.864	424.463	330.418	282.137	34.269	285.743	-4.975
3100	126.284	428.597	333.518	294.745	34.102	294.128	-4.956
3200	126.670	432.613	336.553	307.393	33.906	302.518	-4.938
3300	127.024	436.516	339.523	320.078	33.679	310.916	-4.921
3400	127.350	440.313	342.432	332.797	33.420	319.321	-4.906
3500	127.650	444.009	345.281	345.547	33.127	327.734	-4.891
3600	127.928	447.609	348.074	358.326	32.800	336.156	-4.877
3700	128.186	451.118	350.812	371.132	32.436	344.588	-4.865
3800	128.424	454.539	353.497	383.962	32.035	353.030	-4.853
3900	128.646	457.878	356.130	396.816	31.596	361.482	-4.842
4000	128.852	461.138	358.715	409.691	31.118	369.947	-4.831

Taken from Per-Erik Bengtsson, 2002

Polynomial fits for specific heat of gaseous fuels

$$c_p = a_0 + a_1\theta + a_2\theta^2 + a_3\theta^3 + a_4\theta^{-2}$$

θ = T/1000, T – [K], c_p - [kJ/(mol,K)]

Fuel	a_0	a_1	a_2	a_3	a_4
Propane (C_3H_6)	-6.061	311.034	-163.448	33.699	0.051
Hexane (C_6H_{14})	-86.902	880.648	-686.699	221.049	2.370
Isooctane (C_8H_{18})	-2.314	759.898	-409.141	85.362	-0.129
Methanol (CH_3OH)	-11.321	184.799	-115.064	30.206	0.849
Ethanol (CH_5OH)	29.246	166.276	-49.898	0.000	0.000
Gasoline 1	-100.742	1073.740	-843.829	270.914	2.430
Gasoline 2	-94.144	953.910	-741.656	234.505	2.027
Diesel	-38.101	1033.322	-601.408	135.265	0.209

Physical properties for various solids and liquids (at 298K, 100kPa)			
Name	Density [kg/m^3]	Specific heat [J/kgK]	Thermal conductivity [W/(m K)]
Aluminium (s)	2700	218	890
Brick work (s)	2325	960	1.3
Coal (s)	1300	1300	0.25
Copper (s)	8918	395	385
Paraffin (s)	900	2890	0.24
Paper (s)	930	1340	0.18
Sand (s)	1515	800	0.27
Soil (s)	2050	1840	0.52
Steel (s)	7820	45	420
Water (l)	1000	4182+0.36T	$-0.487+5.887\times10^{-3}T-7.38\times10^{-6}T^2$
Wood (s) (dry)	200-700	-37.7+4.206T	Parallel to fibre direction $k_{c\parallel} = \rho_{wood}\left(\frac{0.73}{1450}+\frac{Y_m k_{c,water}}{1000(1-Y_m)}+ k_{c,gas}\left(\frac{1}{\rho_{wood}}-\frac{1}{1450}-\frac{Y_m}{1000(1-Y_m)}\right)\right)$ Perpendicular to fibre direction $k_{c,\perp} = k_{c,gas} + 2\times10^{-4}\rho_{wood}\left(1+\frac{Y_m k_{c,water}}{c_1(1-Y_m)}\right)$ Y_m as received moisture fraction $Y_m < 0.3 \rightarrow c_1 = 0.29$ $Y_m \geq 0.3 \rightarrow c_1 = 0.24$

PROPERTIES FOR AIR AT 1 ATM

T (K)	ρ kg/m³	c_p (kJ /kg ,K)	$\mu \cdot 10^7$ (Pa · s)	$\nu \cdot 10^6$ (m^2/s)	$k_c \cdot 10^3$ (W/m,K)	$a \cdot 10^6$ (m^2/s)	Pr
100	3.5562	1.032	71.1	2.00	9.34	2.54	0.786
150	2.3364	1.012	103.4	4.426	13.8	5.84	0.758
200	1.7458	1.007	132.5	7.590	18.1	10.3	0.737
250	1.3947	1.006	159.6	11.44	22.3	15.9	0.720
300	1.1614	1.007	184.6	15.89	26.3	22.5	0.707
350	0.09950	1.009	208.2	20.92	30.0	29.9	0.700
400	0.8711	1.014	230.1	26.41	33.8	38.3	0.690
450	0.7740	1.021	250.7	32.39	37.3	47.2	0.686
500	0.6964	1.030	270.1	38.79	40.7	56.7	0.684
550	0.6329	1.040	288.4	45.57	43.9	66.7	0.683
600	0.5804	1.051	305.8	52.69	46.9	76.9	0.685
650	0.5356	1.063	322.5	60.21	49.7	87.3	0.690
700	0.4975	1.075	338.8	68.10	52.4	98.0	0.695
750	0.4643	1.087	354.6	76.37	54.9	109	0.702
800	0.4354	1.099	369.8	84.93	57.3	120	0.709
850	0.4097	1.110	384.3	93.80	59.6	131	0.716
900	0.3868	1.121	398.1	102.9	62.0	143	0.720
950	0.3666	1.131	411.3	112.2	64.3	155	0.723
1000	0.3482	1.141	424.4	121.9	66.7	168	0.726
1100	0.3166	1.159	449.0	141.8	71.5	195	0.728
1200	0.2902	1.174	473.0	162.9	76.3	224	0.728
1300	0.2679	1.189	496.0	185.1	82	238	0.719
1400	0.2488	1.207	530	213	91	303	0.703
1500	0.2322	1.230	557	240	100	350	0.685
1600	0.2177	1.248	584	268	106	390	0.688
1700	0.2049	1.267	611	298	113	435	0.685
1800	0.1935	1.286	637	329	120	482	0.683
1900	0.1833	1.307	663	362	128	534	0.677
2000	0.1741	1.337	689	396	137	589	0.672
2100	0.1658	1.372	715	431	147	646	0.667
2200	0.1582	1.417	740	468	160	714	0.655
2300	0.1513	1.478	766	506	175	783	0.647
2400	0.1448	1.558	792	547	196	869	0.630
2500	0.1389	1.665	818	589	222	960	0.613
3000	0.1135	2.726	955	841	486	1570	0.536
Based on Incropera och DeWitt, Table A.4							

COMBUSTION PROPERTIES OF VARIOUS FUELS

Solid fuels

	Wood				
	Dry		Air dried		
	Density kg/m^3	*HHV* MJ/kg	Moisture %	Density kg/m^3	*LHV* MJ/kg
Wood					
Alder (Al)	310	18.1	25	415	11.9
Aspen (Asp)	260	19.9	25	346	13.3
Birch (Björk)	360	20.2	25	480	13.5
Beech (Bok)	405	19.7	25	480	13.5
Spruce (Gran)	285	20.7	25	380	13.9
Pine (Tall)	290	21.2	25	385	14.2
Wood wastes					
Sawdust	125	20.0	30	179	12.7
Planning shavings (Kutterspån)	80	20.5	15	100	15.9

	Coal								
Quality	**Combustibles**					Proximate analysis			
	Carbon %	**Hydrogen%**	**Nitrogen %**	**Sulphur %**	***HHV* MJ/kg**	**Dry substance %**	**Volatiles %**	**Ash %**	***LHV* MJ/kg**
Anthracite	86.7	2.2	0.8	0.5	31.0	97.7	3.1	6.9	30.5
Low volatile	80.2	3.6	1.1	0.7	31.0	97.0	8.4	9.7	30.3
Semi bituminous	79.6	4.3	1.7	1.0	31.7	96.6	16.2	8.6	30.8
Bituminous	80.1	5.0	1.5	1.0	32.4	96.9	21.8	7.2	31.4
Sub-bituminous	58.8	6.0	1.3	0.3	28.2	80.4	30.5	4.0	27.0
Lignite, Brown coal	42.4	6.7	0.7	0.7	24.6	65.2	28.2	6.2	23.2

		Other solid fuels			
Specie		**Lignite-Briquets**	**Peat fresh**	**Peat dried**	**Bark fresh**
Carbon C	%	55.6	27.7	44.3	24.5
Hydrogen H_2	%	3.0	2.9	4.6	3.2
Oxygen O_2	%	1.52	16.2	25.9	21.1
Nitrogen N_2	%		0.7	1.1	0.2
Sulphur (tot) S	%	0.64	2.5	4.0	1.0
Moisture H_2O	%	19.3	50.0	20.0	50.0
Ash	%	6.3	1-10	1-10	1
Lower Heating value	MJ/kg	18.85	10.25	15.47	8.5

Gaseous fuels

	H_2	CH_4	C_2H_4	CO	CO_2	N_2		Molv. g/mol	LHV MJ/m³
Coal-gas	50	20	2	17	3	8		12.89	15.68
	H_2	CH_4	$C_{2.5}H_{4.2}$	C_2H_6	CO	CO_2	N_2		
City gas	35.3	15	5.5	5.4	11.9	4.9	21.2		
	C_2H_6	C_3H_6	C_3H_8	C_4H_8	$C4H_{10}$	C_5H_{12}			
LPG (gasol): based on propane	3	22	73	-	2	-		43.62	88.4
based on butane	-	-	6	30	62	2		46.1	115.3
	CH_4	C_2H_6	C_3H_8	C_4H_{10}	C_mH_n	CO_2	N_2		
Natural gas: Russia	93	3.3	-	1	-	2.2	0.5		
-"-: Dutch	81.3	2.9	0.4	0.1	0.1	0.8	14.4		
-"-: North sea	90.4	3.8	0.9	0.3	0.5	0.3	3.9		

Thermodynamic properties of various hydrocarbons

Group	Formula	Name	M	$\rho_{(l)}$	T_{boil}	p_{vap}	$c_{p,g}$	$c_{p,l}$	HHV	LHV	H_{evap} (T_{kok})	f	Octane-number	$\Delta h_f°$	p_c	T_c
			g/mol	kg/m³	°C	kPa	kJ/kg°C	kJ/kg°C	kJ/kg	kJ/kg	kJ/kg	-	-	kJ/mol	kPa	K
Alkanes	CH_4	Methane	16.04	466	-161		2.21		55536	50048	510	0.252	120	-74.4	4599	190
	C_2H_6	Ethane	30.07	572	-89	0.507	1.75	2.48	51902	47511	489	0.269	99	-83.8	4883	305
	C_3H_8	Propane	44.1	585	-42	1297	1.62	2.48	50322	46330	432	0.276	97	-105	4244	370
	C_4H_{10}	n-Butane	58.12	579	0	355.6	1.64	2.42	49511	45725	386	0.279	90	-147	3799	425
	C_4H_{10}	Isobutane[1]	58.12	557	-12	500.4	1.62	2.39	49363	45577	366	0.279	98	-154	3647	408
	C_5H_{12}	n-Pentane	72.15	626	36	107.4	1.62	2.32	49003	45343	357	0.283	63	-174	3373	470
	C_5H_{12}	Isopetane[2]	72.15	620	28	140.8	1.6	2.28	48909	45249	342	0.283	90	-179	3394	460
	C_6H_{14}	n-Hexane	86.12	659	69	34.14	1.62	2.27	48674	45099	335	0.285	26	-199	3009	507
	C_6H_{14}	Isohexane[3]	86.18	662	50	50.95	1.58	2.2	48454	44879	305	0.285	94	-207	3130	500
	C_7H_{16}	n-Heptane	100.2	684	99	11.14	1.61	2.24	48438	44925	317	0.285	0	-224	2735	540
	C_7H_{16}	Triptane[4]	100.2	690	81	23.2	1.6	2.13	48270	44757	289	0.285	101		2958	531
	C_8H_{18}	n-Octane	114.23	703	126	3.647	1.61	2.23	48254	44786	301	0.287	17	-250	2492	569
	C_8H_{18}	Isooctane[5]	114.23	692	114	11.85	1.59	2.09	48119	44651	283	0.287	100	-259	2573	544
	C_9H_{20}	n-Nonane	128.26	718	151	1.216	1.61	2.21	48119	44688	288	0.287		-275	2289	595
	$C_{10}H_{22}$	n-Decane	142.28	730	174	0.507	1.61	2.21	48002	44599	272	0.287		-301	2117	618
	$C_{10}H_{22}$	Isodecane[6]	142.28	768	161		1.61	2.21				0.287	92		2512	623
	$C_{11}H_{24}$	n-Undecane	156.31	740	196		1.6	2.21	47903	44524	265	0.289		-327	1965	639
	$C_{12}H_{26}$	n-Dodecane	170.33	749	216		1.6	2.21	47838	44574	256	0.289		-351	1823	658
	$C_{13}H_{28}$	n-Tridecane	184.35	756	236		1.6	2.21			246	0.289			1722	676
	$C_{14}H_{30}$	n-Tetradecane	198.38	763	253		1.6	2.21			239	0.289			1438	693
	$C_{15}H_{32}$	n-Pentadecane	212.45	768	271		1.6	2.21			232	0.289			1520	707
	$C_{16}H_{34}$	n-Hexadecane[7]	226.43	773	287		1.6	2.21	47611	44307	225	0.289		-456	1408	722
	$C_{17}H_{36}$	n-Heptadecane	240.46	778	302		1.6	2.21			221	0.289			1297	733
	$C_{18}H_{38}$	n-Octadecane	254.5	782	317		1.6	2.21	47542	44256	214	0.289			1195	748
Cyclo alkanes	C_5H_{10}	Cyclopentane	70.13	746	49	68.17	1.135	1.836	46936	43798	389	0.293	85	-76.4	4508	512
	C_6H_{12}	Cyclohexane	84.16	779	81	22.69	1.214	1.813	46573	43435	358	0.293	78	-123	4072	553
	C_7H_{14}	Cycloheptane	98.19	810	119	5.875	1.181	1.826	46836	43698	335	0.293	41	-118	3809	604
	C_8H_{16}	Cyclooctane	112.2	835	149	2.127	1.173	1.838	46943	43808	309	0.293	58	-124	3556	647
Aromatics	C_6H_6	Benzene	78.11	874	80	22.69	1.005	1.717	41833	40145	393	0.325	115	82.6	4893	562
	C_7H_8	Toluene[8]	92.14	867	111	7.091	1.089	1.683	42439	40528	362	0.321	109	50.4	4103	592
	C_8H_{10}	Ethyl benzene	106.17	867	136	2.533	1.173	1.721	42996	40923	339	0.316	98	29.9	3596	617
	C_8H_{10}	m-Xylene[9]	106.17	864	139	2.229	1.164	1.692	42873	40800	342	0.316	115	17.3	3535	617

Group	Formula	Name	M	$\rho_{(l)}$	T_{kok}	p_{vap}	$c_{p,g}$	$c_{p,l}$	HHV	LHV	H_{evap} (T_{kok})	f	Octane-number	$\Delta h_f°$	p_c	T_c
			g/mol	kg/m³	°C	kPa	kJ/kg°C	kJ/kg°C	kJ/kg	kJ/kg	kJ/kg	-	-	kJ/mol	kPa	K
Alkenes	C_3H_6	Propene	42.08	519	-47	1560	1.482	2.45	48472	45334	437	0.293	85	20	4599	365
	C_4H_8	1-Butene	56.11	595	-6	434.2	1.487	2.24	48073	44937	390	0.293	80	-0.1	4022	420
	C_5H_{10}	1-Pentene	70.13	641	30	131	1.524	2.178	47766	44528	358	0.293	77	-21.3	3525	465
	C_6H_{12}	1-Hexene	84.16	673	63	41.33	1.533	2.144	47550	44312	335	0.293	63	-43.5	3171	504
	C_4H_6	1,2-Butadien	54.1	658	11.1					45480		0.307				
	C_5H_8	Isopren[10]	68.11	681	34	115.1	1.495	2.199	46382	43798	356	0.305	81	75.5	3849	484
	C_6H_{10}	1,5-Hexadien	82.15	688	59	48.93	1.39	2.136	46796	43582	312	0.303	38	84.1	3434	507
Cyclo alkenes	C_5H_8	Cyclopentene	68.12	772	44		1.064	1.759	45733	43149		0.305	70	33.9	4802	506
	C_6H_{10}	Cyclohexen	82.15	0					45674	42995				-5		
Alkyles	C_2H_2	Acetylene	26	621	-83.9					48200		0.325				
Alcohols	CH_4O	Metanol	32.04	791	65	31.4	1.37	2.531	22663	19915	1099	0.666	92	-202	8084	513
	C_2H_6O	Ethanol	46.07	789	78	15.5	1.42	2.438	29668	26803	836	0.481	89	-235	6139	514
	C_3H_8O	1-Propanol	60.1	803	97	6.179	1.424	2.395	33632	30709	690	0.412		-255	5166	537
	$C_4H_{10}O$	1-Butanol	74.1	805	118	2.229		2.391	36112	33142	584	0.39		-275	4417	563
	$C_5H_{12}O$	1-Pentanol	88.15	814	137			2.361	37787	34791	503	0.37		-299	3910	588
	$C_6H_{14}O$	1-Hexanol	102.18	814	137			2.353	38994	35979	436	0.355		-318	4052	611
Ketones	C_3H_6O	Acetone[11]	58.1	792	56.7		2.175	1.296		30794	523	0.454				
Ethrer	$C_4H_{10}O$	Dietyleter	74.1	714	34.4		2.321	1.457			351	0.386				
Oils		Jet Fuel JP1	150	810						43012		0.294				
		Jet Fuel JP2	112	760						43472		0.294				
		Jet Fuel JP3	126	780						43472		0.294				
		Jet Fuel JP4	170	830						43012		0.299				
		Gasolin								44000		0.29				
		Fuel oil		950						41600		0.308				
Hydrogen gas	H2	Hydrogen	2		-253					119872	451	0.125				

Definitions: M – molar mass, T_{boil} – boiling temperature at 1 atm, p_v – vapour pressure at 38 °C, $c_{p,g}$ – specific heat for the gas at 25 °C, $c_{p,l}$ –specific heat for the liquid at 25 °C, HHV – Higher heating value. The three first are gases the rest are liquids. LHV – lower heating value. H_{evap}, -heat of evaporation at 1 atm and boiling point. f – stoiciometric mass ratio between fuel and oxygen, octane number – engine octane number, $\Delta h_f°$ - Molar enthalpy of formation at 25 °C, p_c – pressure at critical point, T_c - temperature at the critical point.

Remarks: [1] 2-Metyl propane, [2] 2,2-methyl butane, [3] 2,3-dimetyl butane, [4] 2,2,3-trimetyl butane, [5] 2,2,4-trimetyl pentane, [6] 2,2,3,3-tetrametyl hexane, [7] cetane, [8] Methyl benzene, [9] 1,3-dimetyl bensene, [10] 2-metyl-1,3-butadien, [11] Dimetylketon.

Based on Borman och Ragland, table A1 och 2. Sources: Lide, D.L. (ed.), Handbook of Chemistry and Physics, 74th ed., CRC Press, Boca Raton, FL, 1993. Bartok and Sarofim, Fossil Fuel Combustion: A Source Book, Wiley, New York, 1991.

IGNITION RELATED PROPERTIES

Ignition related properties for some stoichiometric mixtures at ambient conditions (room temperature and normal pressure).

Fuel	Oxidant	d_q	E_{min}	T_{ign}	$X_{f,stök}$	Ignition limits	
						Lean	Fat
		mm	10-6*J	°C	vol-%	% stio	% stio
Hydrogen (H_2)	Air	0.64	20.1				
Methane (CH_4)	Air	2.55	331.0	537	9.47	46	164
Acetylene (C_2H_2)	Air	0.76	30.2	305	7.55	31	
Ethane (C_2H_6)	Air			472	5.64	50	272
Ethylene (C_2H_4)	Air	1.25	111.0				
Propane (C_3H_8)	Air	2.03	305.5	470	4.02	51	283
1-3 Butadiene (C_4H_6)	Air	1.25	235.5				
n-Butane (C_4H_{10})	Air			365	3.12	54	330
iso-Butane (C_4H_{10})	Air	2.2	344.4	460			
Cyclo pentane $C_5H_{10}O$	Air			385	2.71		
n-Pentane (C_5H_{12})	Air	3.3	821.2	284	2.55	54	359
iso-Pentane (C_5H_{12})	Air			420			
1-Pentene (C_5H_{12})	Air			298	2.71	47	370
Benzene (C_6H_6)	Air	2.79	551.0	592	2.77	43	336
Cyclohexane (C_6H_{12})	Air	4.06	1381.9	270	2.27	48	401
Cyclohexene (C_6H_{10})	Air	3.3	861.0		2.4		
n-Hexane (C_6H_{12})	Air	3.56	951.5	233	2.16	51	400
l-Hexane (C_6H_{12})	Air	1.87	219.6				
1-Hexene (C_6H_{12})	Air			272			
Toluene (C_7H_8)	Air			568	2.27	43	322
n-Heptane (C_7H_{16})	Air	3.81	1151.8	215	1.87	53	450
Ethyl benzene (C_6H_{10})	Air			460			
m-Xylene (C_8H_{10})	Air			563			
n-Octane (C_8H_{18})	Air			206	1.65	51	425
iso-Octane (C_8H_{18})	Air	2.84	574.4	418			
n-Decane ($C_{10}H_{23}$)	Air	2.06	302.1	232	1.33	45	356
l-Decane ($C_{10}H_{23}$)	Air	1.97	276.5				
Methanol (CH_3OH)	Air			385	12.24	48	408
Ethanol (C_2H_5OH)	Air			365	6.52		
Diethyl ether $C_4H_{10}O$	Air	2.54	490.6				
Hydrogen (H_2)	Oxygen	0.25	4.2				
Methane (CH_3OH	Oxygen	0.3	6.3				
Acetylene (C_2H_2	Oxygen	0.09	0.4				
Ethylene (C_2H_4)	Oxygen	0.19	2.5				
Propane (C_3H_8)	Oxygen	0.24	4.2				
Propane (C_3H_8)	Argon "Air"	1.04	77.1				
Propane (C_3H_8)	Helium "Air"	2.53	453.8				
Hydrogen (H_2)	45% Brome	3.63					

Based on Kanury table 4.2 and 4.3, and Borman och Ragland table A1 and A2.

LAMINAR FLAME SPEED IN AIR

Maximum laminar flame speed			
Fuel	**$u_{L,max}$ m/s**	**$T(u_{L,max})$ K**	**X_b vid $u_{L,max}$ % av stök.**
Acetone (C_2H_6O)	0.5018	2121	131
Acetylene (C_2H_2)	1.5525		133
Benzene (C_6H_6)	0.446	2365	108
1,2-Butadiene (C_4H_6)	0.639	2419	117
n-Butane (C_4H_{10})	0.416	2256	113
1-Butene (C_4H_8)	0.476	2319	116
Cyklobutane (C_4H_{10})	0.6218	2308	115
Cyklohexane (C_6H_{14})	0.4246	2250	117
Cyklopentane (C_3H_8)	0.4117	2264	117
Cyklopropane (C_3H_6)	0.5232	2328	117
n-Dekane ($C_{10}H_{22}$)	0.4031	2286	105
Diethyl ether $C_4H_{10}O$	0.4374	2253	115
Ethane (C_2H_6)	0.4417	2244	112
n-Heptane (C_7H_{16})	0.4246	2214	122
n-Hexane (C_6H_{14})	0.4246	2239	117
Carbon monoxide (CO)	0.39		
Methane (CH_4)	0.3731	2236	106
iso-Octane (C_8H_{18})	0.39		
n-Pentane (C_5H_{12})	0.4246	2250	115
Propane (C_3H_8)	0.4289	2250	114
Propene (C_3H_6)	0.4803	2339	114
Toluene (C_7H_8)	0.386	2344	105
Hydrogen (H_2)	2.9119	2380	170
Based on Kanury table 4.3			

ADIABATIC FLAME TEMPERATURE

Calculated flame temperature and composition of combustion products

Pressure: 1 atm. Reference temperature: 25°C. Gas phase. Air to fuel ratio: 1.0 except for acetylene-oxygen and cyanogen-oxygen. Acetylene-oxygen has a molar ratio of 1, mixtures at maximal temperature contains a bit more oxygen. Cyanogen-oxygen mixture has the molar fraction 1.

		Equilibrium concentrations, mole %									
Fuel	Adiabatic Flame temp.K	H_2O	CO_2	CO	O_2	H_2	OH	H	O	NO	N_2
Oxidant: oxygen											
H_2	3083	57			5	16	10	8	4		
CH_4	3010	37	12	15	7	7	14	5	3		
C_2H_4	3170	24	14	24	10	6	9	6	7		
C_2H_2	3325			61		21		18			
C_3H_8	3091	3.1	13.4	20.0	9.8	6.4	8.7	5.3	5.1		
C_3H_6	3146	24.7	14.0	23.8	10.8	5.7	8.8	5.8	6.4		
n-C_4H_{10}	3096	30.1	13.9	20.8	10.0	6.2	8.6	5.2	5.2		
C_4H_8	3138	25.0	14.2	23.7	10.8	5.7	8.8	5.6	6.2		
n-C_8H_{18}	3082	26	14	22	9	5	14	5	5		
CO	2973		46	35	15				4		
C_2N_2 [a]	4850			66					0.8	0.03	32
Oxidant: air											
H_2	2323	32				2	1				65
CH_4	2222	18	8.5	0.9	0.4	0.4	0.3	0.04	0.02	0.2	70.9
CO[b]	2395	0	29.5	4,3	1,8	0	0	0	0,1	0,5	63,6
C_2H_2	2523	7	12	4	2		1			1	73
C_2H_6[b]	2260	15,6	9,7	1,2	0,5	0,4	0,7	0,05	0,03	0,2	71,7
C_3H_6[b]	2332	12,1	11,1	1,8	0,7	0,3	0,8	0,08	0,06	0,3	72,7
C_3H_8[b]	2267	14,6	10,2	1,3	0,5	0,3	0,7	0,05	0,03	0,2	72,0
C_4H_8[b]	2356	12,0	10,9	2,0	0,8	0,4	0,9	0,09	0,07	0,3	72,6
C_4H_{10}[b]	2261	14,1	10,5	1,3	0,5	0,3	0,6	0,05	0,03	0,2	72,3
C_5H_{12}[b]	2262	13,8	10,7	1,3	0,5	0,3	0,6	0,05	0,03	0,2	72,4
C_6H_6[b]	2343	7,4	13,7	2,2	0,8	0,2	0,7	0,06	0,07	0,4	74,6
C_6H_{14}[b]	2264	13,6	10,8	1,3	0,5	0,3	0,6	0,05	0,03	0,2	72,5
C_7H_8[b]	2329	8,2	13,3	2,0	0,8	0,2	0,7	0,06	0,06	0,3	74,3
C_7H_{16}[b]	2266	13,4	10,4	1,3	0,5	0,3	0,6	0,05	0,03	0,2	72,6
isoC_8H_{18}[b]	2264	13,3	11,0	1,3	0,5	0,3	0,6	0,05	0,03	0,2	72,6
$C_{10}H_{22}$[b]	2268	13,1	11,1	1,4	0,5	0,3	0,7	0,06	0,04	0,02	72,7

[a] Remaining products is mainly N.
[b] calculated from data given here.
Based on Bartock och Sarofim, table G3

SATURATION VAPOUR PRESSURE

Vapour pressure at saturation							
		$p_{sat} = \exp[c_1 - c_2/(T - c_3)], \quad [Pa]$					
Name	Formula	c_1	c_2	c_3	T_{boil} [K]	H_{evap} (T_{boil}) [kJ/kg]	Density (20°C) [kg/m^3]
Methanol	CH_3OH	24.75	4305	12	301.7	1099	791
Ethanol	C_2H_5OH	25.44	4725	12	351.4	836	789
Acetone	C_3H_6O	21.32	2811	43	329.5	523	792
1-Propanol	C_3H_7OH	24.19	4153	43	370.8	690	803
Glycerol	$C_3H_8O_3$	21.65	4178	150	563.0		1270
1-Bytanol	$C_4H_{10}O$	24.41	4473	43	390.0	584	805
Benzene	C_6H_6	18.10	1538	120	353.1	393	874
Cyclohexane	C_6H_{12}	31.36	2595	60	353.7	358	779
Toluene	C_7H_8	21.02	3168	50	383.6	362	867
Heptane	C_7H_{16}	21.00	3048	50	371.4	317	684
2-Xylene	C_8H_{10}	21.35	3610	50	417.4	342	864
iso Octane	C_8H_{18}	20.99	3203	60	398.6	283	692
n-Heptane	C_7H_{16}	21.21	3182	43	371.4	317.8	687.8
Gasoline		20.89	2714	43	333.0	246	724
JP4		22.14	4000	43	420.0	292	773
JP5		22.07	4769	43	495.3	266.5	827
DF2		22.44	5384	43	536.4	254	846
Water	H_2O	23.82	4193	32	373.0	2257	998
Based on Kanury, table 5.3 and Bartock and Sarofim, table 7							

Clausius-Clapeyrons equation:

$$d\ln[p_{sat}]/dT = c_2/\Re T^2$$

Integration under the assumption that the evaporation enthalpy is independent of temperature

$$p_{sat} = p_{sat}{}^0 \exp\left[-(c_2/\Re)\{1/T - 1/T^0\}\right]$$

where $p_{sat}{}^0$ is saturation pressure at an arbitrary reference temperature, T^0.

Periodic Table

1 **H** 1.008																	2 **He** 4.003
3 **Li** 6.941	4 **Be** 9.012											5 **B** 10.81	6 **C** 12.01	7 **N** 14.01	8 **O** 16.00	9 **F** 19.00	10 **Ne** 20.18
11 **Na** 22.99	12 **Mg** 24.31											13 **Al** 26.98	14 **Si** 28.09	15 **P** 30.97	16 **S** 32.07	17 **Cl** 35.45	18 **Ar** 39.95
19 **K** 39.10	20 **Ca** 40.08	21 **Sc** 44.96	22 **Ti** 47.88	23 **V** 50.94	24 **Cr** 52.00	25 **Mn** 54.94	26 **Fe** 55.85	27 **Co** 58.93	28 **Ni** 58.69	29 **Cu** 63.55	30 **Zn** 65.39	31 **Ga** 69.72	32 **Ge** 72.59	33 **As** 74.92	34 **Se** 78.96	35 **Br** 79.90	36 **Kr** 83.80
37 **Rb** 85.47	38 **Sr** 87.62	39 **Y** 88.91	40 **Zr** 91.22	41 **Nb** 92.91	42 **Mo** 95.94	43 **Tc** (98)	44 **Ru** 101.1	45 **Rh** 102.9	46 **Pd** 106.4	47 **Ag** 107.9	48 **Cd** 112.4	49 **In** 114.8	50 **Sn** 118.7	51 **Sb** 121.8	52 **Te** 127.6	53 **I** 126.9	54 **Xe** 131.3
55 **Cs** 132.9	56 **Ba** 137.3	57 **La** *138.9	72 **Hf** 178.5	73 **Ta** 180.9	74 **W** 183.9	75 **Re** 186.2	76 **Os** 190.2	77 **Ir** 190.2	78 **Pt** 195.1	79 **Au** 197.0	80 **Hg** 200.5	81 **Tl** 204.4	82 **Pb** 207.2	83 **Bi** 209.0	84 **Po** (210)	85 **At** (210)	86 **Rn** (222)
87 **Fr** (223)	88 **Ra** (226)	89 **Ac** ~(227)	104 **Rf** (257)	105 **Db** (260)	106 **Sg** (263)	107 **Bh** (262)	108 **Hs** (265)	109 **Mt** (266)	110 **Ds** (271)	111 **Uuu** (272)	112 **Uub** (277)		114 **Uuq** (296)		116 **Uuh** (298)		118 **Uuo** (?)

Lanthanide Series*	58 **Ce** 140.1	59 **Pr** 140.9	60 **Nd** 144.2	61 **Pm** (147)	62 **Sm** 150.4	63 **Eu** 152.0	64 **Gd** 157.3	65 **Tb** 158.9	66 **Dy** 162.5	67 **Ho** 164.9	68 **Er** 167.3	69 **Tm** 168.9	70 **Yb** 173.0	71 **Lu** 175.0
Actinide Series~	90 **Th** 232.0	91 **Pa** (231)	92 **U** (238)	93 **Np** (237)	94 **Pu** (242)	95 **Am** (243)	96 **Cm** (247)	97 **Bk** (247)	98 **Cf** (249)	99 **Es** (254)	100 **Fm** (253)	101 **Md** (256)	102 **No** (254)	103 **Lr** (257)

A COST EFFECTIVE CONCEPT FOR GENERATION OF HEAT, ELECTRICITY AND TRANSPORT FUEL FROM BIOMASS IN FLUIDIZED BED BOILERS – USING EXISTING ENERGY INFRASTRUCTURE

H. Thunman, L.-E. Åmand, B. Leckner, F. Johnsson

Department of Energy and Environment, Division of Energy Technology
Chalmers University of Technology, SE-412 96, Sweden
E-mail: henrik.thunman@chalmers.se

Keywords: Gasification, Demonstration, Fluidized Bed

ABSTRACT: Poly-generation of various energy carriers from biomass is a cost effective option to initiate production of transport fuels from lignocellulosic biomass. Traditionally, the routs for this option have been trough greenfield gasification reactors. Here, on the other hand, the infrastructure of existing boilers is used for introduction of the gasification technology, which lowers cost and minimizes risks. The concept is based on adding a gasifier to existing fluidized bed boilers. An evaluation indicates the possibility of producing between 25 to 50 % of syngas, based on fuel input, without reducing the power output of the boiler. The process uses the thermal flywheel of the fluidized bed as a means to devolatilise the biomass. Only in Sweden there are around 100 fluidized bed boilers, which are potentially appropriate to be retrofitted with the proposed concept, whereof around 40 are large enough to give a low risk option for production of transport fuels within the present energy infrastructure. To demonstrate the concept, the Chalmers 12 MW_{th} circulating fluidized bed boiler will be retrofitted according to this concept, resulting in co-generation of around 2 MW_{th} product gas. The gas will be used temporarily for production of heat and electricity. The unit will, however, be prepared in such a way that the gas in a later stage can produce any Fischer-Tropsch fuel or synthetic natural gas. The retrofit is planed for the summer of 2007 and the plant is planned to be in operation in October 2007. This paper presents and discusses an evaluation of the concept.

1 INTRODUCTION

An efficient use of biomass resources is an important part of the global strategy to reduce the emission of greenhouse gases to the atmosphere. In what way this restricted resource should be used for energy conversion can be discussed, but with the urgent need for action all technical options need to be exploited. From a pure efficiency evaluation the best use of biomass is to just burn it for heat and power production. However, to integrated technologies using renewable sources are generally most efficiently done in the stationary energy sector and the challenge is to find the solutions that could replace fossil fuels for all kinds of energy use. In this context gasification of biomass is attractive as the solid biomass is converted to a gas of suitable quality, which can be used directly, or after further process steps, as a substitute for the fossil fuels in various sectors.

Gasification is, however, not a new technology, nor is the concept of poly-generation, where several energy carriers are produced in a flexible production unit. For example, the same idea that is presented today in many biorefinery concepts has been repeatedly suggested during the last century. Figure 1, shows one such example from 1915 [1] proposed for the Swedish city of Norrköping, where the production unit should produce gas, char coal, process steam, electricity and district heating. In this example the suggested fuel was coal, but all the arguments for the plant and the economics around the project were the same as the ones presented for biorefineries today. It can also be mentioned that the project in Norrköping was stopped due to the First World War and later not continued, due to the large introduction of hydro power in Sweden. This totally changed the economics for the project, as it removed the need for additional production of gas and electricity.

Even though gasification has been identified as having a great potential to become cost-competitive, thermally efficient and environmentally friendly, the market penetration of the technology is slow, especially for biomass. For biomass there have been a large number of pilot and demo projects commissioned during the last twenty to thirty years, but the status of most of them can be summarized: worked fine, now closed down. There are, nevertheless, some exceptions where the gasifier in Güssing [2] perhaps being the best example.

The challenges to be overcome in order to introduce the gasification technology at large scale are to increase the reliability and decrease the investment costs for the gasifier itself as well as for the gas cleaning and the synthesis of the gas for further processes while at the same time increase the overall efficiency. The target of the concept proposed in this work is to provide a solution for the gasifier itself, with the aim to maximize the reliability and the overall efficiency at the same time as the investment cost is minimized.

2 THE CONCEPT

The rationale behind the concept is that poly-generation of various energy carriers from biomass is a cost effective option to initiate production of biofuels. This paper presents a concept for which the available

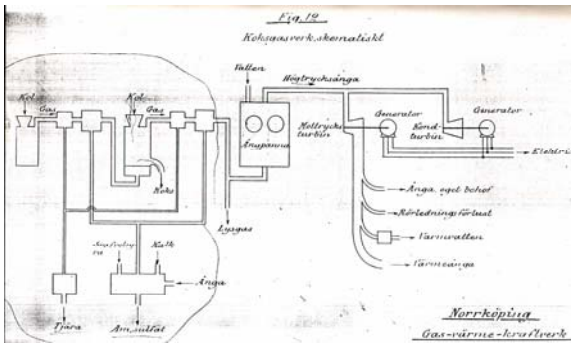

Figure 1 Poly-generation plant proposed for the production of energy carriers needed in Norrköping, Sweden, 1915.

infrastructure of existing boilers can be used as the basis for introducing the gasification technology, which in itself should lower the cost and minimizes risks.

The concept is based on retrofitting existing fluidized bed boilers (FB-boiler). The proposed process uses the thermal flywheel of the fluidized bed as a means of devolatilising the biomass. This is similar to the indirect gasification process which for example is applied in the Güssing gasifier [2]. But, instead of building a single gasification reactor, a fluidized bed boiler, Fig 2, is combined with a gasification reactor. A principle figure of the suggested process is shown in Fig 3, where the circulating fluidized bed (CFB) boiler in Fig 2 is retrofitted with a gasification reactor and one additional particle seal. The second particle seal secures the flow direction of the heat carrier and prevents gas leakage between the combustor and the gasifier. In the process, the heat carrier is transported up through the combustion reactor with the combustion gas, separated from the gas in the cyclone and falls down to the first particle seal. The heat carrier falls, thereafter, down to the gasification reactor, where it releases its heat before it is transported back to the combustion reactor.

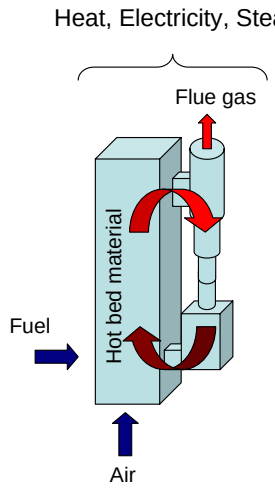

Figure 2: Schematic overview of a circulating fluidized bed boiler

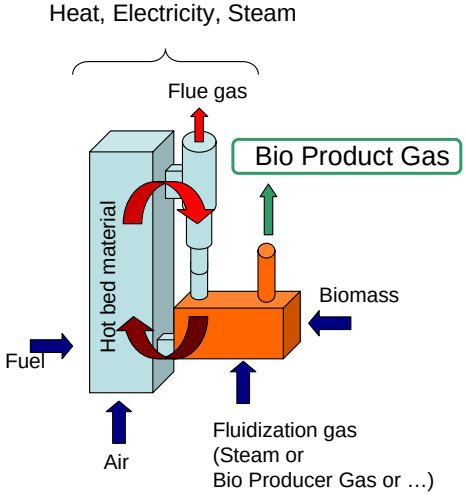

Figure 3: Schematic overview of a circulating fluidized bed boiler when retrofitted with a gasifier

An evaluation of the potential for the process has been carried out on Chalmers 12 MW_{th} CFB boiler. This evaluation shows that it is reasonable to integrate a gasifier with a fuel input of the same order as the thermal power of the boiler on which it is integrated. The size of the gasifier is restricted by:

1. the amount of bed material that can be circulated between the gasification and the combustion reactors,
2. the available space close to the FB-boiler and
3. the available biomass that can be transported to the reactor.

In Fig 4 an energy and material balance is shown for a 100 MW_{fuel} gasifier integrated onto a 100 MW_{th} FB-boiler. The balances assume that a dried biomass (10 % moisture) is fed to the gasifier, 80 % of the dry ash free mass is released as gas in the gasifier and the remaining 20 % is related to the char that is transported to the combustor. Under these conditions the energy stored in the char transported to the combustor is 10 MW_{th} higher than the heat transported from the combustor to the gasifier to support the gasification process. This means that the fuel fed to the combustor should be reduced accordingly to maintain the same production in the combustor. An additional heat source is also available as the gas produced in the gasifier needs to be cooled down. The heat stored in this gas is approximately the same as the heat needed for the gasification. A large part of this heat is, however, difficult to recover and will constitute a loss from the system. This is the case for all gasification systems available today, and is not specific for the proposed process.

There are several technical motivations why one should integrate a gasifier onto a FB-boiler instead of building a pure gasification reactor, for example:

1. Heat balance always fulfilled

In a pure gasification reactor the heat produced for gasification always has to be balanced to the heat requirement for the gasification process. All heat produced on top of this is a loss to the system. In a direct gasifier, where part of the fuel is burned within the gasification reactor, one often has to provide the process with at least 20 % more oxygen than that is required for the process to assure a stable process and compensate for variations in input fuel feed rate. In an indirect gasifier the process tends to become unstable, and as the evenness of the char transport to the combustor varies over time, this often requires that additional fuel is fed into the combustor to stabilize the process. For the proposed process, the heat production in the combustor is always much larger than the heat needed for the gasification, i.e. this assures a stable operation.

2. Minimization of char losses

The rates of gasification reactions with carbon dioxide and water vapour are low at the temperatures present in a fluidized bed gasifier. This means that in a direct gasifier most of the char converted in the gasifier is converted by the oxygen provided to the process. It is difficult to design the process so that the oxygen selects

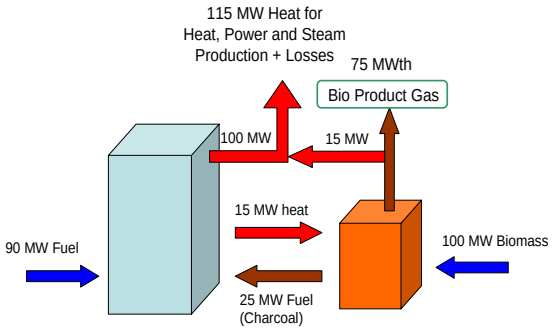

Figure 4: Heat and material balance for the integration of a 100 MW_{fuel} gasifier onto a 100 MW_{th} FB-boiler

the char instead of the more reactive volatile gases. The result is instead that the char remaining in the gasifier undergo attrition, resulting in that a large part of the char leaves the gasifier with the fly ash. An estimate based on data from existing gasifiers indicates that around 50 % of the char leaves the gasifier unconverted. In many cases a lower figure is presented, but then this is often accomplished in combination with high oxygen to fuel ratio. The conversion efficiency of the fuel is one of the great advantages of the indirect gasifier, where the unreacted char is recirculated to the combustor for final combustion. All attempts to increase the gasification of the char in the gasifier results in an increase in the attrition of the char, and consequently, in a loss of char. In the concept proposed here, the fuel conversion can be optimized to minimize the attrition. The variable amount of char transported from the gasifier to the combustor is compensated by the fuel fed to the combustor.

3. Optional fluidization medium

In a pure gasification reactor the reactor design is adjusted for a specific fluidization medium. In the indirect gasifier, and especially in the concept presented here the fluidization medium can be optimized with respect to the gas quality that is going to be produced. This can be done without any significantly negative impact on the heating value of the product gas. The first obvious option is steam that could be removed by condensation during the subsequent gas treatment, producing a medium heating-value gas. The drawback of the use of steam is the energy needed for its production. From an energy-efficiency point of view a more attractive medium is recirculation of hot product gas, which would remove the heat needed for the steam production at the same time as the gas contact time with the bed material is increased and beneficial catalytic effects could be improved. The third choice is recirculation of flue gas. This option will, of course, dilute the gas with nitrogen, but, yet, the gas will have a sufficiently high heating value for many applications.

In some special operations the gasifier could also be fluidized by air or oxygen/steam. In these latter cases the heat needed for the gasification process is produced within the gasifier, but the circulation of the heat carrier makes the process more stable and provides a possibility to reduce the oxygen to fuel ratio, in order to increase the efficiency of the process.

4. Operation at "any" temperature

In the proposed process the conversion temperature in the gasifier could be controlled in a wide temperature range. The ratio of the rate of biomass fed to the gasifier and the circulation rate of the bed material between the two reactors allows control of the bed temperature. As the char produced in the gasifier always is efficiently converted in the combustor, the temperature in the gasifier can be anything between 500 °C, suitable for production of liquids, and 900 °C, suitable for gasification of non-problematic biomass.

5. Secondary oxygen injection

Secondary combustion with air or oxygen could be used to raise the temperature further, in order to reduce the amount of tar, without a significant reduction of the heating value. For a direct gasifier, especially air-blown, the heating value is low from the beginning and a further reduction of the heating value restricts the possible use of the gas.

6. Possibility to gasify wet fuel with a high efficiency

As there is an over production of heat in the system the system could be adjusted so there is a net heat flow to the gasifier and the gasification processes could be operated even for wet biomass, without any significant negative effects on the efficiency of the process. The advantages are that there is no need for a separate dryer, which decrease the complexity and the cost of the plant. This is especially a great advantage for a plant that receives fuels with a wide variation in moister content.

7. Possibility to burn fuel with higher moisture content in combustor

Many fluidized bed boilers especially, bubbling beds, burns wet and problematic fuels. These boilers often use a support fuel that releases its heat in the lower part of the boiler where the moisture is released. By connecting a gasifier to the bubbling fluidized bed the char produced in the gasifier will be transported to the boiler to act as a premium fuel, as it is already heated and consists of more or less pure carbon.

8. The gasifier does not have any negative effect on the combustor

Fluidized bed boilers are well known for their fuel flexibility and the use of external heat exchangers, which will be the function of the gasifier, is a well established technology. On these grounds there are no foreseen negative effects that could be caused by the integration of a gasifier into a FB-boiler.

3 MARKET POTENTIAL

Fluidized bed boilers are common and available all over the world. The major producers outside China and India are Alstom, Foster Wheeler and Metso Power, which have delivered more than 700 plants world wide [3]. The number of installations divided on different sizes could be seen in Fig 5 and the cumulative installed capacity could be seen in Fig 6. A large number of these plants are installed in the Nordic countries with more than 100 installations in Sweden. Fig 7 shows the installed number of units in Sweden. It is interesting to notice that most installations in Sweden are small, a

consequence of their use for biomass and heat production. The largest plants shown in Fig 6 are instead power plants utilizing coal, in which the present concept can be used as co-gasification of biomass as an alternative to co-firing.

The evaluation of the Chalmers CFB-boiler indicates that the installed capacity of this boiler is equal to the potential of gasification, which is true for boiler with a size below 200 MW_{fuel}. For larger sizes the logistics of the biomass transported to the plants are likely to restrict the size. A further look into the installed capacity of the Swedish park of FB units, Fig 8, shows that most of the plants are connected to district heating systems and the time of annual operation is around 4,000 hours. This means that the 5,000 MW_{th} installed capacity has the potential to produce around 20 TWh/year of biomass-based gas.

The size of the biomass gasifier determines what kind of fossil fuel that it is reasonable to substitute. The larger a gasifier is, the more advanced gas cleaning equipment is economically feasible and the wider is the spectrum of applications. Examples of applications for the size ranges in Figs 5-8 are shown in Fig 9. For the smallest sizes (below 20 MW_{fuel}) the numbers of applications are restricted to applications that could use the product gas with little or simplified gas cleaning which in most cases significantly reduces the efficiency of the process. Example of uses, gas for NOx reduction by reburning, substitution of oil or gas in industrial burners, or simple gas engine applications can be mentioned. The last application brought up could be questioned, as the value of electricity close to this kind of boiler most likely is not high enough to motivate an investment in a gas engine.

For a medium-size gasifier (20 to 60 (100) MW_{fuel}) the number of applications increases and rather advanced cleaning equipment could be motivated. The gas produced in this segment could be cooled down and transported to an application outside the site of the gasifier. For example, it could be used as city gas or as substitution of oil and gas in large rotating kilns. A slip stream of hydrogen is also reasonable to derive from gas produced at this scale.

For gasifiers that are considered large in this context (larger than (60) 100 MW_{fuel}) the cleaning and the conditioning of the gas could be economically motivated to be taken all the way to a pure syngas that could be used to produce any synthetic fuel, like methanol, DME or synthetic natural gas.

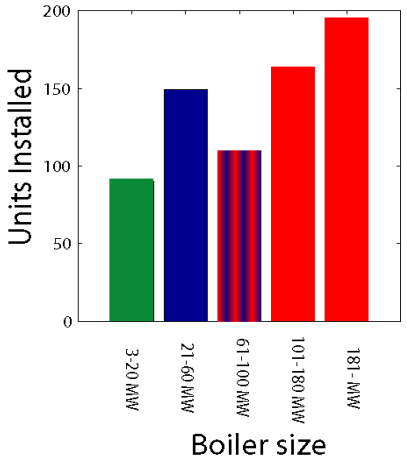

Figure 5 Installed FB-boilers world wide from Alstom, Foster Wheeler and Metso power.

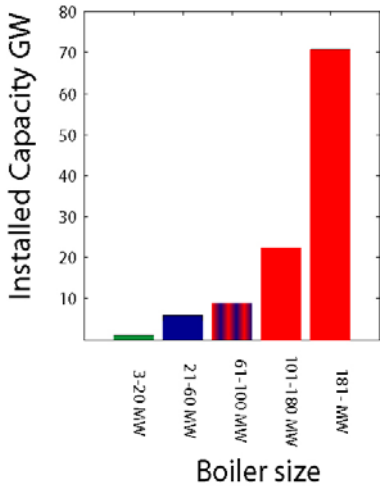

Figure 6 Cumulative installed capacity in FB-boilers world wide from Alstom, Foster Wheeler and Metso power.

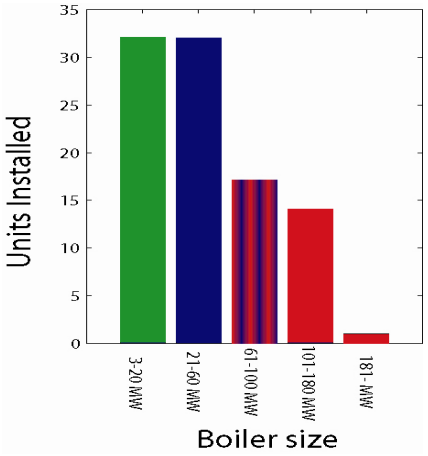

Figure 7 Installed FB-boilers in Sweden from Alstom, Foster Wheeler and Metso power.

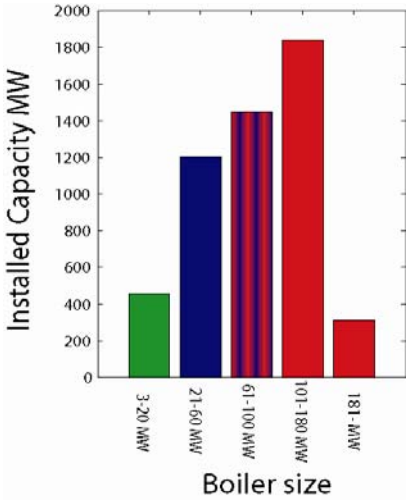

Figure 8 Cumulative installed capacity in FB-boilers in Sweden from Alstom, Foster Wheeler and Metso power.

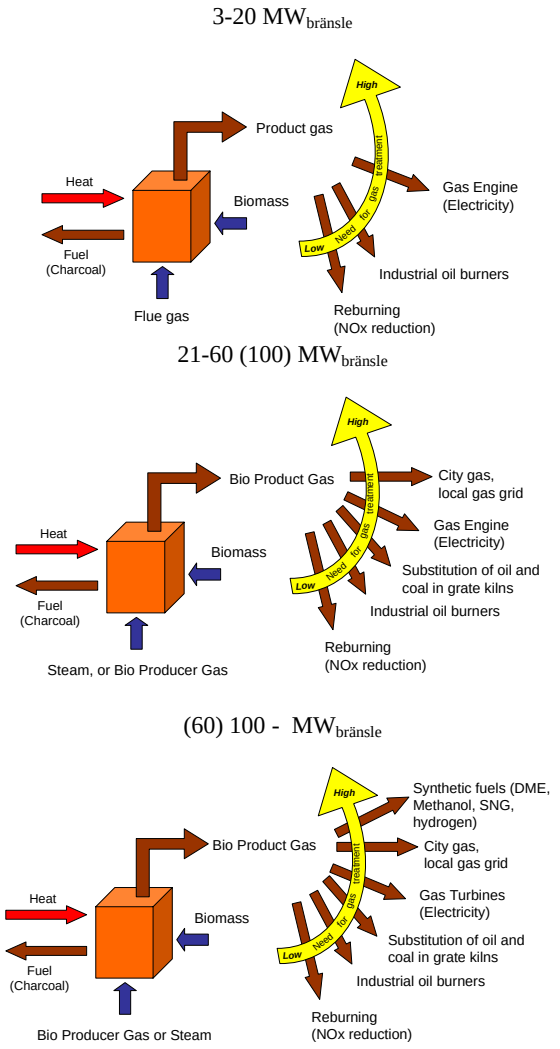

Figure 9 Examples of use of biomass based gas produced from gasifier of different size.

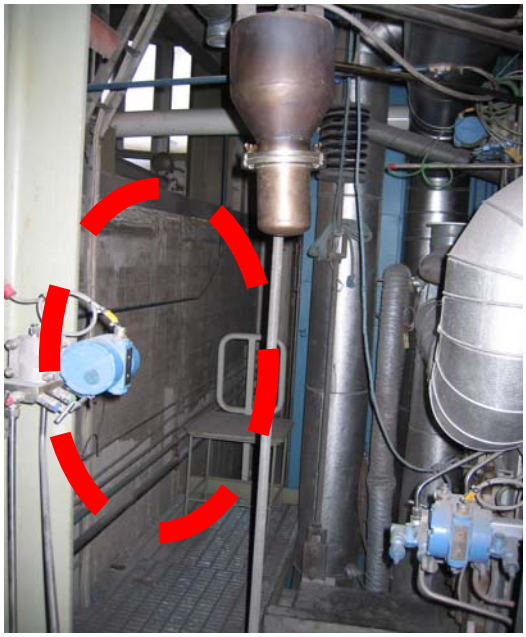

Figure 10 Available space for the 2 MW_{fuel} gasifier

In summary, it can be concluded that the market potential for the gasification concept presented here is large and even larger if one considers the extensive number of fluidized bed installations in China. The major advantages compared to other gasification solutions are the possibility to offer energy companies an alternative to gain experience from biomass gasification at an industrial scale to a relatively low risk. It also provides a way to produce fuels for the transport sector, which could start with substitution of oil and gas in industrial processes. An additional advantage is that the experience and skill built up in companies for several decades related to operating FB-boilers can be used to also operate the integrated gasifier.

4 THE DEMONSTRATION

The concept will be demonstrated on Chalmers 12 MW_{th} CFB-boiler [4]. The basic design started in October 2006. The plan is that the reconstruction and integration of the gasifier will be accomplished in October 2007 and the gasifier will be handed over for research in January 2008.

The integration has been a great challenge as the available space is limited and the condition that the reconstruction should not negatively affect any part of the unique, flexible, research CFB-boiler. In Fig 10 the space available for the gasifier is shown. During the basic design, one parameter that needed to be optimized was the fuel input to the gasifier. After considering all restrictions the requirements on availability for measurement was found to be the most critical parameter and the fuel input to the gasifier was therefore restricted to 2 MW_{fuel}.

In the first step, the new reactor will be connected to the CFB boiler according to Figs 11 and 12. In the first phase of operation the produced gas will be transported back to the boiler and burned, and the heat will be used to heat the buildings in Chalmers' campus area.

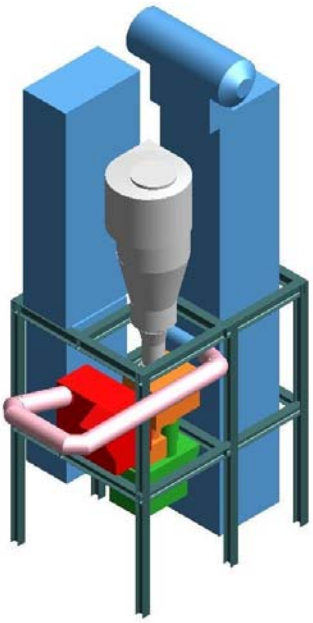

Figure 11 Integration of gasifier onto Chalmers 12 MW_{th} CFB-boiler (Metso Power)

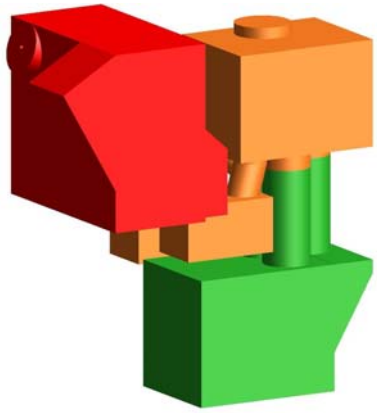

Figure 12 Close up of integration of the gasifier. The top left box is the gasifier; top right box is the particle distributor and inlet of flow of bed material from cyclone. Below the particle distributor the two additional particle seals for separation of gas between gasifier and combustor are seen. The lower box is the existing external particle cooler. (Metso Power)

Figur 13 Chalmers power central

In this first step it will be possible to investigate

- three different fluidization media (steam, flue gas, air),
- dry or wet fuels fed as pellets or wood chips,
- bed temperature could be varied between 500 and 900 °C and
- secondary air to rise the temperature to 900 °C in order to crack tars.

The budget for this first step is 1.4 million euro.

Future plans are to complement the reactor with a thermal reformer, product gas recirculation. The final aim is to include the entire chain required to produce synthetic fuel.

5 CHALMERS 12 MW_{th} CFB-BOILER

At Chalmers power central, Fig 13, there are an existing well functioning and well exploited 12 MW_{th} research CFB-boiler, i.e. a boiler of industrial scale. The flexibility of the boiler is unique and it can handle up to three different solid fuels, if desired simultaneously, one wet fuel like sludge and one oil or gaseous fuel. The boiler itself is equipped with a great number of sensors and measurements ports that allow in-situ measurements in the entire furnace volume at the same time as the global conditions can be monitored. In order to perform measurements in the boiler a unique measurement infrastructure for advanced combustion and gasification investigations has been built up. It has continuously provided high quality data for research projects for more than twenty years. During these years the operators and research staff have improved their skill in performing advanced measurements campaigns at the industrial scale.

6 CONCLUSIONS

A concept using the existing infrastructure of boilers forms the basis for introducing a gasification technology that lowers cost and minimizes risks is here presented. The concept is based on retrofitting existing fluidized bed boilers. The proposed process uses the thermal flywheel of the fluidized bed as a means of devolatilising the biomass. The potential of the concept is extensive and could give a significant push to the introduction of biomass gasification in the world. Moreover, several advantages with integrating a gasifier onto a combustor are identified.

A demonstration project is already initiated and a 2 MW_{fuel} gasifier integrated into a 12 MW_{th} CFB-boiler will be in operation in October this year (2007).

7 REFERENCES

1. Hulten G.S., *Utredning rörande ett kombinerat gas-, värme- och kraftverk för Norrköping*, Pofningsanstalten, Norrköping, (1915).
2. H. Hofbauer, *Scale Up of Fluidized Bed Gasifiers from Laboratory Scale to Commercial Plants: Steam Gasification of Solid Biomass in a Dual Fluidized Bed System* , In F. Winter editor, 19th Int. Conf. on Fluidized Bed Combustion, Vienna (2006).
3. F. Johnsson, *Fluidized Bed Combustion for Clean Energy*, In Proceeding of the *12th Int.Conf. on Fluidization*, (2007)
4. B. Leckner, M. Golriz, W. Zhang, B.-Å. Andersson and F. Johnsson, *Boundary layer-first measurements in the 12 MW CFB research plant at Chalmers University*. In: E.J. Anthony, Editor, *11th Int. Conf. on Fluidized Bed Combustion*, ASME, New York (1991), p. 771.

8 ACKNOWLEDGMENT

This project is made achievable by financing and help with the construction project management from Göteborg Energi AB. A great engagement from Metso Power, Akademiska hus and S.E.P are also a key to the successful progress of the project. Finally the Swedish Energy Agency is recognised in providing resources to maintain the research infrastructure at Chalmers' power station.

BIOMASS CO-COMBUSTION IN AN OXYFUEL POWER PLANT WITH SYNTHESIS GAS PRODUCTION

F. Normann[1], H. Thunman, F. Johnsson

Department of Energy and Environment, Division of Energy Technology
Chalmers University of Technology, SE-412 96, Sweden
[1]Phone: +46 31 772 1486
Fax: +46 31 772 3592
[1]E-mail: fredrik.normann@chalmers.se

ABSTRACT: This paper investigates new possibilities and synergy effects for co-firing of biomass and coal in an oxyfuel fired polygeneration scheme (transportation fuel and electricity) with carbon capture. A way to make the oxyfuel process more effective through a sub stoichiometric combustion is enabled due to the co-combustion of biomass in the process, which keeps the process CO_2 neutral. The sub stoichiometric combustion leads to a production of synthesis gas, which is utilised in an integrated synthesis to DME. The proposed process is simulated with a computer model with a previous study of an oxyfuel power plant as a reference process. The degree of sub stoichiometric combustion, or amount of synthesis gas produced, is optimized with respect to the overall efficiency. The maximal efficiency were found at a stoichiometric ratio of 0.6 were the efficiency for the electricity producing oxyfuel process is 0.35 and the efficiency for the DME process is 0.65. The above mentioned process constitutes a way to improve the oxyfuel carbon capture processes with an efficient use of biomass in a polygeneration process.

Keywords: biomass/coal cofiring, bio-syngas, CO_2 emission reduction

1 INTRODUCTION

The urgent need for reduction of CO_2 emissions from the energy system will not be handled by a single solution. The future system will most certainly include an increased use of renewable energy sources and an implementation of CO_2 capture processes on fossil fuelled based processes. The oxyfuel process (or O_2/CO_2 recycle combustion process) is a promising technique for capture of carbon dioxide from large scale coal fired power plants at a reasonable cost, i.e. < 20 €/ton CO_2 avoided. A series of studies of the process design has been done, e.g. [1,2] and pilot plants are being designed and are under construction, e.g. the construction of a 30 MW_{th} plant outside Berlin which will be commissioned in 2008 [3]. In order to establish a market for biomass on the supply side in the short and medium time co-combustion using a large coal power plant has been proposed as advantageous [4] and the benefits with capture of CO_2 from biomass conversion processes has previously been studied (e.g. [5]). This paper shows that by combining the oxyfuel process with co-combustion of biomass, new possibilities emerge and synergy effects can be gained.

An interesting possibility for the oxyfuel process is to burn the fuel in an oxygen lean mode (i.e. slightly under stoichiometric conditions), yielding a process between combustion and gasification with co-production of synthesis gas. The synthesis gas produced in the process can be utilized either for power generation or as raw gas in chemical synthesis for production of methanol, dimethyl ether (DME) and other chemicals. The sub stoichiometric combustion would also reduce the major drawback of the oxyfuel process, i.e. the expensive oxygen production. When the produced synthesis gas is used for synthesizing transportation fuels the carbon present in the gas is emitted to the atmosphere. The small fraction of biomass co-combusted corresponds to the amount of carbon used for the synthesis gas production and, thus, offsets the CO_2 that is emitted from the further use of the synthesis gas. Refining the synthesis gas to DME in connection with the proposed process can be motivated, because the processes can be well integrated with each other. Such transformation would also make the product easier to handle and to transport because DME liquefies at moderate pressures (5-6bar) at ambient temperature [6]. The end use of DME could be as a clean substitute for diesel and liquefied petroleum gas.

This paper presents a first evaluation of the above mentioned process and possibilities and technical difficulties with the technique are discussed. The purpose of the paper is to investigate new possibilities for synergy effects between the carbon capture processes and a larger implementation of biomass combustion in the energy system.

2 THE PROCESS

The basic principles of the oxyfuel process, described in Figure 1, are that the fuel is burnt in a mixture of oxygen and recycled flue gas. Due to the absence of air borne N_2 the flue gas consists mainly of CO_2 and H_2O. The recycled flue gas is used to control the combustion temperature, burner aerodynamics, residence times and etc., i.e. to make up for the missing N_2. The exhaust flue gas is compressed and separated in various steps before the CO_2 is ready to be stored. In a typical process design the final step consists of CO_2 being condensed to be separated from mainly N_2 and Ar. In the proposed process all the main components are the same as in the standard oxyfuel process, but the stoichiometrics of the combustion is lowered to below one to create a process in between combustion and gasification. This results in production of CO and H_2 (synthesis gas) in the combustor, which are separated from the CO_2 when it is condensed.

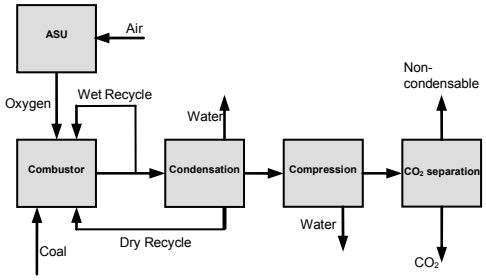

Figure 1: Schematic figure over the basic principles of the oxyfuel process.

The 500 MW_e oxyfuel power plant proposed in [1] is used as the reference in this investigation. This power plant is an assessment made by the IEA based on a thorough investigation of the entire process in cooperation with industry.

The main process data for the reference power plant are given in Table I and the analysis of the black coal used in the study is given in Table II. These values are used throughout this study unless otherwise stated. To investigate the effects of oxygen lean oxyfuel combustion, the stoichiometrics of the combustion is varied from 1.15, i.e. normal combustion, down to 0.4 which can be compared with 0.3 in typical gasification processes. The boiler power of the power plant is kept the same as in the reference plant, leading to a lowered electricity output when the stoichiometrics is decreased and more synthesis gas is produced. This approach will allow for the possibility to change the split between electricity and gas depending on the requirements.

Table I: Main process data for reference oxyfuel power plant.

Net electricity output	532 MW_e
Fuel heat input	1,502 MW
Net efficiency	35.4%$_{vol}$
ASU power	87 MW_e
O2 input	432 tonne/h
Oxygen purity	95%$_{vol}$
O_2/CO_2	30%$_{vol}$
Air ingress	2%$_{vol}$

Table II: Coal specifications.

LHV	25.87 MJ/kg
Ash	12.2 %$_w$
Moisture	9.5 %$_w$
Ultimate Analysis (%$_w$ DAF)	
C	82.5
H	5.5
O	9.0
N	1.8
S	1.1
Cl	0.03

The synthesis gas produced in the combustor is used in a DME synthesis according to [6], performed at 260˚C and 50bar. The DME synthesis is integrated with the gas cleaning section of the oxyfuel power plant so there is no requirement of extra cleaning or compression of the synthesis gas after it leaves the CO_2 condenser. The introduction of H_2 and CO to the CO_2 stream creates a need for a more extensive separation process. Thus, a distillation column is used as an enhancement to the low temperature flash used in the reference work. The composition of the synthesis gas is adjusted to a H_2/CO ratio of 1 (suitable for DME synthesis) for all stoichiometric ratios by controlling the amount of water in the combustor.

Biomass is co-combusted with the coal to an extent required to keep the capture ratio at 95%$_{vol}$, i.e. the same level as for the reference plant. This, since the carbon present in the synthesis gas will be emitted to the atmosphere (i.e. as released from the transportation fuel). The lowest acceptable capture ratio has a considerable impact on the efficiency of the carbon capture process as it sets the demands on the separation and the quantity of CO_2 to compress. It could be argued that a 100% capture ratio, to make the process truly CO_2 neutral, should be aimed at. It would, however, differ from the capture ratio of the reference oxyfuel power plant and make the comparison unfair.

For the fractions of biomass required to offset the CO_2 emissions from the synthesis gas (~20%), no technical difficulties with feeding and handling of the biomass are expected. Therefore, no assessment is made of the pre-treatment or implication of biomass co-firing on the combustion process. Obviously, such an assessment has to be included in further studies and especially if applying higher biomass fractions, to investigate the effect on energy consumption and material issues (e.g. as caused by possible alkali content of the biomass).

3 METHODOLOGY

The process was evaluated with process simulations using the chemical flow sheeting program Aspen Plus [7]. To exploit integration possibilities the combustion, gas cleaning, DME synthesis and steam cycle are all implemented in the same computer model. The Air Separating Unit (ASU) is implemented only to the extent that concerns the current process. That is the power consumption of the compressors and the heat integration with the other parts of the process, which both is dependent on the stoichiometric ratio of the combustion.

Aspen Plus has an extensive database of physical properties and thermodynamic models that were used throughout the study. For the combustion, gas cleaning and synthesis parts of the process the property method of Peng-Robinson with Boston-Mathias alpha function (PR-BM) where used. The PR-BM property method is commonly used for gas processing, especially mixtures of light gases, and is expected to give reasonable results also at elevated temperatures and pressures [8]. For the steam cycle the NBS/NRC steam table of state (STEAMNBS) is used as a property method. The STEAMNBS is specially developed for water/steam systems and is applicable in the pressure range of 0-30,000 bar and temperature range of 260-2,500 K [9].

The gas composition of the combustion processes is calculated from equilibrium at 750˚C, which is estimated as the lowest temperature for which equilibrium is reached. In addition, the adiabatic flame temperature of the combustion is calculated to ensure that a satisfactory temperature, i.e. >1200˚C, is achievable. The outcome of the DME synthesis is also given by equilibrium

calculations at the pressure and temperature of the reference plant, i.e. 50bar and 260˚C.

The efficiency of the DME production (η_{DME}) is expressed with a fixed efficiency for the electricity production in the oxyfuel power plant (η_{oxy}) of 0.35, i.e. the same as in the reference plant, and η_{DME} is calculated according to Equation (1), where P_{DME}, P_e and P_{fuel} are the power of the DME, electricity and added fuel respectively.

$$\eta_{DME} = \frac{P_{DME}}{P_{fuel} - P_e/\eta_{oxy}} \qquad (1)$$

A fixed efficiency of the electricity production is applied, since, the power generation is considered as the principal part of the process. Thus, the work evaluates if an efficient DME production can be attained without any changes in neither the efficiency of the electricity production nor in the carbon capture rate of the oxyfuel process.

4 RESULTS

Figure 2 gives the resulting efficiency of the DME production, as a function of the stoichiometrics of the combustion in the proposed process. The efficiency reaches a maximum of 0.65 at a stoichiometry of 0.6. At higher stoichiometric ratios the efficiency of the DME synthesis suffers due to the negative effect the elevated concentration of inert gases has on the equilibrium. The problems at higher stoichiometric ratios, i.e. when only a small amount of synthesis gas is produced, are primary caused by the argon and nitrogen introduced with the oxygen and from leakage of air into the process. These problems can argue for an enhanced oxygen separation, but, since the fraction of inert gases decreases drastically with a rather small reduction of the stoichiometry, an enhanced oxygen separation is not analysed. At too low stoichiometrics (<0.6) the efficiency of the power production suffers, as the heat transferred is lowered, due to a decrease of the temperature in the combustor. The shift of product from electricity to DME when the stoichiometry is lowered also has a negative effect on the heat economy. The amount of waste heat from the DME synthesis is increasing while the ability to recover waste heat in the pre-heating of the feed water is decreasing. This will lead to a lowered recovery rate of waste heat within the process and negative effects on the plant efficiency. The maximum efficiency achieved for the DME process is just above other processes proposed for DME production from biomass [10]. With the extra advantage of being highly integrated with the oxyfuel process the results shows a good potential for an efficient conversion of biomass to liquid fuel using the proposed technique.

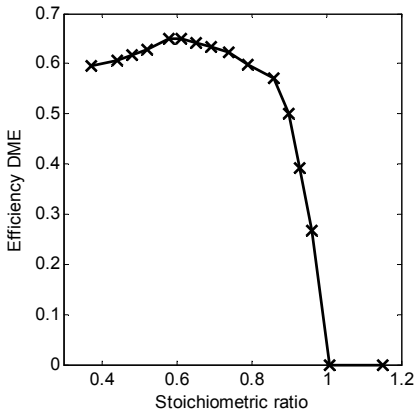

Figure 2: Calculated DME efficiency.

The proposed process offers possibilities for combining of the equipment used in the different processes, an overview are presented in Table III. In the present work only a rough economic evaluation of the proposed process scheme is made. This is based on an assessment on to what extent there are new respectively combined (i.e. an increased or decreased number of) unit operations of the proposed process compared to the reference processes. The largest savings made on the equipment is due to

- the introduction of a combined combustor and gasifier,
- the combined compression of flue gas and synthesis gas, and
- the use of the CO_2 separation to purify the synthesis gas.

The only requirement of enhancement of equipment compared to the reference plants is the upgrading of the low temperature two-step flash to a distillation column for the CO_2 separation.

Table III: Process utilities needed in the different processes and possibilities for equipment integration in the proposed process.

	Oxy-fuel	Gas-ifier	DME plant
Pre-treatment	x	x	
ASU	x	x	
Furnace/Gasifier	x	x	
Particle removal	x	x	
Steam cycle	x		
Flue gas / Syn gas compressor	x		x
Water condensation	x		
Water removal	x		
CO_2 separation	x		
CO_2 compressor	x		
Sulphur separation	x	x	
DME reactor			x
DME distillation columns			x

The major concern with the process is possible complications related to the sub stoichiometric combustion conditions in the combined combustor and gasifier. Under such conditions unwanted formation of hydrocarbons and low burnout of the fuel could occur. For large scale coal facilities the conversion of coal is always a top priority and the combustion most be as

efficient as possible. Nevertheless, the high temperature in the combustor, compared with a gasifier, should ensure satisfactory carbon conversion. The shifting from an oxidizing to a reducing atmosphere could also be an issue for the material used in the combustor, which has to be able to both be resistant against high temperature corrosion and able to transport heat to the steam production. The sub stoichiometric combustion is the central concern for the proposed process and it is most critical for a further investigation of the process.

The recirculation stream containing the combustible gases CO and H_2 could become flammable, if the recirculation stream is mixed with oxygen to create an air like combustion gas. In [11] a method of calculating flammability limits of complex gases, such as those present in the recirculation stream of the proposed process, is presented. A calculation using this method with the recirculation gas composition from the 0.6 stoichiometry case shows that the mixture becomes flammable between 88 and 97%$_{vol}$ of recycled gas in pure oxygen which should be compared with the 69%$_{vol}$ that is present in the recirculation stream of the process. Even so, the mixing of oxygen with combustible gases outside of the combustor is not considered secure but special burners that allows for a mixing inside the combustor has to be designed. Approximations of flammability limits are difficult, especially for a mixture of several fuels and inert gases, and an experimental determination is necessary to reach accuracy.

5 CONCLUSION

A process scheme of a polygeneration plant for co-firing of biomass in a sub stoichiometric oxyfuel combustion is presented and possibilities and synergy effects with the scheme is discussed. The work also points to possible problems that could occur, i.e. where further investigations are required. The investigation was done through a process simulation of the proposed power plant, with previous studies as references.

The results show an optimal DME synthesize at a stoichiometric ration of 0.6 with an efficiency of 0.65 from biomass. The process had a sustained efficiency of 0.35 for the power production and a carbon capture ratio of 95%. The 20%$_{energy}$ co-combustion of biomass creates an efficient way to utilize biomass with the advantage of being done in a large scale coal plant of high efficiency. A central issue, of need of further investigation, is the sub stoichiometric combustion where the conversion ratio of coal and possible presence of high temperature corrosion must be investigated. The process is, however, offering integration possibilities both for heat and for components in the process scheme. Combined use of equipment like the combustor, compressors, and separation processes should lead to lower investment cost and a more profitable process, compared to separate processes for gasification of the biomass and synthesis of DME.

The proposed process would be beneficial both for the oxyfuel process as well as for the biomass combustion and the work shows on possibilities when combining the two processes.

6 ACKNOWLEDGEMENTS

This work is financed by the Swedish Energy Agency.

7 REFERENCES

[1] IEA GHG, Oxy Combustion Processes for CO_2 Capture from power plant - Report Nr 2005/9, (2005)
[2] K. Andersson and F. Johnsson, Process evaluation of an 865 MWe lignite fired O_2/CO_2 power plant, (2005)
[3] L. Strömberg, G. Lindgren and M. Anheden, GHGT8 - Vattenfall's 30 MWth Oxyfuel Pilot Plant Project, (2006)
[4] F. Johnsson, E. Ljunggren, M.Berggren and G. Berndes, 14th European Biomass Conference - Cost competitive bioenergy: Linking lignocellulosic biomass supply with co-firing for electricity in Poland, (2005)
[5] C. Azar, K. Lindgren, E. Larsson and K. Möllersten, Carbon capture and storage from fossil fuels and biomass – Costs and potential role in stabilizing the atmospher, (2006)
[6] T. Ogawa, N. Inoue, T. Shikada and Y. Ohno, Direct Dimethyl Ether Synthesis, (2003)
[7] Aspen Plus (v2004.1), Aspen Tech
[8] C. Barney, Heat exchanger system for reforming in an ammonia process,
[9] L. Haar, NBS/NRC steam tables, (1984)
[10] P Ahlvik and Å. Brandberg, Well to wheel efficiency - Vägverket 2001:85, (2001)
[11] H.F. Coward and G.W. Jones, Limits of flammability of gases and vapours - Bureau of Mines Bulletin 503, (1952)